TÉCNICO LISBOA

Analysis of the Impact of EMF Restrictions on 5G Base Stations Deployment in Existing Networks

Frederico Casal Ribeiro da Maia e Moura

Thesis to obtain the Master of Science Degree in

Electrical and Computer Engineering

Supervisor: Prof. Luís Manuel de Jesus Sousa Correia

Examination Committee

Chairperson: Prof. José Eduardo Charters Ribeiro da Cunha Sanguino

Supervisor: Prof. Luís Manuel de Jesus Sousa Correia

Members of Committee: Prof. Custódio José de Oliveira Peixeiro

Eng. Luis Taborda

January 2021

I declare that this document is an original work of my own authorship and that it fulfils all the requirements of the Code of Conduct and Good Practices of the *Universidade de Lisboa*.

To Carolina, my family, and friends.

Acknowledgements

First of all, I would like to express my deepest gratitude to Professor Luís Correia for giving me the opportunity to develop this thesis under his supervision for the past year. I am extremely grateful for all the patience, good mood and righteous advice, not only for the development of this thesis but also regarding life in general. Without his orientation, all the work performed these last months would not have been possible.

To all GROW members, for the kindness and patience throughout this process. Also, a special thank you to my colleagues Nuno Silva and Sérgio Marinheiro for all the help, important insights, support and friendship.

To Eng. Luís Taborda and Eng. Nuno António from Huawei, for giving me the opportunity to develop this work in close relation to the real world of telecommunications. My deepest gratitude to Eng. Luís Taborda, for all his precious time and effort spent on this thesis, even in this strange and arduous year. I am also very grateful for all the great talks and advice regarding the telecommunications industry as well as all aspects of life.

To my greatest friends, Fernando Lima, Gaspar Ribeiro and Carolina Castilho for all their friendship, support and help throughout these five years, and also for all our good moments inside and outside IST.

To a very special person, my girlfriend Carolina Ribeiro Rato, for all her unconditional love, support, patience and influence, and for always being there for me in the best but also the toughest days of the last five years. Thank you for always pushing me to work harder, to be a better person and for believing in me at all times.

Finally, to my parents and brothers, to whom I will always dedicate my accomplishments, and to whom I am extremely grateful for all the care, education, stability, support, love and everything they have done for me for the last 23 years. I would not be who I am today if not for you.

Abstract

This thesis aims at developing a model to analyse the impact of electromagnetic field restrictions on NR performance in base stations (BSs) with co-location of GSM, UMTS and LTE. A model to estimate the exclusion region of BS antennas was developed. The model estimates the power density as a function of distance for each mobile communication system and any given direction, using far- and near-fields models. One considers that the antennas are continuously radiating at maximum power as a worst-case perspective. A model for the computation of the coverage radius and throughput per resource block (RB) as a function of the NR BS transmitted power was developed. Representative scenarios of BSs with co-location of antennas are analysed. An analysis of the exclusion zone distance is made before and after the installation of NR; for urban scenarios, the highest increase is 248.7%, while it is 131.6% and 56.4% for the suburban and rural ones, respectively. The impact of exclusion zones with restricted dimensions on the coverage radius and throughput per RB at cell-edge is analysed. The highest decrease in coverage radius is 62.9% for rural scenarios and 63.3% for suburban ones; regarding throughput, the highest decrease is 95.9% for both urban and suburban environments. Results show that, in some scenarios, operators may need to reduce the power transmitted by NR and legacy systems in order to comply with exclusion zone restrictions.

Keywords

Exclusion Zones, Mobile Communications Systems, Antennas, Coverage, Throughput, NR.

Resumo

Esta tese visa desenvolver um modelo para analisar o impacto das restrições do campo electromagnético no desempenho das estações base NR com a co-localização de GSM, UMTS e LTE. Foi desenvolvido um modelo para estimar a região de exclusão das antenas de estações base. Este estima a densidade de potência em função da distância utilizando modelos de campos distante e próximo. Considera-se que as antenas transmitem continuamente na potência máxima numa perspectiva de pior caso. Foi desenvolvido um modelo para o cálculo do raio de cobertura e velocidade de transmissão por *resource block* (RB) em função da potência transmitida por estações base NR. São analisados cenários representativos de estações base com co-localização de antenas. É feita uma análise da distância da zona de exclusão antes e depois da instalação de NR. Para os cenários urbanos, o aumento mais elevado é de 248,7%, enquanto que em cenários suburbanos e rurais é de 131,6% e 56,4%, respectivamente. É estudado o impacto de zonas de exclusão com dimensões restritas no raio de cobertura e na velocidade de transmissão por RB. A maior diminuição no raio de cobertura é de 62,9% para os cenários rurais e de 63,3% para os suburbanos. Quanto à velocidade de transmissão, a maior diminuição é de 95,9%, para os ambientes tanto urbanos como suburbanos. Os resultados obtidos mostram que, em alguns cenários, os operadores podem ter de reduzir a potência transmitida pelos sistemas NR e bem como os anteriores, a fim de cumprirem as restrições das zonas de exclusão.

Palavras-Chave

Zona de Exclusão, Sistemas de Comunicações Móveis, Antenas, Cobertura, Velocidade de Transmissão, NR.

Table of Contents

Acknowledgements vii

Abstract ix

Resumo x

Table of Contents xi

List of Figures xiv

List of Tables xvii

List of Acronyms xix

List of Symbols xxii

List of Software xxvii

1 Introduction 1

1.1 Overview and Motivation 2

1.2 Contents 4

2 Fundamental Aspects and State of the Art 7

2.1 Mobile Communications Systems Radio Interface 8

2.2 Coverage, Capacity, and Interference 13

2.3 Services and Applications 16

2.4 Electromagnetic Field Exposure 17

2.4.1 Radiation Regions 18

2.4.2 Electromagnetic Field Recommendations and Measurement 19

2.4.3 Exclusion Zones 22

2.5 State of the Art 24

3 Model Development and Simulator 27

3.1 Model Overview 28

3.2 Power Density Estimation Models 29
3.2.1 Far-Field Model 29
3.2.2 Far-Field Gain-Based Model 30
3.3 Exclusion Zone Evaluation Model 31
3.3.1 Far-Field Zone 31
3.3.2 Near-Field Zone for Linear Arrays 32
3.3.3 Near-Field Zone for Planar Arrays 36
3.3.4 General Zone Model 39
3.4 Coverage and Capacity Planning 44
3.5 Output Evaluation Metrics 47
3.6 Model Assessment 48
3.7 Comparison with Experimental Results 51
4 Results Analysis 57
4.1 Scenarios Description 58
4.2 Variation of $Dfront$ 60
4.3 Exclusion Zone Variation for Other Directions 68
4.4 Influence on Coverage and Throughput 72
5 Conclusions 77
Annex A. Coverage and Capacity 83
A.1 Radio Link Budget 84
A.2 Propagation Models 85
A.3 Users and Resources 88
A.4 SINR versus Throughput 88
Annex B. Additional Model Assessment Data 91
B.1 Exclusion Zone Evaluation Assessment 92
B.2 Coverage and Capacity Assessment 93
Annex C. Measurements Description 101
C.1 Measurements Description of BS1 102
C.1.1 Sector 1 102
C.1.2 Sector 2 103
C.2 Measurements Description of BS2 104
C.3 BS Characteristics 106
Annex D. Measurements Results 107
D.1 Measurements Results of BS1 108

D.1.1 Sector 1 108
D.1.2 Sector 2 112
D.2 Measurements Results of BS2 115
Annex E. 3D Radiation Pattern Interpolation Method 121
Annex F. Antennas Description 125
Annex G. General Zone Model Simulation 127
G.1 Simulation Parameters 128
G.2 Simulation Results 128
Annex H. Variation of the Exclusion Zone Results 131
H.1 Variation of $Dfront$ 132
H.2 Exclusion Distance Results for Other Directions 132
H.3 Downtilt Influence on Physical Barriers 134
Annex I. Influence on Coverage and Throughput Results 137
I.1 Coverage Radius Results 138
I.2 Cell-Edge Throughput per RB Results 143
References 149

List of Figures

Figure 1.1. BS exclusion zone delimited by physical barriers (extracted from [Antu12]). 4
Figure 2.1. LTE's DL resource allocation (adapted from [ROSC08]). 11
Figure 2.2. SCS scalability in NR (adapted from [QUAL18]). 12
Figure 2.3. NR radio frame structure (extracted from [Corr20]). 13
Figure 2.4. Inter-Cell Interference (adapted from [Alme13]). 15
Figure 2.5. NR use cases (extracted from [ITUR15b]). 17
Figure 2.6. Field regions of an antenna (adapted from [Bala05]). 18
Figure 2.7. Reference levels for time-averaged exposures of ≥ 6 minutes from 100 kHz to 300 GHz (extracted from [ICNI20]). 20
Figure 2.8. Exclusion zone surrounding a BS antenna (extracted from [OFRC05]). 22
Figure 2.9. Validity range of the different models (extracted from [OFRC05]). 23
Figure 2.10. Representation of an antenna's exclusion zone (extracted from [OFRC05]). 23
Figure 2.11. Presence of an EMF saturated zone (extracted from [CCMF18]). 25
Figure 3.1. Model Configuration. 28
Figure 3.2. $Dfront$ computation with the far-field model. 33
Figure 3.3. Coordinates system for a linear array antenna (adapted from [Antu12]). 33
Figure 3.4.Geometry comparison between even and odd element arrays. 34
Figure 3.5. Geometry comparison between θ and θ' for a three dipoles linear array. 35
Figure 3.6. Electric field computation for a linear array in the near-field at a distance d. 37
Figure 3.7. Coordinates system for a planar array antenna. 37
Figure 3.8. Electric field computation for a planar array in the near-field at a distance d. 39
Figure 3.9. Power density as a function of distance for an active 3.6 GHz NR antenna in the near-field. 40
Figure 3.10. Power density interpolation over distance for an active 3.6 GHz NR antenna. 41
Figure 3.11. $Sfinal(d)$ over distance for an active 3.6 GHz NR antenna. 42
Figure 3.12. Computation of $Dfront$ with the exclusion zone evaluation model. 43
Figure 3.13. Radiation pattern variances from reactive near-field toward the far-field (adapted from [Bala05]). 44
Figure 3.14. The coverage planning process (based on [Viei18] and [Belc18]). 45
Figure 3.15. Modulation radius distribution in a cell (extracted from [Viei18]). 46
Figure 3.16. $Dfront$ as a function of the antenna input power. 49
Figure 3.17. $Dfront$ vs. number of mobile communications systems present at the BS. 50
Figure 3.18. Cell radius versus BS height for the 700 MHz band. 51
Figure 3.19. Cell radius versus BS height for the 3.6 GHz band. 51
Figure 3.20. Measured versus theoretical results of $S(d)$ for GSM900 and UMTS2100, for set 1 of BS1's sector 1. 53
Figure 3.21. Measured versus theoretical results of $S(d)$ for LTE1800 and NR3600, for set 1 of BS1's sector 1. 53
Figure 4.1. $Dfront$ results for the carrier configuration 1/1. 61
Figure 4.2. $Dfront$ results for the carrier configuration 2/1. 61
Figure 4.3. $Dfront$ results for the carrier configuration 4/2. 62

Figure 4.4. $Dfront$ results for the carrier configuration 4/4. 62
Figure 4.5. Horizontal and vertical radiation patterns of an active NR antenna (extracted from [HUAW19b]). 65
Figure 4.6. Downtilt and vertical SER influence on the exclusion region (adapted from [Antu12]). 65
Figure A.1. Throughput per RB as a function of SINR for MIMO 2x2 and SCS of 15 kHz. 90
Figure B.1. $Dfront$ as a function of the antenna gain. 92
Figure B.2. $Dfront$ as a function of the reference level for EMF exposure. 92
Figure B.3. Cell radius versus MT height for the 700 MHz band. 93
Figure B.4. Cell radius versus MT height for the 3.6 GHz band. 94
Figure B.5. Cell radius versus BS transmitted power for the 700 MHz band. 94
Figure B.6. Cell radius versus BS transmitted power for the 3.6 GHz band. 95
Figure B.7. Cell radius versus frequency for the Okumura-Hata model. 95
Figure B.8. Cell radius versus frequency for the WINNER II model. 96
Figure B.9. Cell radius versus coverage probability for the 700 MHz band. 96
Figure B.10. Cell radius versus coverage probability for the 3.6 GHz band. 97
Figure B.11. Cell radius for different SCS in different scenarios for the 700 MHz band. 97
Figure B.12. Cell radius for different SCS in different scenarios for the 3.6 GHz band. 98
Figure B.13. SINR comparison between LOS and NLOS case for different scenarios. 98
Figure B.14. Comparison of SINR between indoors and outdoors users for the 700 MHz band. 99
Figure B.15 Comparison of SINR between indoors and outdoors users for the 3.6 GHz band.. 99
Figure B.16. Comparison of throughput per RB between indoors and outdoors users at cell edge for the 700 MHz band. 100
Figure B.17. Comparison of throughput per RB between indoors and outdoors users at cell edge for the 3.6 GHz band. 100
Figure C.1. Horizontal plane sketch for sector 1 of BS1. 102
Figure C.2. Vertical plane sketch for sector 1 of BS1. 102
Figure C.3. Point of view from the lower terrace to sector 1 of BS1. 103
Figure C.4. Horizontal plane sketch for sector 2 of BS1. 103
Figure C.5. Vertical plane sketch for sector 2 of BS1. 104
Figure C.6. Point of view from the lower terrace to sector 2 of BS1 104
Figure C.7. Vertical plane sketch of BS2. 105
Figure C.8. Horizontal plane sketch of BS2. 105
Figure C.9. Point of view from the upper terrace to sector 1 of BS2. 105
Figure C.10. Point of view from the upper terrace to sector 2 of BS2. 106
Figure D.1. Measured versus theoretical results of $S(d)$ for GSM900 and UMTS2100, for set 1 of BS1's sector 1. 108
Figure D.2. Measured versus theoretical results of $S(d)$ for LTE1800 and NR3600, for set 1 of BS1's sector 1. 109
Figure D.3. Measured versus theoretical results of $S(d)$ for GSM900 and UMTS2100, for set 2 of BS1's sector 1. 109
Figure D.4. Measured versus theoretical results of $S(d)$ for LTE1800 and NR3600, for set 2 of BS1's sector 1. 110
Figure D.5. Measured versus theoretical results of $S(d)$ for GSM900 and UMTS2100, for set 3 of BS1's sector 1. 110
Figure D.6. Measured versus theoretical results of $S(d)$ for LTE1800 and NR3600, for set 3 of BS1's sector 1. 111
Figure D.7. Measured versus theoretical results of $S(d)$ for GSM900 and UMTS2100, for set 1 of BS1's sector 2. 112

Figure D.8. Measured versus theoretical results of $S(d)$ for LTE1800 and NR3600, for set 1 of BS1's sector 2. 112
Figure D.9. Measured versus theoretical results of $S(d)$ for GSM900 and UMTS2100, for set 2 of BS1's sector 2. 113
Figure D.10. Measured versus theoretical results of $S(d)$ for LTE1800 and NR3600, for set 2 of BS1's sector 2. 113
Figure D.11. Measured versus theoretical results of $S(d)$ for GSM900 and UMTS2100, for set 3 of BS1's sector 2. 114
Figure D.12. Measured versus theoretical results of $S(d)$ for LTE1800 and NR3600, for set 3 of BS1's sector 2. 114
Figure D.13. Measured versus theoretical results of $S(d)$ for GSM900 and UMTS2100, for set 1 of BS2. 116
Figure D.14. Measured versus theoretical results of Sd for LTE1800 and NR3600, for set 1 of BS2. 116
Figure D.15. Measured versus theoretical results of $S(d)$ for GSM900 and UMTS2100, for set 2 of BS2. 117
Figure D.16. Measured versus theoretical results of $S(d)$ for LTE1800 and NR3600, for set 2 of BS2. 117
Figure D.17. Measured versus theoretical results of $S(d)$ for GSM900 and UMTS2100, for set 3 of BS2. 118
Figure D.18. Measured versus theoretical results of $S(d)$ for LTE1800, for set 3 of BS2..... 118
Figure E.1. Azimuth and elevation angle configuration. 122
Figure I.1. Coverage radius for the urban scenarios for the 4/2 configuration with all communications systems. 138
Figure I.2. Coverage radius for the suburban scenarios for the 4/2 configuration with all communications systems. 138
Figure I.3. Coverage radius for the urban scenarios for the 4/2 configuration without UMTS. . 139
Figure I.4. Coverage radius for the suburban scenarios for the 4/2 configuration without UMTS. 139
Figure I.5. Coverage radius for the urban scenarios for the 4/4 configuration with all communications systems. 140
Figure I.6. Coverage radius for the suburban scenarios for the 4/4 configuration with all communications systems. 140
Figure I.7. Coverage radius for the urban scenarios for the 4/4 configuration with 20% of LTE's maximum transmission power. 141
Figure I.8. Coverage radius for the suburban scenarios for the 4/4 configuration without LTE800. 141
Figure I.9. Throughput per RB for the urban scenarios for the 4/2 configuration with all communications systems. 143
Figure I.10. Throughput per RB for the suburban scenarios for the 4/2 configuration with all communications systems. 143
Figure I.11. Throughput per RB for the urban scenarios for the 4/2 configuration without UMTS. 144
Figure I.12. Throughput per RB for the suburban scenarios for the 4/2 configuration without UMTS. 144
Figure I.13. Throughput per RB for the urban scenarios for the 4/4 configuration with all communications systems. 145
Figure I.14. Throughput per RB for the suburban scenarios for the 4/4 configuration with all communications systems. 145
Figure I.15. Throughput per RB for the urban scenarios for the 4/4 configuration with 20% of LTE's maximum transmission power. 146
Figure I.16. Throughput per RB for the suburban scenarios for the 4/4 configuration without LTE800. 146

List of Tables

Table 2.1. Frequency bands assigned to GSM in Portugal (extracted from [ANAC19a]). 8
Table 2.2. GSM BS maximum output power classes (extracted from [ETSI08]). 8
Table 2.3. UMTS bands used in Portugal (extracted from [ANAC19a]). 9
Table 2.4. UMTS BS maximum output power classes (extracted from [Corr20]). 10
Table 2.5. LTE bands used in Portugal (extracted from [ANAC19a]). 10
Table 2.6. LTE's channel bandwidths (adapted from [Corr20]). 11
Table 2.7. LTE BS maximum output power classes (extracted from [Corr20]). 11
Table 2.8. NR bands assigned in Portugal (extracted from [ANAC19b]). 11
Table 2.9. SCS, the minimum and maximum number of RBs (adapted from [SHTN20]). 12
Table 2.10. Cell types and characteristics (adapted from [Corr20]). 14
Table 2.11. Typical antenna gain values (based on [KATH20], [HUAW19b] and [Antu12]). 14
Table 2.12. QoS characteristics for each class (extracted from [Corr20]). 17
Table 2.13. Reference levels for whole body exposure to EMF fields (adapted from [ICNI20]). 20
Table 2.14. Classification of BS antennas installation (extracted from [OFRC05] and [Antu12]). 24
Table 3.1. Empirical tests performed to validate the exclusion zone evaluation model. 49
Table 3.2. Empirical tests performed to validate the coverage and capacity model. 50
Table 3.3. Characteristics of the BSs where the measurements were conducted. 52
Table 3.4. Results for the performance of the theoretical model compared to measurements. . 56
Table 4.1. Used mobile communications systems in each scenario. 58
Table 4.2. Output power per carrier/MIMO element and antenna gain for the systems under analysis. 59
Table 4.3. Number of MIMO elements for each band of LTE and NR. 59
Table 4.4. Reference values for the link budget parameters. 60
Table 4.5. NR contribution to $Dfront$ for each scenario and carrier configuration. 64
Table 4.6. Distance from the visited BSs' sectors to the nearest building. 67
Table 4.7. Analysed directions for the back, side, top and bottom borders of the exclusion zone. 68
Table 4.8. Normalised gains for the analysed directions for each system. 68
Table 4.9. Exclusion borders for the front, back, side, top and bottom for the Urban.1 scenario. 69
Table 4.10. Exclusion borders for the front, back, side, top and bottom for the Urban.2 scenario. 69
Table 4.11. Exclusion borders for the front, back, side, top and bottom for the Urban.3 scenario. 69
Table 4.12. NR transmitted powers for carrier configuration 4/2. 73
Table 4.13. NR transmitted powers for carrier configuration 4/4. 73
Table 4.14. Reference values obtained for the cell radius, and throughput per RB. 74
Table A.1. Okumura-Hata model equations for different scenarios (extracted from [Corr20]). .. 86
Table A.2. Indoors path loss model (extracted from [Corr20]). 86
Table A.3. WINNER II model equations for different scenarios (extracted from [WINN07]). 87
Table A.4. Coding rate for each modulation scheme (extracted from [Belc18] and [Viei18]). 89

Table C.1. BSs radio characteristics. 106
Table D.1. Measurement results for sector 1 of BS1. 111
Table D.2. Measurement results for sector 2 of BS1. 115
Table D.3. Measurement results for BS2 119
Table F.1. Technical characteristics of the passive antenna (extracted from [HUAW19d]). 126
Table F.2. Technical characteristics of the active antennas used in NR3600 (extracted from [HUAW20a] and [HUAW20b]). 126
Table G.1. Simulation parameters for the utilized systems. 128
Table G.2. $Snfnorm$ coefficients and far-field distance for the utilized systems. 129
Table H.1. $Dfront$ variation for the analysed scenarios. 132
Table H.2. Exclusion borders for the front, back, side, top and bottom for the Suburban.1 scenario. 132
Table H.3. Exclusion borders for the front, back, side, top and bottom for the Suburban.2 scenario. 133
Table H.4. Exclusion borders for the front, back, side, top and bottom for the Suburban.3 scenario. 133
Table H.5. Exclusion borders for the front, back, side, top and bottom for the Rural.1 scenario. 133
Table H.6. Exclusion borders for the front, back, side, top and bottom for the Rural.2 scenario. 134
Table H.7. Exclusion borders for the front, back, side, top and bottom for the Rural.3 scenario. 134
Table H.8. Downtilt influence on the definition of physical barriers for the Urban.1 scenario. .. 135
Table H.9. Downtilt influence on the definition of physical barriers for the Urban.2 scenario. .. 135
Table H.10. Downtilt influence on the definition of physical barriers for the Urban.3 scenario. 135
Table I.1. Coverage radius variation for carrier configuration 4/2. 142
Table I.2. Coverage radius variation for carrier configuration 4/4. 142
Table I.3. Throughput per RB variation for carrier configuration 4/2. 147
Table I.4. Throughput per RB variation for carrier configuration 4/4. 147

List of Acronyms

2G	Second-Generation
3G	Third-Generation
4G	Fourth-Generation
5G	Fifth-Generation
ANACOM	Portuguese National Communications Authority
ARFC	Absolute Radio Frequency Channel
ARFCN	ARFC Number
BS	Base Station
CAPEX	Capital Expenditures
CEPT	European Conference of Postal and Telecommunications Administrations
CN	Core Network
CP	Cyclic Prefix
CS	Circuit-Switch
DEM	Digital Elevation Model
DL	Downlink
ECC	Electronic Communications Committee
EDGE	Enhanced Data Rates for GSM Evolution
EIRP	Effective Isotropic Radiated Power
EM	Electromagnetic
eMBB	Enhanced Mobile Broadband
EMF	Electromagnetic Field
FDD	Frequency Division Duplexing
FDMA	Frequency Division Multiple Access
FTBR	Front-to-Back Ratio
GMSK	Gaussian Minimum Shift Keying
GPRS	General Packet Radio Service
GSM	Global System for Mobile Communications
HPBW	Half Power Beam Width
HSPA	High-Speed Packet Access
HSPA+	Evolved HSPA
ICI	Inter-Cell Interference
ICNIRP	International Commission on Non-Ionising Radiation Protection
IoT	Internet of Things

ISI	InterSymbol Interference
LOS	Line-of-Sight
LTE	Long Term Evolution
LTE-A	LTE Advanced
MaMIMO	Massive MIMO
MAPL	Maximum Allowed Path Loss
MIMO	Multiple-Input Multiple-Output
MME	Mobility Management Entity
mMTC	Massive Machine-Type Communication
MSK	Minimum Shift Keying
MT	Mobile Terminal
NEC	Numerical Electromagnetic Code
NIR	Non-Ionising Radiation
NLOS	Non-Line-of-Sight
NR	New Radio
NSA	Non-Standalone
OFDMA	Orthogonal FDMA
OVSF	Orthogonal Variable Spreading Factor
PS	Packet-Switch
PSK	Phase Shift Keying
QAM	Quadrature Amplitude Modulation
QCI	Quality Channel Indicator
QoS	Quality of Service
QPSK	Quadrature Phase Shift Keying
RAN	Radio Access Network
RB	Resource Block
RF	Radio Frequency
RMS	Root Mean Square
RMSE	Root Mean Square Error
SA	Standalone
SAR	Specific Absorption Rate
SC-FDMA	Single-Carrier FDMA
SCS	Subcarrier Spacing
SER	Sweep Envelope Range
SF	Spreading Factor
SINR	Signal to Interference and Noise Ratio
SMS	Short Message Service
TDD	Time Division Duplexing
TDMA	Time Division Multiple Access
TMC	Torrino Mezzocammino

TTI	Transmission Time Interval
TTP	Total Transmitted Power
UARFCN	UTRA ARFCN
UL	Uplink
UMTS	Universal Mobile Telecommunications System
URLLC	Ultra-Reliable and Low-Latency Communication
UTRA	UMTS Terrestrial Radio Access
V2V	Vehicle-to-Vehicle
VoIP	Voice Over IP
W	With
W/O	Without
WCDMA	Wideband Code Division Multiple Access

List of Symbols

$\alpha_{V,SER}$	Sweep envelope range of the vertical radiation pattern
ΔP_r	Difference between the average power received and the receiver's sensitivity
$\Delta_{R_b^{RB}}$	Throughput per RB variation
$\Delta_{R_{cell}}$	Coverage radius variation
ΔS_i	Difference between $S_{model,i}$ and $S_{measure,i}$
$\Delta_{S,max}$	Maximum relative difference between $S_{fit}(d)$ and $S(d)$
Δ_d	Distance between samples
Δ_{es}	Element spacing factor
Δ_{excl}	Exclusion zone distance variation
Δ_{front}	D_{front} variation
Δf_{subc}	Subcarrier spacing
η_{NR}	NR contribution to the exclusion zone distance
θ	Elevation angle
θ'	Elevation angle between element's horizontal axis and direction of observation
θ_{dt}	Downtilt angle
θ_i	Elevation angle of the i^{th} element of the antenna relative to observation point
λ	Wavelength of the transmitted EM wave
μ	Numerology configuration integer
$\mu_{\Delta S}$	Average difference between the model and the measurements for each set of points
μ_{model}	Global average difference between the model and the measurements
$\rho_{SINR\,min}$	Minimum SINR required for the service
ρ_{SINR}	Signal to interference plus noise ratio
ρ_u	Active user density
σ	Standard deviation of the used propagation model
$\sigma_{\Delta S}$	Standard deviation for each set of points
σ_{model}	Standard deviation of μ_{model}
τ_{SF}	Subframe duration
φ	Azimuth angle
φ_i	Azimuth angle of the i^{th} element of the antenna relative to observation point
ϕ_{total}	Total inclination angle

ψ_i	Phase shift of the i^{th} element
A_{4^i-QAM}	Area of the cell served by the $4^i - QAM$ modulation
A_{cell}	Cell coverage area
a_0	Rational coefficient of the term d^0
a_1	Rational coefficient of the term d^1
a_2	Rational coefficient of the term d^2
a_3	Rational coefficient of the term d^3
a_{pd}	Average power decay
B_{RB}	Bandwidth per RB
B_{symb}	Symbol bandwidth
$D_{H,el}(\varphi)$	Element radiation pattern in the horizontal plane
$D_{V,el}(\theta)$	Element radiation pattern in the vertical plane
D_{ant}	Largest dimension of the antenna
D_{back}	Back border of the exclusion zone
D_{bottom}	Bottom border of the exclusion zone
D'_{bottom}	Bottom border of the exclusion zone when downtilt is used
$D_{excl}(\theta, \varphi)$	Exclusion zone distance in the direction of θ and φ
$D_{excl}^{W\ NR}$	Exclusion zone distance with NR
$D_{excl}^{W/O\ NR}$	Exclusion zone distance without NR
D_{front}	Front border of the exclusion zone
D'_{front}	Front border of the exclusion zone when downtilt/SER are used
$D_{front}^{W\ NR}$	Front border of the exclusion zone with NR installed
$D_{front}^{W/O\ NR}$	Front border of the exclusion zone without NR installed
D_{side}	Side border of the exclusion zone
D_{top}	Top border of the exclusion zone
D'_{top}	Top border of the exclusion zone when downtilt is used
d_{BP}	Urban breaking point distance
d'_{BP}	Suburban and rural breaking point distance
d_{es}	Distance between each antenna element
$d_{ff,i}$	Far-field distance for the i^{th} system
d_{ff}	Far-field boundary
d_{ff}^{min}	Minimum distance containing all the far-field distances of the BS systems
$d_{i,obs}$	Distance from the i^{th} element to point of observation
d_{max}	Maximum simulation distance
d_{min}	Minimum simulation distance
d_{obs}	Distance from the antenna to point of observation
d_{rnf}	Reactive near-field limit

E	Electric field
$E(d,\theta,\varphi)$	Electric field at a distance d from the antenna in the direction of θ and φ
F_N	Noise figure of the receiver
$F_p(\theta)$	Radiation pattern factor
f	Frequency of the carrier
$G_{\theta_1}(\varphi)$	Top/bottom antenna gain
$G_{\theta_2}(\varphi)$	Antenna gain in the horizontal plane for φ
$G_{\varphi_1}(\theta)$	Antenna gain in the vertical plane for θ at the front of the antenna ($\varphi = 0$)
$G_{\varphi_2}(\theta)$	Antenna gain in the vertical plane for θ at the back of the antenna ($\varphi = \pi$)
$G(\theta,\varphi)$	Antenna gain in the direction of θ and φ
$\hat{G}(\theta,\varphi)$	Interpolated antenna gain in the direction of θ and φ
G_{BF}	Beamforming gain
$G_{M,i}$	Maximum antenna gain for the i^{th} system
G_M	Maximum antenna gain
G_{MIMO}	MIMO gain
$\hat{G}_H(\theta,\varphi)$	Weighted contribution from the horizontal plane
G_{TX}	Antenna gain per transmitter
G_{Tx}	Transmitter antenna gain
$\hat{G}_V(\theta,\varphi)$	Weighted contribution from the vertical plane
$G_{el}(\theta_i,\varphi_i)$	Antenna element gain
$G_{r\ tot}$	Total receiver antenna gain
G_r	Receiver antenna gain
H	Magnetic field
h_{BS}	Height of the BS
h_{MT}	Height of the mobile terminal
h_{ant}	Height of the antenna
h_{ele}	Height of rectangle occupied by planar array element
$h_{i,even}$	Distance from the i^{th} element to the array centre for an even element array
$h_{i,odd}$	Distance from the i^{th} element to the array centre for an odd element array
$h_{min,BS}$	Minimum BS height required to ensure acceptable exposure levels
$h_{min,ant}$	Minimum antenna height to ensure acceptable exposure levels
h_{person}	Typical person height
h_{person}	Height of person
k_0	Free-space wavenumber
$L_{P\ ind}$	Indoors path loss
L_c	Cable losses between transmitter and antenna
L_{dip}	Length of the dipole

L_{ref}	Reference path loss
L_{ref}^{ind}	Indoors reference path loss
L_u	Losses due to the user's body
M	Modulation order
M_I	Interference margin
M_{SF}	Slow-fading margin
$N_{H,el}$	Number of horizontal elements of the planar array
N_{MIMO}	MIMO order
$N_{RB,cell}$	Total number of RBs in a cell
N_{RB}^{max}	Maximum number of RBs
N_{RB}^{min}	Minimum number of RBs
N_{RB}^{user}	Number of RBs allocated to each user
N_{SC}^{RB}	Number of subcarriers in an RB
N_{TX}	Number of transmitters of planar array
$N_{V,el}$	Number of vertical elements of the planar array
$N_{c\ GSM900}$	Number of carriers for GSM900
$N_{c\ UMTS}$	Number of carriers for UMTS
N_c	Number of carriers
N_{el}	Number of radiating elements of the antenna
$N_{f\ th}$	Threshold floor number
N_f	Floor number of the user
N_{points}^{set}	Number of points per set
N_{samp}	Number of samples of simulation
N_{sets}	Total number of measurement sets
N_{symb}^{SF}	Number of symbols per subframe
N_{sys}	Number of communications systems in a BS
$N_{users}^{4^i-QAM}$	Number of users served by the $4^i - QAM$ modulation
N_{users}	Total number of users
N_{users}^{cell}	Number of users in a cell
P_{EIRP}	Effective isotropic radiated power
P_{EIRP}^{UL}	Uplink EIRP
P_{SAR}	Specific Absorption Rate
P_{Tx}	Transmitter output power
$P_{Tx/BW,max}$	Maximum power transmitted for the total bandwidth
$P_{Tx/sc,max}$	Maximum power transmitted per subcarrier
$P_{coverage}$	Probability of being covered
$P_{i,in}$	Input power to the i^{th} element of the antenna

P_i	Input power for the i^{th} system
P_{in}	Input power of the antenna
$\overline{P_{r,R}}$	Average power received at distance R
$P_{r\,min}$	Receiver sensitivity
P_r	Power available at the receiving antenna
P_r^{DL}	Downlink received power
P_r^{UL}	Uplink received power
R_{4^i-QAM}	Radius for the $4^i - QAM$ modulation
$R_{b,4^i-QAM}^{RB}$	Throughput per RB for the $4^i - QAM$ modulation
$R_{b,ref}^{RB}$	Reference value for the throughput per RB
R_b^{user}	DL throughput for each user
$R_{cell,ref}$	Reference value for the coverage radius
R_{cell}	Cell radius
$\hat{r}(\theta_i, \varphi_i)$	Unitary vector of the i^{th} element
S	Power density
$S_{final,i}(d)$	Global expression for the power density for the i^{th} system
$S_{final}(d)$	Global expression for the power density
$S_{fit}(d)$	Interpolation function based on maxima of $S(d)$
S_i	Power density at frequency i
$S_{measure,i}$	Power density obtained from the measurements at point i
$S_{model,i}$	Power density computed with the model at point i
$S_{near-field}(d)$	Interpolation function for the power density in the near-field
$S_{nf}^{norm}(d)$	Normalised power density function for the near-field
S_{norm}^{tot}	Total normalised power density
$S_{ref,i}$	Power density reference level at frequency i
S_{up}	Upper bound of $S(d)$ in the near-field model
$W_1(\theta)$	Weight function 1 for the interpolated 3D antenna radiation pattern
$W_2(\varphi)$	Weight function 2 for the interpolated 3D antenna radiation pattern
$W_3(\theta, \varphi)$	Weight function 3 for the interpolated 3D antenna radiation pattern
w_{ant}	Width of the antenna
w_{ele}	Width of rectangle occupied by planar array element
y_{ij}	Y coordinate of the element placed in the i^{th} and j^{th} column
y_{obs}	Y coordinate of the observation point
Z	Field impedance
Z_0	Characteristic impedance of free space
z_{ij}	Z coordinate of the element placed in the i^{th} and j^{th} column
z_{obs}	Z coordinate of the observation point

List of Software

Matlab R2018a	Numerical computing software
Microsoft Excel 2016	Spreadsheet application
Microsoft Paint 3D	Graphics and 3D modelling software
Microsoft Power Point 2016	Presentation and slide program
Microsoft Word 2016	Text editor software

Chapter 1

Introduction

This chapter provides a brief history of the mobile communications systems evolution, and also an overview of the work performed as well as the motivations behind it. At the end of the chapter, the structure of the thesis is presented.

1.1 Overview and Motivation

Mobile communications systems have changed the way humans communicate with each other. As our civilization becomes more and more globalised and our day-to-day objects become more “intelligent”, the need for an overall higher connectivity increases. This need acts as a driving gear for mobile communications systems to evolve in order to provide new services and applications that meet the needs of our society.

The first digital mobile communications system was the second-generation (2G) Global System for Mobile Communications (GSM), which was first deployed in 1991 in Finland [GSMA20]. GSM was initially designed for voice and Short Message Service (SMS), although it has later evolved to the General Packet Radio Service (GPRS) and Enhanced Data Rates for GSM Evolution (EDGE) in order to support data services like internet access.

The third-generation (3G), which included Universal Mobile Telecommunications System (UMTS), was first deployed in Japan in 2001 and then in Europe in 2002 [HoTo04]. Its network architecture is similar to GSM’s since it was built upon it. UMTS was designed for multimedia communications purposes, achieving data-rates much higher that GSM, which allowed consumers to transmit and receive high-quality images and video, as well as better access to web browsing. Although initially the available theoretical throughput was up to 2 Mbit/s, UMTS evolved to support new modulation techniques and also Multiple-Input Multiple-Output (MIMO), among other features, allowing a maximum theoretical throughput of 84 Mbit/s for DL in the latest releases.

The fourth-generation (4G), also known as Long Term Evolution (LTE), was approved at the end of 2007 and its commercial deployment started in 2010. Opposed to GSM’s and UMTS’s network, which use circuit-switch (CS) for voice and packet-switch (PS) for data, LTE is only dedicated to data with a full PS network. As the number of mobile terminals (MTs) grew, as well as consumers demand, higher available data-rates were required. With the improvement of MIMO systems and other new techniques, such as carrier aggregation, LTE provided a maximum theoretical throughput of 300 Mbit/s in an initial release and a maximum throughput of 1 Gbit/s with the release of LTE-Advanced (LTE-A).

According to [STAT20], the total number of mobile subscriptions reached 8.3 billion in 2019. With a global population of around 7.7 billion in 2020, the number of devices connected to cellular networks has already exceeded the number of people on the planet. As connectivity becomes more and more vital to the general public, as well as to companies and commerce in general, the number of connected devices increases, and thus traffic and capacity demands for the cellular networks also increase. The fifth-generation (5G), also known as New Radio (NR), offers the solution to this problem by implementing a network with a higher device capacity, higher offered throughput and also extremely low latency. High gain antennas and other new techniques, such as beamforming and massive MIMO (MaMIMO), help

increasing the system coverage and capacity. According to [STAT20], the number of NR mobile subscriptions is forecast to exceed 2.7 billion by 2025. According to [3GPP19], there are two deployment options defined for NR, the Non-standalone (NSA) architecture and the Standalone (SA) one, meaning that, initially, NR Radio Access Network (RAN) will be supported on LTE's RAN and core, and later it will have its network infrastructure separated from the LTE one.

Since the beginning of mobile communications systems, awareness has been raised and studies have been performed on the potential health risk caused by electromagnetic radiation from these systems. Due to the increase in BS deployment, the popularity of these systems and massive publicly available information, the general public has been more and more concerned about the research and impact of Electromagnetic Fields (EMFs) on the human body. The International Commission on Non-Ionising Radiation Protection (ICNIRP) is a scientific body that works together with experts from different countries and fields, such as biology, epidemiology, medicine, physics and chemistry to assess the risk of non-ionising radiation (NIR) exposure, and provide guidelines for the maximum allowed exposure levels from the quantification of adverse health effects. Most European countries, such as Portugal, adopt these reference threshold values established by the ICNIRP, although there are countries that establish their own exposure guidelines with lower values than the ones established by ICNIRP. Mobile communications operators are obliged to comply with the limits imposed by their respective countries.

Although these guidelines have been reviewed and reimplemented over the years, this topic has been, and will continue to be, generating a great deal of controversy and misinformation, regarding the adverse non-thermal effects of electromagnetic radiation, such as mood influence, infertility and cancer. According to [ICNI20], several experimental studies testing for acute changes to wellbeing or symptoms on humans are available, and that these provide evidence that "belief about exposure", and not exposure itself, is the relevant symptom determinant. As discussed in [ICNI20], evidence of non-thermal adverse health effects may be found on contradictory, non-reproducible and biased studies.

In the vicinity of BS antennas, exposure levels may be higher than the ones defined in the guidelines. Such regions are called the exclusion zone of a BS and, if they are in regions accessible to the general public, physical barriers should be implemented by operators in order to protect the public from potentially dangerous levels of radiation. A sketch of an exclusion zone represented by an imaginary semi-sphere and limited by physical barriers is illustrated in Figure 1.1. EMF measurement campaigns, electromagnetic (EM) simulations and mathematical models can be performed to assess EMF compliance near BS antennas.

A procedure for the measurement of EMFs originated by multiple BSs is presented in [CFCO04], and in [OFRC05] several models with different validity ranges are presented for the estimation of BS exclusion zones. With the introduction of MaMIMO and beamforming in NR, traditional EMF measurement methods and exposure models may lead to significantly overestimated results. In [TFCT17], a model for the time-averaged realistic maximum power transmitted by an NR antenna is presented, considering factors such as BS usage and users' spatial distribution. In [PKZu19], an alternative method of EMF exposure assessment based on mathematical models and EM simulations is also presented.

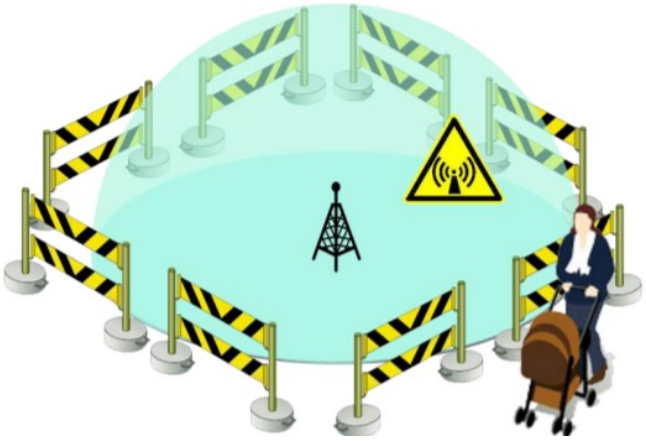

Figure 1.1. BS exclusion zone delimited by physical barriers (extracted from [Antu12]).

With each new mobile communications system generation, and since in Portugal no system has been decommissioned, the number of active systems increases. In order to reduce the costs of network deployment, operators take advantage of legacy BSs to install NR antennas. Since these BSs already possess GSM, UMTS and LTE, the addition of another system increases the exposure levels near the BS, thus increasing the size of the exclusion zone around it. In BS installations where the exclusion zone must have limited dimensions, a decrease in the transmitted power may be necessary, thus affecting network roll-out and performance.

The purpose of this thesis was to develop a model, and a simulator to implement it, to compute the exclusion zone of a BS in order to understand the impact of NR installations on the increase of the existing exclusion regions, and to verify in which circumstances this increase requires the definition of physical barriers for public protection. The evaluation of the exposure levels in the vicinity of the BSs requires the knowledge of several antenna parameters, such as transmitted power, radiation patterns, and frequency band. The implemented model is also used to analyse the impact of EMF restrictions implemented at the BSs on coverage and throughput. In the BSs where already exists some degree of EMF saturation prior to the installation of NR, restrictions must be implemented at the level of the transmission powers of NR antennas. These restrictions have a negative impact on the quality of the services offered by operators and create difficulties in the process of NR network roll-out. The novelty in this thesis is the computation of EMF exposure for planar arrays that are used in active NR antennas. This thesis is done in collaboration with Huawei, one of the main worldwide vendors of telecommunications equipment and consumer electronics.

1.2 Contents

This thesis is divided into five chapters, followed by a set of annexes containing additional information, as well as complementary results and analysis. The present chapter contains a brief overview of the problem and the motivations behind the developed work.

In Chapter 2, the fundamental aspects of mobile communications systems are addressed. It begins with a brief description of the radio interface of GSM, UMTS, LTE and NR. Then, an overview of the concepts of coverage, capacity and interference is made, followed by the main services and applications enabled by NR deployment. EMF exposure is discussed by introducing the radiation regions around a BS, the international safety guidelines for exposure and EMF measurement, and also the main concepts on the definition of BS exclusion zones. Finally, the state of the art on the problem of NR BSs deployment in an EMF restricted environment is presented.

In Chapter 3, the issues regarding the model development and implementation are presented. Firstly, a model overview is presented, where the model's objective and both input and output parameters are defined. Then, the far- and near-fields power density estimation models used in this thesis are laid out. A simulator for the definition of a BS exclusion zone was then created by developing a general model linking the near- and far-fields zones of an antenna. For the near-field zone, two methods were developed: one concerning linear arrays and the other for planar arrays (used in active NR antennas). A model to estimate the coverage radius and the throughput at cell-edge was also developed. Then, empirical tests were performed in order to assess the models for exclusion zone, and coverage and capacity. Finally, at the end of the chapter, the theoretical results from the exclusion zone model are compared with experimental ones from an EMF measurement campaign performed on real BSs.

In Chapter 4, the analysis of results is presented. Firstly, the analysed scenarios and the main simulation parameters are described. Then, an analysis is made on the variation of the exclusion zone for the front, side, back, top and bottom regions of the antenna by computing the exclusion zone dimensions before and after the installation of the NR antenna. An analysis of the impact of the exclusion zone dimensions, as well as the downtilt, on the definition of physical barriers for public protection is performed. Finally, the impact of the restrictions imposed for the size of exclusion zones on the coverage radius and throughput at cell-edge is analysed.

Finally, in Chapter 5, the main conclusions of the work performed are summarised, and some insight for future work is suggested.

Regarding the annexes at the end of the thesis, the basic concepts of coverage and capacity are presented in Annex A. In Annex B, additional results and analysis on the theoretical model assessment are presented. The characteristics of the performed EMF measurements and corresponding BSs are presented in Annex C, and the results from these measurements are laid out in Annex D. In Annex E, a three-dimensional radiation pattern interpolation is described. The main characteristics of the antennas used in the exclusion zone simulations are presented in Annex F. The parameters and results of the exclusion zone model for the frequency bands considered in this thesis are presented in Annex G. Finally, additional results regarding the variation of the exclusion zone and influence of EMF restrictions on coverage and throughput are presented in Annexes H and I respectively.

Chapter 2

Fundamental Aspects and State of the Art

This chapter provides a general overview of the fundamental concepts of GSM, UMTS, LTE and NR. A comparison among all cellular communications systems is done in Section 2.1 regarding the radio interface. An overview of coverage, capacity, and interference is done in Section 2.2. The possible services and applications of NR are presented in Section 2.3 and an introduction to electromagnetic field exposure is done in Section 2.4. Finally, Section 2.5 concludes this chapter with the state of the art on the thesis subject.

2.1 Mobile Communications Systems Radio Interface

This section focuses primarily on the radio interface of GSM [Moli11], UMTS [Moli11], [HoTo04], [WSAl03], LTE [HoTo11], [Alca13] and NR [3GPP17], [3GPP19] respectively.

GSM

GSM uses a combination of Frequency Division Multiple Access (FDMA) and Time Division Multiple Access (TDMA) regarding multiple access techniques, and Frequency Division Duplexing (FDD) for the duplexing scheme.

The frequency bands assigned to GSM in Portugal are presented in Table 2.1. The total bandwidth refers to the sum of Uplink (UL) and Downlink (DL) ones, being distributed among Portugal's operators.

Table 2.1. Frequency bands assigned to GSM in Portugal (extracted from [ANAC19a]).

GSM Bands		
UL [MHz]	**DL [MHz]**	**Total Bandwidth [MHz]**
[885, 915]	[930, 960]	60
[1710, 1770]	[1805, 1865]	120

Since GSM employs FDMA, both UL and DL frequency bands are divided into 200 kHz Radio Frequency (RF) channels. Each pair of UL/DL RF channels is called an Absolute Radio Frequency Channel (ARFC) and is assigned an ARFC Number (ARFCN).

TDMA is then used to increase the system's capacity by dividing the time axis into timeslots, each RF channel containing 8 timeslots. The combination of a timeslot number and an RF channel is called a physical channel.

The modulation technique used in plain GSM is the Gaussian Minimum Shift Keying (GMSK) [ETSI19a], which is a variant of the Minimum Shift Keying (MSK), which allows data rates up to 9.6 kbit/s. GPRS uses the same technique, but it can aggregate the timeslots, possibly up to 8, allowing a maximum data rate of 171 kbit/s. As opposed to GPRS and plain GSM, EDGE uses 8 Phase Shift Keying (8-PSK) as a modulation technique, the maximum data rate going up to 384 kbit/s.

The maximum output power per carrier in a GSM BS is presented in Table 2.2. For a macro-cell BS, the output power per carrier is measured at the input of the BS transmission combiner, [ETSI08]. For micro- and pico-cells, the output power per carrier is measured at the antenna connector after all stages of combining.

Table 2.2. GSM BS maximum output power classes (extracted from [ETSI08]).

GSM BS Maximum Output Power [dBm]		
Macrocell	**Microcell**	**Picocell**
[34, 58]	[9, 32]	[13,23]

UMTS

UMTS uses Wideband Code Division Multiple Access (WCDMA) and FDD. The UMTS bands used in Portugal are shown in Table 2.3.

Table 2.3. UMTS bands used in Portugal (extracted from [ANAC19a]).

UMTS Bands		
UL [MHz]	**DL [MHz]**	**Total Bandwidth [MHz]**
[885, 915]	[930, 960]	60
[1920, 1980]	[2110, 2170]	120

With WCDMA, each user is given two types of codes, a spreading code (also called channelisation code) and a scrambling one: the spreading code is used to spread the transmitted signal's spectrum, being given in chip/s, and is assigned to different users in an orthogonal way to minimise channel interference; scrambling codes are pseudo-random and have the same chip rate as the spreading code, therefore they do not spread the signal. Although with this technique the transmitted signals from different users lose their orthogonality to one another, their cross-correlation is still very small and thus the channel interference remains low.

In UMTS, the separation between carriers is 5 MHz, and to increase capacity, the carrier spacing can be any multiple of 200 kHz. Therefore, just as in GSM, carriers are referred to using the UMTS Terrestrial Radio Access (UTRA) ARFCN (UARFCN). The spreading and scrambling code's chip rate is 3.84 Mchip/s, which provides a channel bandwidth of 4.4 MHz.

The ratio between the spreading code chip rate and the transmitted signal symbol rate is called the spreading factor (SF). The orthogonal codes used in UMTS have a variable SF and they all belong to the same family, the Orthogonal Variable Spreading Factor (OVSF). The use of OVSF codes allows the SF to vary amongst users while maintaining orthogonality. The SF can vary from 4 to 256 in UL and from 4 to 512 in DL.

The modulation technique used in plain UMTS is the Quadrature Phase Shift Keying (QPSK), allowing for a maximum theoretical data rate of 2 Mbit/s. UMTS/High-Speed Packet Access (HSPA) uses 16-Quadrature Amplitude Modulation (16-QAM) and is capable of reaching a data rate of 14.4 Mbit/s in DL and 5.76 Mbit/s in UL, [ITUR15a] and [ETSI19b]. The UMTS/Evolved HSPA (HSPA+) uses 64-QAM modulation and, using 2×2 MIMO and dual carrier aggregation, can reach up to 84 Mbit/s in DL and 34.5 Mbit/s in UL.

Both UMTS/HSPA and UMTS/HSPA+ use adaptive modulation, i.e., the modulation technique varies according to the channel's quality. This means that, in poorer radio conditions, UMTS/HSPA can use QPSK and UMTS/HSPA+ can use 16-QAM or QPSK.

The maximum output power for UMTS BSs is presented in Table 2.4. Note that there is no upper limit for the maximum power of UMTS macro-cells.

Table 2.4. UMTS BS maximum output power classes (extracted from [Corr20]).

UMTS BS Maximum Output Power [dBm]			
Macrocell	**Microcell**	**Picocell**	**Femtocell**
-	≤ 38	≤ 24	≤ 20

LTE

LTE, differently from GSM and UMTS, uses slightly different multiple access methods for each link. For DL, it uses Orthogonal FDMA (OFDMA), and for UL, it uses Single-Carrier FDMA (SC-FDMA). The duplexing method is the FDD. The bands used for LTE in Portugal are shown in Table 2.5.

Table 2.5. LTE bands used in Portugal (extracted from [ANAC19a]).

LTE Bands		
UL [MHz]	**DL [MHz]**	**Total Bandwidth [MHz]**
[832, 862]	[791, 821]	60
[1710, 1770]	[1805, 1865]	120
[1920, 1980]	[2110, 2170]	120
[2510, 2570]	[2630, 2690]	120

In OFDMA, each user is assigned a set of orthogonal subcarriers with a fixed subcarrier spacing (SCS) between them. To allow multiple users to access the available bandwidth, each user is allocated a set of resources called Resource Blocks (RBs). An RB is composed of 12 subcarriers in the frequency domain and 7 OFDMA symbols in the time domain. Since in LTE the SCS is 15 kHz, an OFDMA symbol has a duration of 66.7 μs.

In order to reduce Intersymbol Interference (ISI), LTE uses the Cyclic Prefix (CP) concept where the initial part of the symbol is attached to the end of the symbol. The CP has a duration of 4.7 μs, which gives a total symbol duration of 71.4 μs. As it can be seen in Figure 2.1, the 7 OFDMA symbols in an RB form a slot of 0.5 ms. The minimum set of resources assigned to a user is two consecutive RBs in the time domain. The allocation in the frequency domain is then modified every Transmission Time Interval (TTI) of 1 ms or subframe.

The major difference between OFDMA and SC-FDMA is that in OFDMA the modulated data symbols are transmitted in parallel, one per subcarrier, whereas in SC-FDMA the modulated data symbols are transmitted in series at M times the rate, where M is the modulation order. Each modulated data symbol in SC-FDMA has a bandwidth defined as:

$$B_{symb\,[\mathrm{kHz}]} = M \times 15 \tag{2.1}$$

The composition and allocation of RBs, as well as the periodical addition of the CP, for SC-FDMA, is the same as in OFDMA.

LTE allows flexible bandwidth allocation, depending on the number of subcarriers assigned to the user. LTE's available channel bandwidths are shown in Table 2.6. The types of modulation used in LTE are QPSK, 16-QAM, 64-QAM for UL and DL, and 256-QAM for DL. LTE also features 2×2, 4×4, and 8×8 MIMO, carrier aggregation, and adaptive modulation and coding.

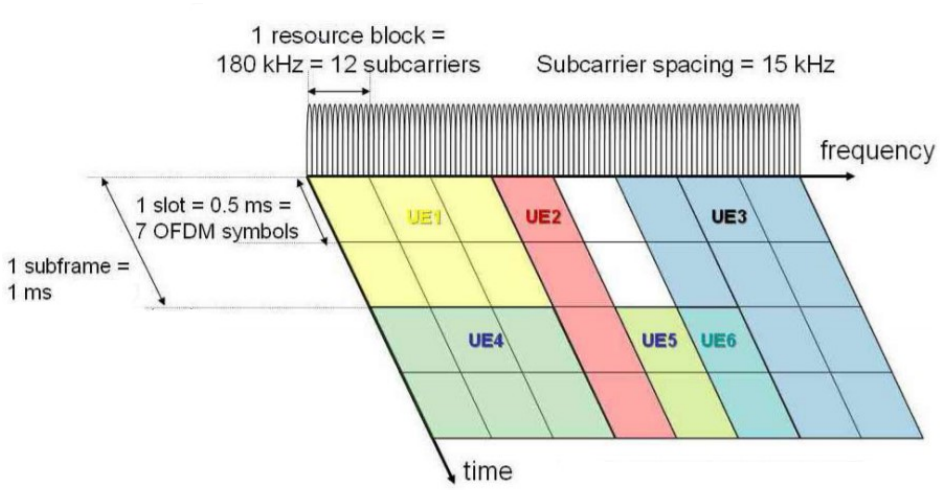

Figure 2.1. LTE's DL resource allocation (adapted from [ROSC08]).

Table 2.6. LTE's channel bandwidths (adapted from [Corr20]).

Bandwidth [MHz]	1.4	3	5	10	15	20

The maximum output power for LTE BSs is presented in Table 2.7. in LTE the maximum output power depends on the link, [Corr20]: for DL, it is the maximum power transmitted per subcarrier ($P_{Tx/sc,max}$), and for UL it is the maximum power transmitted for the total maximum bandwidth ($P_{Tx/BW,max}$).

Table 2.7. LTE BS maximum output power classes (extracted from [Corr20]).

LTE BS Maximum Output Power [dBm]		
Macrocell	**Microcell**	**Femtocell**
-	≤ 24	≤ 20

NR

NR radio interface is similar to LTE's one. For DL, it uses OFDMA, and for UL, differently from LTE, it can use OFDMA or SC-FDMA. The duplexing methods are FDD and Time Division Duplexing (TDD): FDD is to be used in the 700 MHz band and TDD in the 3.6 GHz bands. These bands are the ones currently assigned in Portugal and are represented in Table 2.8.

Table 2.8. NR bands assigned in Portugal (extracted from [ANAC19b]).

NR Bands		
UL [MHz]	**DL [MHz]**	**Total Bandwidth [MHz]**
[703, 733]	[758, 788]	60
[3400, 3800]		400

A key feature of the NR radio interface is the concept of variable SCS, Figure 2.2. In contrast to LTE, which has a fixed SCS of 15 kHz, NR supports multiple SCS configurations or numerologies. The supported transmission numerologies are represented in Table 2.9, and the SCS is given by:

$$\Delta f_{subc[\text{kHz}]} = 2^{\mu} \times 15 \tag{2.2}$$

where:

- μ: numerology configuration integer.

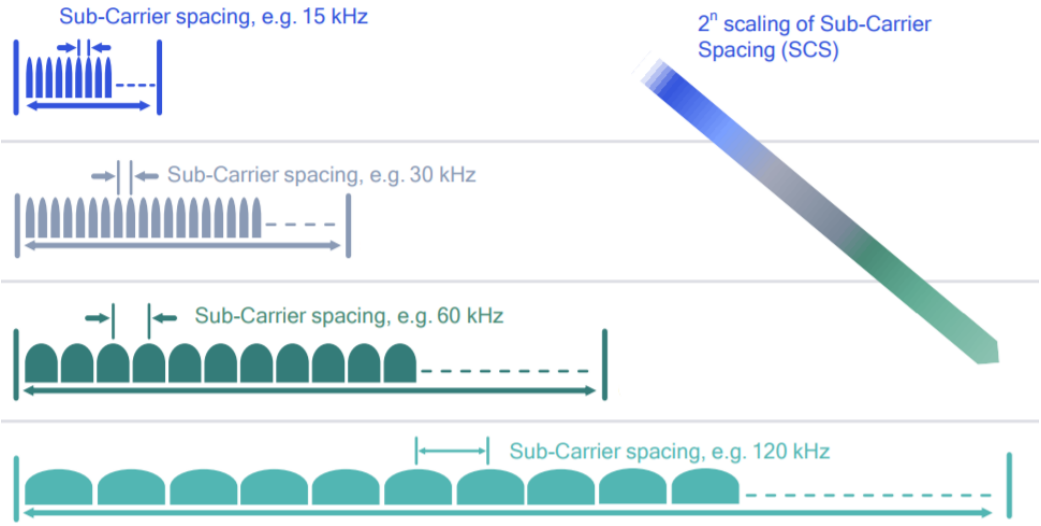

Figure 2.2. SCS scalability in NR (adapted from [QUAL18]).

Differently from LTE, in NR an RB is expressed only in the frequency domain, which corresponds to 12 consecutive subcarriers, independently of the used numerology, [HUAW19a]. The total bandwidth of an RB depends on the used configuration. The minimum (N_{RB}^{min}) and maximum (N_{RB}^{max}) number of RBs allocated to a user are also defined in Table 2.9, being the same for UL and DL. Regarding the radio frame structure, the length of a radio frame is 10 ms and is composed of 10 subframes of 1 ms each, a subframe being the aggregation of several timeslots. Since in NR a timeslot is defined as 14 consecutive OFDMA symbols, the number of timeslots in a subframe depends on the SCS, as shown in Figure 2.3.

Table 2.9. SCS, the minimum and maximum number of RBs (adapted from [SHTN20]).

μ	N_{RB}^{min}	N_{RB}^{max}	$\Delta f_{subc[kHz]}$
0	24	275	15
1	24	275	30
2	24	275	60
3	24	275	120
4	24	138	240

NR supports carrier aggregation as well as all LTE modulation orders for UL and DL. A new type of modulation is introduced for UL, the $\pi/2$-BPSK, [HUAW19]. MaMIMO and beamforming are also being introduced in the NR radio interface.

As the name suggests, MaMIMO is a MIMO system that uses a large number of antennas at the BS. The NR radio interface supports up to 256 antennas at the BS, [3GPP16], which is considerably higher than the current MIMO systems like LTE, which can use up to 8 antennas.

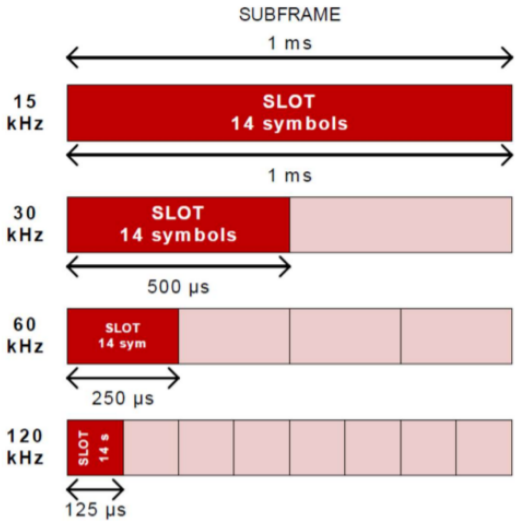

Figure 2.3. NR radio frame structure (extracted from [Corr20]).

Beamforming is a DL multi-antenna feature that forms a beam with a narrow Half Power Beam Width (HPBW) towards the target users [HUAW19b], thereby increasing signal strength on the user side. By controlling the current's phase at the input of each antenna element, the beam can be steered to the target user. This new feature is possible due to the use of active antennas, contrary to the previous systems that used passive antennas without beamforming and beam steering. Beamforming makes use of the large number of antennas available in MaMIMO technology.

The maximum output power in NR is defined the same way as in LTE's case, [Corr20]. The BSs maximum output power classes are also the same.

2.2 Coverage, Capacity, and Interference

This sub-section analyses the main aspects related to coverage, capacity and interference for NR. The coverage and capacity of a given system, as well as how interference affects it, are of paramount importance to design and deploy a network correctly.

The main objective of coverage estimation is to calculate the cell radius in a given environment to determine the system's BSs deployment. In mobile communications systems there are four types of cell sizes, [Shar17]:

- **Macro-cell:** It is used as outdoor cells and characterised by offering a larger coverage area compared to other types. Antennas are usually mounted on top of the buildings' rooftops.
- **Micro-cell:** It is characterised by covering areas with a high populational density. such as malls, hotels and special events. Its radius can go up to 1 km.
- **Pico-cell:** Its radius is usually less than 100 m and antennas are omnidirectional. They are generally used for indoor purposes, such as offices or railway stations.
- **Femto-cell:** Low-powered BSs with omnidirectional antennas, typically used inside houses. Its radius can go up to 50 m.

The generic characteristics of these types of cells regarding their radius and Effective Isotropic Radiated Power (EIRP) are presented in Table 2.10. The EIRP depends on the transmitted power and the antenna gain. The typical values of antenna gain, depending on the type of antenna, for the frequency bands assigned in Portugal, are presented in Table 2.11.

Table 2.10. Cell types and characteristics (adapted from [Corr20]).

Cell Type		Radius [km]	P_{EIRP} [dBm]
Macro	Large	> 3	[50, 60]
	Small	1 - 3	[47, 50]
Micro		0.1 - 1	[30, 47]
Pico		< 0.1	[22, 33]
Femto		< 0.05	[10, 25]

Table 2.11. Typical antenna gain values (based on [KATH20], [HUAW19b] and [Antu12]).

Gain [dBi]	Antenna Type	
Frequency Bands [MHz]	Omnidirectional	Sectorial
700	[2, 10.9]	[13.4, 17]
800	[2, 12.1]	[2.9, 19.3]
900	[2, 11.1]	[5, 22]
1800	[2, 11.8]	[5, 24.2]
2100	[2, 11.8]	[2.9, 24.2]
2600	[2, 11]	[8, 19.5]
3600	[6.8, 7]	[15.5, 25]

The coverage radius of a cell can be theoretically calculated by combining a suitable propagation model for the path loss with the link budget expression. The fundamental formulations for the link budget are presented in Section A.1 (Annex A). Combining (A.1) and (A.5), the cell radius can be computed by:

$$R_{cell\ [\mathrm{km}]} = 10^{\frac{P_{EIRP\ [\mathrm{dBm}]} + G_{r\ tot\ [\mathrm{dBi}]} - P_{r\ \min\ [\mathrm{dBm}]} - L_{ref\ [\mathrm{dB}]}}{10\ a_{pd}}} \tag{2.3}$$

The system capacity must be estimated in order to compute the number of required resources, defined as RBs in NR, which can be offered to the end-user within a certain quality of service (QoS), [Viei18].

In order to plan the capacity of a given cell it is necessary to know the demanded resources for a certain user that guarantee a minimum bit rate required for the user's intended service. Then, knowing the total number of resources available and the throughput for each user, the cell capacity can be computed. The fundamental formulations regarding the available resources and the number of served users are presented in Section A.3 (Annex A). Combining (A.14) and (A.15), the number of users that the system is able to serve can be computed by:

$$N_{users} = \frac{N_{RB,cell}\ N_{SC}^{RB}\ N_{MIMO}\ N_{symb}^{SF}\ \log_2(M)_{[\text{bits/symbol}]}}{\tau_{SF\,[\text{s}]}\ R_{b\,[\text{bit/s}]}^{user}} \quad (2.4)$$

Logically, one can observe that the number of users that the system should be able to cover in a cell can be expressed by:

$$N_{users}^{cell} = \left\lceil \rho_{u\,[\text{user/km}^2]}\ A_{cell\,[\text{km}^2]} \right\rceil \quad (2.5)$$

where:

- ρ_u : active user density inside the cell coverage area;
- A_{cell}: cell coverage area.

Considering that the area covered by the cell is a regular hexagon and that the radius of the cell is the one computed in (2.3), the cell coverage area can be expressed as:

$$A_{cell\,[\text{km}^2]} = \frac{3\sqrt{3}\ R_{cell\,[\text{km}]}^2}{2} \quad (2.6)$$

The propagation between transmitter and receiver introduces signal quality degradation, the main responsible agents being attenuation and interference. While attenuation, given by the environment, reduces the signal power received, interference is responsible for signal distortion. It is a major factor that limits coverage, capacity and transmission efficiency, [SDRh17] and [Alme13].

In mobile communications systems, the complete frequency band is shared among cells in a repeated pattern to maximise coverage and capacity, which is done over reuse rules and mechanisms adapted to each system. As indicated above, this frequency reuse causes interference problems, thus the trade-off between capacity and interference is of key importance in cellular networks.

In NR, Inter-Cell Interference (ICI) is the main interference agent. ICI, as illustrated in Figure 2.4, occurs when a user receives signals from other BSs that contain subcarriers with the same frequency. This interference problem aggravates at the cell-edge where the intended signal power is lowest and the interfering signal power is at a maximum, thus the Signal to Interference and Noise Ratio (SINR) may become bellow the threshold accepted for each system.

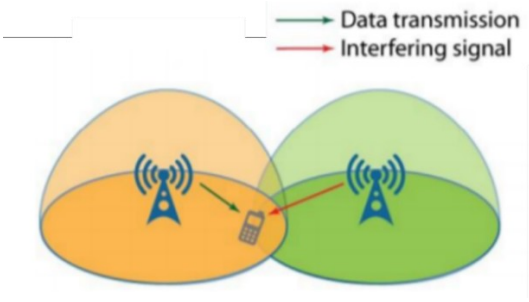

Figure 2.4. Inter-Cell Interference (adapted from [Alme13]).

Since interference causes the SINR to drop, consequently it causes throughput reduction through the reduction of the modulation order. This way, the interference reduces cell capacity and thus the throughput received by the user may not be enough for the required service, especially, as stated above, for cell-edge users. Therefore, the increase in interference also causes decreased coverage by cell radius reduction.

Interference can be reduced by downtilting the main lobe of the BS antenna, lowering the BS antenna, optimising the location of the BS, using power control and using sectorised cells, which lowers the number of interfering cells, [Corr20].

2.3 Services and Applications

The goal of this sub-section is to identify and analyse the main services and applications of NR.

Several new services and use cases, such as the Internet of Things (IoT), remote surgery and augmented reality are expected to emerge with NR network deployment. These use cases belong to three main categories [ITUR15b], defined as:

- **Enhanced Mobile Broadband (eMBB):** It targets the human interaction use cases for access to multimedia content, services, and data. The demand for higher data rates continues to increase and eMBB aims to improve the existing mobile broadband. There are two main scenarios covered by eMBB, wide-area coverage and hotspot coverage, both with different requirements. For the wide-area coverage case, the main requirements are uninterrupted coverage, medium to high mobility and improved throughput compared to today. For the hotspot case, i.e., a high user density area, a very high capacity is needed while mobility requirements are low.
- **Massive Machine Type Communications (mMTC):** It is characterised by a very large number of connected devices, which typically transmit a small volume of data and are required to be low cost with a very long battery lifespan. It includes IoT services, such as smart cities.
- **Ultra-Reliable and Low-Latency Communications (URLLC):** It is characterised by having strict requirements for mobility, latency and availability. Some use cases include remote medical surgery, remote driving and Vehicle-to-Vehicle (V2V) communication.

Figure 2.5 illustrates several use cases and their respective categories.

In order to measure the overall performance of each service, one can quantify QoS characteristics offered to the end-user. Regarding QoS, NR will still support the service categories defined for previous generations of mobile communications:

- **Conversational Services:** It is characterised by real-time conversation services between users, for example, Voice Over IP (VoIP). It is very delay-strict due to human perception.
- **Streaming Services:** It is characterised by unidirectional real-time data flow, for example, video streaming. It is not as delay-strict as conversational services since it is not restricted by human perception.
- **Interactive Services:** It is characterised by accessing remote equipment, continuously or not, for example, web-browsing.
- **Background Services:** It is characterised by sending and receiving data in the background, for example, reception of e-mails. It is the least delay-sensitive service.

Table 2.12 describes the QoS characteristics of the service categories stated above.

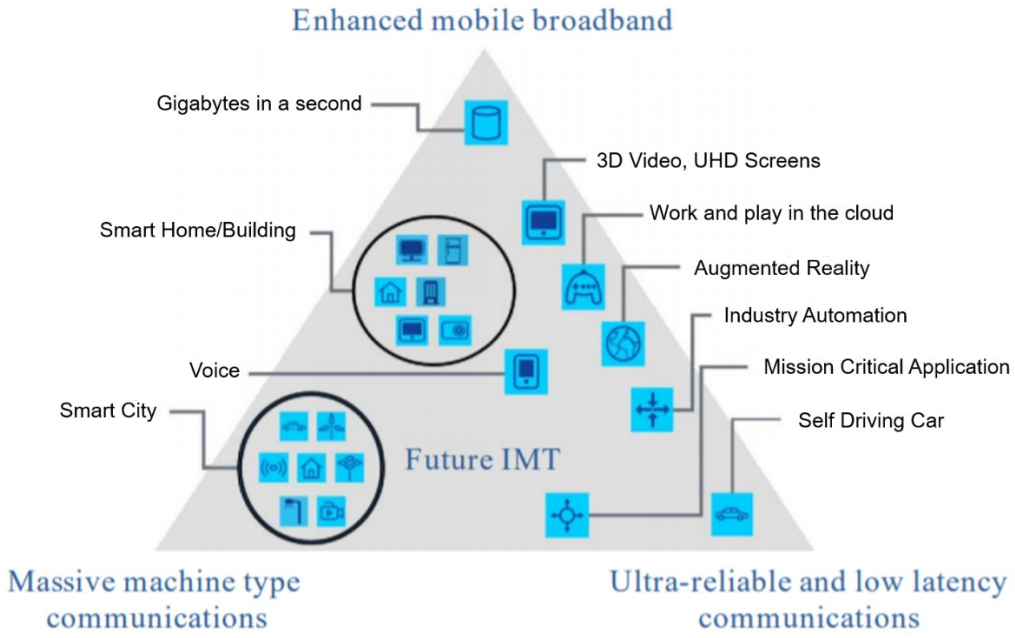

Figure 2.5. NR use cases (extracted from [ITUR15b]).

Table 2.12. QoS characteristics for each class (extracted from [Corr20]).

Characteristics	Service Class			
	Conversational	Streaming	Interactive	Background
Real Time	Yes	Yes	No	No
Symmetric	Yes	No	No	No
Guaranteed Rate	Yes	Yes	No	No
Delay	Minimum/Fixed	Minimum/Variable	Moderate/Variable	High/Variable
Buffer	No	Yes	Yes	Yes
Bursty	No	No	Yes	Yes
Example	Voice Call	Video-Clip	www	e-mail

2.4 Electromagnetic Field Exposure

In this subsection, the objective is to analyse the main subjects regarding Electromagnetic Field (EMF) exposure. Firstly, an introduction to radiation regions is done. Secondly, EMF measurement and international safety recommendations are presented, and finally the exclusion regions around the BSs are defined.

2.4.1 Radiation Regions

EMFs around an antenna have complex and non-homogeneous behaviour characteristics [OFRC05]. The space surrounding an antenna is usually subdivided into three regions, [Bala05]: (a) reactive near-field, (b) radiating near-field, and (c) far-field, as shown in Figure 2.6. These regions are so designated to identify the field structure inside each one. It is important to note that the boundaries that separate these regions are not uniquely defined, using different criteria to establish its values, depending on the error tolerance specified for the project.

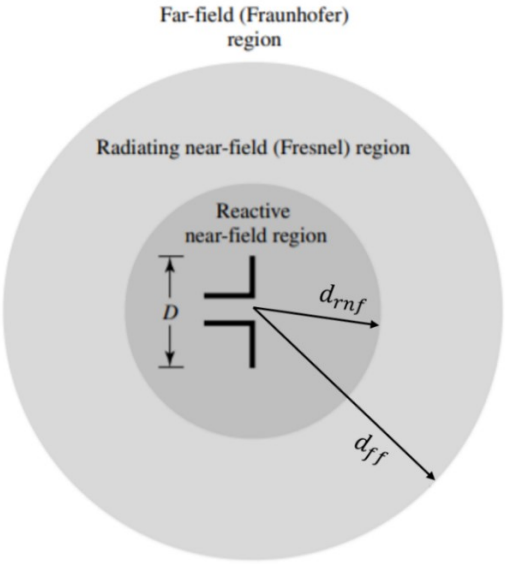

Figure 2.6. Field regions of an antenna (adapted from [Bala05]).

The reactive near-field is the closest to the antenna and its boundary is defined by [OFRC05]:

$$d_{obs\,[\mathrm{m}]} < d_{rnf\,[\mathrm{m}]}, \quad \text{where} \quad d_{rnf\,[\mathrm{m}]} = \frac{\lambda_{[\mathrm{m}]}}{4} \tag{2.7}$$

and:

- d_{rnf}: reactive near-field limit;
- d_{obs}: the distance from the antenna to the point of observation;
- λ: the wavelength of the transmitted EM wave.

Due to the structure of the field, Electric (E) and Magnetic (H) fields have to be separately estimated in order to determine power density (S) [OFRC05], which also involves the field impedance (Z). It can be seen that in this region, due to the characteristics of the E and H fields, the reactive power density is predominant over the radiating power density (no radiation phenomenon), and the E field decays with d^{-3} [Bala05].

The radiative near-field, also defined as Fresnel zone, is delimited by:

$$d_{rnf\,[\mathrm{m}]} \leq d_{obs\,[\mathrm{m}]} < d_{ff\,[\mathrm{m}]}, \quad \text{where} \quad d_{ff\,[\mathrm{m}]} = \frac{2\ D^2_{ant\,[\mathrm{m}]}}{\lambda_{[\mathrm{m}]}} \tag{2.8}$$

and:

- d_{ff}: the far-field boundary;
- D_{ant}: the largest dimension of the antenna.

Inside this region the radiating power density is predominant over the reactive power density (radiation phenomenon), the radiation pattern depends upon the distance from the antenna and the E field decays with d^{-2}. The E and H fields measured inside the Fresnel zone are directly interrelated by the characteristic impedance of free space (Z_0), and thus, only the measurement of E is needed to know the two components of the EM fields, [OFRC05].

The far-field region, also known as the Fraunhofer region, is defined as:

$$d_{obs\,[\mathrm{m}]} \geq d_{ff\,[\mathrm{m}]} \tag{2.9}$$

In this region, the field components (E and H) are essentially orthogonal to each other and transverse to the radial direction of propagation, and the E field decays with d^{-1} [Bala05]. The E and H fields measurements are directly related to the characteristic impedance of free space as in the radiative near-field region [OFRC05]. The radiation pattern is now independent of the radial distance.

It is important to note that the characteristics of the fields, as the boundaries from one region to the other are crossed, do not change abruptly but undergo a gradual transition [Bala05].

2.4.2 Electromagnetic Field Recommendations and Measurement

The massification of cellular communications, and consequently the number of BS antennas, has caused major concerns in the general population regarding the potential health hazards of EMFs. The biological effects of EMFs in humans can be considered a very sensitive subject [OFRC05]. Up to today, there are still uncertainties due to lack of trustful medical information on certain radiation effects, and inconclusive/inconsistent studies on possible health effects due to crude exposure assessment and failure to control for confounding factors, [ICNI98], [ICNI09], and [ICNI20]. The few studies with adequate exposure assessment did not reveal any adverse health-related effects, [ICNI09] and [ICNI20],

The EMFs generated in RF (100 kHz to 300 GHz) can have three potential effects on human beings: thermal effects, non-thermal effects and psycho-somatic effects [Corr20]. Regarding psycho-somatic effects, they are a consequence of the perception of danger, even when it does not exist. A well-known example is people feeling symptoms even when the antennas are not connected. This effect may be a consequence of the alarm raised by the media on this matter [Corr20].

Regarding non-thermal effects, these are still under study and the occurrence of long-term biological effects are still inconclusive. The thermal effects of RF are well-known and quantifiable [OFRC05], which consist of the increase in tissue temperature resulting from the interaction between the tissue molecules and the EMF. Biological damage occurs when the level of heating exceeds the body capacity of dissipating the excessive energy. Since the relation between the amount of radiation absorbed by the body and the corresponding temperature elevation is well-known, the establishment of rules and guidelines regarding exposure to RF is possible [OFRC05].

From a health risk perspective, there is the need to know how much EMF power is absorbed by biological

tissue, as this is responsible for the thermal effects stated above, [ICNI20]. This EMF power absorbing capability is typically a function of the incident field frequency. As stated in [ICNI20], for frequencies below 6 GHz it is useful to describe this effect in terms of the Specific Absorption Rate (SAR), which is the power absorbed per unit mass (W kg^{-1}), since for these frequencies EMFs penetrate deep into tissue and thus depth needs to be considered.

Since SAR can be difficult to measure, other, more easily evaluated quantities, named reference levels, are also specified. These quantities relevant to the guidelines are the E field, the H field and the power density S.

The basic restrictions and reference threshold presented by ICNIRP are established differently for two main groups of the population: the occupational public and the general public, [Antu12]. The occupational public is the group of professional workers that are exposed to known conditions and are trained to be aware of potential risks and to take appropriate precautions. The general public is defined as individuals of all ages and health status, including what is defined as sensitive groups, such as children and elderly people. In this thesis, only the thresholds defined for the general public are presented.

The reference levels for the general public regarding E, H and S, for exposures higher than 6 minutes that are under the frequencies of interest in this thesis are represented in Table 2.13 and Figure 2.7.

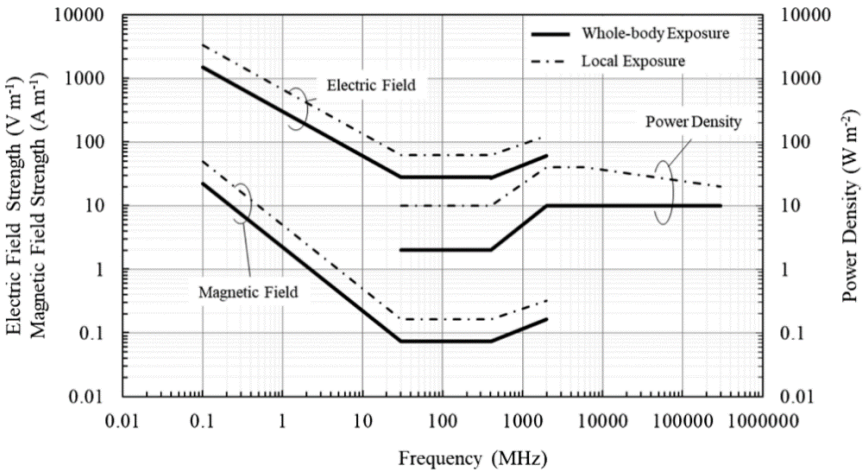

Figure 2.7. Reference levels for time-averaged exposures of ≥ 6 minutes from 100 kHz to 300 GHz (extracted from [ICNI20]).

Table 2.13. Reference levels for whole body exposure to EMF fields (adapted from [ICNI20]).

Frequency Range, f [MHz]	E ($V \times m^{-1}$)	H ($A \times m^{-1}$)	S ($W \times m^{-2}$)
]400, 2000]	$1.375 \times f^{0.5}$	$0.0037 \times f^{0.5}$	f/200
> 2000	----	----	10

One needs to take S, E^2 and H^2 averaged over 30 minutes, over the whole body space, and E and H fields are to be derived from these averaged values [ICNI20]. For frequencies up to 2 GHz, compliance

in the far-field zone is demonstrated if either E, H or S values are within the reference ones. For the radiative near-field zone, compliance is demonstrated if either S or both E and H do not exceed the above reference values. Within the reactive near-field zone, compliance is demonstrated if both E and H do not exceed the reference values. For frequencies above 2 GHz, within the far-field and radiative near-field zones, compliance is demonstrated if S does not exceed the above reference values. For the reactive near-field zone, reference levels cannot be used to determine compliance and so basic restrictions must be assessed. The "----" indicates that the cell is not relevant for the reference levels.

It is important to observe that in situations of simultaneous exposure to fields of different frequencies, these exposures are additive in their effect, and thus it is possible to analyse separately each frequency exposure [ICNI20]. The following criterion regarding the reference values for the power density should then be applied as:

$$\sum_{i=30\ \mathrm{MHz}}^{300\ \mathrm{GHz}} \left(\frac{S_{i,[\mathrm{W/m^2}]}}{S_{ref,i,[\mathrm{W/m^2}]}} \right) \leq 1 \qquad (2.10)$$

where:

- S_i: the power density at frequency i;
- $S_{ref,i}$: the power density reference level from Table 2.12 at frequency i.

To verify compliance with the reference levels established by ICNIRP, measurements of the quantities described above must be performed around areas of interest, e.g., BSs. The definition of measurement guidelines is of extreme importance for results to be replicated, and in doing so, it becomes possible to compare different measurement values [Antu12].

The Electronic Communications Committee (ECC) issued a recommendation [ECCC07], within the European Conference of Postal and Telecommunications Administrations (CEPT), on measuring non-NR in the 9 kHz to 300 GHz frequency band. This recommendation is applied by the Portuguese National Communications Authority (ANACOM), [ANAC07].

The measurement method present in the ECC recommendation is based on three cases: the quick overview (case 1), the variable frequency band scan (case 2) and the detailed investigation (case 3).

The quick overview method can only be applied in far-field situations. The equipment used in this case is RF radiation meters with isotropic field probes capable of measuring the field's Root Mean Square (RMS) value. The variable frequency band scan is also applied only in far-field situations and should be used when it is required to know the exposure levels per frequency. The equipment for this case should be a spectrum analyser. The detailed investigation method is the more complex method of all three and so, it should be used when cases 1 and 2 are not applicable. This case should then be used for near-field measurements and strong field measurements. These methods for the measurement of EMF exposure are explained in detail in [ECCC07].

The current methodology dedicated to EMF measurements on GSM, UMTS and LTE, may not be suitable for NR [PKZu19], due to the new radio techniques introduced, such as MaMIMO and beamforming. The existing measurement methods can then result in significantly overestimated results

when applied to NR. [PKZu19] suggests that an alternative way to assess EMF exposure is a new method that exploits both simulations and calculations. This new method would need to take into account the topology of the location of investigation, including digital maps of the terrain and buildings in 3D format, propagation phenomena (such as diffraction, reflection and EM waves interference) and the technical parameters of the involved BS.

Several approaches at the establishment of models to assess EMF in NR have already been proposed. [TFCT17] suggests a model based on a statistical approach considering factors such as BS utilisation, MaMIMO, TDD and spatial distribution of users within the cell. [BWWG18] also proposes a statistical approach for EMF exposure assessment on systems with MaMIMO technology.

2.4.3 Exclusion Zones

Exclusion zones are regions around BS antennas that may exceed the established human exposure thresholds, Figure 2.8, which are usually inside the near-field region of the radiating antenna. These regions can be physically delimited by warning signs and perimeter fences to protect the general public from potentially harmful levels of NIR.

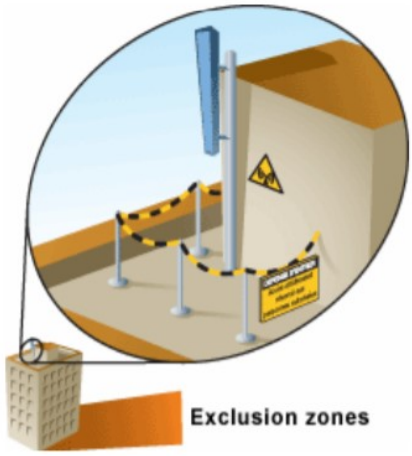

Figure 2.8. Exclusion zone surrounding a BS antenna (extracted from [OFRC05]).

Measurement procedures to assess EMF components, as well as the maximum localised SAR in a human model, can be time-consuming and BS type dependent [SLAO10]. As an alternative to these procedures, software simulations of EMFs around BS antennas may be run, although this approach typically requires a large amount of time to obtain precise results.

The most practical solution to estimate exclusion zones around BSs is to select adequate mathematical models [SLAO10], which usually provide a good prediction of radiation levels and are simple to apply. In [OFRC05], several models for the estimation of EMFs around BS antennas are presented:

- Far-field model;
- Far-field approximation;
- Cylindrical exclusion zone;
- Far-field gain-based model;

- Synthetic and gain-based model;
- Hybrid prediction.

These models aim at presenting simple formulations, typically assessed through complex simulations. Their validity is presented in Figure 2.9.

	Propagation models validity range (expression of the power density)							
Validity range [m]	0	$\frac{\lambda}{2}$	λ	2λ	3λ	$\frac{D^2}{4\lambda}$	$\frac{\alpha_{3dB}G(\theta,\phi)D}{4\pi}$	$\frac{2D^2}{\lambda}$
Far-field model								
Far-field Approximation								
Far-field gain-based model								
Gain based model								
Synthetic based model								
Cylindrical exclusion zone								
Hybrid								

Figure 2.9. Validity range of the different models (extracted from [OFRC05]).

In a simple approach to the estimation of exclusion zones, simple models, like the far-field one or the far-field approximation, are used to assess the dimension of these zones [SLAO10]. A model for the representation of an exclusion zone of a BS antenna is illustrated in Figure 2.10.

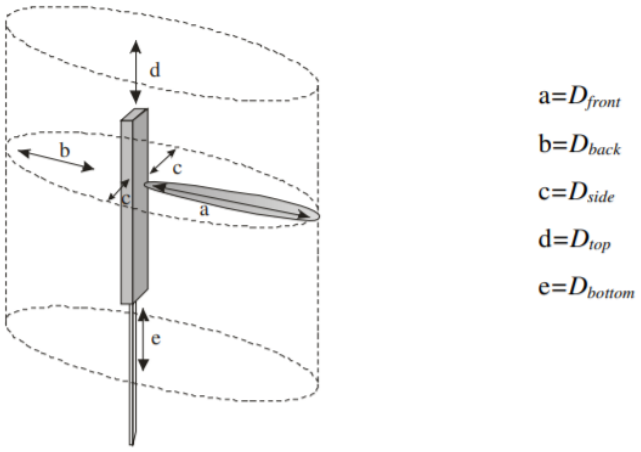

Figure 2.10. Representation of an antenna's exclusion zone (extracted from [OFRC05]).

The distance values calculated from these models are obtained for the worst-case scenario and in the direction of the antenna's main lobe (D_{front}). As stated in [OFRC05], to obtain de distances for the sides (D_{side}), back (D_{back}), top (D_{top}) and bottom of the antenna (D_{bottom}), correction factors are applied to D_{front}, which depends on the desired direction. These correction factors for D_{side} and D_{back} are determined from the typical antenna characteristics found in the antenna's catalogue.

The correction factor for D_{top} and D_{bottom} is the same, being $0.3 \times D_{front}$ [OFRC05]. When a downtilt is used, a correction factor must be applied to the top and bottom distances:

$$D'_{top\,[\mathrm{m}]} = D_{top\,[\mathrm{m}]}\ \cos(\theta_{dt}) \tag{2.11}$$

$$D'_{bottom\,[\mathrm{m}]} = D_{bottom\,[\mathrm{m}]}\ [1 + \sin(\theta_{dt})] \tag{2.12}$$

where:

- θ_{dt}: downtilt angle.

One must begin by estimating the far-field region of the antennas to check if it is reasonable to use the far-field model since this is the simplest one [OFRC05]. If the far-field distance is large and, at this distance, the power density calculated is several times below the threshold value, then it means there is the need to use models with smaller validity ranges. As it can be seen in Figure 2.9, the validity distance for the far-field approximation model is eight times smaller than the far-field one. This allows one to obtain results at a much closer distance from the BS antennas. As stated in [OFRC05], if the calculated distance is feasible according to the type of BS installation, even if the power density is below the threshold level, the exclusion can be considered as the minimum valid distance for the model. This decision is taken as a more simple but precautionary approach.

The values for the exclusion zone distances, as well as the need to implement physical barriers for public protection, depend on the type of BS antennas installation and cell type. Different cell types possess different transmitted powers, thus varying the exclusion zone dimensions. Regarding BS installation type, different types of BSs require different proximities to the general public, which, depending on the transmitted powers, may require the need for physical barriers. The classification of different types of infrastructure supporting the BS antennas for the interest of this work, as well as the respective cell type and the involving environment, are presented in Table 2.14.

Table 2.14. Classification of BS antennas installation (extracted from [OFRC05] and [Antu12]).

Denomination	Cell Type	Environment	Installation Type	Antenna Height [m]
Rtower	Macrocell	Rural, Suburban	Tower, Mast, Water sump, "Tree"	20-50
Uroof	Micro/Macrocell*	Urban	Roof-top	2-5**
Utower			Tower	20-40
Ufaçade	Microcell		Bulding Façade	3-10
Upole			Light Pole or other	3-5

**: The cell type will depend on the coverage area*

***: Height from the rooftop*

2.5 State of the Art

In this subsection, an overview of the research performed by other authors regarding the implementation and planning of NR networks under EMF restrictions is done.

Planning the deployment of NR networks under EMF exposure restrictions is a complex challenge. Under these limits, the task becomes especially harder under densely populated areas where multiple NR radio infrastructures of different operators need to coexist. As discussed previously, the exposure to multiple sources of EMFs is additive in its effects, and thus, the new NR infrastructures plus the already existing legacy technologies, namely GSM, UMTS and LTE, only add to a more EMF saturated environment. Addressing the planning problem is critical for the roll-out of NR [CCMF18], A network planning that does not take the established EMF restrictions into account may result in a negative impact on the Capital Expenditures (CAPEX), poor coverage and limited support for the new services.

[CCMF18] states that stringent EMF restrictions set heavy limitations for the operators in the installation of new NR equipment, and highlights three different scenarios regarding how these restrictions may affect the planning of the NR cellular network:

- NR cell densification;
- EMF saturation zones (caused by legacy technologies);
- EMF regulation based on minimum distance.

In this thesis, the problem addressed is the installation of NR BSs in sites with legacy technologies, also termed the Brownfield approach. Figure 2.11 represents the scenario where a pre-NR site is already covering a given area. Since the BS surrounding is already at the limit of the EMF exposure levels established, the new NR equipment cannot be installed in the same location.

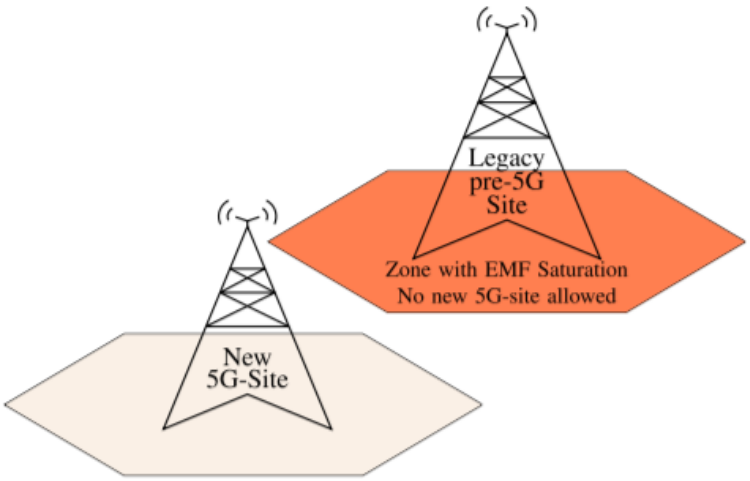

Figure 2.11. Presence of an EMF saturated zone (extracted from [CCMF18]).

This may increase CAPEX costs, since the operator would have to install the NR BS in a new site or decrease the QoS offered by legacy technologies by lowering their transmitted power. [CCMF18] also stated that the case of EMF saturation may be exploited by operators already serving the area by denying the installation of the competitor's NR BS.

[CCMF18] considers two real-world case-studies of currently deployed cellular networks to support the discussion of the impact of EMF restrictions on NR network planning. The first case-study concentrates on a portion of the Fuorigrotta district, in Naples, Italy, and the main goal is to assess the EMF levels in the given area. To assess EMF exposure, [CCMF18] utilises a ray-tracing simulator developed in

[FIRR04]. This simulator requires, as inputs, a Digital Elevation Model (DEM) of the area, a vector file containing the position and height of the buildings, and the characterisation of the BSs antennas in terms of location, input power, radiation diagram and azimuthal pointing angles. The results show that for the maximum input power and 75% of the maximum input power, there are several zones within the studied area that exceeds the Italian limits for EMF exposure. These results highlight the concern that some areas may already have reached EMF saturation with the use of legacy networks, which can significantly limit the deployment of future NR BSs. It is important to note that the limits imposed by the Italian government are considerably below the ones proposed by ICNIRP.

The second case study focuses on the impact of current regulations on network planning and the QoS offered to the end-user on the Torrino Mezzocammino (TMC) area in Rome, Italy. To this end, [CCMF18] used CellMapper, a monitoring application that collects different cellular metrics of the BSs serving the user. The measurements were made outdoors and mainly by foot inside the TMC area with three LTE-A enabled smartphones, one for each operator. It is important to note that, due to municipal regulations, which impose a minimum distance of 100 m between a sensitive place and the BS, the TMC area does not have any BS installed in it, and thus, users are served by BSs outside TMC. These BSs were identified using the CellMapper application. Different zones of TMC experience very low values of the received power, which are equal or below -110 dBm. These results were manually confirmed by experiencing frequent drop calls and difficulty in accessing internet applications. The lack of installed BSs inside TMC has an impact on the quality of experience perceived by the user and on the type of service offered by the operator, and the regulation that integrates a minimum distance between the BS and a sensitive place has quite an impact on network planning.

Chapter 3

Model Development and Simulator Description

This chapter provides an overview of the general model as well as a description of the developed models for this thesis. Firstly, power density estimation models are presented and an exclusion zone evaluation model is built. Secondly, the coverage and capacity planning is made and the output evaluation metrics are presented, and finally, at the end of the chapter, a theoretical model assessment and comparison with EMF measurements are done.

3.1 Model Overview

Having studied the fundamental aspects of mobile communications systems regarding network architecture, radio interface, coverage, capacity and interference, as well as EMF exposure and recommendations, a model to address the problem of this thesis is presented in this section, Figure 3.1 showing the general configuration.

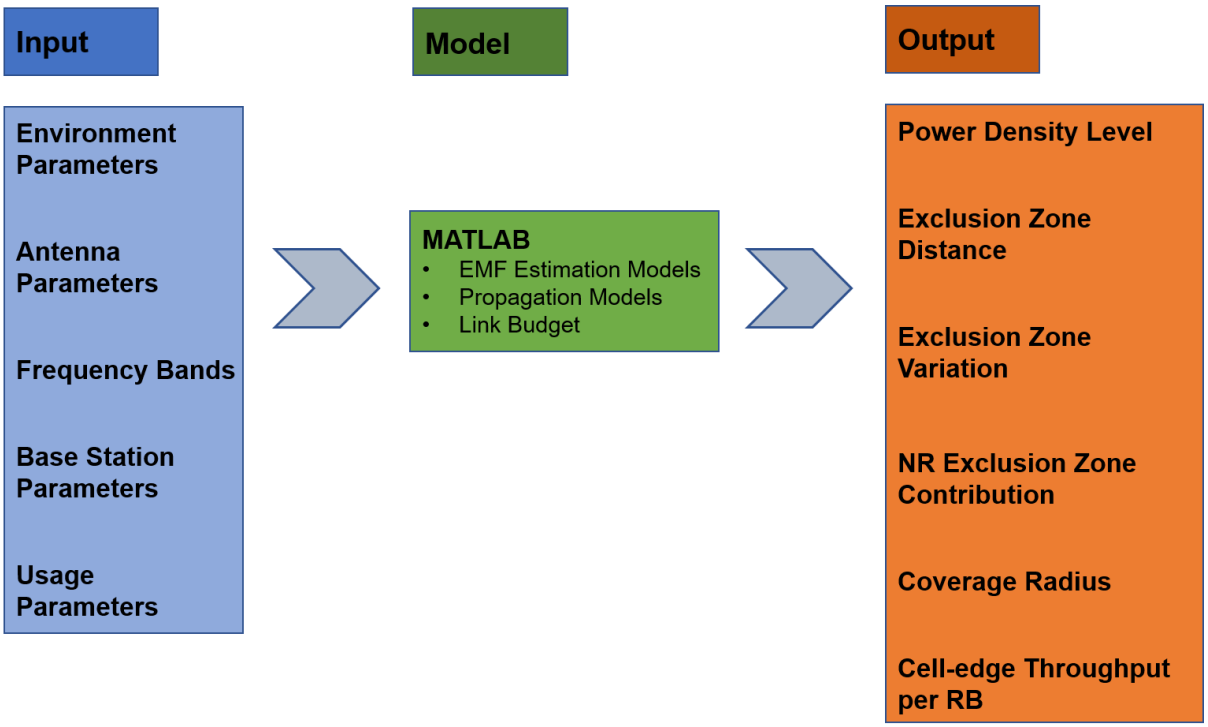

Figure 3.1. Model Configuration.

The main goal of this thesis is to develop a model and a simulator to implement it, to analyse the impact of EMF restrictions on NR BS deployment in sites with legacy technologies already installed (GSM, UMTS and LTE). This model consists of developing, through MATLAB, an exclusion zone evaluation model, and a coverage and capacity planning model to analyse BS performance under the implemented EMF restrictions.

The input parameters for the model are divided into environment, antenna, frequency bands, BS and usage. The environment parameters take the surroundings where the considered BS is inserted into account, which are classified as urban, suburban or rural. The antenna parameters, such as its dimension, input power, gain and frequency bands, are used as inputs for the exclusion zone evaluation, coverage and capacity models. The BS parameters, such as its height and type of installation, need to be considered as the propagation model inputs. The usage parameters take the type of service of the end-user into account, whether it is a voice service or a data one. The different types of services require different quality levels that influence the capacity of the cell as well as its radius.

The output parameters are divided into power density level, exclusion zone distance, exclusion zone variation, NR exclusion zone contribution, coverage radius and throughput per RB at cell-edge. The developed model is able to compute the power density levels at any given instance from the antenna, enabling then the calculation of the exclusion zone distance and consequently the exclusion zone variation with the installation of the NR antenna. The coverage radius and throughput per RB are computed through the link budget and adequate propagation models.

Two situations are considered regarding exclusion zone evaluation via simulation: one considers only the legacy antenna and the other takes both the legacy and the NR antennas working simultaneously. The analysis of both simulations allows one to evaluate the power density levels before and after the installation of NR, allowing for the computation of the variation of the BS exclusion zone and also the contribution of NR to the obtained variation. Regarding the impact of the exclusion zone restrictions in the performance of NR BSs, reference values for the coverage radius and cell-edge throughput per RB are defined and then a comparison is made with the results obtained from the imposed restrictions.

3.2 Power Density Estimation Models

In this subsection, models for the estimation of EMF levels are presented. As studied in Chapter 2, the computation of the EMF strength is needed to establish the exclusion zones around BSs. As discussed earlier, the most practical solution to estimate these zones is the application of adequate mathematical models. Since exclusion zones are usually in the near-field of the BS antenna, near-field models must be employed in order to obtain suitable field level approximations. The models for EMF estimation presented below do not take the environment topology into account, and thus the conditions are assumed to be free space propagation.

3.2.1 Far-Field Model

The far-field model is one of the most common EMF level estimation models and is also the simplest one, the RMS value for the power density being expressed by [SLAO10]:

$$S(d,\theta,\varphi)_{[\mathrm{W/m^2}]} = \frac{P_{in\,[\mathrm{W}]}\; G(\theta,\varphi)}{4\pi\;\; d^2_{obs\,[\mathrm{m}]}} \quad , \quad d_{obs[\mathrm{m}]} \geq d_{ff\,[\mathrm{m}]} \tag{3.1}$$

$$d_{ff\,[\mathrm{m}]} = \frac{2\;\; D^2_{ant\,[\mathrm{m}]}}{\lambda_{[\mathrm{m}]}} \tag{3.2}$$

where:

- θ: elevation angle;
- φ: azimuth angle;
- P_{in}: input power of the antenna;
- $G(\theta,\varphi)$: antenna gain in the direction of the elevation and azimuth angles.

Although the far-field model is of great simplicity, its range of applicability is rather limited, as it can only be applied when the distance from the antenna to the observation point is greater than the far-field distance of the antenna under study. If the far-field model is applied in the near-field region of the antenna, the computed field strength is overestimated.

3.2.2 Far-Field Gain-Based Model

The far-field gain-based model is a fast and efficient method for the evaluation of EMF levels inside the near-field region of the BS antenna [OFRC05]. For this method, the gain of the entire antenna is derived from the combination of the far-field radiation pattern of an antenna element with the array factor. The model considers that BS antennas are uniform arrays and that the coupling between the dipoles of the array can be neglected. A good estimate of the near-field can thus be obtained as a combination of the far-field radiated by each antenna element:

$$S(d,\theta,\varphi)_{[\mathrm{W/m^2}]} \approx \frac{\left| \sum_{i=1}^{N_{el}} \frac{\sqrt{30 \ P_{i,in\,[\mathrm{W}]} \ G_{el}(\theta_i,\varphi_i)}}{d_{i,obs\,[\mathrm{m}]}} \ e^{-j(k_0 d_{i,obs}+\psi_i)} \ \hat{r}(\theta_i,\varphi_i) \right|^2}{Z_{0[\Omega]}}, \qquad d_{obs\,[\mathrm{m}]} > 3\lambda_{[\mathrm{m}]} \tag{3.3}$$

$$G_{el}(\theta_i,\varphi_i) \approx \frac{G_M \ D_{V,el}(\theta_i) \ D_{H,el}(\varphi_i)}{N_{el}} \tag{3.4}$$

$$k_{0\,[\mathrm{rad/m}]} = \frac{2\pi}{\lambda_{[\mathrm{m}]}} \tag{3.5}$$

where:

- N_{el}: number of radiating elements of the antenna;
- $P_{i,in}$: input power to the the i^{th} element;
- θ_i: elevation angle of the i^{th} element relative to point of observation;
- φ_i: azimuth angle of the i^{th} element relative to point of observation;
- $d_{i,obs}$: distance from the i^{th} element to the point of observation;
- $\hat{r}(\theta_i,\varphi_i)$: unitary vector of the i^{th} element;
- $G_{el}(\theta_i,\varphi_i)$: antenna element gain;
- G_M: maximum antenna gain;
- $D_{V,el}(\theta)$: element radiation pattern in the vertical plane;
- $D_{H,el}(\varphi)$: element radiation pattern in the horizontal plane;
- ψ_i: phase shift of the i^{th} element.
- k_0: free space wavenumber.

Note that in (3.3) the expression inside the absolute value bars corresponds to the radiated electric field. The far-field gain-based model presents good agreement with Numerical Electromagnetic Code (NEC) results for distances above three wavelengths, [SLAO10].

3.3 Exclusion Zone Evaluation Model

This subsection aims at developing a model for the estimation of the exclusion zone around a BS, which takes the models discussed previously for the estimation of EMF into account. Within the scope of this thesis, the goal is to compute the variation of the exclusion zone when an NR antenna is inserted in a BS with GSM, UMTS and LTE technologies already installed. For this purpose, the exclusion zone needs to be computed before and after the installation of the NR antenna.

3.3.1 Far-Field Zone

In general, the exclusion zone is located in the near-field of the BS antenna. Nevertheless, the far-field model can be used in a first instance, since it is the simplest one and requires little computation time, to ensure whether the exclusion zone is in the near- or the far-fields.

As discussed in Section 2.4.2, the simultaneous exposure to fields of different frequencies possesses an additive effect, meaning that the total normalised exposure can be regarded as the sum of the exposure for each frequency in relation to its reference value. This effect is reflected in (2.10), where the total normalised exposure cannot be greater than 1, taking all sources that radiate between 30 MHz and 300 GHz into account. For the purpose of this thesis, the only sources of radiation are the BS antennas since the exposure from other sources inside the exclusion zone is rather weak in comparison, thus, only the frequencies used in the BS are considered and the exposure from other sources is assumed to be zero. Taking this into consideration, (2.10) can be rewritten as:

$$S_{norm}^{tot} = \sum_{i=1}^{N_{sys}} \left(\frac{S_{i\,[\mathrm{W/m^2}]}}{S_{ref,i\,[\mathrm{W/m^2}]}} \right) \leq 1 \tag{3.6}$$

where:

- N_{sys}: the number of communications systems used in the BS;
- S_{norm}^{tot}: the total normalised power density.

For example, a BS that operates with three technologies such as LTE 800, GSM 900 and LTE 2600 has a number of communications systems equal to 3.

Taking (3.6) as a reference, the goal is to calculate a distance such that the total normalised power density is equal to 1. This distance, in the direction of maximum radiation, is the value for the front border of the exclusion zone, D_{front}.

As stated earlier, the first analysis for D_{front} can be done using the far-field model. For this analysis, one needs to note that the output result is only valid if the computed distance is inside the far-field zone for all the technologies present in the BS. For this purpose, one can define a distance such that it contains all the far-field zones considered:

$$d_{ff,[\mathrm{m}]}^{min} = \max\{d_{ff,i\,[\mathrm{m}]} : i = 1, \dots, N_{sys}\} \tag{3.7}$$

where:

- d_{ff}^{min}: the minimum distance containing all the far-field distances of the BS antennas;
- $d_{ff,i}$: the far-field distance for the i^{th} system.

In order to compute the power density in the far-field region of an antenna, (3.1) is used. Combining (3.1) with (3.6) one has:

$$S_{norm}^{tot} = \sum_{i=1}^{N_{sys}} \left(\frac{P_{i\,[\mathrm{W}]}\ G_{M,i}}{4\pi\ d_{obs\,[\mathrm{m}]}^2}\ \frac{1}{S_{ref,i\,[\mathrm{W/m^2}]}} \right) \tag{3.8}$$

where:

- P_i: the input power for the i^{th} system;
- $G_{M,i}$: the maximum antenna gain for the i^{th} system.

As stated above, the front border of the exclusion zone is such that the total normalised power density must be equal to 1 at that distance. Taking into account this and the fact that the d_{obs} is the same for all used frequencies, D_{front} can be computed as follows:

$$\frac{1}{D_{front\,[\mathrm{m}]}^2} \sum_{i=1}^{N_{sys}} \left(\frac{P_{i\,[\mathrm{W}]}\ G_{M,i}}{4\pi}\ \frac{1}{S_{ref,i\,[\mathrm{W/m^2}]}} \right) = 1 \tag{3.9}$$

and so:

$$D_{front\,[\mathrm{m}]} = \sqrt{\sum_{i=1}^{N_{sys}} \left(\frac{P_{i\,[\mathrm{W}]}\ G_{M,i}}{4\pi}\ \frac{1}{S_{ref,i\,[\mathrm{W/m^2}]}} \right)} \tag{3.10}$$

The flowchart corresponding to the D_{front} computation for a BS using the far-field model is shown in Figure 3.2. One should notice that if the computed D_{front} is less than the minimum distance that contains all the BS's far-field distances, then the exclusion zone is inside the near-field of the BS and thus a near-field model is needed to compute the EMF exposure.

3.3.2 Near-Field Zone for Linear Arrays

The near-field model used to assess exposure from a BS is the far-field gain-based model presented in Section 3.2.2. As stated earlier, the model considers that BS antennas are linear uniform arrays and that the coupling between the dipoles can be neglected. The coordinates system for a linear array composed of elements of two dipoles with orthogonal polarisation is represented in Figure 3.3.

In a BS antenna, the number of elements of the array is usually a power of 2 in order for the input power to be more easily divided among its elements. The spacing between elements is uniform and can be given by the wavelength multiplied by a factor:

$$d_{es\,[\mathrm{m}]} = \Delta_{es}\ \lambda_{[\mathrm{m}]} \tag{3.11}$$

where:

- d_{es}: the distance between each element;
- Δ_{es}: the element spacing factor.

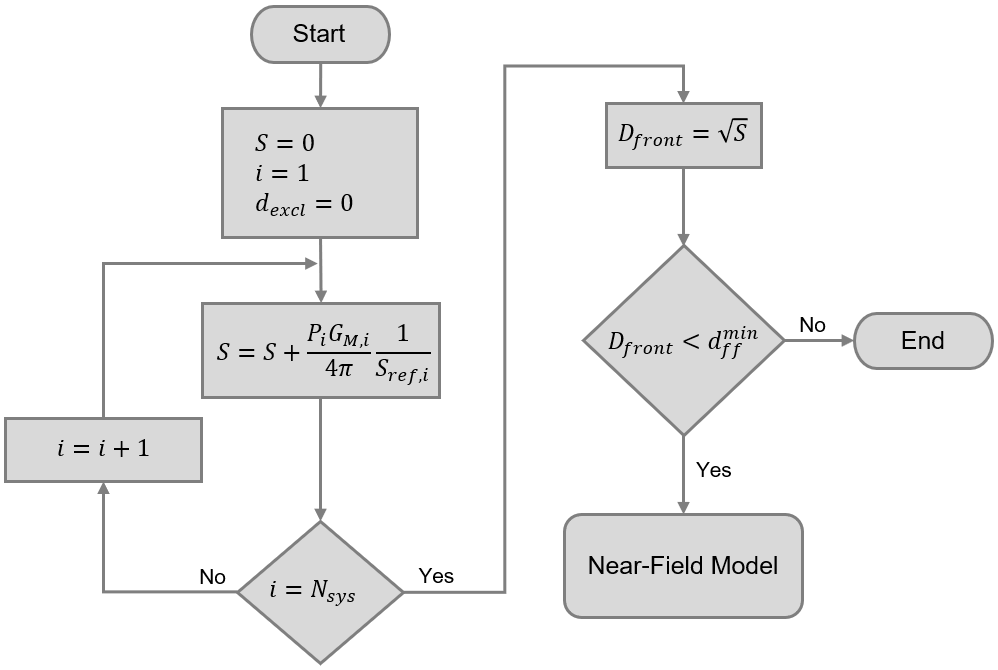

Figure 3.2. D_{front} computation with the far-field model.

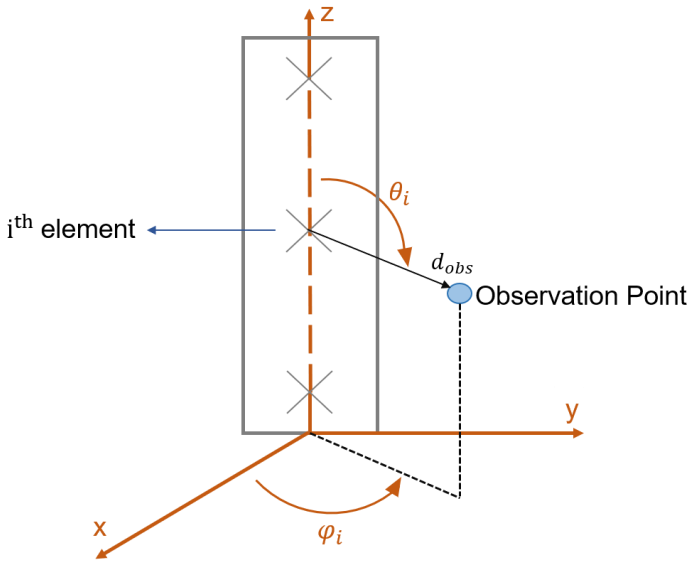

Figure 3.3. Coordinates system for a linear array antenna (adapted from [Antu12]).

In mobile communications systems, the distance between each array element usually corresponds to a wavelength, although in some cases its value can vary. The element spacing can be provided by the antenna manufacturer and it is not usually present in the equipment's datasheet.

In order to use the far-field gain-based model for the computation of the EMF exposure in the near-field of the antenna, first one needs to define the geometry of the problem. Figure 3.4 represents the considered geometries for both even and odd numbers of elements in a uniform array.

The point of observation is at a distance d_{obs} from the antenna and it is chosen to have a height that corresponds to the midpoint of the antenna. Due to the existing symmetry, one can now make the analysis of the problem focusing only on half of the array elements.

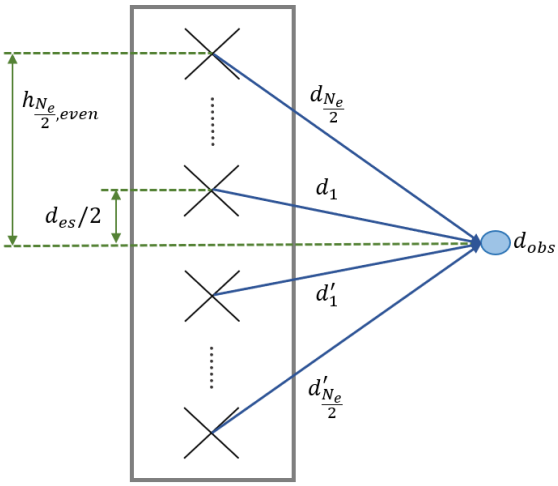

a) Even element array.

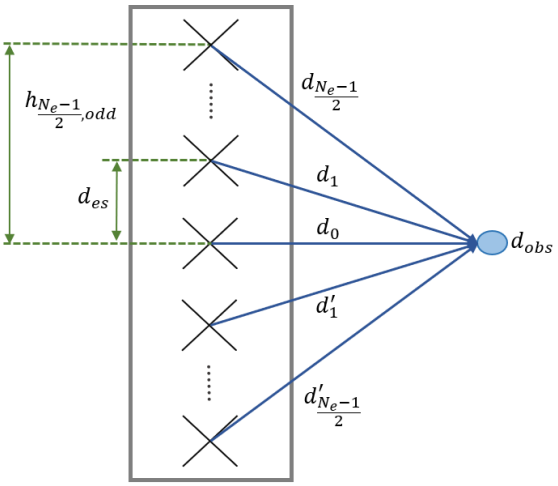

b) Odd element array.

Figure 3.4.Geometry comparison between even and odd element arrays.

The distance from the i^{th} element of the array to the point of observation $d_{i,obs}$ can be described as a function of d_{obs}. According to Figure 3.4, for an array with an even number of elements, the expression for $d_{i,obs}$ as a function of d_{obs} is given by:

$$d_{i,obs\,[\mathrm{m}]} = \sqrt{h^2_{i,even\,[\mathrm{m}]} + d^2_{obs\,[\mathrm{m}]}} \tag{3.13}$$

$$h_{i,even\,[\mathrm{m}]} = \frac{(2i-1)}{2}\ d_{es\,[\mathrm{m}]} \tag{3.14}$$

where:

- $h_{i,even}$: the distance from the i^{th} element centre to the array centre for an even element array.

For an odd element array the expression for $d_{i,obs}$ is as follows:

$$d_{i,obs\,[\mathrm{m}]} = \sqrt{h^2_{i,odd\,[\mathrm{m}]} + d^2_{obs\,[\mathrm{m}]}} \tag{3.15}$$

$$h_{i,odd\,[\mathrm{m}]} = i\ d_{es\,[\mathrm{m}]} \tag{3.16}$$

where:

- $h_{i,odd}$: the distance from the i^{th} element centre to the array centre for an odd element array.

One can note that for an array with an odd number of elements, the element at the array centre is considered to be the 0^{th} element and in this manner its distance to the observation point, as can be confirmed by (3.15) and (3.16), degenerates to d_{obs}. From the considerations adopted above, the electric field expression from (3.3) can be rewritten as:

$$E(d,\theta,\varphi) \approx \begin{cases} \left| \sum_{i=1}^{\frac{N_{el}}{2}} \frac{2\sqrt{30\,P_{i,in}\,G_{el}(\theta_i,\varphi_i)}}{d_{i,obs}} e^{-j(k_0 d_{i,obs}+\psi_i)} \right|, & N_{el}\ even \\ \left| \frac{\sqrt{30\,P_{0,in}\,G_{el}(\theta_0,\varphi_0)}}{d_{obs}} e^{-j(k_0 d_{obs}+\psi_0)} + \sum_{i=1}^{\frac{N_{el}-1}{2}} \frac{2\sqrt{30\,P_{i,in}\,G_{el}(\theta_i,\varphi_i)}}{d_{i,obs}} e^{-j(k_0 d_{i,obs}+\psi_i)} \right|, & N_{el}\ odd \end{cases} \tag{3.17}$$

The phase shift associated with each element, ψ_i, is used to control the direction of maximum radiation, meaning that a tilt angle can be implemented by varying the feeding current's phase between each element. The direction of maximum radiation is considered to be perpendicular to the antenna axis ($\theta = \pi/2$) and thus the phase shift of each element is considered to be 0. It is also assumed that the array power efficiency is equal to 1 and that the input power is equally distributed over all elements:

$$P_{i,in\,[\mathrm{W}]} = \frac{P_{in\,[\mathrm{W}]}}{N_{el}} \tag{3.18}$$

The gain of one element is given by (3.4) and it depends on N_{el}, G_M, the element vertical radiation pattern, $D_{V,el}(\theta)$, and the element horizontal radiation pattern, $D_{H,el}(\varphi)$. The horizontal radiation pattern for a dipole is omnidirectional and therefore it is considered to be equal to 1, meaning that the element gain does not vary with the azimuth angle; the vertical radiation pattern is a well-known function of the elevation angle and the dipole's length relative to the wavelength, being defined as [Silv20]:

$$D_{V,el}(\theta) = \left| \frac{\cos\left(\frac{k_0 L_{dip\,[\mathrm{m}]}}{2}\cos(\theta)\right) - \cos\left(\frac{k_0 L_{dip\,[\mathrm{m}]}}{2}\right)}{\sin(\theta)} \right|^2 = |F_P(\theta)|^2 \tag{3.19}$$

where:

- L_{dip}: the dipole's length;
- $F_P(\theta)$: the radiation pattern factor.

In order to simplify the analysis, one can make another geometry consideration, as represented in Figure 3.5 for a linear array composed of three dipoles.

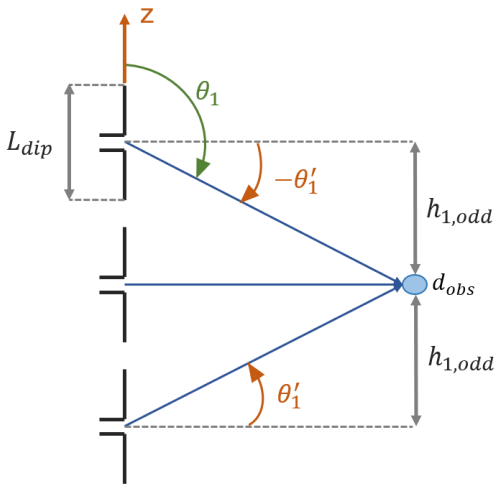

Figure 3.5. Geometry comparison between θ and θ' for a three dipoles linear array.

Since the model analysis takes advantage of the symmetry between the upper and lower half of the array, it is easier to analyse the contribution of each element if the elevation angle is replaced by the angle formed by the element's horizontal axis and the direction of observation, θ'. As it can be seen from Figure 3.5, due to the array's symmetry and the fact that the element's radiation pattern is symmetrical in relation to the horizontal axis, the EMF contribution of symmetrical elements, i.e., elements at the same distance from the array's centre, is the same. The new angle variable, as represented in Figure 3.5, can then be defined as:

$$\theta' = \frac{\pi}{2} - \theta \tag{3.20}$$

One can extract from Figure 3.5 and, from (3.14) and (3.16), that θ_i' can be computed as follows:

$$\theta_i' = \begin{cases} \tan^{-1}\left(\dfrac{d_{es\,[\mathrm{m}]}\ (2i-1)}{2\ d_{obs\,[\mathrm{m}]}}\right), & N_{el}\ even \\ \tan^{-1}\left(\dfrac{i\ d_{es\,[\mathrm{m}]}}{d_{obs\,[\mathrm{m}]}}\right), & N_{el}\ odd \end{cases} \tag{3.21}$$

Taking all the previous considerations into account, the gain of each element, given by (3.4), can be rewritten as:

$$G_{el}(\theta_i') \approx \frac{G_M}{N_{el}}\ |F_P(\theta_i')|^2 \tag{3.22}$$

where:

$$F_P(\theta_i') = \frac{\cos\left(\frac{k_0 L_{dip}}{2}\cos\left(\frac{\pi}{2} - \theta_i'\right)\right) - \cos\left(\frac{k_0 L_{dip}}{2}\right)}{\sin\left(\frac{\pi}{2} - \theta_i'\right)} \tag{3.23}$$

All the relevant elements for the far-field gain-based model are now fully defined and thus (3.17) can be further simplified:

$$E(d, \theta_i') \approx \begin{cases} \dfrac{2\sqrt{30 P_{in} G_M}}{N_{el}} \left| \displaystyle\sum_{i=1}^{\frac{N_{el}}{2}} \frac{|F_P(\theta_i')|}{d_{i,obs}} e^{-jk_0 d_{i,obs}} \right|, & N_{el}\ even \\ \dfrac{2\sqrt{30 P_{in} G_M}}{N_{el}} \left| \dfrac{|F_P(0)|}{2 \times d_{obs}} e^{-jk_0 d_{obs}} + \displaystyle\sum_{i=1}^{\frac{N_{el}-1}{2}} \frac{|F_P(\theta_i')|}{d_{i,obs}} e^{-jk_0 d_{i,obs}} \right|, & N_{el}\ odd \end{cases} \tag{3.24}$$

The flowchart corresponding to the electric field computation in the near-field based on the far-field gain-based model is presented in Figure 3.6.

3.3.3 Near-Field Zone for Planar Arrays

The previous considerations apply to BS antennas that are linear arrays, i.e., there are N_{el} vertical elements, which is the case for GSM, UMTS and LTE. For active NR antennas, the number of horizontal elements is different from one and therefore the antenna is formed by a matrix of dipoles, i.e., a planar array. In order to assess exposure from a planar array, a different geometrical approach is taken. Figure 3.7 represents the coordinate system for a planar array, where both antenna elements and observation point are represented in a 3D space, the antenna being placed at the zOy plane ($x = 0$).

The observation point is assumed to be at a distance d_{obs} from the antenna centre. To simplify the analysis, one assumes that each element occupies a rectangle with width w_{ele} and height h_{ele} given by:

$$h_{ele\,[\mathrm{m}]} = \frac{h_{ant\,[\mathrm{m}]}}{N_{V,el}} \tag{3.25}$$

$$w_{ele\,[\mathrm{m}]} = \frac{w_{ant\,[\mathrm{m}]}}{N_{H,el}} \tag{3.26}$$

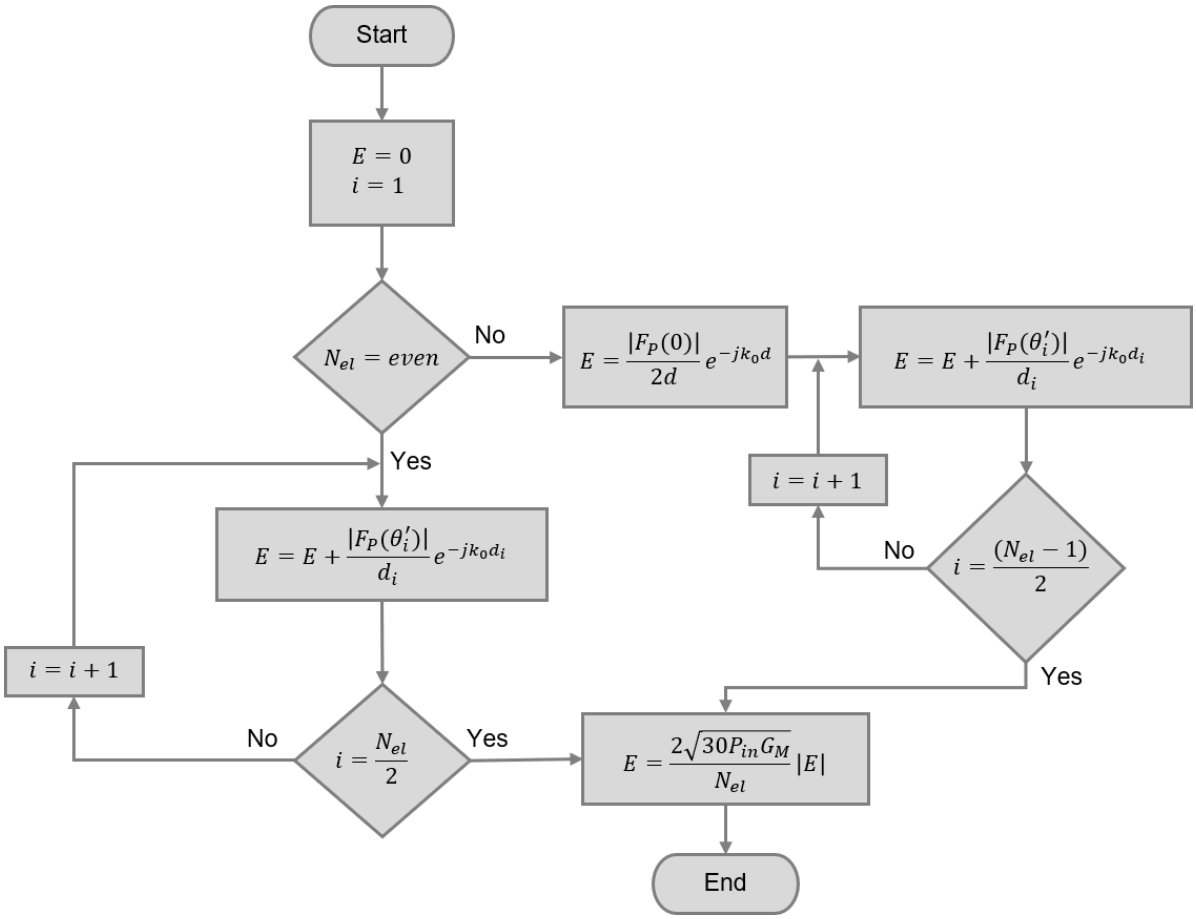

Figure 3.6. Electric field computation for a linear array in the near-field at a distance d.

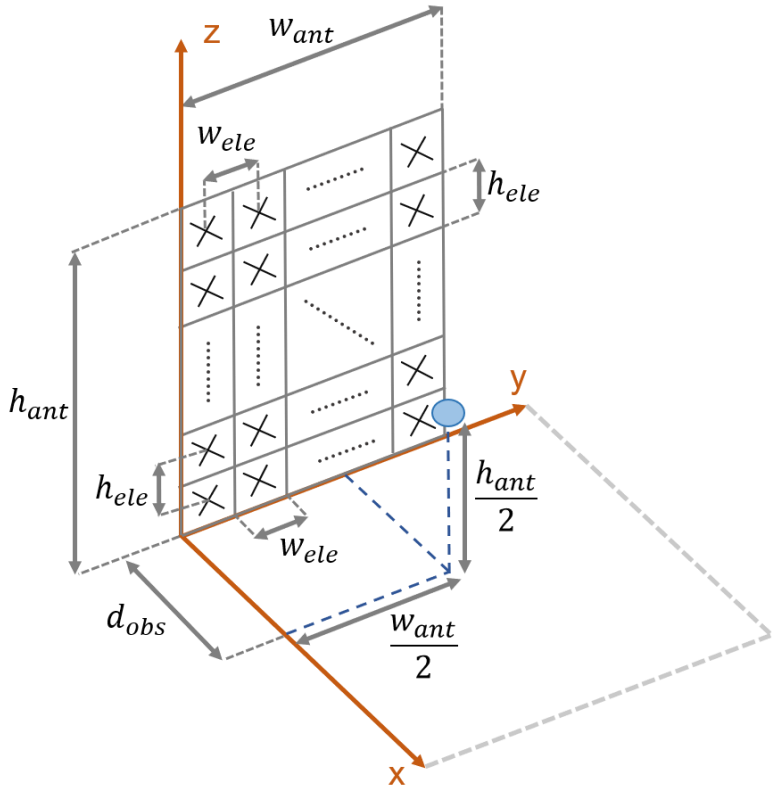

Figure 3.7. Coordinates system for a planar array antenna.

where:

- h_{ant}: the height of the antenna;
- w_{ant}: the width of the antenna;
- $N_{V,el}$: the number of vertical elements of the planar array;
- $N_{H,el}$: the number of horizontal elements of the planar array.

Assuming that each element is placed at the centre of each rectangle, the y and z coordinates of the element placed in the i^{th} line and j^{th} column are expressed respectively by:

$$y_{ij\,[\mathrm{m}]} = \frac{w_{ele\,[\mathrm{m}]}}{2} + (j-1)\ w_{ele\,[\mathrm{m}]} \tag{3.27}$$

$$z_{ij\,[\mathrm{m}]} = \frac{h_{ele\,[\mathrm{m}]}}{2} + (i-1)\ h_{ele\,[\mathrm{m}]} \tag{3.28}$$

From (3.28), one can note that the first line of dipoles starts at the bottom of the antenna, increasing from bottom to top. Taking the previous considerations into account, the distance from an element to the observation point is expressed as follows:

$$d_{ij,obs\,[\mathrm{m}]} = \sqrt{{d_{obs\,[\mathrm{m}]}}^2 + \left(y_{obs\,[\mathrm{m}]} - y_{ij\,[\mathrm{m}]}\right)^2 + \left(z_{obs\,[\mathrm{m}]} - z_{ij\,[\mathrm{m}]}\right)^2} \tag{3.29}$$

where:

- y_{obs}: the y coordinate of the observation point ($w_{ant}/2$);
- z_{obs}: the z coordinate of the observation point ($h_{ant}/2$).

It is assumed that the total power is equally distributed over all elements:

$$P_{el\,[\mathrm{W}]} = \frac{P_{in\,[\mathrm{W}]}}{N_{el}} = \frac{P_{in\,[\mathrm{W}]}}{N_{V,el}\ N_{H,el}} \tag{3.30}$$

The gain of each element is still given by (3.22) although the maximum antenna gain is expressed, in linear units, as:

$$G_M = G_{TX}\ G_{BF} \tag{3.31}$$

where:

- G_{TX}: the antenna gain per transmitter;
- G_{BF}: the beamforming gain.

The transmitters are linear arrays formed by elements in the antenna's columns. The number of transmitters (N_{TX}) in the planar array defines the MIMO level of the antenna. Both the transmitter gain and the beamforming gain are provided by the antenna's manufacturer.

The elevation angle of an element in relation to the observation point is given by:

$$\theta_{ij} = \frac{\pi}{2} - \theta'_{ij} \tag{3.32}$$

where:

$$\theta'_{ij} = \tan^{-1}\left(\frac{z_{obs} - z_{ij}}{d_{ij,obs}}\right) \tag{3.33}$$

Taking all the previous considerations into account, the electric field for a planar array in the near-field

is given by:

$$E(d,\theta_{ij}) \approx \frac{\sqrt{30\ P_{in}\ G_M}}{N_{el}} \left| \sum_{i=1}^{N_{V,el}} \sum_{j=1}^{N_{H,el}} \frac{|F_P(\theta_{ij})|}{d_{ij,obs}} e^{-jk_0 d_{ij,obs}} \right| \tag{3.34}$$

The flowchart corresponding to the electric field computation in the near-field for a planar array is presented in Figure 3.8.

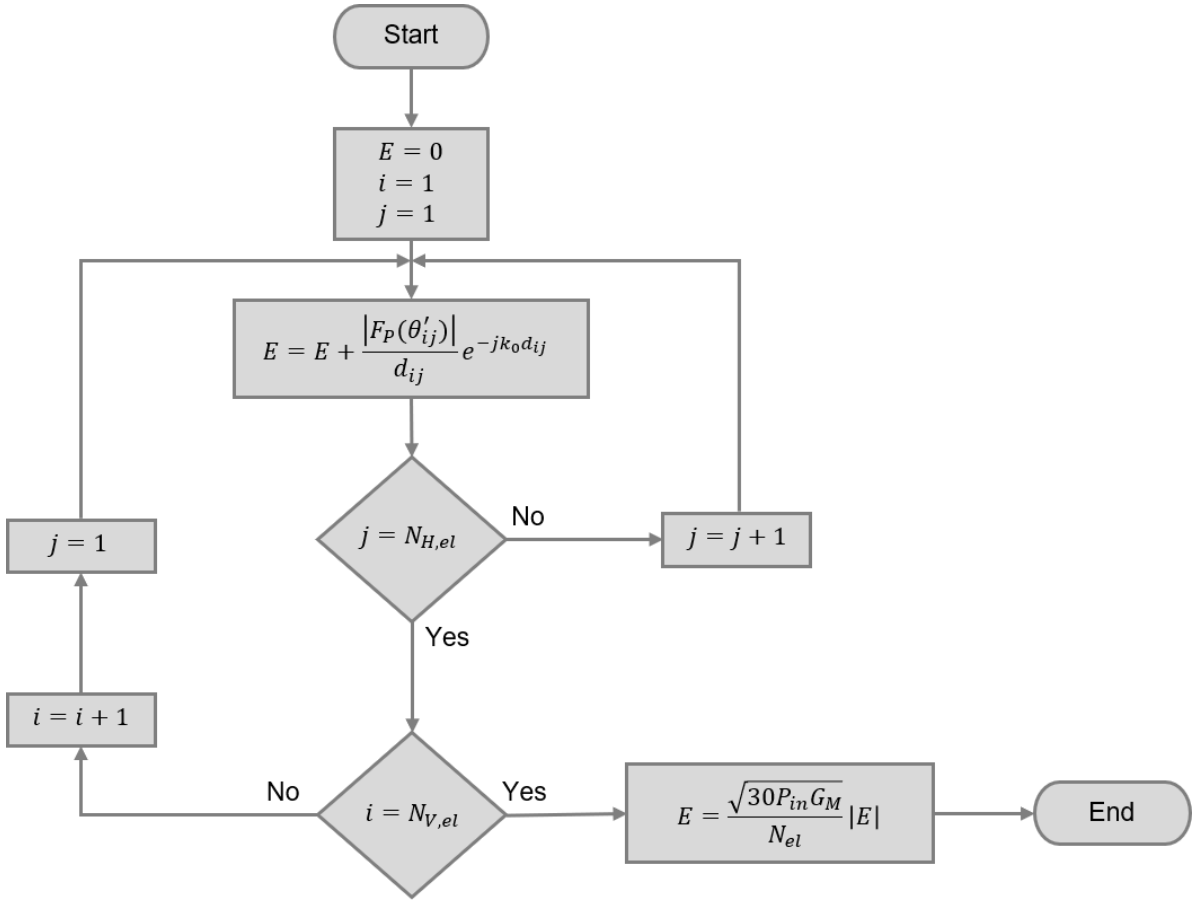

Figure 3.8. Electric field computation for a planar array in the near-field at a distance d.

Note that, for example, for an antenna formed by 12 vertical elements, 8 horizontal elements and 4 transmitters per column, meaning 3 elements per transmitter, the analysis is done for a planar array composed of 3 vertical elements and 8 horizontal elements, the number of elements being 24 and the input power being the power delivered to said section.

3.3.4 General Zone Model

Since the far-field gain-based model is suited for distances above 3λ, the near-field analysis is performed inside the radiative near-field zone. As discussed in Section 2.4.1, in this zone the electric and magnetic fields are directly interrelated by Z_0 (120π). Figure 3.9 shows the power density as a function of distance for an active NR antenna operating in the 3.6 GHz band, with a total input power of 10 W, 12 vertical elements, 8 horizontal elements and 4 transmitters per column.

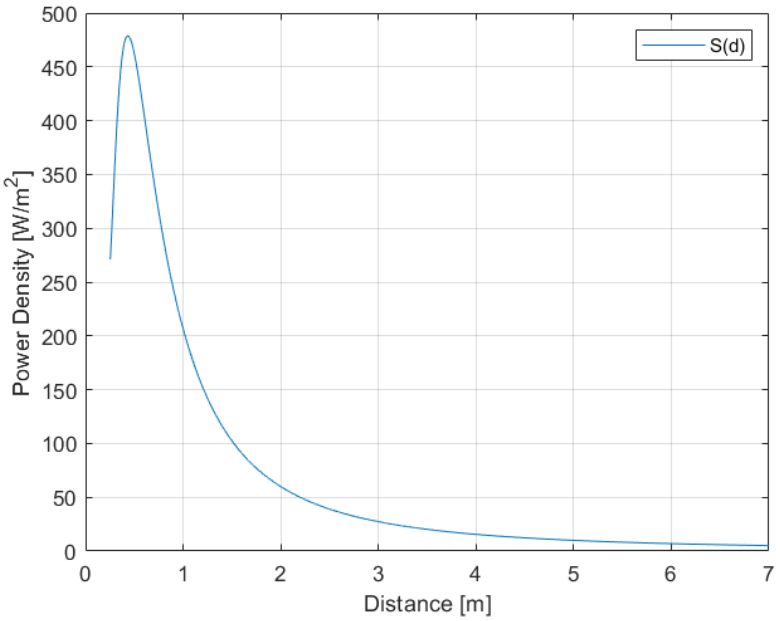

Figure 3.9. Power density as a function of distance for an active 3.6 GHz NR antenna in the near-field.

In order to account for the monotonically decreasing behaviour of the power density with distance, an interpolation method is applied in the near-field. Note that the following methods for the exclusion zone estimation are based on [Antu12]. The interpolation function that best suits the power density behaviour depends on the number of vertical elements, or simply the number of elements for linear arrays, being:

$$S_{fit}(d) = \begin{cases} \frac{P_{in}G_M}{4\pi} \frac{1}{(a_0 + a_1 d + a_2 d^2)}, & N_{el}, N_{V,el} < 8 \\ \frac{P_{in}G_M}{4\pi} \frac{1}{(a_0 + a_1 d + a_2 d^2 + a_3 d^3)}, & N_{el}, N_{V,el} \geq 8 \end{cases} \quad (3.35)$$

where a_0, a_1, a_2 and a_3 are the coefficients of the rational function $S_{fit}(d)$. One should note that these coefficients are normalised to the input power and gain of the antenna. The interpolation is based on the maxima of $S(d)$ and, since $S(d)$ may have a low number of maxima, equally spaced points along the power density curve after the last maximum are also used. The number of equally spaced points equal to 50 leads to acceptable results, although this parameter can be chosen by the user.

In order to determine the maximum values of the power density function, all samples are analysed along d, where each sample is compared with the previous and the following ones, $S(d - \Delta_d)$ and $S(d + \Delta_d)$ respectively, where Δ_d is the distance between samples. The second sample is the first to be analysed and thus, by comparing it with the previous one, the first sample is also analysed. In order to comply with the monotonically decreasing behaviour of the power density, a maximum is neglected when it is less than the following one. The interpolation method is done using the Curve Fitting Toolbox in MATLAB. The tool determines the fitting coefficients and returns the root mean square error (RMSE). If the RMSE is high the function runs up again until the best possible RMSE is found.

The obtained function $S_{fit}(d)$ may have, for a given distance, lower values than $S(d)$. To ensure the worst-case scenario, the upper bound method is used [Antu12], i.e., the largest relative difference between $S_{fit}(d)$ and $S(d)$, $\Delta_{S,max}$, is applied to $S_{fit}(d)$, the upper bound power density function being

$$S_{up}(d) = \left(1 + \Delta_{S,max}\right)\ S_{fit}(d) \tag{3.36}$$

where:

$$\Delta_{S,max} = \max\left\{\left(\frac{S(d) - S_{fit}(d)}{S_{fit}(d)}\right)\right\} \tag{3.37}$$

The upper bound method ensures that $S_{up}(d)$ is the vertically moved $S_{fit}(d)$, Figure 3.10. In order to estimate $S_{up}(d)$, the minimum value used for d is imposed by the model's minimum distance of 3λ. With the increase in distance, the upper bound method starts to perform poorly due to the values of the power density being some orders of magnitude less than 1. The program has shown to have acceptable results for a maximum distance between 8 m and half of the antenna's far-field distance, although this parameter can be changed by the user.

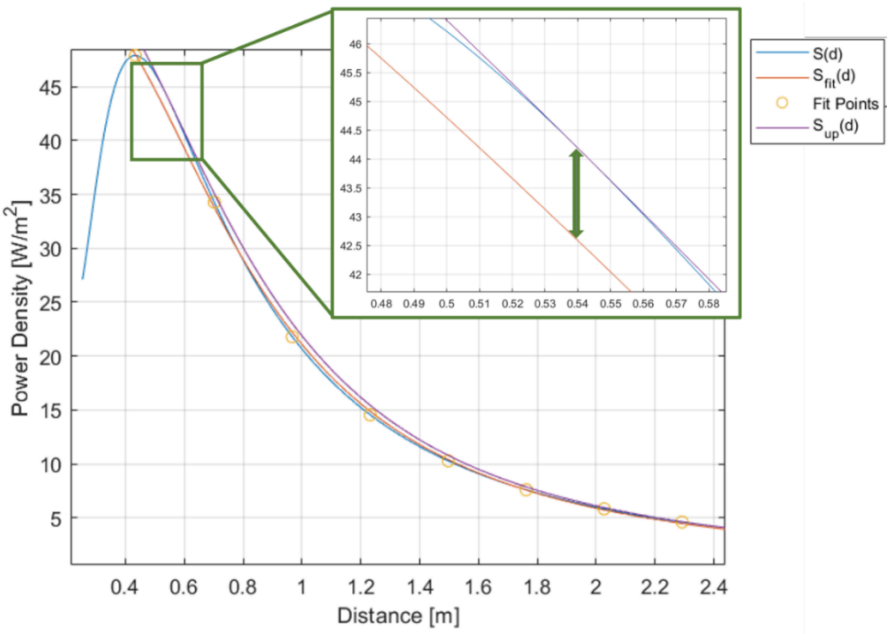

Figure 3.10. Power density interpolation over distance for an active 3.6 GHz NR antenna.

For distances above the far-field one, the far-field model becomes more accurate and, due to its simplicity, it is used in such circumstances. In order for the complete model to be realistic, it needs to vary continuously from the near-field zone to the far-field one because, as stated in Section 2.4.1, EMFs vary continuously as a function of distance. This continuity can be ensured by applying a final interpolation. The interpolation points are equally spaced and along the $S_{up}(d)$ curve with the final point being at the far-field distance with the far-field value for the power density. In order to ensure the interpolation is accurate, the number of points should be the minimum needed for the interpolation process, guarantying that the function passes through the far-field point. The interpolation function is also given by (3.35). The final power density expression is then as follows:

$$S_{final}(d) = \begin{cases} S_{near-field}(d), & 3\lambda \leq d < d_{ff} \\ \dfrac{P_{in} G_M}{4\pi d^2}, & d \geq d_{ff} \end{cases} \tag{3.38}$$

where:

- $S_{near-field}(d)$: the final interpolation function obtained for the power density in the near-field.

In this way, for distances up to the far-field distance the complete model coincides with the estimated one for the near-field region, and it coincides with the far-field model for distances above the far-field distance, Figure 3.11.

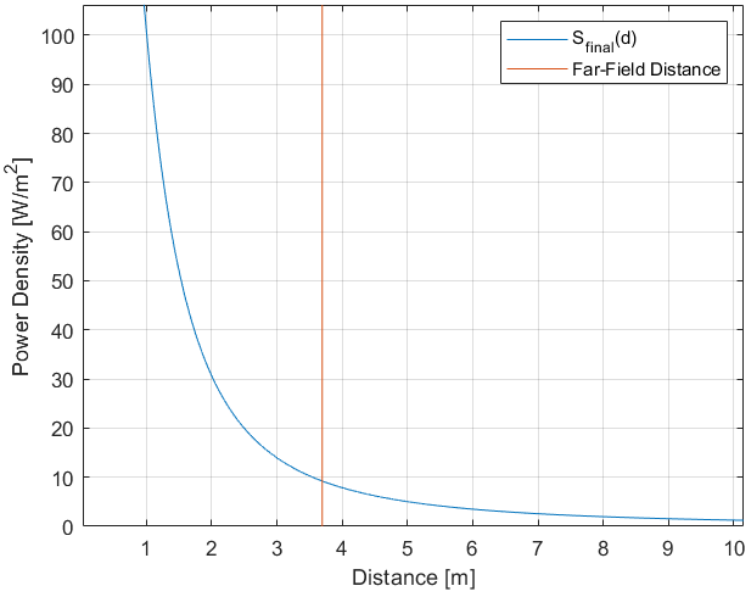

Figure 3.11. $S_{final}(d)$ over distance for an active 3.6 GHz NR antenna.

The relevant variables used in the simulation are the minimum, d_{min}, and maximum, d_{max}, distances and the number of samples, N_{samp}, contained in this range. The value of d_{min} is 3λ, which is the lower boundary for the near-field model and d_{max} should be greater than the far-field distance. According to [Antu12], for an acceptable model accuracy, the number of samples should exceed 60 000. The number of samples used in simulations is 100 000, although it is a parameter that can be chosen by the user. Logically, the more samples used in the simulation, the better the model's accuracy and the longer the computation time. The sampling interval, or the distance between samples, is given by:

$$\Delta_d = \frac{d_{max} - d_{min}}{N_{samp}} \tag{3.39}$$

As stated at the beginning of Section 3.3, the goal of the exclusion zone evaluation model is to determine its dimensions for a given BS. The model developed so far estimates the power density for any given distance, inside the model's range, at the direction of maximum radiation. The value for the front border, D_{front}, can thus be computed. The dimensions for the remaining directions can be calculated by applying correction factors to D_{front}, or the maximum antenna gain, as described in Section 2.4.3 for the cylindrical exclusion zone [OFRC05].

Under the circumstances of the developed model, the total normalised power density as a function of distance is given by:

$$S_{norm}^{tot}(d) = \sum_{i=1}^{N_{sys}} \left(\frac{S_{final,i}(d)}{S_{ref,i}} \right) \tag{3.40}$$

where:

- $S_{final,i}(d)$: power density function obtained by the model for the i^{th} communication system.

As previously mentioned, the distance D_{front} is such that the total normalised power density is equal to 1. Since solving (3.40) as a function of distance has great computation complexity, considering that $S_{norm}^{tot}(d)$ is a function of N_{sys} terms with 2 equations to describe each one, instead (3.40) is iterated over the distance samples. Bearing in mind that $S_{norm}^{tot}(d)$ is a discrete function with Δ_d as the sampling interval, and due to the approximations and numerically precision of MATLAB, there may be no defined distance in which $S_{norm}^{tot}(d)$ is exactly 1. Taking this fact into account, and in a more conservative approach, D_{front} is then given by the minimum distance that ensures $S_{norm}^{tot}(d) < 1$, Figure 3.12.

Regarding the simulation, d_{min} should be equal to $3\lambda_{max}$, where λ_{max} is the maximum wavelength of all the systems present in the simulation, i.e., of the system working at the lowest frequency. The maximum distance used, d_{max}, should be greater than D_{front}. The main input parameters of the MATLAB program are the systems' frequency, P_{in}, G_M, Δ_{es}, N_{el}, $N_{V,el}$, $N_{H,el}$, antenna dimensions, N_{samp}, d_{max} and d_{min}.

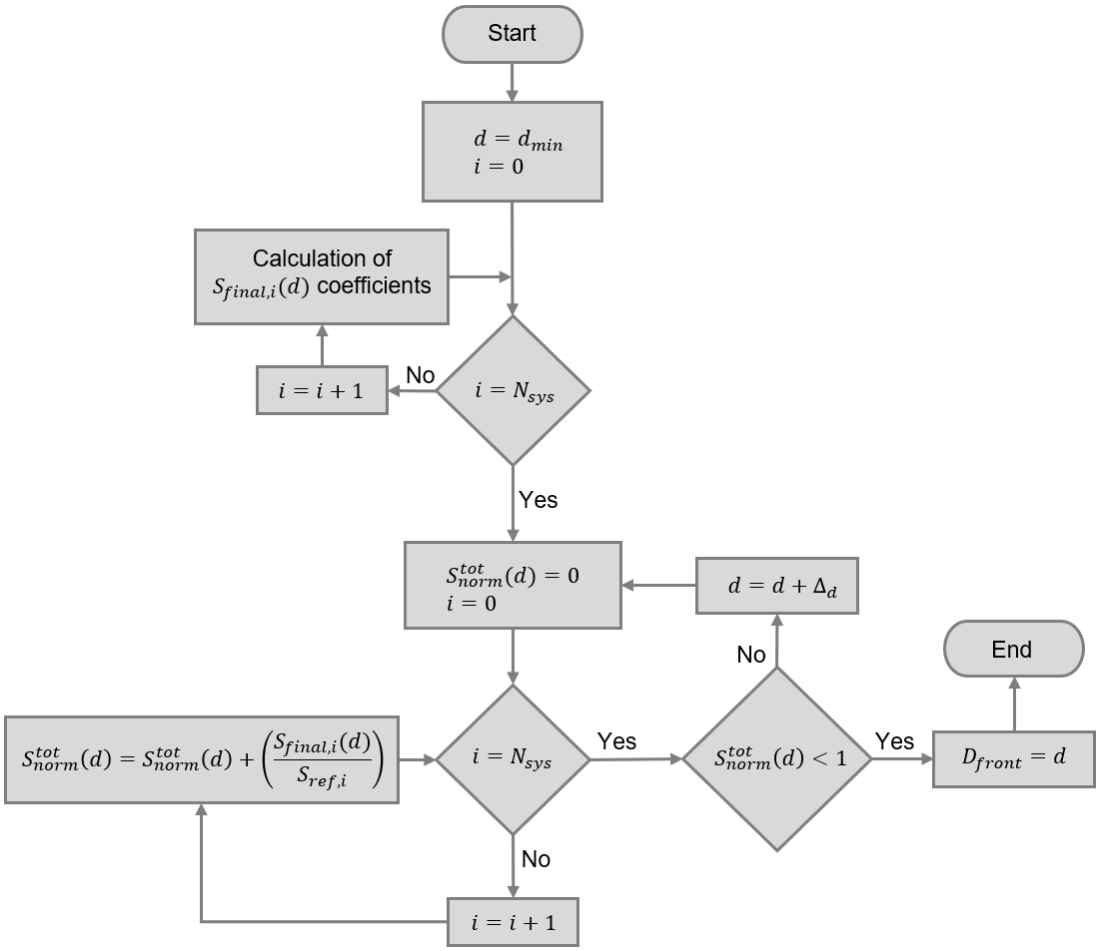

Figure 3.12. Computation of D_{front} with the exclusion zone evaluation model.

The number of carriers, N_c, and the level of MIMO in a communication system can be accounted for in the input power of the antenna. For example, a system with 2 carriers with 20 W per carrier has P_{in} equal to 40 W. The same reasoning is applied to systems with MIMO technology. This method leads again to a more conservative approach, since it assumes that the direction of maximum radiation is the same for different carriers and different MIMO beams. Equal results are achieved by instead multiplying $S_{final,i}(d)$ by the system's N_c and MIMO level.

In order to compute the complete BS exclusion zone, the distances for the remaining directions are calculated by either applying correction factors to D_{front} or to the antenna gain. From the analysis of the radiation patterns of each system, the normalised gains for each direction are extracted and applied as correction factors for the antenna gain. The simulation is run again with the new antenna gain for each system involved and the compliance distance for the desired direction is calculated. The front-to-back ratio (FTBR) present in the antenna's catalogue should be used as a correction factor to the antenna gain in order to compute D_{back}.

One should note that both the antenna's radiation pattern and the FTBR refer only to distances in the far-field zone. As discussed in Section 2.4.1, in the near-field region the radiation pattern is a function of distance, Figure 3.13. Nevertheless, for the lack of suitable information, the antenna's radiation pattern and the FTBR should be used to calculate the desired correction factors since they overestimate the EMFs in the vicinity of the antenna. When a downtilt is used, the correction factors applied to D_{top} and D_{bottom} are given respectively by (2.11) and (2.12).

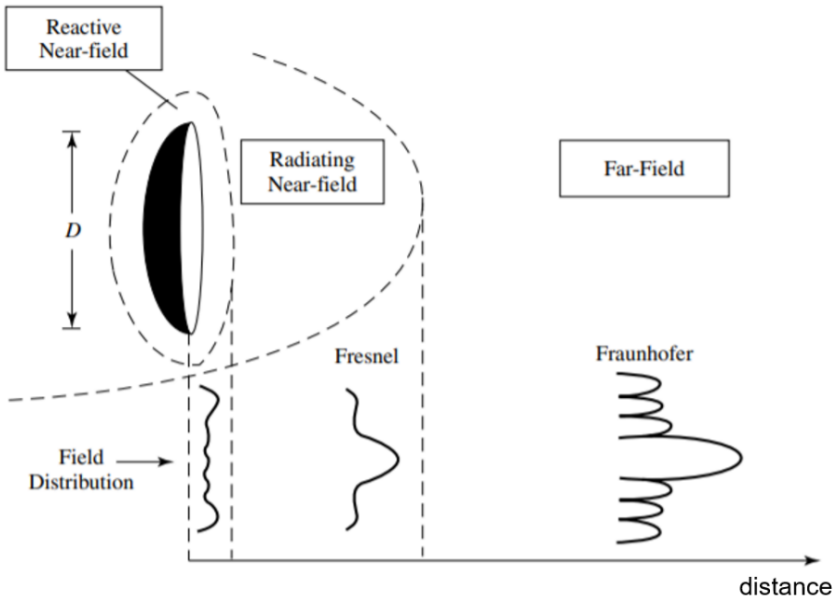

Figure 3.13. Radiation pattern variances from reactive near-field toward the far-field (adapted from [Bala05]).

One needs to note that the methods approached in this model do not take into consideration the surrounding environment. The presence of different objects in the vicinity of the antenna, such as poles, masts, and buildings, will influence the power density levels in this region.

3.4 Coverage and Capacity Planning

The main goal of this subsection is to develop a model for the estimation of the BS's coverage radius as well as the cell-edge throughput. The purpose is to understand how the coverage and capacity of a cell vary according to the imposed EMF restrictions at the BS. Coverage planning is defined by the radio

link budget evaluation for both UL and DL with no specific concern for the capacity, [Viei18]. As described in Section A.1, the maximum allowed path loss (MAPL) is computed from the link budget evaluation. As it can be seen from (A.1) and (A.4), the MAPL depends on the receiver sensitivity, which in turn depends on the SINR required for the intended service. With the appropriate propagation model, which depends on the scenario, frequency bands and BS/MT heights, it is then possible to compute the coverage radius of the BS. This sequence of steps is summarised in Figure 3.14.

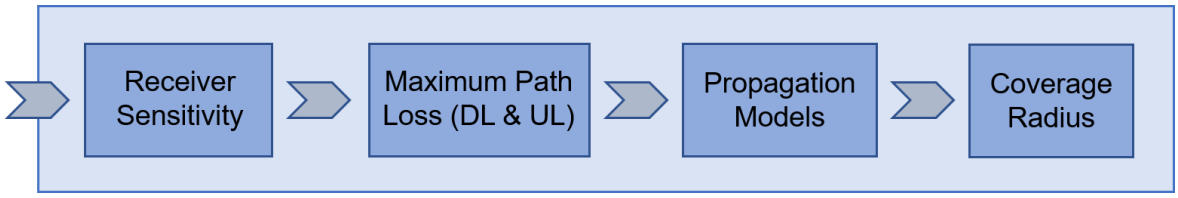

Figure 3.14. The coverage planning process (based on [Viei18] and [Belc18]).

As it can be interpreted by (A.4), by fixing the receiver's noise figure and the minimum required SINR, the sensitivity of the receiver depends on the used numerology. As the numerology increases, the required minimum received power increases, therefore the numerology that minimises the receiver's sensitivity, and in turn maximises the coverage radius, is the numerology 0 with SCS of 15 kHz. The interference margin may range from 1 to 3 dB and it depends on the cell structure, the number of active users and their respective services, [Corr20].

Regarding the coverage given by a BS, a parameter with paramount importance for the QoS offered to the user is the probability of being covered at a given distance from the BS. Logically, a mobile operator is interested in offering a high coverage probability inside the cell area. The definition of coverage probability is presented in Section A.1. As it can be interpreted from (A.6) and (A.7), for a given coverage probability set by the operator, the coverage radius can be computed for the value of $\overline{P_{r,R}}$ instead of $P_{r\,min}$. One may notice that, for a coverage radius calculated for the receiver's sensitivity, the probability of being covered at cell-edge is 50%, which is a small value compared to the operators' usual goal of 90% of coverage probability for the edge of the cell.

Having computed the necessary receiver's sensitivity, the next step is to compute the MAPL for the DL, which is the connection of interest for this thesis. The expressions for the EIRP and received power in the DL are given by (A.2) and (A.8) respectively, and the MAPL is then defined in (A.9). Once the MAPL is computed, the coverage radius can be calculated by applying a suitable propagation model. Combining (A.5) with (A.9), (2.3) can be rewritten as:

$$R_{cell\,[\mathrm{km}]} = 10^{\frac{P_{Tx\,[\mathrm{dBm}]}+G_{Tx\,[\mathrm{dBi}]}-L_{Tx\,[\mathrm{dB}]}-P_{r\,\min\,[\mathrm{dBm}]}-\Delta P_{r\,[\mathrm{dB}]}+G_{r\,tot\,[\mathrm{dBi}]}-L_{Rx\,[\mathrm{dB}]}-L_{ref\,[\mathrm{dB}]}}{10\ a_{pd}}} \tag{3.41}$$

The average power decay with distance and the reference path loss are obtained from the propagation models. The propagation models used in this work are presented in Section A.2 (Annex A). For the NR 700 MHz band, the used propagation model is the Okumura-Hata, which is valid for [150, 1 500] MHz, [Corr20]. For the NR 3.6 GHz band, the WINNER II model is used, which is valid for [2, 6] GHz, [WINN07]; the WINNER II model also includes the Line-of-Sight (LOS) and Non-LOS (NLOS) cases. It is important to note that these propagation models are only valid for outdoors path loss. To completely

characterise coverage, one needs to also include a model for the extra indoors attenuation, presented also in Section A.2. This is a statistical model based on measurements in Lisbon and it takes into consideration the building floor at which the user is located relative to a threshold floor value based on the used frequency.

As stated in Section 2.2.2, capacity dimensioning considers the hexagon as the typical cell shape, nevertheless, a uniform circular distribution of users is shown in Figure 3.15 for illustration purposes.

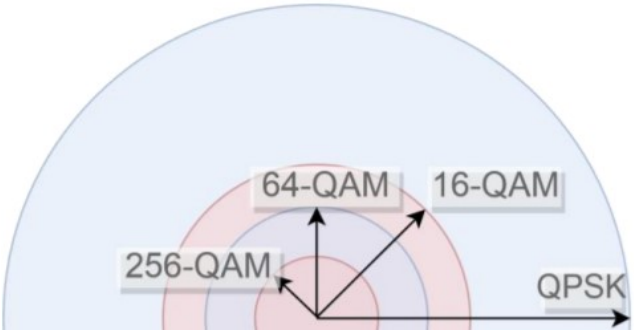

Figure 3.15. Modulation radius distribution in a cell (extracted from [Viei18]).

The total number of users in a given cell can be given by the sum of users served by each modulation, which is a good approximation if the traffic profile consists mainly of mobile data services:

$$N_{users}^{cell} = \sum_{i=1}^{4} N_{users}^{4^i-QAM} \tag{3.42}$$

where:

$$N_{users}^{4^i-QAM} = \left\lfloor N_{users}^{cell} \ \frac{A_{4^i-QAM}\,[\mathrm{km}^2]}{A_{cell}\,[\mathrm{km}^2]} \right\rfloor = \left\lfloor N_{users}^{cell} \ \frac{R_{4^i-QAM}^2\,[\mathrm{km}] - R_{4^{i+1}-QAM}^2\,[\mathrm{km}]}{R_{QPSK}^2\,[\mathrm{km}]} \right\rfloor \tag{3.43}$$

and:

- A_{4^i-QAM}: area of the cell served by the $4^i - QAM$ modulation;
- R_{4^i-QAM}: radius for the $4^i - QAM$ modulation.

One must note that (3.43) is independent of the shape considered for the cell, and that, since the 256-QAM modulation is the highest modulation considered for NR, the radius for the modulation above is 0.

The modulation borders are established when with an inferior modulation scheme it is possible to achieve a better throughput than with a higher one. This means that there is a value for the SINR in which the throughput is equal for adjacent modulations, which is where the location of the modulation border is established. In order to establish these borders, expressions that relate the throughput with the SINR were obtained, being presented in Section A.4 of Annex A.

In any given scenario, the operator installing the BS has a minimum QoS goal for cell-edge users, as well as a target coverage radius for the desired area. Assuming constant noise and interference, for a fixed distance from the BS, the SINR at the receiver decreases as the power transmitted by the BS antennas decreases and increases as the transmitted power increases. Since the throughput per RB is a function of the received SINR, the restrictions imposed on the BS transmitted powers have a clear

impact on the QoS offered by the operator. Depending on the EMF level of a given location, the NR antennas may have to transmit at a power lower than desired by the operator, which may cause a decrease in service quality or a reduction in the coverage radius, which in turn increases the need for more BSs to cover the desired area, increasing the operator's cost.

3.5 Output Evaluation Metrics

This subsection aims at defining and organising the evaluation metrics corresponding to the model's outputs presented in Figure 3.1, which are:

- Power Density Level;
- Exclusion Zone Distance;
- Exclusion Zone Variation;
- NR Exclusion Zone Contribution;
- Coverage Radius;
- Cell-edge Throughput per RB.

The power density level as a function of distance for any given direction can be given by:

$$S_{final}(d,\theta,\varphi) = \frac{P_{in}G(\theta,\varphi)}{4\pi} \begin{cases} S_{nf}^{norm}(d), & 3\lambda \leq d < d_{ff} \\ \dfrac{1}{d^2}, & d > d_{ff} \end{cases} \tag{3.44}$$

$$S_{nf}^{norm}(d) = \begin{cases} \dfrac{1}{(a_0 + a_1 d + a_2 d^2)}, & N_{el}, N_{V,el} < 8 \\ \dfrac{1}{(a_0 + a_1 d + a_2 d^2 + a_3 d^3)}, & N_{el}, N_{V,el} \geq 8 \end{cases} \tag{3.45}$$

where:

- $S_{nf}^{norm}(d)$: power density function for the near-field, normalised to input power and antenna gain.

The coefficients in (3.45) are obtained by the interpolation method demonstrated in Section 3.3.4.

The exclusion zone distance for any given direction, $D_{excl}(\theta,\varphi)$, is such that:

$$\sum_{i=1}^{N_{sys}} \left(\frac{S_{final,i}(d,\theta,\varphi)}{S_{ref,i}} \right) = 1 \tag{3.46}$$

Due to the computational complexity discussed in Section 3.3.4, an iteration over the distance samples is executed until (3.47) is satisfied. Note that D_{excl} is being defined as the general nomenclature for the compliance distance in an undefined direction. For example, for the back of the antenna, D_{excl} degenerates into D_{back}, and for the front, D_{excl} degenerates into D_{front}.

The exclusion zone variation in any given direction is then given by:

$$\Delta_{excl\,[\%]} = \left(\frac{D_{excl\,[\mathrm{m}]}^{W\,NR} - D_{excl\,[\mathrm{m}]}^{W/O\,NR}}{D_{excl\,[\mathrm{m}]}^{W/O\,NR}} \right) 100 \tag{3.47}$$

where:

- $D_{excl}^{W\ NR}$: exclusion zone distance with NR (W NR);
- $D_{excl}^{W/O\ NR}$: exclusion zone distance without NR (W/O NR).

In order to evaluate the contribution of NR to the exclusion zone distance, a metric is given by:

$$\eta_{NR\,[\%]} = \left(\frac{D_{excl\,[\mathrm{m}]}^{W\ NR} - D_{excl\,[\mathrm{m}]}^{W/O\ NR}}{D_{excl\,[\mathrm{m}]}^{W\ NR}} \right) 100 \tag{3.48}$$

where:

- η_{NR}: NR contribution to the exclusion zone distance.

The coverage radius of a cell in any given environment is given by:

$$R_{cell\,[\mathrm{km}]} = 10^{\frac{P_{Tx\,[\mathrm{dBm}]} + G_{Tx\,[\mathrm{dBi}]} - L_{Tx\,[\mathrm{dB}]} - P_{r\,\min\,[\mathrm{dBm}]} - \Delta P_{r\,[\mathrm{dB}]} + G_{r\,tot\,[\mathrm{dBi}]} - L_{Rx\,[\mathrm{dB}]} - L_{ref\,[\mathrm{dB}]}}{10\ a_{pd}}} \tag{3.49}$$

where:

$$P_{r\,\min\,[\mathrm{dBm}]} = -174 + 10\log_{10}\left(B_{RB\,[\mathrm{Hz}]}\right) + F_{N\,[\mathrm{dB}]} + \rho_{SINR\,\min\,[\mathrm{dB}]} + M_{I\,[\mathrm{dB}]} + M_{SF\,[\mathrm{dB}]} \tag{3.50}$$

$$\Delta P_{r\,[\mathrm{dB}]} = \overline{P_{r,R\,[\mathrm{dBm}]}} - P_{r\,\min\,[\mathrm{dBm}]} \tag{3.51}$$

Note that all the above parameters necessary to compute the cell radius are defined in Section A.1.

The cell-edge throughput per RB is defined as:

$$R_{b\,[\mathrm{bit/s}]}^{RB} = 2^{\mu}\ \frac{N_{MIMO}}{2} \begin{cases} \dfrac{2.34201 \times 10^{6}}{14.0051 + e^{-0.577897\ \rho_{SINR\,[\mathrm{dB}]}}}, & -10 \le \rho_{SINR\,[\mathrm{dB}]} \le 5.56 \\ \dfrac{47613.1}{0.0926275 + e^{-0.295838\ \rho_{SINR\,[\mathrm{dB}]}}}, & 5.56 < \rho_{SINR\,[\mathrm{dB}]} \le 13.03 \\ \dfrac{26405.8}{0.0220186 + e^{-0.24491\ \rho_{SINR\,[\mathrm{dB}]}}}, & 13.03 < \rho_{SINR\,[\mathrm{dB}]} \le 25.75 \\ \dfrac{26407.1}{0.0178868 + e^{-0.198952\ \rho_{SINR\,[\mathrm{dB}]}}}, & \rho_{SINR\,[\mathrm{dB}]} > 25.75 \end{cases} \tag{3.52}$$

As it can be observed, a minimum SINR is necessary to define the radius of the cell, defining also the throughput per RB for that given SINR.

3.6 Model Assessment

In order to assess the developed models, a series of empirical tests were performed before the comparison with measurements and analysis of results. Since the general model comprises two major parts, the exclusion zone evaluation, and the coverage and capacity planning, the assessment was divided accordingly, the tests being detailed in Tables 3.1 and 3.2 respectively. The complementary data regarding model assessment, as well as the corresponding descriptions, are presented in Annex B.

The validity of the exclusion zone evaluation model can be evaluated according to the behaviour of the front border of the exclusion zone, D_{front}, under different circumstances. Since the compliance distances for all directions are computed based on the antenna gain, it is reasonable to extrapolate the behaviour

of D_{front} when considering the remaining directions. As it can be seen in Figures 3.16 and B.1, an increase in input power and maximum antenna gain causes D_{front} to increase as expected. It is only logical that when the antenna radiates more intensely in one direction, the compliance distance also increases in the said direction.

Table 3.1. Empirical tests performed to validate the exclusion zone evaluation model.

Test ID	Validation Element
1	Verify if the exclusion zone front border increases with the increase of the antenna input power and antenna gain.
2	Verify if the exclusion zone front border increases with the increase of the number of mobile communication systems present at the BS.
3	Verify if the exclusion zone front border decreases with the increase on the reference values for exposure.

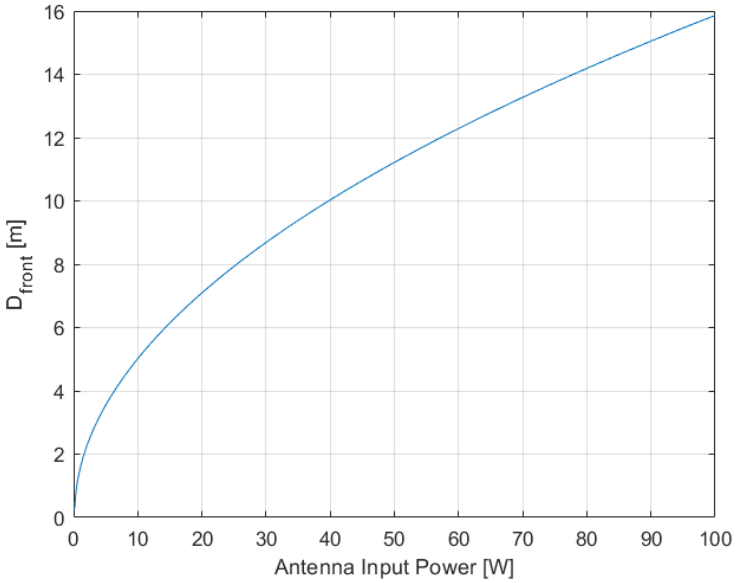

Figure 3.16. D_{front} as a function of the antenna input power.

Figure 3.17 represents the behaviour of D_{front} according to the number of systems present at the considered BS. For one system, it is considered that only NR at the 3.6 GHz band is present. The remaining systems considered for this scenario are GSM900, UMTS2100, LTE800, LTE1800 and LTE2600. As the number of systems increase at the BS, the number of radiating elements also increases, elevating the EMF level in the vicinity of the BS and increasing the compliance distance.

In order to verify the coverage and capacity model, the cell radius, the SINR and the cell-edge throughput were evaluated for different parameters indicated in Table 3.2. For all the performed tests, the urban, suburban and rural environments were compared, as well as the Okumura-Hata and WINNER II models, so as to verify if the program performs as expected. For example, for the same input parameters, an urban environment should have a higher propagation loss than a rural one. For the test of the SINR against the LOS and NLOS situations, the only propagation model used is the WINNER II since this is

the only one that differentiates these scenarios. The test IDs number 2, 3, 4, and 5 are presented and thoroughly described in Section B.2 (Annex B).

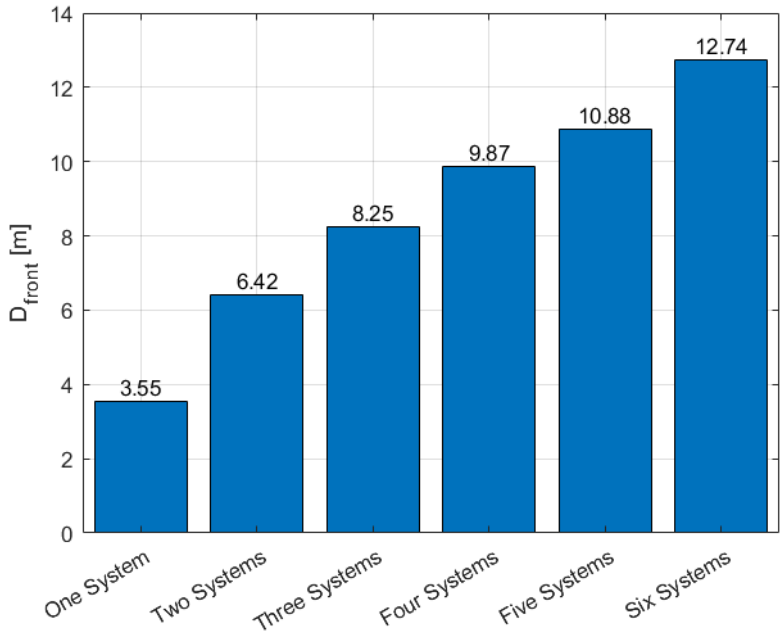

Figure 3.17. D_{front} vs. number of mobile communications systems present at the BS.

Table 3.2. Empirical tests performed to validate the coverage and capacity model.

Test ID	Validation Element
1	Verify if the cell radius increases with the BS height, MT height and input power.
2	Verify if the cell radius decreases with the increase in frequency and coverage probability.
3	Verify if the cell radius is higher for higher numerology configurations.
4	Verify if the SINR is higher for the LOS situation when compared with the NLOS one.
5	Verify if the SINR and the cell-edge throughput increase with the input power, and comparison between outdoors and indoors users

The cell radius as a function of the BS height for the 700 MHz and the 3.6 GHz bands is represented in Figures 3.18 and 3.19 respectively. As it can be observed in all cases, as the BS height increases, the cell radius also increases as expected. One may notice that the cell radius is greater for the 700 MHz band than for the 3.6 GHz one, which is due to the propagation loss being higher for higher frequencies. The cell radius is also considerably greater in rural scenarios comparing to urban and suburban ones, due to the fact that rural scenarios have a lower propagation loss.

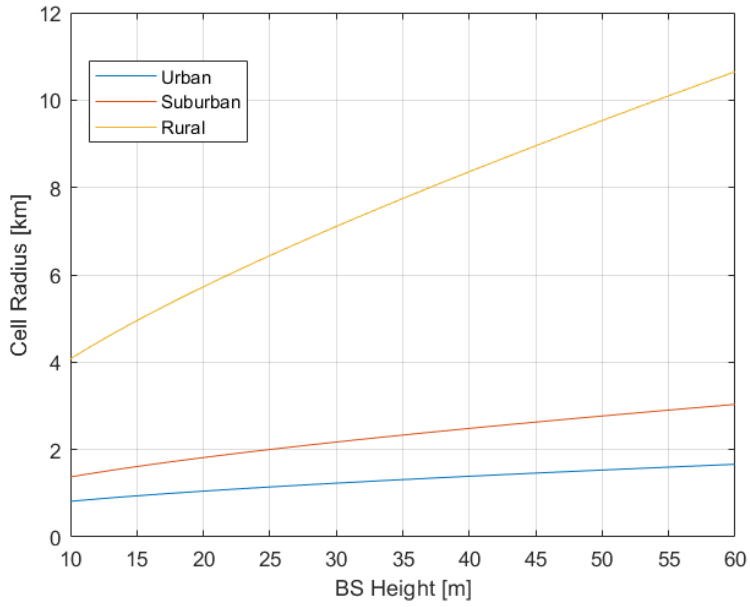

Figure 3.18. Cell radius versus BS height for the 700 MHz band.

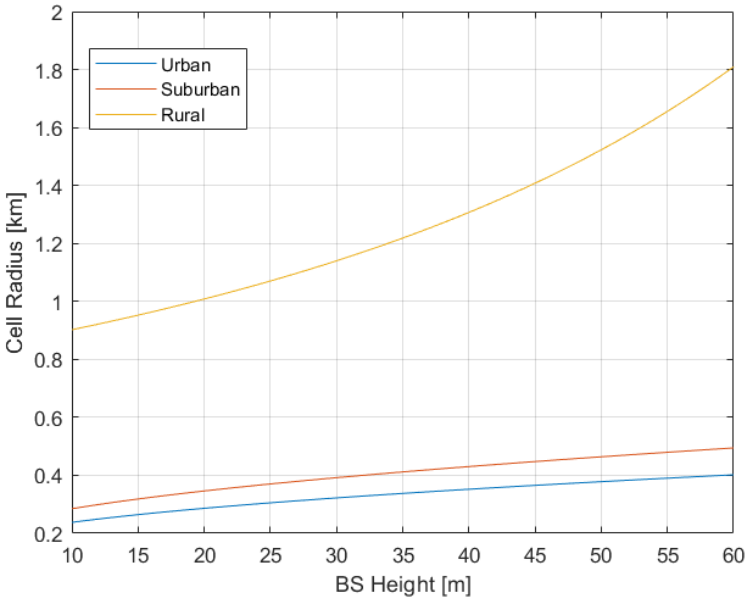

Figure 3.19. Cell radius versus BS height for the 3.6 GHz band.

3.7 Comparison with Experimental Results

Experimental EMF measurements were conducted in operational BSs in order to analyse the real behaviour of the power density in the vicinity of the BSs' antennas. These measurements allow for the comparison of the measured data with the developed theoretical model, thus evaluating its deviation from the experimental results.

In order to carry out the measurements, a spectrum analyser (Anritsu MS2713E) together with a near-isotropic antenna (Anritsu 2000-1791-R) were used, since the analyser allows for the separate examination of each frequency band. The results were then stored as retrievable text files where the average power density for each measured frequency was recorded. The analyser is also capable of testing whether the performed measurement is within the ICNIRP limits performing a fail/pass test.

The characteristics of the BSs where the measurements were performed are presented in Table 3.3. Note that a single passive antenna was used for the legacy systems. As it can be observed, the measurements were conducted in 4 sectors, 2 for each BS. Ideally, the measurement campaign for each sector should be such that the sets of measurement points are offset 90º from each other, forming a cross-like pattern, which would allow the analysis of the power density behaviour for the front, sides, and back of the antennas. Due to constraints in the access and layout of the BSs, 3 sets of points separated by 45º were measured for each sector in BS1. For the BS2, measurements were performed for the front and back of the antennas. The measurement points were spaced by 0.5 m and the measured values were recorded for 1 minute for each point for the entire frequency band, [0.7, 4] GHz. Note that, as stated in Section 2.4.2, the compliance reference levels are for exposures with a duration higher or equal to 6 minutes. According to [OSLA08], the 1-minute measurement window is sufficient in order to obtain values with an error inferior to 10%.

Table 3.3. Characteristics of the BSs where the measurements were conducted.

BS	Sector	Environment	Systems	Access Type	Measurement Directions
BS1	1	Urban Macrocell	GSM900, UMTS2100, LTE1800 and NR3600	Public, Upper Terrace	0º, 45º and 315º
	2			Public, Lower Terrace	
BS2	1			Restricted, Upper Terrace	180º
	2			Restricted, Lower and Upper Terrace	0º and 180º

The power density as a function of distance, $S(d)$, obtained from the measurement results and the theoretical model for set 1 of sector 1 of BS1, is presented in Figures 3.20 for GSM900 and UMTS2100, and 3.21 for LTE1800 and NR3600.

As it can be observed in Section C.1.1, the legacy antenna and the NR one are, respectively, 1.7 m and 2.7 m above the measuring equipment in the vertical plane. The computation of the power density for the desired directions should then take the three-dimensional radiation pattern into account by applying the normalised gains to the maximum antenna gain, as explained in Section 3.3.4. Since the 3-dimensional radiation pattern is not provided by antenna manufacturers, a 3D radiation pattern interpolation method based on the vertical and horizontal planes was used, [LCSF16], shown in Annex E. Note that, for the 0º measurement direction in BS1, the vertical radiation pattern should be used for NR3600 instead since the azimuthal angle is 0º with respect to the active antenna. In order to

compute the theoretical results, the downtilt of each system was considered so as to obtain the correct inclination angle of the radiation pattern.

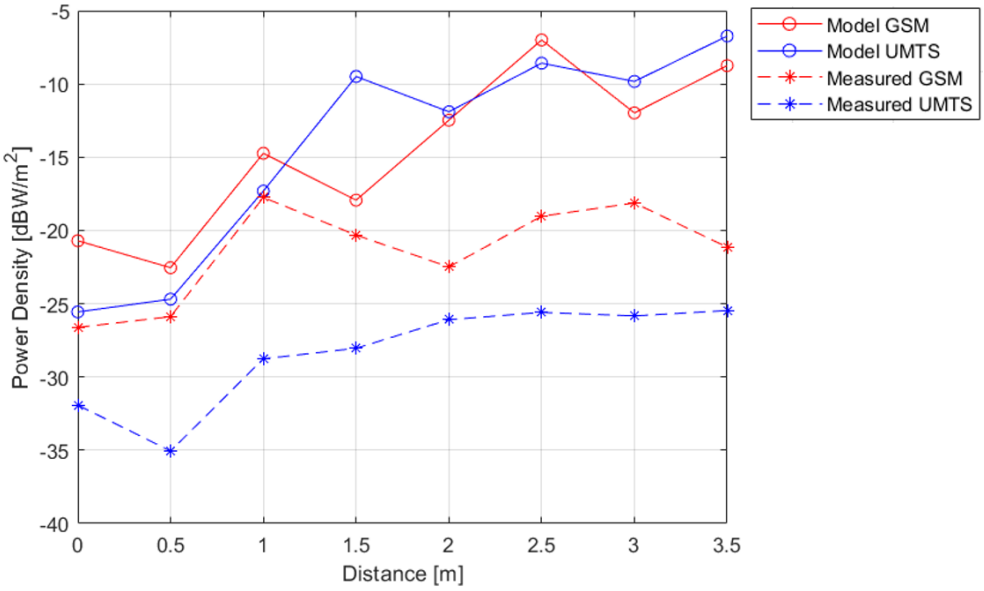

Figure 3.20. Measured versus theoretical results of $S(d)$ for GSM900 and UMTS2100, for set 1 of BS1's sector 1.

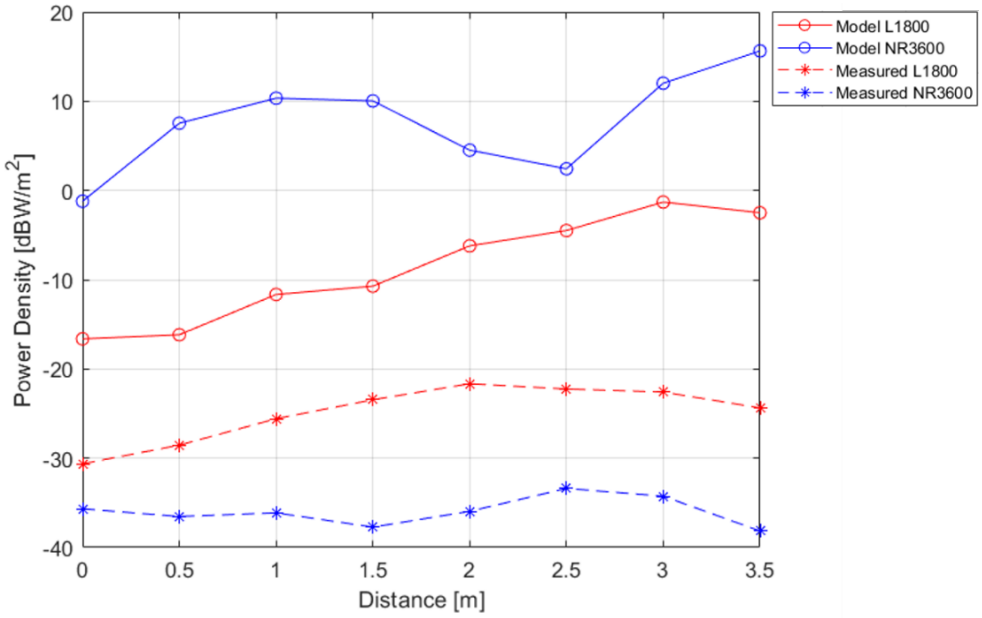

Figure 3.21. Measured versus theoretical results of $S(d)$ for LTE1800 and NR3600, for set 1 of BS1's sector 1.

As it can be observed from Figures 3.20 and 3.21, the exposure levels from the experimental results are lower than the exposures obtained from the theoretical model. The lowest differences obtained for GSM and UMTS are 2.39 dB and 6.36 dB respectively. Regarding LTE1800 and NR3600, the model further overestimates the results with minimum differences of 12.37 dB and 34.47 dB respectively. As one can observe from the measurements, the power density tends to increase with the increase of the distance to the BS. This may be due to the fact that, in the vicinity of the BS, the variations in the antenna

gain, which can be seen in the radiation pattern, possess a higher weight in determining exposures than small variations in distance. As the distance increases, the measurement direction becomes closer to the direction of the antenna's main lobe. The fluctuations in power density that occur throughout the measurements may be due to nulls and secondary lobes on the antenna's radiation pattern.

The comparison between the measurements and the theoretical model results for sets 2 and 3 of sector 1 of BS1 is presented in Section D.1.1 from Figures D.1 to D.4. As it can be observed, the exposure levels obtained from the measurements are lower than the theoretical model results. The lowest differences for the second set are 3.39 dB for GSM, 1.33 dB for UMTS, 3.73 dB for LTE1800 and 37.87 dB for NR3600. For the third set, the lowest differences are 9.9 dB for GSM, 7.32 dB for UMTS, 11.8 dB for LTE1800 and 31.60 dB for NR3600.

The power density measurements and theoretical results for the first set of sector 2 of BS1 are presented in Section D.1.2, in Figures D.5 and D.6. As it can be observed, the model's results follow the behaviour of the measurements, overestimating exposure levels except for one point in GSM, two points in UMTS, and one point in LTE1800, where the model underestimates the measured power density. Excluding these points, the minimum differences obtained are 1.0 dB for GSM, 0.67 dB for UMTS, 4.03 dB for LTE1800 and 21.42 dB for NR3600. The results for the second and third set are presented also in Section D.1.2 from Figures D.7 to D.10. It can be seen that, generally, the results from the theoretical model also follow the behaviour of the measurements except for one point in GSM and another in UMTS, for the second set, where the model underestimates exposure. Excluding these, the minimum difference for set 2 is 0.18 dB for GSM, 4.02 dB for UMTS, 4.68 dB for LTE1800 and 30.88 dB for NR3600. Regarding the third set, the minimum difference is 1.20 dB for GSM, 2.73 dB for UMTS, 9.74 dB for LTE1800 and 33.93 dB for NR3600.

Regarding the points where the theoretical model underestimates exposure, the curves for each communication system obtained from the model suggest that these points coincide with nulls in the antennas' radiation pattern. Since the computation of the three-dimensional radiation pattern is subjected to errors, and that a radiation pattern can present large variations in gain over a small degree variation, the value for the antenna gain being used as an input for the theoretical model may be a few orders of magnitude lower than the real antenna gain at those points. Another source of error for this antenna gain drop is the total downtilt considered for the simulations. While, in reality, the total tilt angle is the sum of the mechanical and electrical downtilts, for simplicity purposes the total downtilt used in the theoretical model was considered to be fully mechanical. Since the electrical tilt produces changes in the radiation pattern and the mechanical one only rotates it, this simplification may cause differences between the considered and the real radiation patterns.

The results obtained from the measurements and the theoretical model for BS2 are presented in Section D.2 in Figures D.11 and D.12 for set 1, D.13 and D.14 for set 2, and D.15 and D.16 for set 3. The measurements for set 1 and 2 were conducted for the back and at the antenna level with respect to the passive antenna, Figure C.7, and thus the FTBR was used for the normalised gain of each legacy system. The measurements of NR3600 were performed 2 m below the active antenna in the vertical plane, being used the vertical radiation pattern for the computation of the theoretical results. For the

third set, the measurements were conducted at the front side and 2.2 m below the passive antenna, thus being used the vertical radiation pattern for the model's results. Due to technical difficulties, measurements for NR3600 were not conducted for the third set.

Since, for set 1 and 2, the measurements were performed practically at the antenna level, the power density tends to decrease with the increase in distance to the BS, as seen from the results. For the third set, the power density behaviour is similar to that of BS1's results, where the exposure tends to increase with distance due to the increase in antenna gain. As it may be observed, again the theoretical model overestimates the power density exposure levels in the vicinity of the antennas. The minimum exposure difference, regarding set 1, is then 13.39 dB for GSM, 18.55 dB for UMTS, 18.26 dB for LTE1800 and 24.90 dB for NR3600. For set 2, the minimum difference is 9.34 dB for GSM, 14.12 dB for UMTS, 12.05 dB for LTE1800 and 28.47 dB for NR3600. Regarding the third set, the minimum difference is 5.22 dB, 3.58 dB and 6.16 dB for GSM, UMTS and LTE1800 respectively.

In order to evaluate the performance of the theoretical model against the experimental data, the total average difference between the model's results and the measurements, μ_{model}, and its corresponding standard deviation, σ_{model}, were analysed. Firstly, the average difference for each set of points is computed:

$$\mu_{\Delta S} = \frac{1}{N_{points}^{set}} \sum_{i=1}^{N_{points}^{set}} (\Delta S_i) \tag{3.53}$$

$$\Delta S_i = S_{model,i} - S_{measure,i} \tag{3.54}$$

where:

- N_{points}^{set}: the number of points per set;
- $S_{model,i}$: the power density computed with the model at point i;
- $S_{measure,i}$: the power density obtained from measurements at point i.

The total average difference between the model's results and the measurements is then given by:

$$\mu_{model} = \frac{1}{N_{sets}} \sum_{i=1}^{N_{sets}} \mu_{\Delta S,i} \tag{3.55}$$

where:

- N_{sets}: the total number of measurement sets.

The standard deviation for each set of points is calculated by:

$$\sigma_{\Delta S} = \sqrt{\frac{1}{N_{points}^{set}} \sum_{i=1}^{N_{points}^{set}} (\Delta S_i - \mu_{\Delta S})^2} \tag{3.56}$$

The total standard deviation for the performance of the model is then computed as:

$$\sigma_{model} = \sqrt{\frac{1}{N_{sets}} \sum_{i=1}^{N_{sets}} \sigma_{\Delta S,i}^2} \tag{3.57}$$

The results are presented in Table 3.4. As it can be observed, due to higher exposure differences for the 180º direction, the averages for GSM, UMTS and LTE1800 were divided into two groups (0º/45º/315º and 180º). The results from the performance evaluation suggest that the model's results correctly follow the measurements' behaviour, due to the relatively low values of σ_{model}, and that it overestimates exposure levels, as seen previously from the theoretical results. One may note that the model significantly overestimates exposure regarding NR3600. This is due to the fact that the measurements for NR were obtained for 1 active user in the network. It is expected that when NR becomes commercially available in Portugal, the increase in the number of users will increase the radiation levels near the BS.

Table 3.4. Results for the performance of the theoretical model compared to measurements.

System	μ_{model} [dB]		σ_{model} [dB]
	0º/45º/315º	180º	
GSM900	7.25	14.00	3.48
UMTS2100	9.41	18.36	4.32
LTE1800	14.06	17.12	4.34
NR3600	38.17		6.02

There are, however, a few other considerations to point out regarding the simplifications assumed in the calculations that may explain differences between theoretical and experimental results.

For the purpose of simplicity, reflections on nearby surfaces (obstacles, ground, etc.) and radiated power from other sectors are not considered in the model's results, which may increase real exposure at the considered BS.

In order to obtain the antenna gain for the desired directions, the vertical and horizontal radiation patterns were used, and, as stated in Section 3.3.4, these provide the angular distribution of the antenna gain in the far-field zone only. Since the measurements were conducted in the near-field zone, the model may be overestimating exposure levels.

Another conservative approach being taken by the theoretical model is the assumption that the BS is always radiating the maximum power in each system. In reality, the transmitting power will depend on the traffic profile of the BS, as well as the implemented power control, which may decrease exposure levels near the BS.

The proposed model is then a practical tool for the estimation of power density levels in the vicinity of the BS, and consequently exclusion zone distances, with a confident safe margin as indicated by the results from Table 3.4.

Chapter 4

Results Analysis

This chapter presents the description of the considered scenarios as well as the simulation results and their respective analysis.

4.1 Scenarios Description

The variation of the EMF levels on BSs before and after the installation of NR, as well as the BS performance regarding coverage radius and throughput per RB, were evaluated by applying the developed models to representative cases of BS installations possessing GSM, UMTS and LTE. The scenarios chosen for this purpose are presented in Table 4.1, as well as the corresponding systems.

Table 4.1. Used mobile communications systems in each scenario.

Scenarios	Mobile Communications Systems Frequency Bands								
	GSM	UMTS		LTE				NR	
	900	900	2100	800	1800	2100	2600	700	3600
Urban.1	X		X		X				X
Urban.2	X		X				X		X
Urban.3	X		X		X		X		X
Suburban.1	X	X	X	X	X				X
Suburban.2	X	X		X		X		X	
Suburban.3	X		X	X	X	X		X	X
Rural.1	X	X		X				X	
Rural.2	X	X	X			X		X	
Rural.3	X	X	X	X		X		X	

This analysis takes the general three environments into account: three urban (Urban.1, Urban.2 and Urban.3), three suburban (Suburban.1, Suburban.2 and Suburban.3) and three rural (Rural.1, Rural.2 and Rural.3). The output powers per carrier/MIMO element for each system present in the considered scenarios are represented in Table 4.2. Note that multiple carriers are transmitted only in GSM and UMTS, while MIMO is only implemented in LTE and NR. The number of MIMO elements for each LTE and NR band is presented in Table 4.3.

The exclusion zone distances for the direction of maximum radiation, D_{front}, were computed for different number of carriers for GSM ($N_{c\ GSM900}$) and UMTS ($N_{c\ UMTS}$), since for any BS installation, the number of carriers used in a system may differ. Four different configurations on the ratio $N_{c\ GSM900}/N_{c\ UMTS}$ were used to obtain a wide variety of results: 1/1, 2/1, 4/2 and 4/4; $N_{c\ UMTS}$ refers to the number of carriers for both the 900 and 2100 bands. For example, the Suburban.1 scenario makes use of the UMTS900 and UMTS2100 bands and thus, for the 4/2 configuration, two carriers are considered for each UMTS band.

The analysis for this thesis was performed using two different active antennas for the NR3600 band. For the urban scenarios one considered the AAU5613 antenna and for the suburban scenarios the AAU5339w one (these are antennas manufactured by Huawei): the AAU5613 possesses 64x64 MIMO,

which ensures a higher capacity compared to the AAU5339w that possess 32x32, thus being a more suitable deployment for more densely populated environments. Regarding GSM, UMTS, LTE and NR700, a single passive antenna was considered, the ASI4517R3v06. The technical characteristics of these antennas are presented in Annex F.

Table 4.2. Output power per carrier/MIMO element and antenna gain for the systems under analysis.

System			Output Power per Carrier/MIMO Element [W]	Maximum Antenna Gain [dBi]
GSM	900		20	16.0
UMTS	900		20	16.0
	2100		30	15.9
LTE	800		40	15.5
	1800			15.5
	2100		10	15.9
	2600		40	16.7
NR	700		40	15.2
	3600	AAU5613	2.5	25.0
		AAU5339w	5	23.8

Table 4.3. Number of MIMO elements for each band of LTE and NR.

System			Number of MIMO Elements
LTE	800		2
	1800		
	2100		
	2600		4
NR	700		2
	3600	AAU5613	64
		AAU5339w	32

The values used for the link budget parameters are presented in Table 4.4, which are reference values, extracted from [HUAW19c], for the DL channel, since it is the connection of interest for this thesis. Since the scope of this thesis is to analyse the impact of EMF restrictions solely on outdoors BSs, indoors users served by indoors BSs are not considered. Furthermore, for the analysed scenarios that consider the use of active antennas for NR3600, the cable losses can be considered to be non-existing, since the radio module is part of the antenna hardware instead of being separated from it; for the 700 MHz band of NR, a passive antenna is used and thus cable losses cannot be neglected. Regarding the MIMO order used for the link budget, it is the number of simultaneous streams of data considered for the user.

Table 4.4. Reference values for the link budget parameters.

Parameter	Urban	Suburban		Rural
		NR3600	NR700	
Slow-Fading Margin [dB]	7.0	6.0		5.0
Interference Margin [dB]	6.0	4.0		2.0
Cable Losses [dB]	0.0	0.0	2.0	2.0
SCS [kHz]	30.0	30.0	15.0	15.0
Number of RBs	273	273	55	55
MT Height [m]	1.8			
BS Height [m]	42.0			
MT Antenna Gain [dBi]	3.0			
MT Losses [dB]	3.0			
MT Noise Figure [dB]	7.0			
SINR [dB]	5.0			
Coverage Probability [%]	90.0			
MIMO Order	2x2			

4.2 Variation of D_{front}

The computations of the exclusion zone distances were performed for the scenarios presented above using (3.44) for the power density contribution of each system and (3.46) to compute the exclusion zone distance. The model results for the antenna coefficients as well as the used parameters are presented in Annex G. One needs to consider that the values used for the transmitting powers in GSM, UMTS, LTE and NR are the maximum ones. The actual transmitted power for each system varies along the day and depends on BS usage and power control, which means that the exclusion zone of a BS is variable and may be actually lower than the one obtained in this design.

The results of D_{front} for every scenario are presented in Figures 4.1 to 4.4, and the D_{front} variation, Δ_{front}, is presented in Table H.1 (Annex H), considering the absence (W/O NR) and presence (W NR) of NR. The increase in the compliance distance due to the installation of NR ranges from 92.3% to 248.7% for the urban scenarios, from 17.3% to 131.6% for the suburban ones, and from 14.3% to 56.4% for the rural ones. One should note that the increase in D_{front} is overall lower for the rural scenarios since they only consider the deployment of NR700, as opposed to urban and suburban ones where NR3600 is installed. As it can be observed from the antennas' characteristics and the radio configurations present in Tables 4.2 and 4.3, the transmitted power, as well as the antenna gain, are significantly higher for NR3600 than for NR700, causing a higher overall increase in D_{front}.

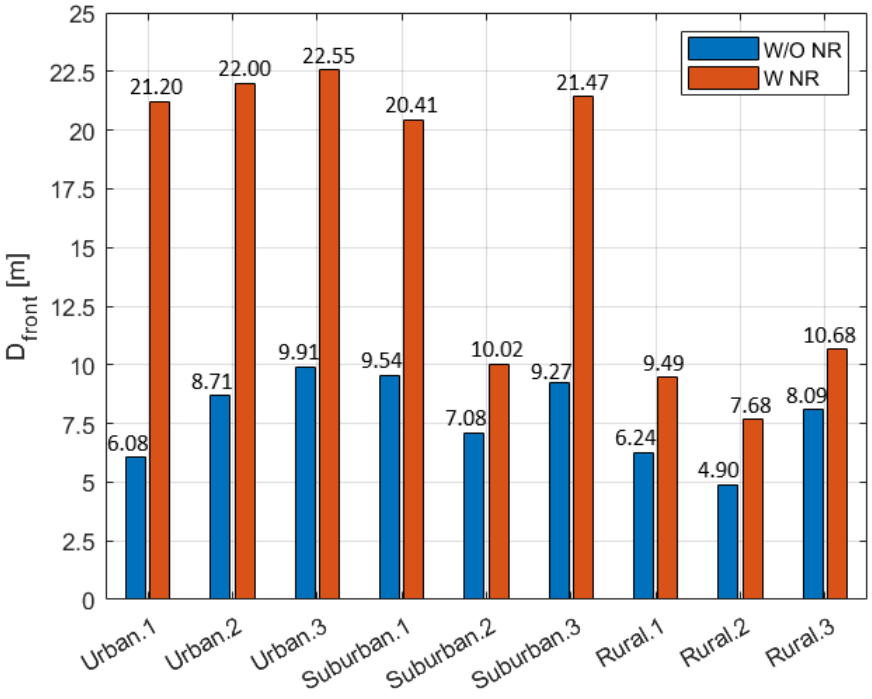

Figure 4.1. D_{front} results for the carrier configuration 1/1.

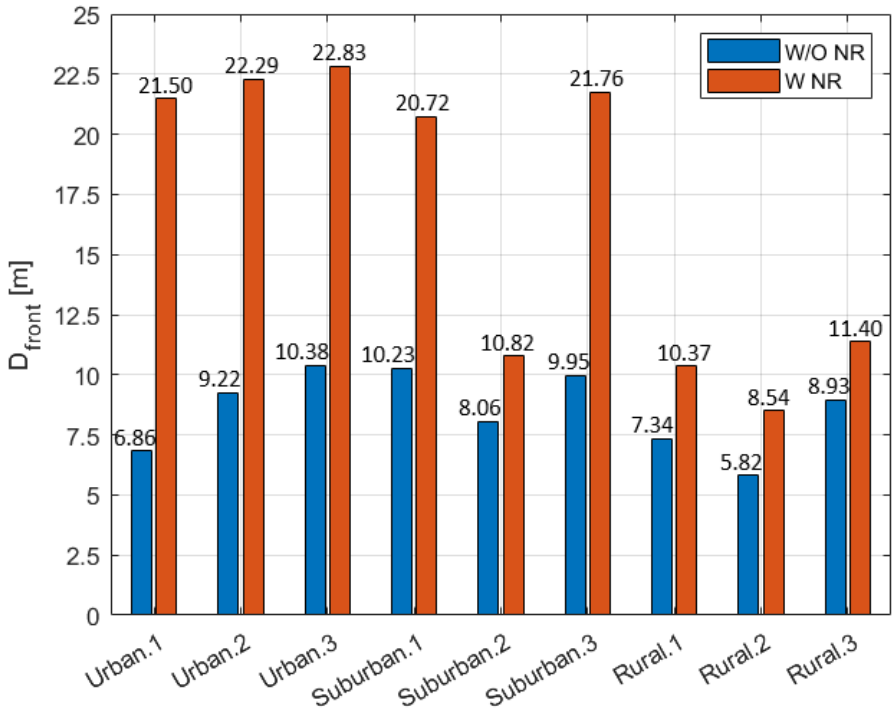

Figure 4.2. D_{front} results for the carrier configuration 2/1.

Regarding the carrier configuration 1/1 for urban scenarios, the D_{front} values W/O NR go from 6.08 m for the Urban.1 scenario to 9.91 m for the Urban.3 scenario; the increase in the compliance distance from Urban.1 to Urban.2 results from the higher gain and higher transmitted power, due to the use of a higher order of MIMO of LTE2600 comparing to LTE1800. As explained earlier, a conservative approach

is taken by assuming that all carriers and MIMO elements radiate in the same direction. For Urban.3, the compliance distance is higher than for Urban.1 and Urban.2, as expected, since for this scenario both LTE1800 and LTE2600 are present. The D_{front} values after the installation of NR range from 21.20 m for Urban.1 to 22.55 m for Urban.3.

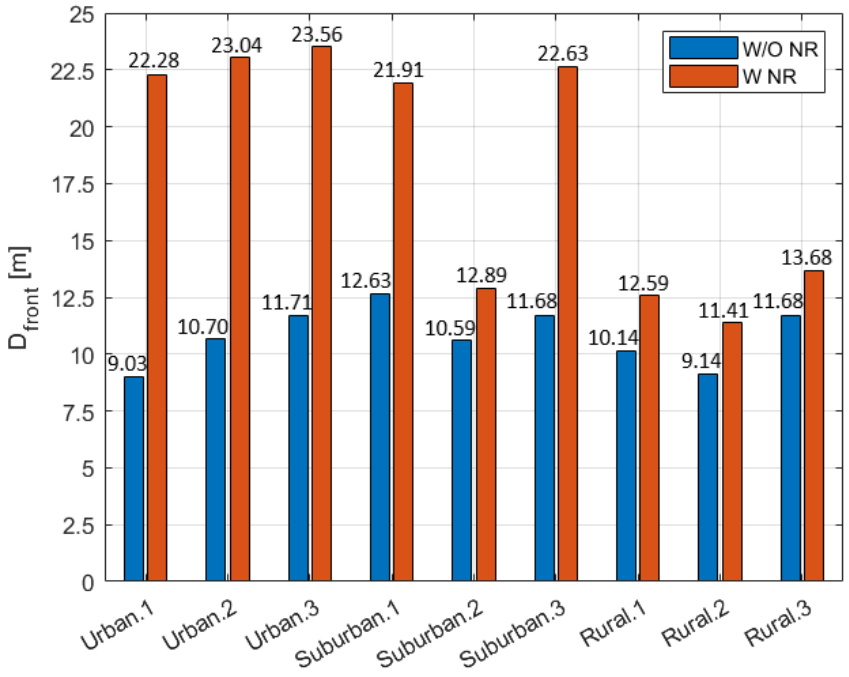

Figure 4.3. D_{front} results for the carrier configuration 4/2.

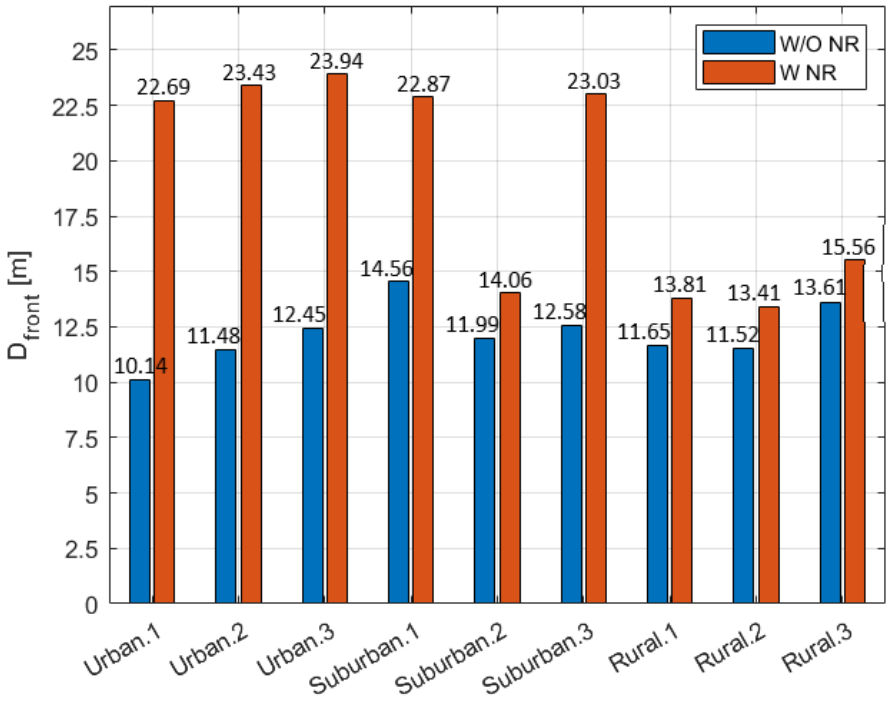

Figure 4.4. D_{front} results for the carrier configuration 4/4.

Regarding the suburban scenarios, the values for D_{front} W/O NR vary from 7.08 m to 9.54 m, the lowest result being obtained for Suburban.2, as expected, due to reduced transmitted power compared to the other two scenarios. The values for D_{front} after the deployment of NR confirm the higher increase in compliance distance associated with the installation of active antennas in the 3.6 GHz band. For Suburban.1 and Suburban.3, where NR3600 is implemented, the value for D_{front} is 20.41 m and 21.47 m, respectively; this increase is substantially higher than the increase produced by NR700 in Suburban.2, with D_{front} as 10.02 m.

For the rural scenarios, the values for D_{front} W/O NR range from 4.91 m to 8.09 m, which can be explained by the total transmitting power for each scenario. The values for D_{front} with NR vary between 7.68 m for Rural.2 and 10.68 m for Rural.3. As expected, this increase for the exclusion distance is significantly lower than the one obtained with the installation of NR3600 since, for the rural scenarios the deployment of NR700 has only passive antennas of lower gain and output power.

For the carrier configuration 2/1, the D_{front} results are higher than for the 1/1 one. Since every scenario includes GSM900 and its transmitted power doubles for the 2/1 configuration, the results behave as expected. The compliance distance increases from 6.96 m to 21.50 m for Urban.1 W/O NR and W NR, respectively. For Urban.2, with the installation of NR, the compliance distance increases from 9.22 m to 22.29 m, and for Urban.3, the compliance distance increases from 10.38 m to 22.83 m. As expected, for the urban scenarios, D_{front} is higher for the scenario with GSM900, UMTS2100, LTE2600 and LTE1800, and it has the lowest value for the scenario with only GSM900, UMTS2100 and LTE1800.

Regarding suburban and rural scenarios, the values for D_{front} W/O NR range from 8.06 m to 12.23 m and from 5.82 m to 8.93 m respectively, while in the W NR case they vary between 10.82 m and 21.76 m for suburban and between 8.54 m and 11.41 m for rural ones. As explained for the 1/1 configuration, smaller increases for D_{front} with NR in rural scenarios are expected.

Regarding the carrier configuration 4/2, the results increase as expected compared to the previous scenario since both GSM900 and UMTS2100 double the number of transmitted carriers. For Urban.1, D_{front} increases from 9.03 m W/O NR to 22.28 m W NR, for Urban.2 from 10.70 m W/O NR to 23.04 m W NR and for Urban.3 from 11.71 m W/O NR to 23.56 m W NR.

For the suburban scenarios, with the installation of NR, D_{front} increases from 12.63 m to 21.91 m for Suburban.1, from 10.59 m to 12.89 m for Suburban.2 and from 11.68 m to 22.63 m for Suburban.3. Regarding the rural scenarios, this increase is from 10.14 m W/O NR to 12.59 m W NR for Rural.1, from 9.14 m W/O NR to 11.41 m W NR for Rural.2, and from 11.68 m W/O NR to 13.68 m W NR for Rural.3.

Regarding the carrier configuration 4/4, for the urban scenarios D_{front} W/O NR ranges between 10.14 m and 12.45 m, and W NR from 22.69 m and 23.94 m; while the suburban and rural scenarios, the ranges are W/O NR between 11.99 m and 14.56 m, and 11.52 m and 13.61 m, respectively. With the installation of NR, D_{front} has values between 14.06 m and 23.03 m for the suburban cases, and between 13.41 m and 15.56 m for the rural ones. Since this is the highest carrier configuration presented, the values for the compliance distance are also the highest compared to the previous configurations.

One may note that in some situations, the scenarios with higher total transmitted power (TTP) do not produce the highest compliance distances. For example, for the 4/4 configuration W/O NR, Rural.2 has a TTP of 300 W and D_{front} equal to 11.52 m, while Rural.1 has a TTP of 240 W and D_{front} equal to 11.65 m. Although Rural.1 transmits 60 W less than Rural.2, its compliance distance is 13 cm higher, which may be explained by the lower exposure reference values existing to lower frequencies, Table 2.13. Since the exposure limits are lower for lower frequencies (below 2 GHz), it is expected that scenarios working with lower bands possess higher compliance distances. Note that this behaviour is only expected if the antennas gain and the transmitted powers are comparable between scenarios.

Since the radio configuration of NR700 and NR3600 does not change among environments, it is expected that the D_{front} growth decreases for BSs with a higher transmitting power of legacy systems, which can be observed in all scenarios. This is due to the EMF influence of NR decreasing as the influence of the legacy systems increases. The results for the contribution of NR to D_{front}, obtained from (3.48), are presented in Table 4.5; comparing these with the D_{front} results for the urban, suburban, and rural scenarios, it can be observed that for smaller D_{front} growths the contribution of NR is lower and consequently, the contribution of the legacy systems is higher.

Table 4.5. NR contribution to D_{front} for each scenario and carrier configuration.

Scenario	η_{NR} [%]			
	$N_{c\,GSM900}/N_{c\,UMTS2100}$			
	1/1	2/1	4/2	4/4
Urban.1	71.3	67.6	59.5	55.3
Urban.2	60.4	58.6	53.6	51.0
Urban.3	56.1	54.5	50.3	48.0
Suburban.1	53.3	50.6	42.4	36.3
Suburban.2	29.3	25.5	17.8	14.7
Suburban.3	56.8	54.3	48.4	45.4
Rural.1	34.2	29.2	19.5	15.6
Rural.2	36.1	31.9	19.9	14.1
Rural.3	24.3	21.7	14.6	12.5

The contribution of NR3600 to D_{front} is significantly higher than the contribution of each legacy system individually. One may note that the lowest contribution of NR3600 is 36%, which leaves 64% of the total contribution to be distributed among legacy systems. This overall high increase in D_{front} due to the installation of NR3600 can be explained by the high gain of the active antennas and the high transmitted power used in the 3.6 GHz band of NR. Regarding NR700, one may notice that the contribution to D_{front} is not as high as the contribution of NR3600 as expected, due to lower transmission power and antenna gain, as seen in Suburban.2 and the rural scenarios.

As stated in Section 2.1, there are several novelties introduced in NR's radio interface, such as MaMIMO, beamforming and beam steering. Due to these new characteristics, there is the possibility of

multiple beams targeting different directions in both the horizontal and vertical planes. These active antennas are then capable of performing horizontal and vertical sweeps that allow for better coverage in both planes. These sweeps, performed with the beam steering technique, need to be accounted for in the radiation pattern by introducing a Sweep Envelope Range (SER), Figure 4.5.

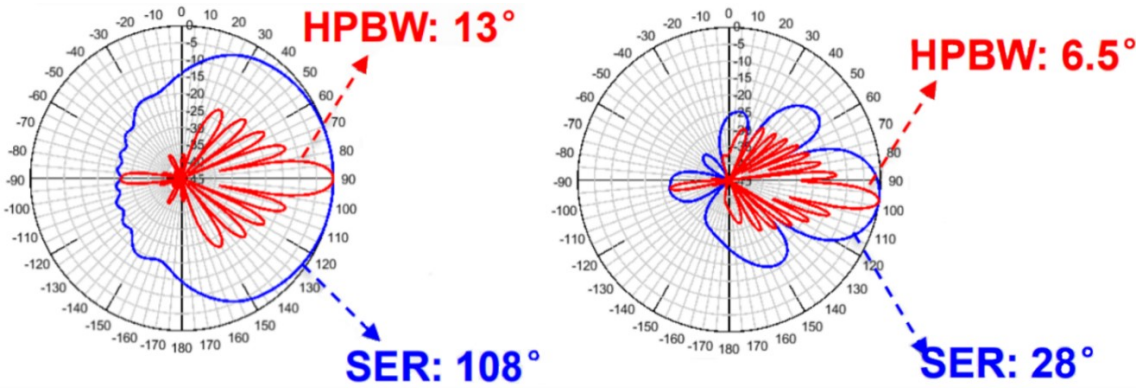

Figure 4.5. Horizontal and vertical radiation patterns of an active NR antenna (extracted from [HUAW19b]).

As a consequence of the sweeping, there is a wide range of directions in front of the antenna that must have D_{front} as the border of the exclusion zone. This consequence needs to be analysed and taken into account by the operators when defining the exclusion zone around the antennas, which leads again to conservative results for the boundaries, since not all power is focused in all directions at once in a realistic scenario.

Due to the high results for D_{front} in urban scenarios, between 21.20 m (Urban.1 with 1/1 configuration) and 23.94 m (Urban.3 with 4/4 configuration), there are some considerations to be taken into account regarding public exposure. For scenarios with the antennas installed close to the ground, Ufaçade and Upole installations, physical barriers may need to be implemented at street level due to the typical minimum height of 3 m. The use of high values for the downtilt also increases the amount of exposure at the street, Figure 4.6.

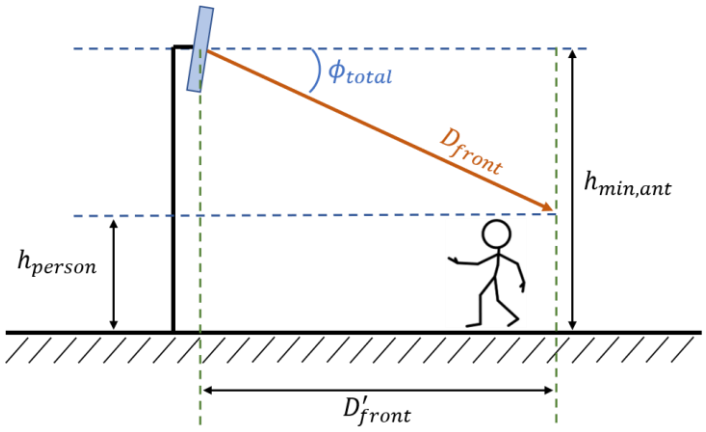

Figure 4.6. Downtilt and vertical SER influence on the exclusion region (adapted from [Antu12]).

As stated earlier, the NR active antennas perform horizontal and vertical beam sweeping, increasing the range of directions that coincide with the maximum antenna gain. The vertical sweeping increases then the exposure at street level by maintaining the high antenna gain for lower angles, Figure 4.6. As shown in Figure 4.5, the sweeping angle is given by the SER. An evaluation can then be made to compute the minimum antenna height, $h_{min,ant}$, required in order not to install physical barriers:

$$D'_{front\,[\mathrm{m}]} = D_{front\,[\mathrm{m}]} \ \cos(\phi_{total}) \tag{4.1}$$

$$h_{min,ant\,[\mathrm{m}]} = h_{person\,[\mathrm{m}]} + \left(D_{front\,[\mathrm{m}]} \ \sin(\phi_{total})\right) \tag{4.2}$$

$$\phi_{total} = \theta_{dt} + \frac{\alpha_{V,SER}}{2} \tag{4.3}$$

where:

- D'_{front}: front border of the exclusion zone when downtilt/SER are used;
- h_{person}: the height of a person;
- ϕ_{total}: the total inclination angle;
- $\alpha_{V,SER}$: SER of the vertical radiation pattern.

Thus, if the height of the antenna is above $h_{min,ant}$ no physical barriers are necessary, but, on the other hand, if the height of the antenna is below $h_{min,ant}$, D'_{front} corresponds to the distance at which physical barriers must be installed. The results for the urban scenarios are presented in Section H.3 (Annex H) from Table H.8 to H.10. The results were computed for the 4/2 and 4/4 carrier configurations, a downtilt of 12º, which can be considered a high value for urban scenarios, and a vertical SER of 30º, which corresponds to the active antenna considered for the urban scenarios. The height of the person was considered to be 1.80 m, which is higher than the average height for adults in Portugal according to [ELIF16]. One should note that for the results W/O NR, the value of the SER is 0º since no active antenna is used. The suburban and rural scenarios were not considered for the simulation since the typical BS height for these environments, Table 2.14, should be sufficient to ensure that physical barriers at ground level are not required.

According to the results, there is no need for physical barriers at ground level for urban BSs with a height higher than 12.67 m (Urban.3, 4/4 configuration, W NR). As observed in Table 2.14, the BS installations that may cause overexposure at street level are the Upole and Ufaçade topologies due to the low typical installation height. For Uroof scenarios, there may also be overexposure for BSs installed on top of small buildings in which the total antenna height is below 12 m above ground. For example, considering a building with 3 floors and 3 m per floor, [Corr20], and an antenna installation height of 2 m, the total antenna height will be 11 m. Thus, even in some Uroof scenarios, the installation of NR3600 may cause overexposure and thus a more detailed analysis regarding the need for physical barriers at street level should be performed.

It needs to be emphasised though that for these installations, the type of cell is usually micro-cell and thus the power needed to cover the respective area is much lower than the ones used in the analysed scenarios thus lowering the compliance distances. The implemented tilt is also lower in order to increase the coverage area.

For this approach, based on [Antu12], it is assumed that the direction of maximum radiation is situated in the centre of the total vertical sweep and thus half of the value of the SER is added to the downtilt angle, resulting thus in the total inclination of the maximum gain of the antenna, ϕ_{total}. It is also assumed, for simplification purposes, that the considered downtilt is only mechanical and not electrical, ensuring that the radiation pattern remains the same and it is only rotated by θ_{dt}, as explained in Section 3.7. Finally, it also considered that all the antennas and systems possess the same downtilt.

Another aspect to be taken into account in Uroof scenarios is the impact of D_{front} on the buildings in front of the BS. In these buildings, the rooftop, top floor balconies and/or top floor indoor spaces may be inside the BS's exclusion zone, depending on the width of the street. One assumes a sidewalk with a width of 2.25 m and each traffic lane with 3.5 m, [IMTT11], although these values may vary from place to place. For a street with 2 traffic lanes, the width of the street is 11.5 m, which is well below the 21.20 m obtained for D_{front} for Urban.1 with the 1/1 configuration. The top floor and rooftop of the frontal building would then be inside the BS's exclusion zone, assuming identical heights for the buildings.

One must note that, typically, in order to obtain better coverage, the height of the BS is higher than the nearby buildings, increasing the BS-to-building distance. Also, the BS antennas may not be installed at the edge of the building, further increasing this distance. The attenuation caused by the glass (12 to 34 dB) and the building's walls (12 to 58 dB), [HUAW19c], may provide additional safety.

For the BSs where the measurements were conducted, presented in Section 3.7, the distance from each sector to the nearest building was measured with a laser rangefinder (Nikon Laser 1200S). The results are presented in Table 4.6: the distances from each sector to the nearest building are well above the maximum D_{front} value, obtained for Urban.3 for the 4/4 configuration (23.94 m).

Table 4.6. Distance from the visited BSs' sectors to the nearest building.

BS	Sector	Distance to nearest bulding [m]
BS1	1	36.0
	2	41.5
	3	50.5
BS2	1	46.5
	2	80.0
	3	59.5

Since NR3600 uses TDD as the duplexing method and the beams obtained from MaMIMO may not all be allocated at the same time, the actual power transmitted by the BS may be lower than the maximum transmitted power. A study performed by [TFCT17] aimed to assess the time-averaged realistic maximum transmitted power for MaMIMO antennas, a number of factors being required to be considered, such as BS usage, TDD UL/DL time ratio, scheduling time and spatial distribution of users within the cell. The results show that, for an 8×8 array antenna, the realistic maximum transmitted power takes values between 7% and 22% of the theoretical maximum, which translates to a reduction in

compliance distance. For example, for Urban.3 with 4/4 carrier configuration and 22% of the maximum transmitted power for NR3600, the value of D_{front} would reduce from 23.94 m to 15.59 m, which is a 34.9% reduction. As stated by [TFCT17], this reduction in the compliance distance may facilitate the installation of NR BSs.

4.3 Exclusion Zone Variation for Other Directions

Regarding the exclusion distances for different directions, one presents in Tables 4.7 and 4.8 the analysed directions and normalised gains that allow the computation of D_{back}, D_{side}, D_{top}, D_{bottom} and also D_{front}. The results for the urban scenarios are shown in Tables 4.9 to 4.11, and for the suburban and rural ones from Tables H.2 to H.7 (Annex H). A colour code scheme is presented in these results in order to better analyse the impact of NR on the exclusion zone distance in the direction of maximum radiation. For values of D_{front} up to 11.5 m, the results are considered acceptable and thus the colour is green. For $11.5 < D_{front\,[m]} \leq 15.0$, the results may be acceptable in some situations and thus the colour is orange, and for $D_{front\,[\mathrm{m}]} > 15.0$ the colour is red. The values of 11.5 m and 15.0 m correspond to the width of a street with 2 and 3 traffic lanes respectively, as assumed in the previous section.

Table 4.7. Analysed directions for the back, side, top and bottom borders of the exclusion zone.

Back (H plane)	Side (H plane)	Top (V plane)	Bottom (V plane)
180º	90º and 270º	270º	90º

Table 4.8. Normalised gains for the analysed directions for each system.

System	Normalised Gains [dB]			
	Back	Side	Top	Bottom
GSM/UMTS 900	-24.0	-14.1	-27.7	-29.2
UMTS/LTE 2100	-25.0	-18.9	-21.9	-33.3
LTE 800	-25.0	-14.2	-25.9	-41.5
LTE1800	-25.0	-15.4	-31.9	-32.0
LTE 2600	-25.0	-25.8	-30.2	-27.2
NR 700	-22.0	-12.6	-30.0	-31.7
NR 3600 (AAU5613)	-24.8	-13.7	-26.6	-28.6
NR 3600 (AAU5339w)	-27.5	-14.1	-23.7	-27.6

In order to compute the exclusion zone borders for the back, side, top and bottom directions, the absolute value of the normalised gain is subtracted from the maximum antenna gain for each system and the simulation is run again. To compute D_{side}, the used gain value is the highest between the two directions (90º and 270º, in the horizontal plane), ensuring the highest compliance distance is calculated.

For D_{back}, the gain values for 180º, in both horizontal and vertical planes, are compared to the antenna's FTBR, the highest value among these three being chosen. As explained in Section 3.3.4, the use of the radiation patterns for the computation of the exclusion zone leads to overestimated results, since these patterns represent the angular distribution of the radiated fields in the far-field.

Table 4.9. Exclusion borders for the front, back, side, top and bottom for the Urban.1 scenario.

	$N_{c\,GSM900}/N_{c\,UMTS}$		D_{front} [m]	D_{back} [m]	D_{side} [m]	D_{top} [m]	D_{bottom} [m]
Urban.1	1/1	W/O NR	6.08	0.95	0.95	0.95	0.95
		W NR	21.20	1.06	4.23	0.95	0.95
	2/1	W/O NR	6.96	0.95	0.95	0.95	0.95
		W NR	21.50	1.06	4.26	0.95	0.95
	4/2	W/O NR	9.03	0.95	0.95	0.95	0.95
		W NR	22.28	1.07	4.31	0.95	0.95
	4/4	W/O NR	10.14	0.95	0.95	0.95	0.95
		W NR	22.69	1.08	4.34	0.95	0.95

Table 4.10. Exclusion borders for the front, back, side, top and bottom for the Urban.2 scenario.

	$N_{c\,GSM900}/N_{c\,UMTS}$		D_{front} [m]	D_{back} [m]	D_{side} [m]	D_{top} [m]	D_{bottom} [m]
Urban.2	1/1	W/O NR	8.71	0.95	0.95	0.95	0.95
		W NR	22.00	1.08	4.19	0.95	0.95
	2/1	W/O NR	9.22	0.95	0.95	0.95	0.95
		W NR	22.29	1.08	4.22	0.95	0.95
	4/2	W/O NR	10.70	0.95	0.95	0.95	0.95
		W NR	23.04	1.09	4.27	0.95	0.95
	4/4	W/O NR	11.48	0.95	0.95	0.95	0.95
		W NR	23.43	1.10	4.29	0.95	0.95

Table 4.11. Exclusion borders for the front, back, side, top and bottom for the Urban.3 scenario.

	$N_{c\,GSM900}/N_{c\,UMTS}$		D_{front} [m]	D_{back} [m]	D_{side} [m]	D_{top} [m]	D_{bottom} [m]
Urban.3	1/1	W/O NR	9.91	0.95	0.95	0.95	0.95
		W NR	22.55	1.09	4.25	0.95	0.95
	2/1	W/O NR	10.38	0.95	0.95	0.95	0.95
		W NR	22.83	1.09	4.27	0.95	0.95
	4/2	W/O NR	11.71	0.95	0.95	0.95	0.95
		W NR	23.56	1.10	4.33	0.95	0.95
	4/4	W/O NR	12.45	0.95	0.95	0.95	0.95
		W NR	23.94	1.11	4.35	0.95	0.95

For the urban environments W/O NR, the exclusion zone border for the back, side, top and bottom of the antenna is less than $3\lambda_{GSM900}$, 0.95 m. After the installation of the active antenna, the distances for the top and bottom of the antenna remain less than $3\lambda_{GSM900}$. In these cases, the compliance distance is below the range of the model and thus the border is set at this value. For the urban scenarios, the highest working wavelength corresponds to the GSM900 system and so the lower limit for the implemented model is $3\lambda_{GSM900}$.

For Urban.1, after the installation of NR3600, the values for D_{back} increase to 1.06 m for the 1/1 and 2/1 configuration, and to 1.07 m and 1.08 m for the 4/2 and 4/4 ones, respectively. For the top and bottom of the antenna, the compliance distances remain less than $3\lambda_{GSM900}$. The border for the sides of the antenna increases to 4.23 m, 4.26 m, 4.31 m and 4.34 m for the 1/1, 2/1, 4/2 and 4/4 configurations respectively.

For Urban.2, the compliance distances for the back increase by 2 cm compared to Urban.1 for the same carrier configuration, which is negligible. Regarding the sides of the antenna, the compliance distance increases to 4.19 m, 4.22 m, 4.27 m and 4.29 m for the configuration 1/1, 2/1, 4/2 and 4/4 respectively. These values, for the respective configuration, are lower than the D_{side} values obtained for Urban.1, which is due to the side gain of LTE2600 being close to 10 dBi lower than the side gain of LTE1800, thus decreasing the side exposure levels.

Regarding Urban.3, the compliance distances for the back increase by 1 cm compared to Urban.2 results for the same carrier configuration. For D_{side}, its value increases to 4.25 m for the 1/1 configuration, to 4.27 m for the 2/1 configuration, and 4.33 m and 4.35 m for the 4/2 and 4/4 configurations, respectively. Since this is the urban scenario with the highest number of installed systems, it is expected that exposure gets higher and thus the compliance distance is greater compared to the previous scenarios.

Regarding the suburban and rural scenarios, for the installations W NR, the highest working wavelength corresponds to NR700, except in Suburban.1, where NR3600 is installed instead, and thus LTE800 has the highest wavelength. For the suburban scenarios, the distances for the back, top and bottom are less than $3\lambda_{LTE800}$ or $3\lambda_{NR700}$. Note that $3\lambda_{LTE800} = 1.10$ m and $3\lambda_{NR700} = 1.18$ m. For Suburban.2, the values for D_{side} are also less than $3\lambda_{LTE800}$ (W/O NR) and $3\lambda_{NR700}$ (W NR). Regarding Suburban.1, D_{side} increases to 3.64 m, 3.66 m, 3.74 m, and 3.81 m for the 1/1, 2/1, 4/2, and 4/4 configurations respectively. For Suburban.3, D_{side} increases to 3.72 m for the 1/1 configuration, 3.74 m for 2/1, 3.80 m for 4/2, and 3.83 m for 4/4. One can observe that, for the same carrier configuration, the values of D_{side} W NR are higher for Suburban.3, as expected, due to the installation of both NR700 and NR3600.

For the rural scenarios, it can be observed that the distances for the back, side, top and bottom of the antenna are less than $3\lambda_{LTE800}$ for installations W/O NR, or $3\lambda_{GSM900}$ in Rural.2, and less than $3\lambda_{NR700}$ for installations W NR.

After presenting the model's results, the goal is to analyse the typical BS installations, Table 2.14, and verify how the obtained results influence the definition of physical barriers, intended to protect the general public from potentially harmful exposures. As stated earlier, the computed results are obtained

for the worst-case scenario, where the maximum power is being continuously transmitted for all systems.

Regarding the suburban and rural environments, there is no need for physical barriers in any direction since, as observed in Table 2.14, the antennas are typically installed in towers 20 to 50 m high with no access to the general public.

Considering the urban scenarios analysed in this thesis, the values for D_{top} and D_{bottom} are reduced and may not present the need to install public protection barriers. Regarding D_{top}, its value is below 0.95 m and also the top of the antenna is not usually accessed by the general public, and thus a physical barrier is not necessary. Regarding D_{bottom}, the concern might be the users on the top floor of the building, for Uroof scenarios and, depending on the installation's location, the public access to the bottom part of the antennas. For Utower scenarios, the general public is not allowed and thus physical barriers are not necessary. For the Uroof scenarios, depending on the type of access available to the general public and the height of the antennas, physical barriers might be required. In this context, the downtilt must also be considered since, as observed in (2.12), D_{bottom} increases with the increase of the downtilt angle. Regarding the public on the top floor of the building, there is no cause for concern, since the attenuation caused by the roof (concrete and brick) is above 16 dB [HUAW19c] and the height at which the antennas are installed, Table 2.14, provide additional safety.

For D_{back}, the values vary from 1.06 m (Urban.1 with 1/1 configuration) to a maximum of 1.11 m (Urban.3 with 4/4 configuration). As explained earlier, there is no need for physical barriers that comprise the back of the antennas for the Utower scenarios since these have no public access. For the Uroof scenarios, it should be considered whether the public has access to the zones comprising the back of the antenna. If the back of the antennas is easily accessible, then, according to the results, physical barriers need to be considered. Regarding the Ufaçade scenarios, there is usually no danger of exposure due to the attenuation of the outer wall of the building. This attenuation can range from 12 dB (12 cm plasterboard wall) to 58 dB (external wall plus 2 inner ones) [HUAW19c].

As it can be observed from the results, for the sides of the antenna, the compliance distance increases significantly with the introduction of NR. This increase is due to the side gain of the active antennas being significantly higher than the side gain of the legacy systems. The values for D_{side} vary between 4.19 m (Urban.2 with 1/1 configuration) and 4.55 m (Urban.3 with 4/4 configuration). For the Ufaçade installation, the concern for high exposure levels may be the approximation of the antenna's laterals to zones with public access like windows and balconies. Regarding the Uroof installation, an evaluation should be made whether the public has access or not to the sides of the BS. If these zones are accessible, due to the considerable values for D_{side}, then protective barriers should be installed. For Utower scenarios, there is no cause for concern since these do not have public access and are not built very close to buildings.

4.4 Influence on Coverage and Throughput

In this section, the goal is to analyse the consequences of EMF restrictions on the coverage radius and cell-edge throughput in the scenarios taken in the previous sections. As the number of systems increases in a single BS, so does the exclusion zone around it. In some scenarios, the exclusion zone may have limited dimensions and thus it cannot increase even further. In this situation, the solution may be to decrease the transmitted power of the systems present in the BS or even shut down a frequency band or system. This decrease in the transmitted power may have a relevant impact on the overall network performance and QoS offered to the user.

As it can be observed from the results of the previous sections, the values for D_{front} W NR differ with the scenarios, ranging between 21.20 m and 23.94 m for urban, 10.02 m and 23.03 m for suburban, and 7.68 m and 15.56 m for rural ones.

Regarding rural scenarios, there are usually no constraints for the exclusion zone dimensions, since the antennas are typically installed on towers 20 to 50 m high and are relatively far from buildings. This ensures that no public accessed areas are within the BS's exclusion zone and thus no reduction in the transmitted powers is necessary.

For suburban scenarios, although the BSs installation may be similar to the rural ones, there are circumstances where the antennas may be installed closer to public accessed areas, such as residential buildings, schools and hospitals. In these cases, the transmitted powers may be reduced and thus the impact of these restrictions must be analysed. As discussed in the previous section, for example, on the impact of D_{front} on the buildings in front of Uroof BSs, the results for D_{front} for the urban scenarios exceed acceptable values and thus a reduction in the BS's transmitted power is necessary.

The scenarios to be analysed in this section are then the urban and suburban ones with 4/2 and 4/4 carrier configurations, which are the more realistic configurations for BS deployments and also the ones that provide higher exposure and thus higher compliance distances. In order to analyse the impact of EMF restrictions on these scenarios, three maximum values were considered for D_{front}: 18.5 m, 15 m, and 11.5 m, which are the widths of streets with 4, 3, and 2 traffic lanes respectively, for the assumption discussed in Section 4.2. The aim is then to compute the reduction in the transmission power necessary to meet the requirements, for each scenario, and analyse the impact of such reduction on the performance of NR BSs. One must note that, for Suburban.2, the values of D_{front} W NR are always below 15 m and thus the power reduction is performed only for 11.5 m.

In order to study the performance variation, two parameters are analysed:

- Coverage radius;
- Cell-edge throughput per RB.

For the coverage radius analysis, the SINR is set to the reference value of 5 dB, Table 4.4, and the behaviour of the coverage radius with the decrease in the transmitted power is analysed. Regarding the cell-edge throughput per RB, the coverage radius is now set to a fixed value, and the throughput variation with the transmitted power is analysed. In this case, since the throughput is a function of SINR,

(3.52), SINR varies with the transmitted power and the throughput is computed accordingly. This analysis allows one to understand the compromise that operators may have to achieve in order to deploy NR BSs in locations where EMF exposure levels are limited.

The results obtained for the NR transmitted power for carrier configurations 4/2 and 4/4 are presented in Tables 4.12 and 4.13, respectively. For both configurations, the transmitted powers were computed for all systems present in each scenario as shown in Table 4.1. For the 4/2 configuration, the transmitted powers were also computed in the absence of UMTS, and for the 4/4 configuration, the transmitted powers were computed without LTE800 for the suburban scenarios and 20% of LTE's maximum power for the urban ones.

Table 4.12. NR transmitted powers for carrier configuration 4/2.

Characteristics	D_{front} [m]	Transmitted Power [W]						
		Scenario						
		Urban.1	Urban.2	Urban.3	Suburban.1	Suburban.2	Suburban.3	
							NR3600	NR700
All Communications Systems	11.5	18	7	0	0	30	0	0
	15.0	52	45	35	29	-	27	40
	18.5	98	84	74	88	-	83	50
Without UMTS	11.5	25	14	5	10	78	5	10
	15.0	59	51	42	52	-	40	30
	18.5	105	91	81	112	-	90	59

Table 4.13. NR transmitted powers for carrier configuration 4/4.

Characteristics	D_{front} [m]	Transmitted Power [W]						
		Scenario						
		Urban.1	Urban.2	Urban.3	Suburban.1	Suburban.2	Suburban.3	
							NR3600	NR700
All Communications Systems	11.5	11	0	0	0	0	0	0
	15.0	45	37	27	6	-	24	20
	18.5	90	76	67	65	-	76	40
Without LTE800 for Suburban and 20% of LTE for Urban	11.5	18	16	14	0	72	10	5
	15.0	52	51	49	32	-	44	40
	18.5	98	95	93	92	-	97	60

One must note that the transmitted powers for Suburban.2 correspond to NR700, for Suburban.3 they are separated between NR3600 and NR700, and for the remaining scenarios they correspond to NR3600. When the transmitted power in a certain scenario is 0 it is due to D_{front} being already higher than the compliance distance limit even W/O NR, thus no deployment is possible. Regarding Suburban.2, the D_{front} value is always less than 15 m and thus the analysis is only performed for D_{front} equal to 11.5 m, hence the "-" sign for 15 and 18.5 m. Note also that for Suburban.3, the combinations of the transmitted power for NR3600 and NR700 may vary for the same value of D_{front}.

The reference values obtained for the coverage radius and throughput per RB at cell-edge for the urban and suburban scenarios are presented in Table 4.14, which were obtained for a transmitted power of 160 W for NR3600 and 80 W for NR700. As stated earlier, the reference coverage radius and throughput were computed for SINR equal to 5 dB. Note that the coverage radius and throughput per RB were calculated as discussed in Annex A and Section 3.4, and thus different propagation models and coding rates can result in different reference values. For the NR3600, the results were obtained for the NLOS situation. The reference values were obtained for outdoors users.

Table 4.14. Reference values obtained for the cell radius, and throughput per RB.

Environment		Transmitted Power [W]	Coverage Radius [km]	Throughput per RB [kbit/s]
Urban		160	0.35	333.1
Suburban	NR3600	160	0.49	333.1
	NR700	80	2.24	166.6

The results for the coverage radius and throughput per RB obtained for the transmitted powers shown in Tables 4.12 and 4.13 are presented in Sections I.1 and I.2 (Annex I), respectively. As stated earlier, the analysis for Suburban.2 is performed only for D_{front} equal to 11.5 m, since no power reduction is necessary for the other D_{front} values, thus, by default, these results were set to 0 for 15 and 18.5 m. In Figures I.6 and I.14, Suburban.2 is not presented since either no power reduction is necessary (D_{front} equal to 15 m and 18.5 m) or NR cannot be installed (D_{front} equal to 11.5 m).

In order to analyse the impact of the decrease in the transmitted power in each scenario, the obtained results are compared to the reference values of Table 4.14. The variations of the coverage radius and throughput per RB are then given by:

$$\Delta_{R_{cell}\,[\%]} = \frac{\left(R_{cell} - R_{cell,ref}\right)}{R_{cell,ref}}\ 100 \tag{4.4}$$

$$\Delta_{R_b^{RB}\,[\%]} = \frac{\left(R_b^{RB} - R_{b,ref}^{RB}\right)}{R_{b,ref}^{RB}}\ 100 \tag{4.5}$$

where:

- $R_{cell,ref}$: reference value for the coverage radius;
- $R_{b,ref}^{RB}$: reference value for the throughput per RB.

The results obtained for the coverage radius variation and throughput per RB variation are presented in Tables I.1 to I.4. A colour code scheme is also implemented in the results in Annex I: a reduction in coverage radius and throughput up to 20% is considered acceptable and thus the assigned colour is green; for reductions up to 40%, the colour is orange; for a reduction higher than 40% the results are unacceptable and thus the colour is red.

Regarding the coverage radius variation of the urban scenarios for the 4/2 configuration, the decrease can go up to 45.7% for Urban.1 and 60.0% for Urban.2 for the lowest value of D_{front} and with all systems

installed. For this configuration, the decrease can go up to 34.3% for Urban.3 for D_{front} equal to 15 m, since, for D_{front} equal to 11.5 m, the restrictions prevent the installation of NR3600. As expected, when UMTS is removed the variation decreases, going up to 40% for Urban.1, 51.4% for Urban.2 and 62.9% for Urban.3. The removal of UMTS enables the installation of NR3600 for Urban.3.

For the suburban scenarios with all communications systems installed, the decrease can go up to 38.8% for Suburban.1, 25.0% for Suburban.2 and 40.8% and 18.3% for NR3600 and NR700 of Suburban.3, respectively. Note that for Suburban.1 and Suburban.3, NR cannot be deployed for D_{front} equal to 11.5 m. As discussed earlier, no reduction is observed regarding Suburban.2 for 15 m and 18.5 m. As can be observed, the removal of UMTS enables the installation of NR for Suburban.1 and Suburban.3, and the decrease in Suburban.2 to only 0.9%.

Regarding the 4/4 configuration, since the exposure from legacy systems is higher compared to the 4/2 configuration, the decrease in coverage radius is also higher when all systems are installed. The decrease for Urban.1 goes up to 54.3%, and NR cannot be deployed for both Urban.2 and Urban.3 for the lowest value of D_{front}.

For the suburban scenarios, NR can only be installed for D_{front} equal to 15 and 18.5 m. Regarding these scenarios, with the removal of LTE800, it is now possible to deploy NR for D_{front} equal to 11.5 m except for Suburban.1. The reduction in coverage radius can go up to 38.8% for Suburban.1, 3.1% for Suburban.2, and 55.1% and 55.4% for NR3600 and NR700 of Suburban.3, respectively. For the urban scenarios, with LTE transmitting 20% of maximum power, the deployment of NR is now possible for D_{front} equal to 11.5 m for the 3 scenarios. The decrease in coverage radius can go up to 45.7% for Urban.1, 48.6% for Urban.2, and 51.4% for Urban.3. Note that, for Suburban.2 and Suburban.3, this decrease is lower compared with the decrease enabled by the removal of UMTS in the 4/2 configuration.

The results for the variation of the throughput per RB follow the same behaviour as the coverage radius variation. For the 4/2 carrier configuration with all systems installed, it can be observed that the decrease in throughput is 91.1% for the Urban.2 scenario and D_{front} equal to 11.5 m, representing a throughput per RB of 29.7 kbit/s, Figure I.9. With the removal of UMTS and for D_{front} equal to 11.5 m, the decrease in throughput can reach 95.9% for both Urban.3 and Suburban.3 with NR3600, representing a throughput per RB of 13.5 kbit/s, Figure I.11 and I.12. Although for D_{front} equal to 11.5 m the decrease in throughput can be quite significant as observed, for D_{front} equal to 18.5 m this decrease varies between 0.9% and 2.3% with all systems installed, and between 0.6% and 1.3% without UMTS.

Regarding the 4/4 carrier configuration with all systems installed, the decrease is generally higher for the same values of D_{front} compared to the 4/2 configuration. For the urban scenarios, the highest decrease corresponds to 76.6% for Urban.1, representing a throughput per RB of 77.9 kbit/s, Figure I.13.

For the suburban scenarios, the highest decrease is 93.7% for Suburban.1 and D_{front} equal to 15 m, representing a throughput per RB of 20.9 kbit/s, Figure I.14. With the removal of LTE800 for the suburban scenarios and 20% of LTE's maximum transmitted power for the urban ones, the throughput

decrease is lower as expected. For example, without the presence of LTE800, the throughput per RB of Suburban.1 for D_{front} equal to 15 m increases from 20.9 kbit/s to 273.1 kbit/s, corresponding to a decrease with respect to the reference value of 18.0% instead of 93.7%.

As it can be observed from the results obtained for throughput and coverage radius variation, the restrictions imposed to the dimensions of the exclusion zone can greatly impact on the deployment of NR BSs as well as their performance. It is observed that in order to obtain reasonable results for the coverage radius/throughput per RB, the exclusion zone must have larger dimensions, and, in some situations, the performance of legacy systems can be compromised by reducing the transmitting powers or even shutting down entire working frequency bands. One may observe from the results that this solution has a higher impact in circumstances where the compliance distance is reduced. In situations where the exclusion zone may possess larger dimensions, for example for D_{front} equal to 18.5 m, it can be observed that the variation in throughput is not significant between the scenarios with all systems installed and the scenarios without UMTS/LTE, thus the removal of these systems may not be necessary.

Chapter 5

Conclusions

This chapter finalises the thesis, summarising the main conclusions as well as some suggestions for future work.

The goal of this thesis was to develop a model to estimate exclusion zones of BSs with co-location of NR with legacy systems, and in particular, to study the influence of the deployment of NR on the variation of the exclusion zones. As these zones are usually inside the near-field zone of the BS antennas, near-field models for linear and planar arrays were developed. A model was also developed in order to analyse how the influence of NR on the exclusion zones and the EMF restrictions in BSs impact the performance of the NR system in terms of coverage radius and cell-edge throughput per RB.

In Chapter 1, a brief description of the evolution of mobile communications systems and the need for NR is presented. Then, an introduction to EMF exposure and BS exclusion zones is done, followed by the enumeration of some studies regarding EMF measurement and exclusion zone models. The main objectives of this work are also discussed. Finally, the contents of the work are briefly described.

In order to achieve the proposed goals, the fundamental concepts of GSM, UMTS, LTE and NR are studied in Chapter 2. First, a basic description of the radio interface, as well as the working frequency bands in Portugal, of each system is performed. Fundamental concepts on coverage, capacity, and interference, such as cell types, cell radius definition, number of users in a cell, and SINR as a function of received power are discussed. The main service categories enabled by NR deployment, eMBB, mMTC and URLLC, and the respective use cases are identified. EMF exposure is then discussed by introducing the different radiation regions around the antenna and the respective borders' definition. The radiation exposure guidelines developed by ICNIRP are also presented, as well as EMF measurement recommendations from international entities. The study of EMF exposure is finished with the presentation of different approaches for the estimation of the exclusion zones around the BS. Finally, one presents the state of the art on the problem of planning NR networks under EMF restrictions.

In Chapter 3, the models used in this thesis as well as their assessment and implementation are described. First, an overview of the general model and its characteristics is presented, describing the input and output parameters as well as the main ideas behind the model's goal. Then, the mathematical models that served as a basis for the power density estimation in this thesis are presented: the far-field ($d > 2D^2/\lambda$) and the far-field gain-based for near-field ($d > 3\lambda$) ones. With these mathematical models, an exclusion zone evaluation method linking the near- and far-field zones was developed. For the near-field zone exposure estimation, two types of antenna arrays were identified: linear arrays, used in legacy systems and NR700, and planar arrays, used for the active antennas of NR3600. The main simulation parameters were also identified. Then, the coverage and capacity planning model is also presented by describing the equations used in the simulator for the coverage radius of the cell and the throughput per RB. The propagation models used for the simulations are also discussed. The model's output parameters and the main corresponding mathematical expressions are presented in the Output Evaluation Metrics section. A theoretical assessment of the exclusion zone and coverage and capacity models was performed, with the goal of verifying the correctness of the developed models.

At the end of Chapter 3, the results of the EMF measurement campaign performed on active BSs are compared to the results of the theoretical model developed for the exclusion zone evaluation. The results

show that, on average, the theoretical model overestimates the exposure levels for every communication system and measurement direction and, due to the relatively low values of standard deviation, it correctly follows the behaviour of the power density near the antenna. For GSM900, the model is on average 7.25 dB above the measurements for the 0º/45º/315º directions and 14.00 dB for the back direction, with a standard deviation of 3.48 dB. For UMTS2100, the average is 9.41 dB for the 0º/45º/315º directions and 18.36 dB for the antenna's back, with a standard deviation corresponding to 4.32 dB. For LTE1800 the average is 14.06 dB for the 0º/45º/315º directions and 17.12 dB for the 180º direction, with a standard deviation of 4.34 dB. Regarding NR3600, the results maintained their average difference across all measured directions, with an average of 38.17 dB and a standard deviation of 6.02 dB. Since NR networks are not yet commercial in Portugal, the NR measurements were obtained for only one authorised mobile terminal. It is expected that, as NR becomes publicly available, exposure levels with NR increase near the BS antennas. These results provide a certain degree of confidence in the developed model, concluding that it can be a useful tool to assess exposure levels in the vicinity of BS antennas.

The exclusion zone evaluation model was developed and implemented in Matlab R2018a, allowing the computation of the exclusion distance in the direction of maximum radiation, D_{front}. In order to compute the compliance distance for the other directions, the normalised antenna gains obtained from the radiation patterns are applied to the maximum antenna gain. Ideally, radiation patterns for the near-field of the antennas should be obtained for a more accurate exposure estimation, although the use of far-field radiation patterns overestimates antenna gains in the near-field allowing for a more conservative computation. It is also considered that the antennas radiate the maximum power continuously, being thus considered the worst-case scenario with respect to EMF exposure.

For the BS scenarios, three scenarios were considered for each environment (urban, suburban and rural), representing the most likely configurations of frequency bands in BS deployment. It was also considered that NR3600 is only deployed in urban and suburban environments, while NR700 is only deployed in suburban and rural ones. In order to obtain a wide variety of results, four different carrier configurations for GSM and UMTS were analysed in terms of the ratio $N_{c\,GSM900}/N_{c\,UMTS}$: 1/1 2/1, 4/2, and 4/4. Note that, usually, GSM deployments do not consider the use of just one carrier.

The first analysis was performed for the variation of D_{front} in the considered BS scenarios. The results for D_{front} clearly demonstrate the impact of NR, especially NR3600, on the variation of compliance distances. For the 1/1 configuration, D_{front} increases up to 10.68 m with NR700 and 22.55 m with NR3600, with variations between 32% and 248.7%. For the 2/1 configuration, the variation in D_{front} is between 27.8% and 213.4%, and for the 4/2 configuration D_{front} increases between 17.1% and 146.7%. Finally, for the 4/4 configuration, D_{front} increases from 14.3% to 123.8%, with values up to 15.56 m for NR700 and 23.94 m for NR3600.

As the transmitted power from legacy systems increases with the increase in the number of carriers, the increase in D_{front} due to the installation of NR decreases. This is visible in the results from the NR

contribution in the exclusion zone variation. Regarding NR3600, the maximum contribution for the exclusion zone dimensions is 71.3%, 67.6%, 59.5% and 55.3% for the carrier configuration 1/1, 2/1, 4/2, and 4/4, respectively. For NR700, the maximum contribution is 34.2% for the 1/1 configuration, 29.2% for the 2/1 configuration, 19.5% for the 4/2 configuration and 15.6% for the 4/4 configuration. The contribution of NR decreases as the power transmitted from legacy systems increases.

Due to the relatively high values of D_{front} with the installation of NR3600 in urban scenarios, there may be overexposure at street level due to the reduced minimum height of 3 m for Ufaçade and Upole installations, and thus physical barriers for public protection may be installed. The use of downtilt and vertical sweep for NR3600 was analysed to assess the compliance of EMF restrictions at ground level. For a downtilt of 12º and a vertical SER of 30º, there is no need to install physical barriers at ground level if the BS is more than 12.67 m high. Due to the maximum height of 10 m and 5 m for Ufaçade and Upole installations respectively, a detailed analysis to assess the need for physical barriers at ground level should be performed. The conclusions are the same for Uroof installations where the BS height is lower than 12.67 m. For this analysis, it was assumed that the downtilt is the same for all systems.

No analysis was performed for the suburban and rural scenarios, since the BS installation in these environments should ensure that no physical barriers are necessary at ground level. One should also note that, for BSs installed at relatively low heights, the transmitted powers are much lower than the ones used in this work.

For Uroof installations, the impact of D_{front} on the buildings in front of the BS was also analysed. In these scenarios, public accessed spaces in the front building, such as rooftops, balconies and even indoor zones, may possess high levels of exposure depending on the distance between buildings. For these cases, the width of the street should then be taken into account. For example, in streets with 2 and 3 traffic lanes, 11.5 m and 15 m wide respectively, it is observed that D_{front} is higher than the street width. A careful exposure analysis at the time of BS installation should then be performed to ensure that the reference levels are not exceeded on nearby buildings.

Regarding the back, side, top, and bottom of the BS, the results obtained with NR are usually not a complication for rural and suburban environments due to the installation characteristics of the BSs and the relatively low values for the compliance distances. For the suburban scenarios, the maximum value for D_{side} is 3.83 m, and for the remaining directions the compliance distance is below 1.18 m ($3\lambda_{NR700}$). For the rural scenarios, the compliance distance in any direction is below $3\lambda_{NR700}$. For the urban environments, the dimensions of D_{back}, D_{side}, D_{back} and D_{bottom} should be taken into account whenever the BS antennas may be accessible to the general public, for example, in some Uroof installations. Although D_{back} and D_{bottom} possess low values, 1.11 m and below 0.95 m ($3\lambda_{GSM900}$) respectively, physical barriers should be considered if the antennas are easily accessed by the public. Regarding D_{side}, with a maximum value of 4.55 m, physical barriers must be considered whenever public access is within the compliance distance.

Finally, the impact of the exclusion zone restrictions for the urban and suburban scenarios on the

coverage radius and cell-edge throughput per RB was analysed. The analysis of the coverage radius was performed by fixing the SINR and obtaining the coverage radius value for the respective transmitted power. For the throughput analysis, the cell radius was fixed and the SINR was computed for each value of the transmitted power, obtaining then the throughput per RB. It is found that, in some situations, the size of the exclusion zone without NR does not allow its installation. For the cases where NR can be installed, the coverage radius decreases up to 62.9% for the urban scenarios and 63.3% for the suburban ones. Regarding the throughput per RB, whenever it is possible to deploy NR, the decrease can reach up to 95.9% for both urban and suburban scenarios. One must note that no analysis was performed for the rural scenarios, since the obtained exclusion zone dimensions do not have an impact on these environments.

From the results, it can be concluded that, due to the high values for the exclusion zone dimensions, operators may need to reduce the transmission power of NR antennas, or even increase the investment in order to install NR BSs without the presence of legacy systems. Operators may also need to re-evaluate exposure levels in the vicinity of the BS in order to verify if physical barriers for public protection need to be implemented. For BSs with co-location, the power transmitted by legacy systems may also need to be reduced in order to install NR, which can bring a lot of complexity in the deployment of NR networks. It can also be observed that for D_{front} equal to 15 and 18.5 m, the decrease in coverage radius is generally higher than the decrease in throughput. For these cases, it may be preferable to allow the reduction in throughput while maintaining the coverage radius. Also, for the highest values of D_{front}, the decommission or power reduction of legacy bands may not be necessary since the difference in throughput per RB is not significant and may not justify the compromise of legacy systems.

For future work, it would be interesting to study how the BS surrounding environment, such as the floor, building walls and antenna supports (such as masts and poles) influence the shape and size of exclusion zones. This could be accomplished with EM simulations using CST and Antenna Magus. EM simulations can also be used to assess the correctness of the developed exposure models. Another interesting research would be to develop better techniques for measuring EMF exposure of MaMIMO systems near the BS in already loaded commercial NR networks, ensuring that exposure levels are as realistic as possible. These results could then be compared with new exposure assessment mathematical models for MaMIMO systems that consider factors such as BS utilisation and spatial distribution of users. One suggests also the study and development of near-field radiation pattern models as a function of distance, for linear and planar antenna arrays, in order to obtain more accurate results in near-field exposure estimation.

Annex A

Coverage and Capacity

This annex presents the fundamental formulations of coverage and capacity as well as the propagation models used in this thesis.

A.1 Radio Link Budget

The fundamental formulations for the link budget and its parameters, based on [Corr20], are described in this section.

The maximum allowed path loss (MAPL) is defined as:

$$L_{p\,\max\ [\mathrm{dB}]} = P_{EIRP\ [\mathrm{dBm}]} + G_{r\ tot\ [\mathrm{dBi}]} - P_{r\,\min\ [\mathrm{dBm}]} \quad (A.1)$$

where:

- $G_{r\ tot}$: total receiver antenna gain;
- $P_{r\ min}$: receiver sensitivity;
- P_{EIRP}: Effective isotropic radiated power.

The P_{EIRP} being taken into consideration for this thesis is in the DL connection so it is defined as:

$$P^{DL}_{EIRP\ [\mathrm{dBm}]} = P_{Tx\ [\mathrm{dBm}]} + G_{Tx\ [\mathrm{dBi}]} - L_{c\ [\mathrm{dB}]} \quad (A.2)$$

where:

- P_{Tx}: transmitter output power;
- G_{Tx}: transmitter antenna gain;
- L_c: losses in the cable between transmitter and antenna.

In NR, the DL transmitter output power is the power transmitted per subcarrier.

Notice that if MIMO is used at the reception, its gain is already included in the definition of total receiver antenna gain since this is defined as:

$$G_{r\ tot\ [\mathrm{dBi}]} = G_{r\ [\mathrm{dBi}]} + G_{MIMO\ [\mathrm{dB}]} \quad (A.3)$$

where:

- G_r: receiver antenna gain;
- G_{MIMO}: MIMO gain.

According to [Viei18] and [Corr20], the receiver sensitivity in NR is computed as follows:

$$P_{r\,\min\ [\mathrm{dBm}]} = -174 + 10\log_{10}\left(B_{RB\ [\mathrm{Hz}]}\right) + F_{N\ [\mathrm{dB}]} + \rho_{SINR\,\min\ [\mathrm{dB}]} + M_{I\ [\mathrm{dB}]} + M_{SF\ [\mathrm{dB}]} \quad (A.4)$$

where:

- B_{RB}: bandwidth per RB (SCS dependent);
- F_N: receiver's noise figure;
- $\rho_{SINR\ min}$: minimum SINR required for the service;
- M_I: interference margin;
- M_{SF}: slow-fading margin.

Based on [Corr20], taking the model of the average power decay with distance, $L_{p\,max}$ can also be defined as:

$$L_{p\,\max\,[\mathrm{dB}]} = L_{ref\,[\mathrm{dB}]} + 10\ a_{pd}\ \log_{10}\left(R_{cell\,[\mathrm{km}]}\right) \tag{A.5}$$

where:

- L_{ref} : reference path loss (propagation model dependent);
- a_{pd}: average power decay (propagation model/environment dependent);
- R_{cell}: cell radius.

According to [Corr20], the probability of being covered at a given distance from the BS is given by:

$$P_{coverage} = \frac{1 + \mathrm{erf}\left(\frac{\Delta P_{r\,[\mathrm{dB}]}}{\sqrt{2}\sigma_{[\mathrm{dB}]}}\right)}{2} \tag{A.6}$$

$$\Delta P_{r\,[\mathrm{dB}]} = \overline{P_{r,R\,[\mathrm{dBm}]}} - P_{r\,\min\,[\mathrm{dBm}]} \tag{A.7}$$

where:

- $\overline{P_{r,R}}$: the average power received at a distance R;
- ΔP_r: difference from the average received power to the receiver's sensitivity;
- σ: standard deviation of the propagation model.

The expression for the received power in the DL is given by:

$$P^{DL}_{r\,[\mathrm{dBm}]} = P_{r\,[\mathrm{dBm}]} - L_{u\,[\mathrm{dB}]} \tag{A.8}$$

where:

- P_r: power available at the receiving antenna.
- L_u: losses due to the user's body.

The losses due to the user's body depend on the service being used. According to [Corr20], if the service being used is voice the attenuation ranges between 3 and 10 dB. If the service being used is data then the attenuation ranges between 0 and 3 dB.

From the equations defined above, the MAPL expression can then be rewritten as:

$$L_{p\,\max\,[\mathrm{dB}]} = P_{Tx\,[\mathrm{dBm}]} + G_{Tx\,[\mathrm{dBi}]} - L_{c\,[\mathrm{dB}]} - P_{r\,\min\,[\mathrm{dBm}]} - \Delta P_{r\,[\mathrm{dB}]} + G_{r\,tot\,[\mathrm{dBi}]} - L_{u\,[\mathrm{dB}]} \tag{A.9}$$

A.2 Propagation Models

In this section, the propagation models used for the 700 MHz and 3.6 GHz bands of NR, as well as the indoors path loss model are presented. The propagation model for the 700 MHz band is the Okumura-Hata model, presented in Table A.1. The indoors path loss model is presented in Table A.2 and, for the

3.6 GHz band, the WINNER II model is used and it is presented in Table A.3.

Table A.1. Okumura-Hata model equations for different scenarios (extracted from [Corr20]).

Scenario	Okumura-Hata Equations
Urban	$L_{ref\ [\mathrm{dB}]} = 69.55 + 26.16\log_{10}(f_{[\mathrm{MHz}]}) - 13.82\log_{10}(h_{BS\ [\mathrm{m}]}) - H_{mu\ [\mathrm{dB}]}(h_{MT}, f)$
	$H_{mu\ [\mathrm{dB}]}(h_{MT}, f) = h_{MT\ [\mathrm{m}]}[1.10\log_{10}(f_{[\mathrm{MHz}]}) - 0.70] - [1.56\log_{10}(f_{[\mathrm{MHz}]}) - 0.8]$
	$\sigma_{[\mathrm{dB}]}(f) = 0.70\log_{10}(f_{[\mathrm{MHz}]})^2 - 2.50\log_{10}(f_{[\mathrm{MHz}]}) + 11.10$
Suburban	$L_{ref\ [\mathrm{dB}]} = 69.55 + 26.16\log_{10}(f_{[\mathrm{MHz}]}) - 13.82\log_{10}(h_{BS\ [\mathrm{m}]}) - H_{mu\ [\mathrm{dB}]}(h_{MT}, f) -2.0\log_{10}\left(\frac{f_{[\mathrm{MHz}]}}{28}\right)^2 - 5.40$
	$H_{mu\ [\mathrm{dB}]}(h_{MT}, f) = h_{MT\ [\mathrm{m}]}[1.10\log_{10}(f_{[\mathrm{MHz}]}) - 0.70] - [1.56\log_{10}(f_{[\mathrm{MHz}]}) - 0.8]$
	$\sigma_{[\mathrm{dB}]}(f) = 0.98\log_{10}(f_{[\mathrm{MHz}]})^2 - 3.40\log_{10}(f_{[\mathrm{MHz}]}) + 11.88$
Rural	$L_{ref\ [\mathrm{dB}]} = 69.55 + 26.16\log_{10}(f_{[\mathrm{MHz}]}) - 13.82\log_{10}(h_{BS\ [\mathrm{m}]}) - H_{mu\ [\mathrm{dB}]}(h_{MT}, f) -4.78\log_{10}(f_{[\mathrm{MHz}]})^2 + 18.33\log_{10}(f_{[\mathrm{MHz}]}) - 40.9$
	$H_{mu\ [\mathrm{dB}]}(h_{MT}, f) = h_{MT\ [\mathrm{m}]}[1.10\log_{10}(f_{[\mathrm{MHz}]}) - 0.70] - [1.56\log_{10}(f_{[\mathrm{MHz}]}) - 0.8]$
	$\sigma_{[\mathrm{dB}]}(f) = 0.98\log_{10}(f_{[\mathrm{MHz}]})^2 - 3.40\log_{10}(f_{[\mathrm{MHz}]}) + 11.88$
All	$a_{pd} = 4.49 - 0.655\log_{10}(h_{BS\ [\mathrm{m}]})$

One uses:

- h_{BS}: height of the BS;
- h_{MT}: height of the MT.

Table A.2. Indoors path loss model (extracted from [Corr20]).

Scenario	Indoors Path-Loss Equations	$\sigma_{[\mathrm{dB}]}$	Validity Range
All	$L_{P\ ind\ [\mathrm{dB}]} = 6.6 + 2.1f_{[\mathrm{GHz}]} - 1.5N_f$	6	$N_f \leq N_{f\ th}$
	$L_{P\ ind\ [\mathrm{dB}]} = 0$		$N_f > N_{f\ th}$

where:

$$N_{f\ th} = \left\lfloor \frac{6.6 + 2.1f_{[\mathrm{GHz}]}}{1.5} \right\rfloor \quad (A.10)$$

and:

- $L_{P\ ind}$: indoors path loss;
- f: carrier frequency;
- N_f: user's floor number;

- $N_{f\ th}$: threshold floor number.

For the users that are indoors, the reference path loss is then given by:

$$L_{ref\ [\mathrm{dB}]}^{ind} = L_{ref\ [\mathrm{dB}]} + L_{P\ ind\ [\mathrm{dB}]} \qquad (A.11)$$

One may notice that for users on the floors above the threshold floor number, there is no additional indoors attenuation. This behaviour may be explained due to, generally, the BS's height being above the average height of the buildings in the considered scenario. Consequently, the highest building floors may have LOS to the BS, while at the lowest floors may occur severe shadowing. The indoors model is valid for frequencies between 700 MHz and 3.8 GHz.

Table A.3. WINNER II model equations for different scenarios (extracted from [WINN07]).

Scenario		WINNER Equations	$\sigma_{[\mathrm{dB}]}$	Validity Range
Urban	LOS	$L_{ref\ [dB]} = 117 + 20\log_{10}\left(\frac{f_{[GHz]}}{5}\right)$ $a_{pd} = 2.6$	4	$0.01 \le d_{[\mathrm{km}]} < d_{BP}$
		$L_{ref\ [dB]} = 133.47 + 6\log_{10}\left(\frac{f_{[GHz]}}{5}\right) - 14\log_{10}(h_{BS\ [\mathrm{m}]}) - 14\log_{10}(h_{MT\ [\mathrm{m}]})$ $a_{pd} = 4$	6	$d_{BP} \le d_{[\mathrm{km}]} \le 5$
	NLOS	$L_{ref\ [dB]} = 30a_{pd} + 34.46 + 23\log_{10}\left(\frac{f_{[GHz]}}{5}\right) + 5.83\log_{10}(h_{BS\ [\mathrm{m}]})$ $a_{pd} = 4.49 - 0.655\log_{10}(h_{BS\ [\mathrm{m}]})$	8	$0.05 \le d_{[\mathrm{km}]} \le 5$
Suburban	LOS	$L_{ref\ [dB]} = 112.6 + 20\log_{10}\left(\frac{f_{[GHz]}}{5}\right)$ $a_{pd} = 2.38$	4	$0.03 \le d_{[\mathrm{km}]} < d'_{BP}$
		$L_{ref\ [dB]} = 131.65 + 3.8\log_{10}\left(\frac{f_{[GHz]}}{5}\right) - 16.2\log_{10}(h_{BS\ [\mathrm{m}]}) - 16.2\log_{10}(h_{MT\ [\mathrm{m}]})$ $a_{pd} = 4$	6	$d'_{BP} \le d_{[\mathrm{km}]} \le 5$
	NLOS	$L_{ref\ [dB]} = 30a_{pd} + 31.46 + 23\log_{10}\left(\frac{f_{[GHz]}}{5}\right) + 5.83\log_{10}(h_{BS\ [\mathrm{m}]})$ $a_{pd} = 4.49 - 0.655\log_{10}(h_{BS\ [\mathrm{m}]})$	8	$0.05 \le d_{[\mathrm{km}]} \le 5$
Rural	LOS	$L_{ref\ [dB]} = 108.7 + 20\log_{10}\left(\frac{f_{[GHz]}}{5}\right)$ $a_{pd} = 2.15$	4	$0.01 \le d_{[\mathrm{km}]} < d'_{BP}$
		$L_{ref\ [dB]} = 130.5 + 1.5\log_{10}\left(\frac{f_{[GHz]}}{5}\right) - 18.5\log_{10}(h_{BS\ [\mathrm{m}]}) - 18.5\log_{10}(h_{MT\ [\mathrm{m}]})$ $a_{pd} = 4$	6	$d'_{BP} \le d_{[\mathrm{km}]} \le 10$
	NLOS	$L_{ref\ [dB]} = 130.7 + 21.3\log_{10}\left(\frac{f_{[GHz]}}{5}\right) - 0.13(h_{BS\ [\mathrm{m}]} - 25) - 0.9\log_{10}(h_{MT\ [\mathrm{m}]} - 1.5)$ $a_{pd} = 2.51 - 0.013(h_{BS\ [\mathrm{m}]} - 25)$	8	$0.05 \le d_{[\mathrm{km}]} \le 5$

One uses:

- d_{BP}: urban breaking point distance;

- d'_{BP}: suburban and rural breaking point distance.

where:

$$d_{BP\ [\mathrm{m}]} = \frac{4\left(h_{BS\ [\mathrm{m}]} - 1\right)\left(h_{MT\ [\mathrm{m}]} - 1\right)}{\lambda_{[\mathrm{m}]}} \quad (A.12)$$

$$d'_{BP\ [\mathrm{m}]} = \frac{4 h_{BS\ [\mathrm{m}]} h_{MT\ [\mathrm{m}]}}{\lambda_{[\mathrm{m}]}} \quad (A.13)$$

A.3 Users and Resources

In this section, the fundamental formulations regarding the BS's resources and the throughput for each user are described.

According to [Belc18] the number of RBs allocated to each user is given by:

$$N_{RB}^{user} = \frac{N_{RB,cell}}{N_{users}} \quad (A.14)$$

where:

- $N_{RB,cell}$: total number of RBs in a cell;
- N_{users}: the total number of users.

The theoretical throughput in DL for each user can be calculated as follows:

$$R_{b\ [\mathrm{bit/s}]}^{user} = \frac{N_{RB}^{user}\ N_{SC}^{RB}\ N_{MIMO}\ N_{symb}^{SF}\ \log_2(M)_{[\mathrm{bits/symbol}]}}{\tau_{SF\ [\mathrm{s}]}} \quad (A.15)$$

where:

- N_{SC}^{RB}: number of subcarriers in an RB (12 for all numerologies);
- N_{MIMO}: MIMO order (e.g. 2×2 MIMO means the order is 2);
- N_{symb}^{SF}: number of symbols per subframe (numerology dependent);
- τ_{SF} : subframe duration (1 ms for all numerologies).

Note that the throughput computed in (A.15) is not taking into consideration the inclusion of control and synchronisation data.

A.4 SINR versus Throughput

In this section, the relationship between the SINR and the throughput for the different modulation schemes and coding rates supported by NR is presented.

The expressions for each modulation and the corresponding coding rates were extracted from [Viei18] and [Belc18]. According to [Belc18], the coding rate assigned to each modulation is the average value of the coding rates obtained according to the QCI (Quality Channel Indicator)reported by the MT. These are represented in Table A.4.

Table A.4. Coding rate for each modulation scheme (extracted from [Belc18] and [Viei18]).

Modulation Scheme	Coding Rate
QPSK	1/3
16-QAM	1/2
64-QAM	3/4
256-QAM	[0.70, 0.94]

For the QPSK modulation, the throughput per RB and the respective SINR are expressed as follows:

$$R^{RB}_{b,QPSK\ [\text{bit/s}]} = \frac{2.34201 \times 10^6}{14.0051 + e^{-0.577897 \rho_{SINR\ [\text{dB}]}}} \quad (A.16)$$

$$\rho_{SINR\ [\text{dB}]} = -\frac{1}{0.577897} \times \ln\left(\frac{2.34201 \times 10^6}{R^{RB}_{b,QPSK\ [\text{bit/s}]}} - 14.0051\right) \quad (A.17)$$

For the 16-QAM modulation, the throughput per RB and the respective SINR are given by:

$$R^{RB}_{b,16-QAM\ [\text{bit/s}]} = \frac{47613.1}{0.0926275 + e^{-0.295838 \rho_{SINR\ [\text{dB}]}}} \quad (A.18)$$

$$\rho_{SINR\ [\text{dB}]} = -\frac{1}{0.295838} \ln\left(\frac{47613.1}{R^{RB}_{b,16-QAM\ [\text{bit/s}]}} - 0.0926275\right) \quad (A.19)$$

For the 64-QAM modulation, the throughput per RB and the respective SINR are defined as:

$$R^{RB}_{b,64-QAM\ [\text{bit/s}]} = \frac{26405.8}{0.0220186 + e^{-0.24491 \rho_{SINR\ [\text{dB}]}}} \quad (A.20)$$

$$\rho_{SINR\ [\text{dB}]} = -\frac{1}{0.24491} \ln\left(\frac{26405.8}{R^{RB}_{b,64-QAM\ [\text{bit/s}]}} - 0.0220186\right) \quad (A.21)$$

For the 256-QAM, the expressions for the throughput per RB and the respective SINR are given by:

$$R^{RB}_{b,256-QAM\ [\text{bit/s}]} = \frac{26407.1}{0.0178868 + e^{-0.198952 \rho_{SINR\ [\text{dB}]}}} \quad (A.22)$$

$$\rho_{SINR\ [\text{dB}]} = -\frac{1}{0.198952} \ln\left(\frac{26407.1}{R^{RB}_{b,256-QAM\ [\text{bit/s}]}} - 0.0178868\right) \quad (A.23)$$

One must note that these expressions were determined for MIMO 2x2 and numerology configuration 0. According to [Viei18], for other SCS configurations, the maximum throughput difference per modulation should be the ratio between the higher SCS and the 15 kHz standard spacing (numerology configuration 0). The same logic can be applied to higher MIMO orders, for example, in the best-case scenario, for a

connection using MIMO 4x4, the throughput is 2 times the referenced one.

In order to define the modulation borders, a general formula for the throughput per RB comprising the best modulation for each SINR must be computed. With the MATLAB software, it is possible to plot the previous equations and find the intersection points, Figure A.1, in order to specify the borders of each modulation with relation to the SINR.

The general expression for the throughput per RB as a function of the SINR is then given by:

$$R_{b\,[\mathrm{bit/s}]}^{RB} = 2^{\mu}\ \frac{N_{MIMO}}{2}\begin{cases}\dfrac{2.34201\times 10^{6}}{14.0051+e^{-0.577897\rho_{SINR\,[\mathrm{dB}]}}}, & -10 \le \rho_{SINR\,[\mathrm{dB}]} \le 5.56\\ \dfrac{47613.1}{0.0926275+e^{-0.295838\rho_{SINR\,[\mathrm{dB}]}}}, & 5.56 < \rho_{SINR\,[\mathrm{dB}]} \le 13.03\\ \dfrac{26405.8}{0.0220186+e^{-0.24491\rho_{SINR\,[\mathrm{dB}]}}}, & 13.03 < \rho_{SINR\,[\mathrm{dB}]} \le 25.75\\ \dfrac{26407.1}{0.0178868+e^{-0.198952\rho_{SINR\,[\mathrm{dB}]}}}, & \rho_{SINR\,[\mathrm{dB}]} > 25.75\end{cases} \qquad (A.24)$$

Note that, since the expressions for the throughput were computed for numerology configuration 0 and 2x2 MIMO, the general expression for any given numerology and MIMO level must be given by (A.24) for the best-case scenario, as explained above.

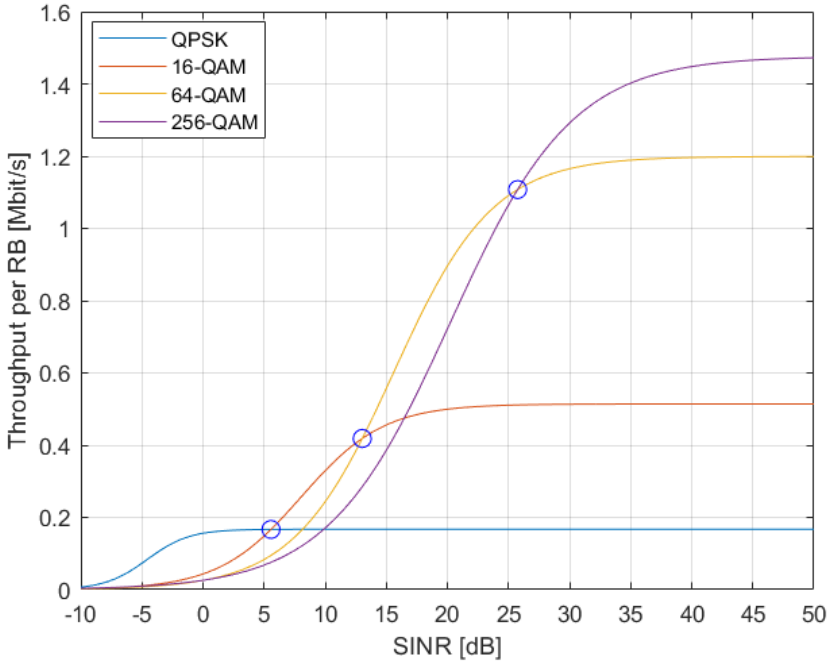

Figure A.1. Throughput per RB as a function of SINR for MIMO 2x2 and SCS of 15 kHz.

Annex B

Additional Model Assessment Data

This annex presents complementary data and respective analysis regarding the assessment of the exclusion zone evaluation model and the coverage and capacity planning model.

B.1 Exclusion Zone Evaluation Assessment

The complementary data regarding the assessment of the exclusion zone evaluation model is presented in figures B.1, D_{front} as a function of antenna gain, and B.2, the variation of D_{front} with respect to the reference values for power density exposure.

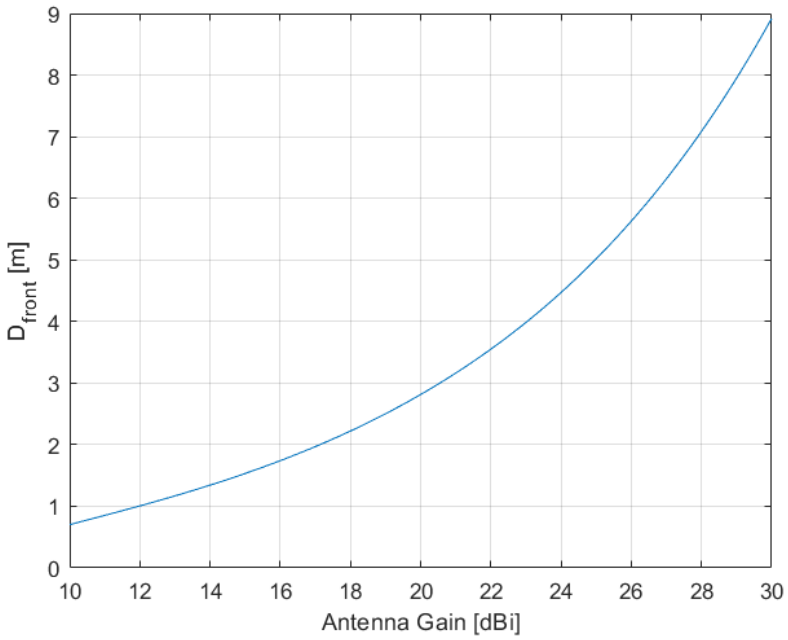

Figure B.1. D_{front} as a function of the antenna gain.

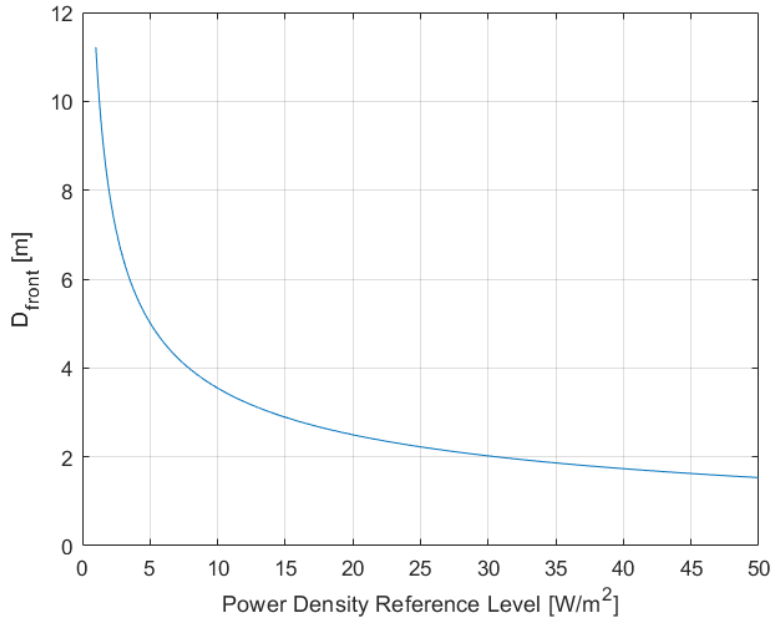

Figure B.2. D_{front} as a function of the reference level for EMF exposure.

As can be observed, the increase in the reference values means that the threshold for the maximum allowed exposure is higher. This is the case for the occupational public, e.g. maintenance workers, which possess the proper equipment and need to be closer to the antennas, thus having a higher value for the allowed maximum exposure. In some countries, the regulators impose, for the general public, exposure limits that are below the ones presented by ICNIRP. This causes compliance distances to be greater than those of countries that impose the limits set by ICNIRP. As can be observed in Figure B.2, the front border of the exclusion zone follows this behaviour. By limiting the exposure reference values, the compliance distance increases when compared to higher values for the maximum allowed exposure.

B.2 Coverage and Capacity Assessment

The complementary data regarding the assessment of the coverage and capacity planning is presented from figures B.3 and B.17.

The variation of the cell radius with respect to the MT's height is represented in figures B.3 and B.4. As can be observed, the behaviour is similar to the test for the BS height due to the same reasons. One must note that the scenario chosen for the simulation of the 3.6 GHz band is the NLOS one. Since for this case, the WINNER II equations for the urban and suburban environments do not depend on the MT's height, the cell radius remains constant as observed.

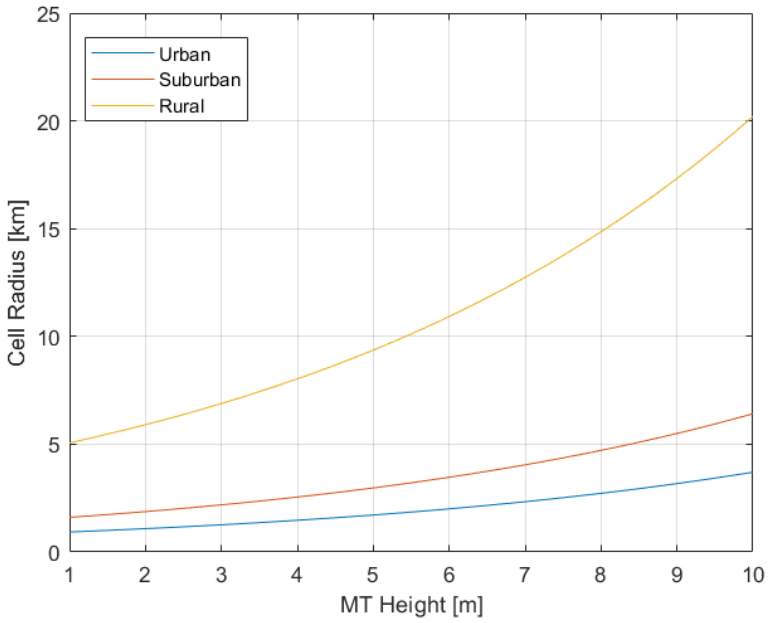

Figure B.3. Cell radius versus MT height for the 700 MHz band.

In figures B.5 and B.6, it is represented the dependency of the cell radius with regard to the transmitted power for the 700 MHz and 3.6 GHz bands respectively. As is expected, as the transmitted power increases the cell radius also increases. From this behaviour, it can be understood how the restrictions

in the transmitted powers can affect cellular planning. Lower transmitted powers may cause severe cell densification or even a reduced QoS offered to the user.

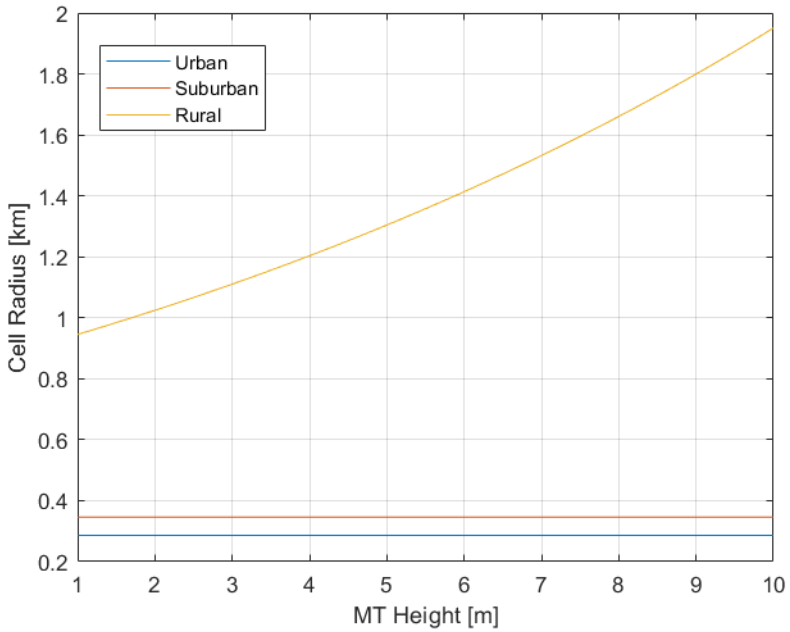

Figure B.4. Cell radius versus MT height for the 3.6 GHz band.

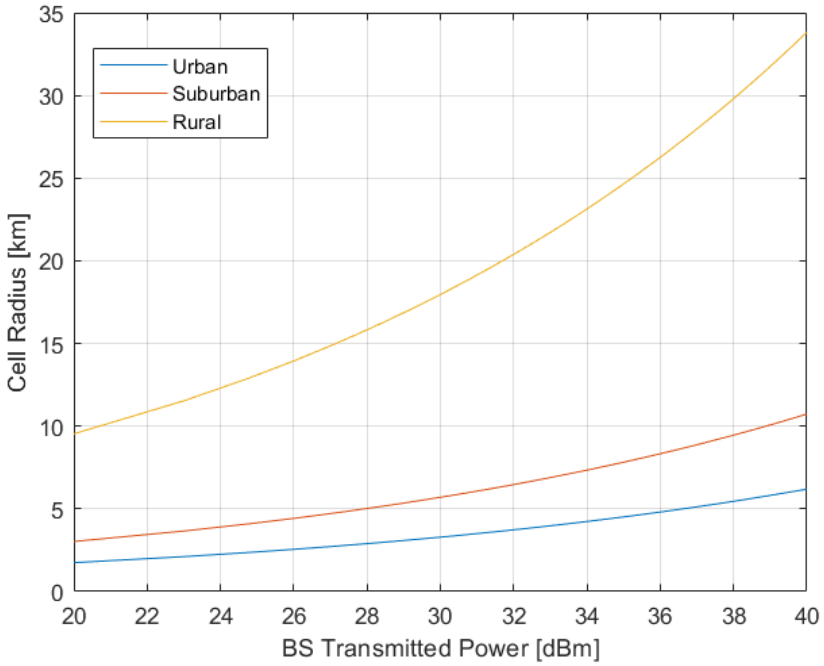

Figure B.5. Cell radius versus BS transmitted power for the 700 MHz band.

The cell radius variation as a function of frequency for both Okumura-Hata and WINNER II models is represented in figures B.7 and B.8 respectively. Since the path loss is greater for higher frequencies the decreasing behaviour of the cell radius, as can be observed, is the expected one. Both propagation models are represented separately since they do not share the same frequency interval. One should

observe that, given these properties, the 700 MHz band in NR can be used when wider cells are required for a higher coverage, while the 3.6 GHz band can be used in an environment where the need for capacity is greater and smaller cells are required.

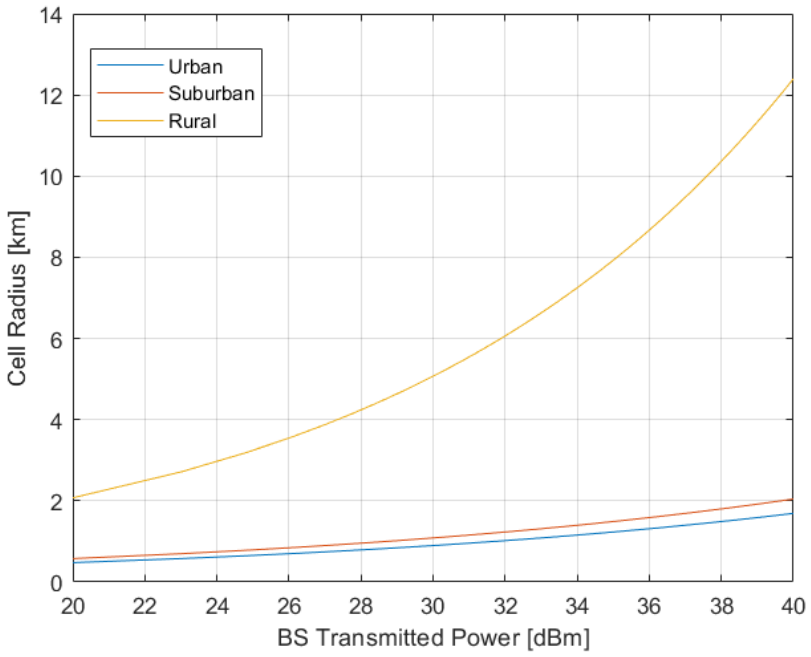

Figure B.6. Cell radius versus BS transmitted power for the 3.6 GHz band.

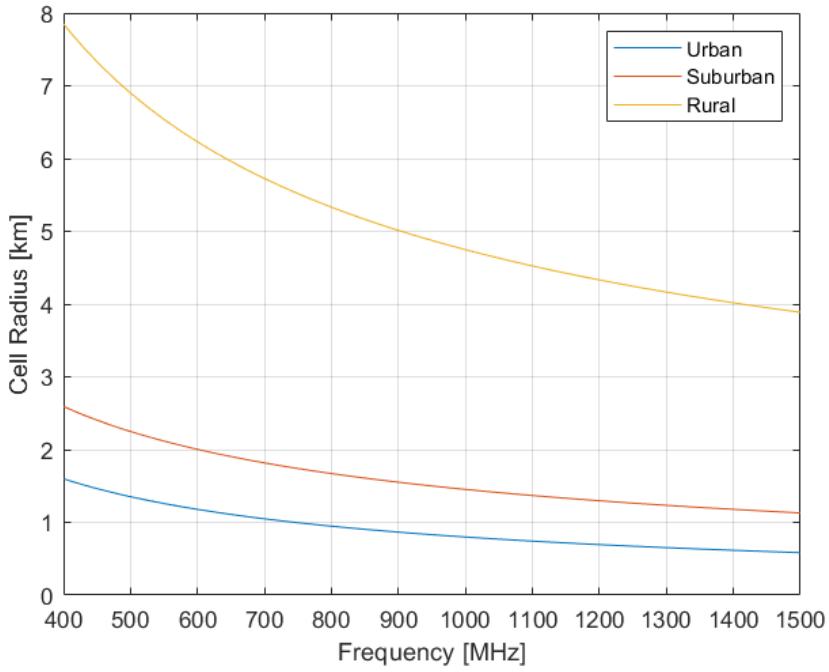

Figure B.7. Cell radius versus frequency for the Okumura-Hata model.

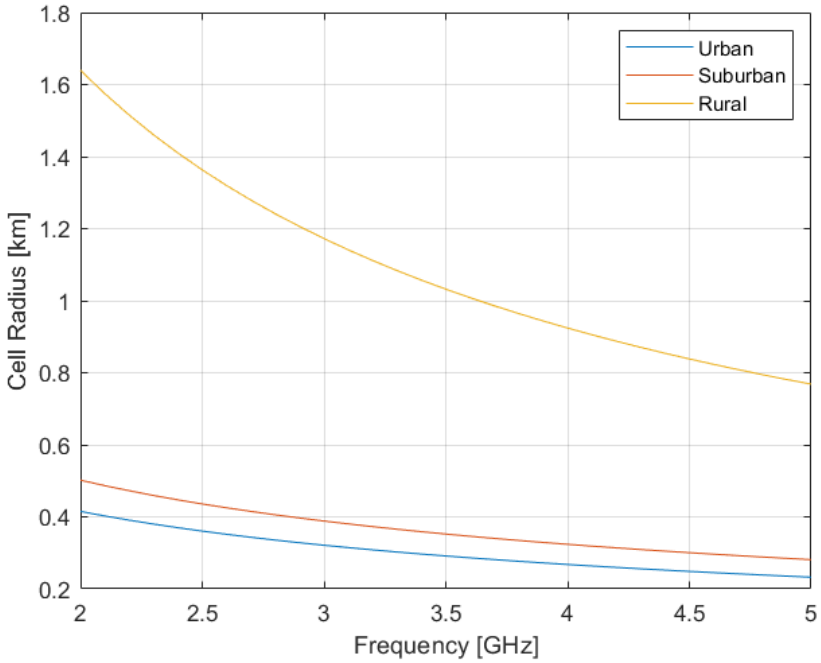

Figure B.8. Cell radius versus frequency for the WINNER II model.

In figures B.9 and B.10 is represented the variation of cell radius as a function of the coverage probability. As stated in Section 3.4, for a coverage probability of 50% the received power must be equal to the receiver's sensitivity. Usually, operators set the coverage probability to be 90% or higher, for cell-edge, in order to offer to the user a good overall service. In order to increase the coverage probability, the received power must also be increased as can be interpreted by (A.6) and (A.7). For example, for a coverage probability of 90%, the received power must be 10.25 dB above the receiver's sensitivity. This result is taken for an urban environment using the WINNER II propagation model in an NLOS situation.

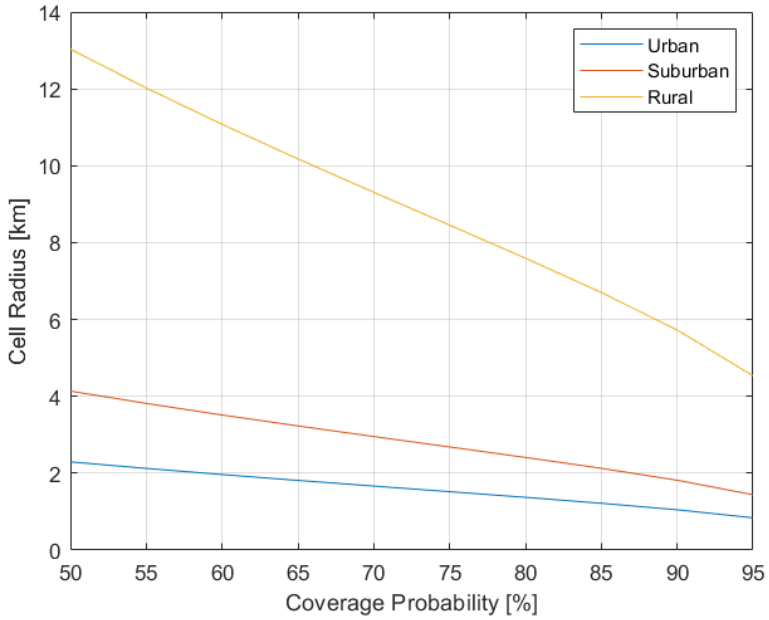

Figure B.9. Cell radius versus coverage probability for the 700 MHz band.

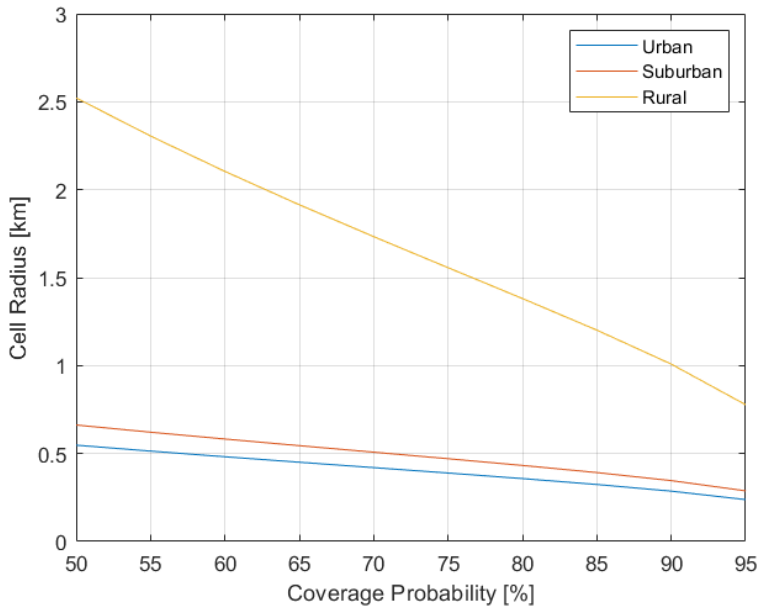

Figure B.10. Cell radius versus coverage probability for the 3.6 GHz band.

One of the novelties introduced in NR is the concept of numerology where the SCS can vary, as opposed to LTE where the SCS is 15 kHz and constant. As can be observed in (A.4), the receiver's sensitivity depends on the bandwidth of the SCS. The higher the SCS's bandwidth, the higher the receiver's sensitivity, meaning that the cell radius should be lower for higher numerologies. As explained in Section 3.4, by increasing the SCS, the available throughput in an RB is increased. This causes a reduction in cell radius, or, by fixing the cell radius, the coverage probability is decreased. In figures B.11 and B.12 is represented the variation of the cell radius for different SCS and different scenarios, for the 700 MHz and 3.6 GHz bands respectively. As can be observed for all scenarios, the cell radius decreases by increasing the SCS.

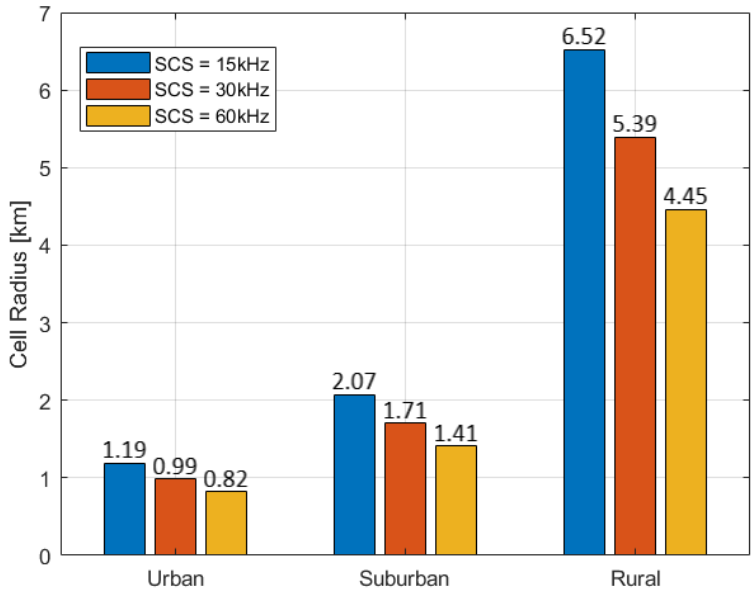

Figure B.11. Cell radius for different SCS in different scenarios for the 700 MHz band.

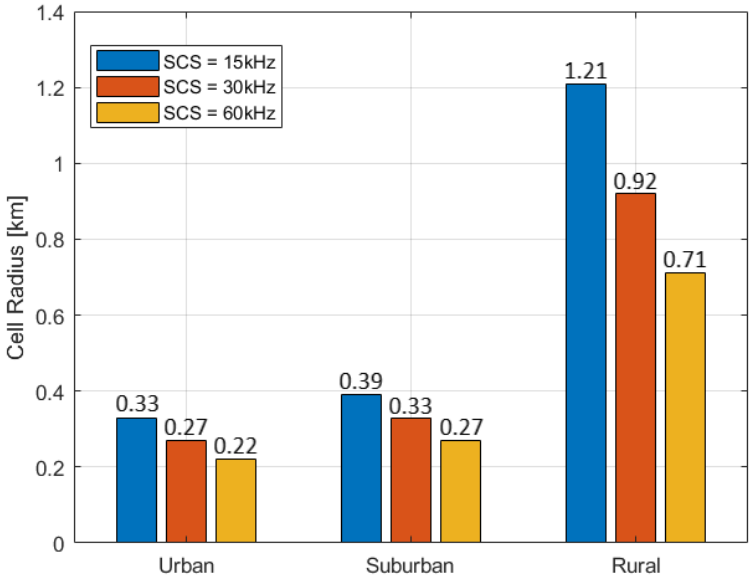

Figure B.12. Cell radius for different SCS in different scenarios for the 3.6 GHz band.

An important parameter to take into account when providing a certain service is the user's SINR. As seen in the previous section, the offered throughput per RB is a direct function of the SINR. For a fixed location where the noise and interference power is constant, the higher the received power the higher the SINR. In a situation where the user is not in LOS with the BS, the communication is established through multipath, which causes a decrease in received power and the possibility of occurring deep signal fading. For the LOS situation, besides the multipath components, there is the direct component which increases the received power significantly. The comparison of the SINR between the LOS and NLOS situation is presented in Figure B.13. As can be observed, the differences in the SINR are significant between the LOS and NLOS case.

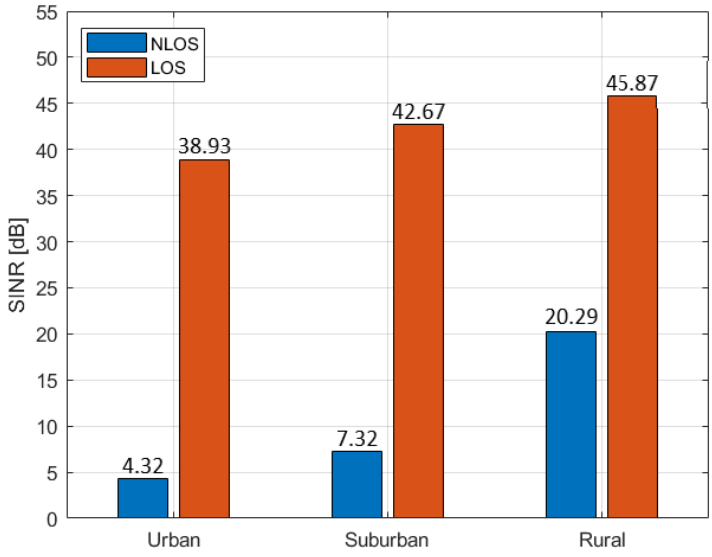

Figure B.13. SINR comparison between LOS and NLOS case for different scenarios.

Another important aspect that needs to be taken into account is the performance of the service offered to indoors users. Usually, as can be observed from Table A.2, indoors users can have a severe reduction in the SINR, and consequently, the throughput, when compared to outdoors users due to the extra propagation loss associated. Depending on the location of the user inside the building, this reduction may cause an important decrease in the offered QoS. The SINR and the throughput per RB for both the 700 MHz and 3.6 GHz bands and for indoors and outdoors users are represented from figures B.14 to B.17.

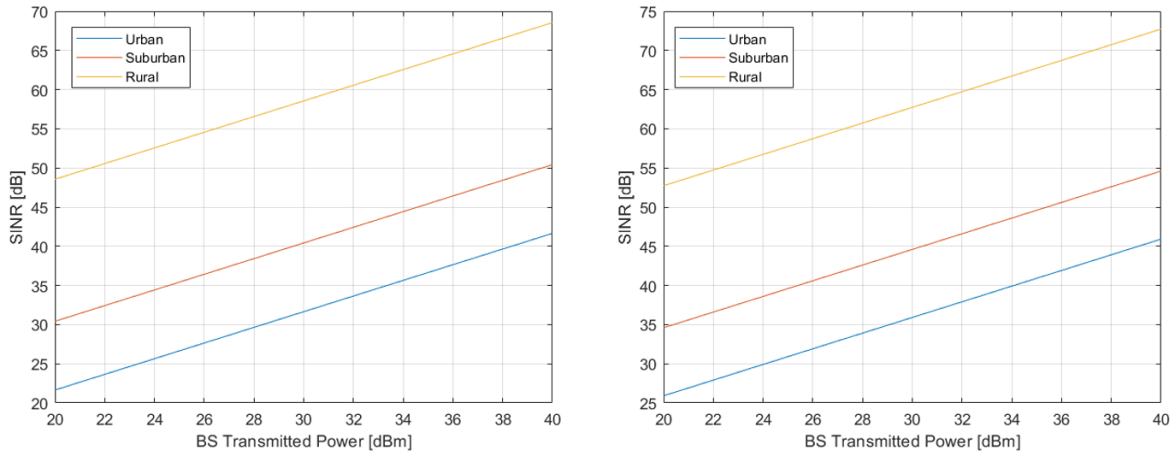

a) Indoors users. b) Outdoors users.

Figure B.14. Comparison of SINR between indoors and outdoors users for the 700 MHz band.

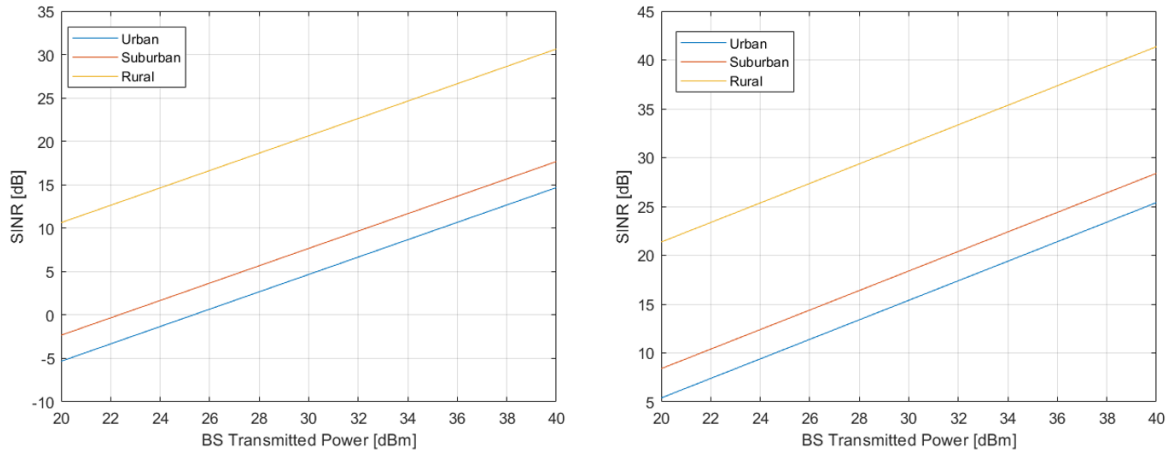

a) Indoors users. b) Outdoors users.

Figure B.15 Comparison of SINR between indoors and outdoors users for the 3.6 GHz band.

As can be observed in figures B.14 and B.15, the difference in SINR from indoors to outdoors is higher for the 3.6 GHz band. This is due to the penetration loss being higher for higher frequency bands. While for the 700 MHz band this difference may not cause a severe loss in service quality, the issue can be worst when considering the 3.6 GHz band. This is confirmed by figures B.16 and B.17. One may note that the difference in the throughput per RB is not very accentuated in the 700 MHz band. On the other hand, for the 3.6 GHz band, the throughput can be more than two times higher for outdoor users

comparing to indoor ones. The abrupt changes that occur in the throughput can be explained by the change in the modulation order as the SINR increases. One may also notice that the throughput per RB is generally higher for the 700 MHz band than for the 3.6 GHz band. This is purely due to the lower propagation loss on lower bands which in turn, for a fixed location, translates in a higher SINR. It needs to be taken into account that higher bands will provide a higher overall bandwidth, meaning that the available number of RBs will be higher, increasing the total available throughput. Note also that it is being assumed that the interference is equal and fixed for both frequency bands.

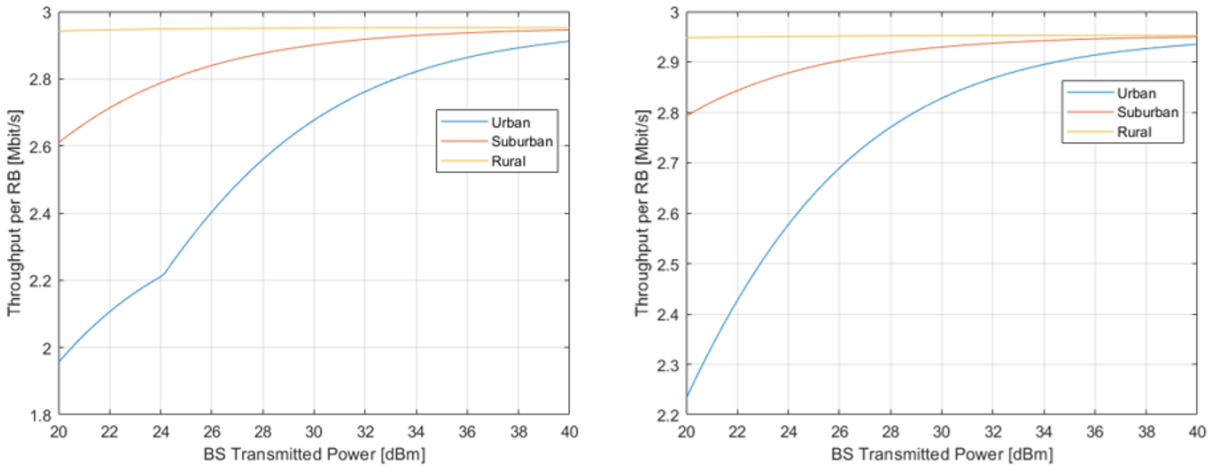

a) Indoors users. b) Outdoors users.

Figure B.16. Comparison of throughput per RB between indoors and outdoors users at cell edge for the 700 MHz band.

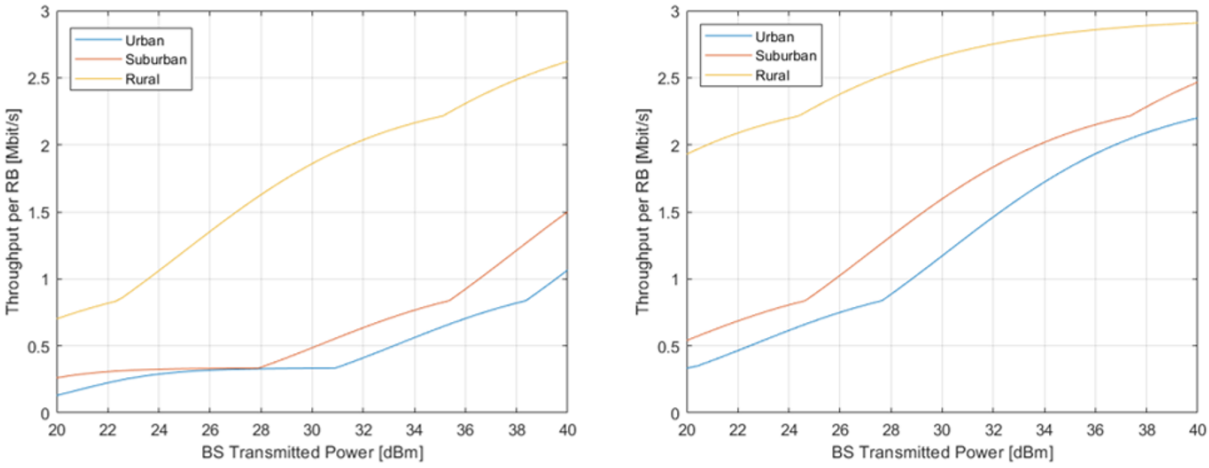

a) Indoors users. b) Outdoors users.

Figure B.17. Comparison of throughput per RB between indoors and outdoors users at cell edge for the 3.6 GHz band.

Annex C

Measurements Description and BS Characteristics

This annex presents the layout of the BSs where the measurements were performed, as well as their characteristics.

C.1 Measurements Description of BS1

In this subsection, the measurement layout for both sector 1 and sector 2 of BS1 are shown.

C.1.1 Sector 1

The horizontal and vertical plane sketches of sector 1 are presented in figures C.1 and C.2 respectively, and a photograph of the NR and legacy antennas is then presented in Figure C.3. Note that, in Figure C.1, the measurement point 1.1 is directly below the NR antenna.

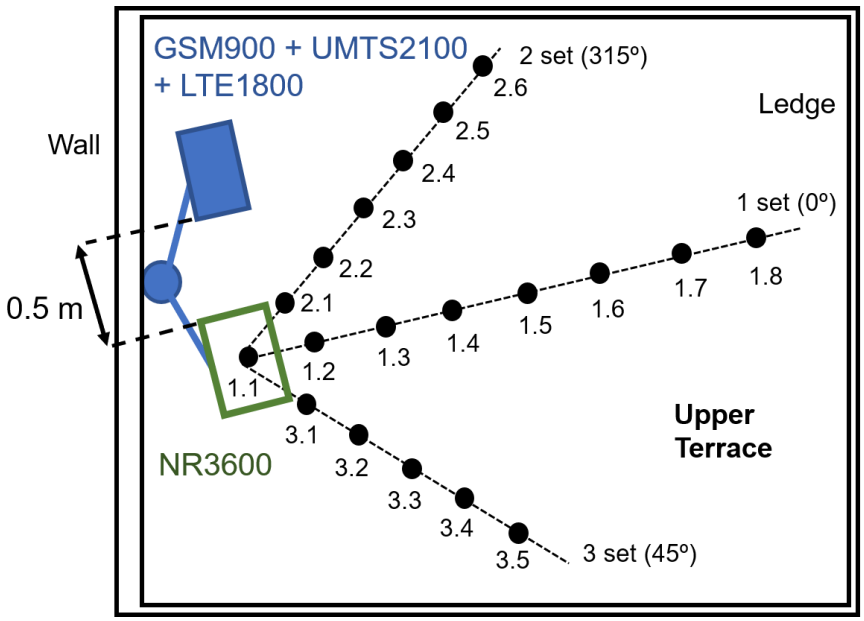

Figure C.1. Horizontal plane sketch for sector 1 of BS1.

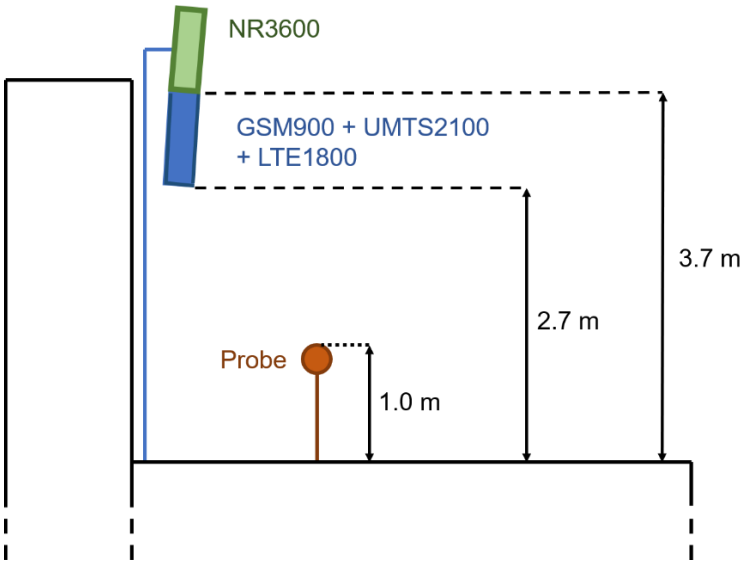

Figure C.2. Vertical plane sketch for sector 1 of BS1.

Figure C.3. Point of view from the lower terrace to sector 1 of BS1.

C.1.2 Sector 2

The horizontal and vertical plane sketches of sector 2 are presented in figures C.4 and C.5 respectively, and a photograph of the NR and legacy antennas is then presented in Figure C.6.

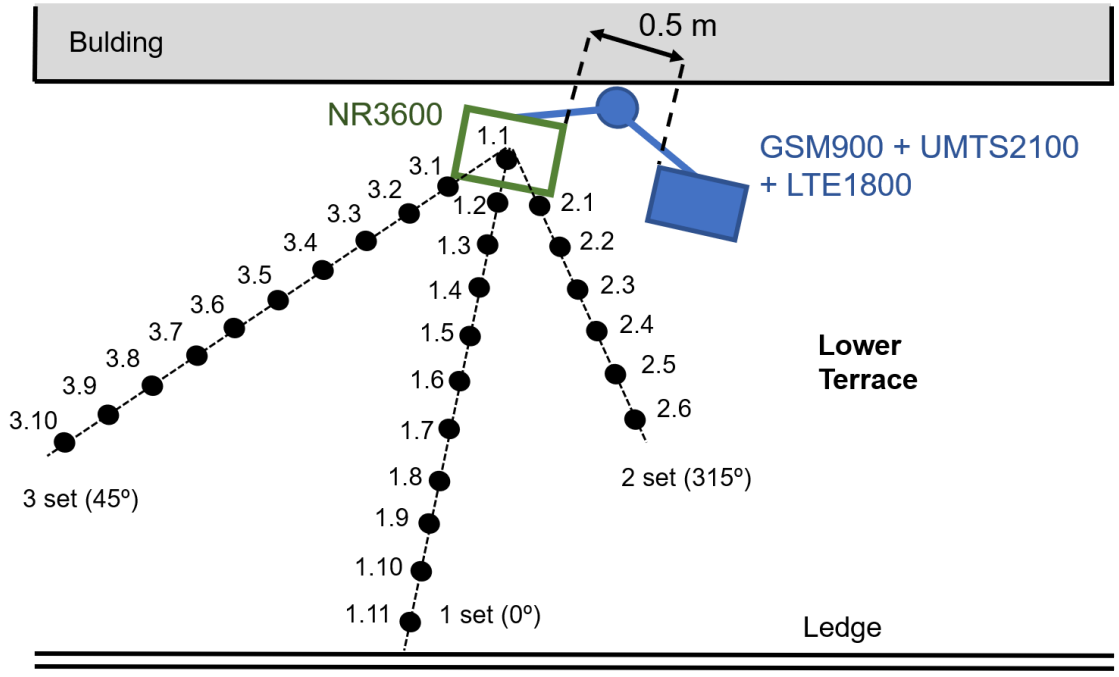

Figure C.4. Horizontal plane sketch for sector 2 of BS1.

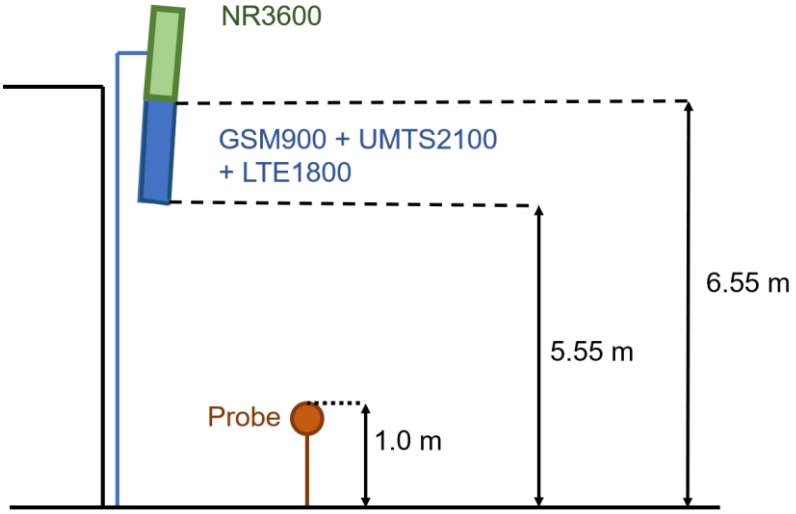

Figure C.5. Vertical plane sketch for sector 2 of BS1.

Figure C.6. Point of view from the lower terrace to sector 2 of BS1

C.2 Measurements Description of BS2

In this subsection, the experimental results and the measurement layout for both sector 1 (first set) and sector 2 (second and third set) of BS2 are shown. The vertical and horizontal plane sketches are presented in figures C.7 and C.8 respectively. The vertical configuration is the same for both sectors and thus the vertical sketch is representing sectors 1 and 2. As can be observed, in this BS the NR antenna is installed on top of the passive antenna. Photographs of sectors 1 and 2 are presented in figures C.9 and C.10 respectively.

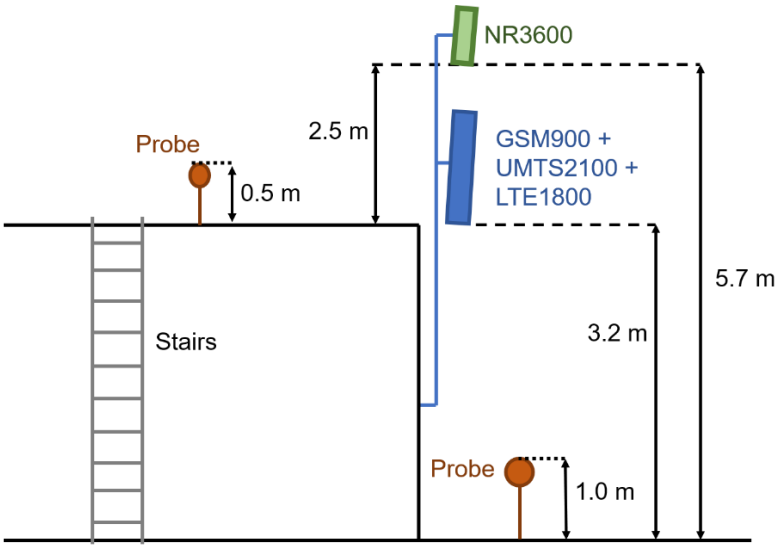

Figure C.7. Vertical plane sketch of BS2.

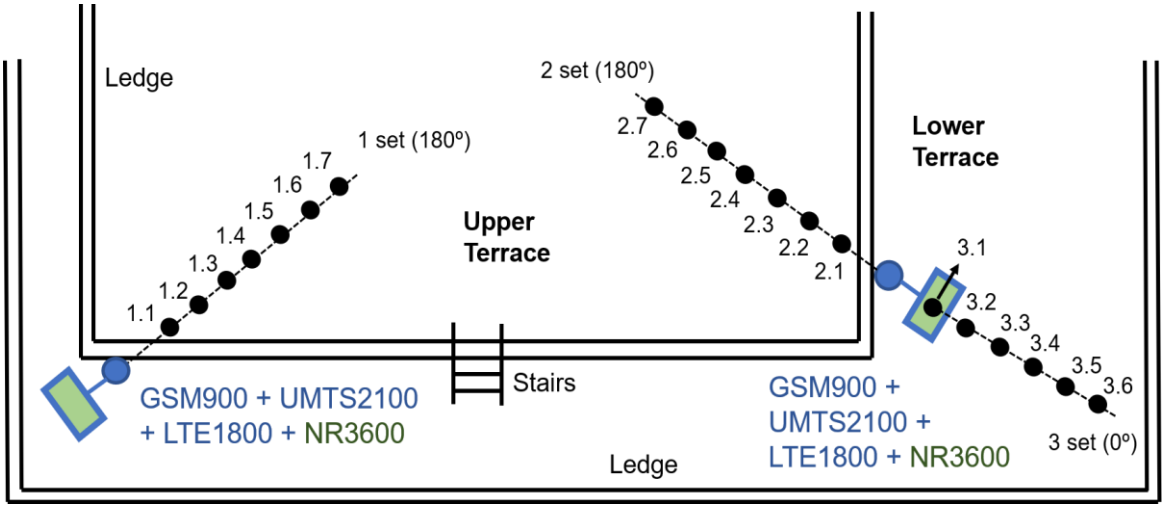

Figure C.8. Horizontal plane sketch of BS2.

Figure C.9. Point of view from the upper terrace to sector 1 of BS2.

Figure C.10. Point of view from the upper terrace to sector 2 of BS2.

C.3 BS Characteristics

The radio characteristics of the BSs where measurements were conducted are presented in Table C.1. Note that the number of carriers corresponds to GSM and UMTS while the number of MIMO elements corresponds to LTE and NR.

Table C.1. BSs radio characteristics.

BS	Sector	Systems	Tilt [º]	N_c/MIMO Elements	Transmitted Power [W]
BS1	1	GSM900	7	3	60
		UMTS2100	11	1	30
		LTE1800	11	2	80
		NR3600	11	64	160
	2	GSM900	7	3	60
		UMTS2100	6	1	30
		LTE1800	6	2	80
		NR3600	5	64	160
BS2	1	GSM900	6	4	80
		UMTS2100	7	2	60
		LTE1800	7	2	80
		NR3600	5	64	160
	2	GSM900	6	4	80
		UMTS2100	10	1	30
		LTE1800	10	2	80
		NR3600	10	64	160

Annex D

Measurements Results

This annex presents the results obtained for the conducted measurements and the comparison between these and the theoretical model results.

D.1 Measurements Results of BS1

In this subsection, the measurements results for both sector 1 and sector 2 of BS1 are shown, as well as the comparison between the results computed by the theoretical model and the measurements.

D.1.1 Sector 1

The comparison between the measurements and theoretical results for the first, second, and third set are presented from figures D.1 to D.6, and the results obtained from the measurements are presented in Table D.1.

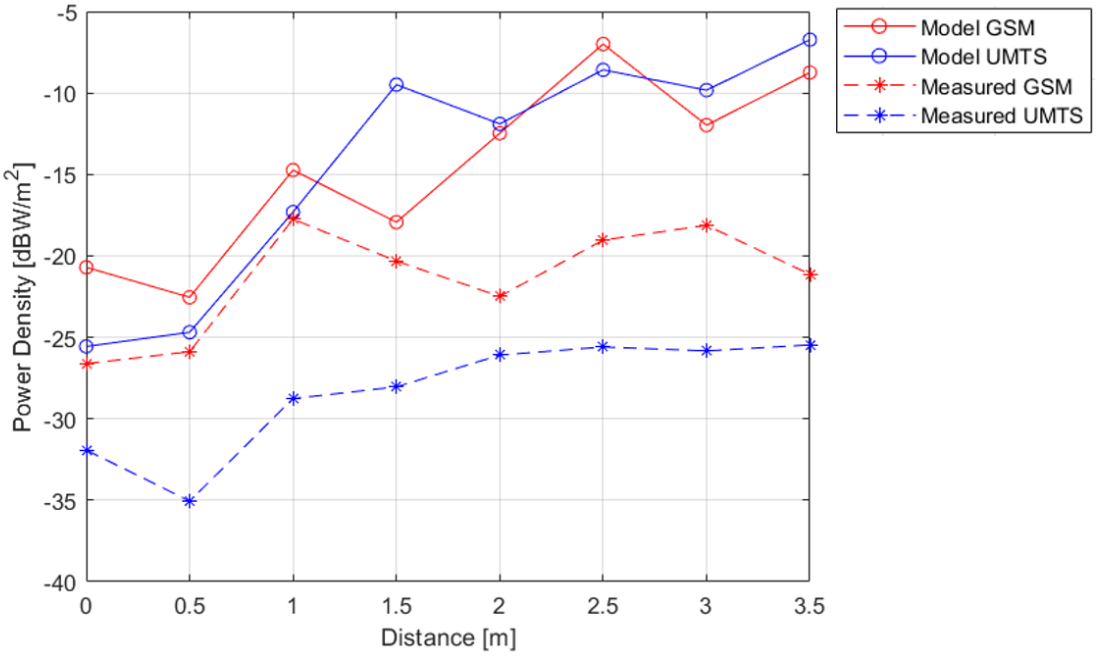

Figure D.1. Measured versus theoretical results of $S(d)$ for GSM900 and UMTS2100, for set 1 of BS1's sector 1.

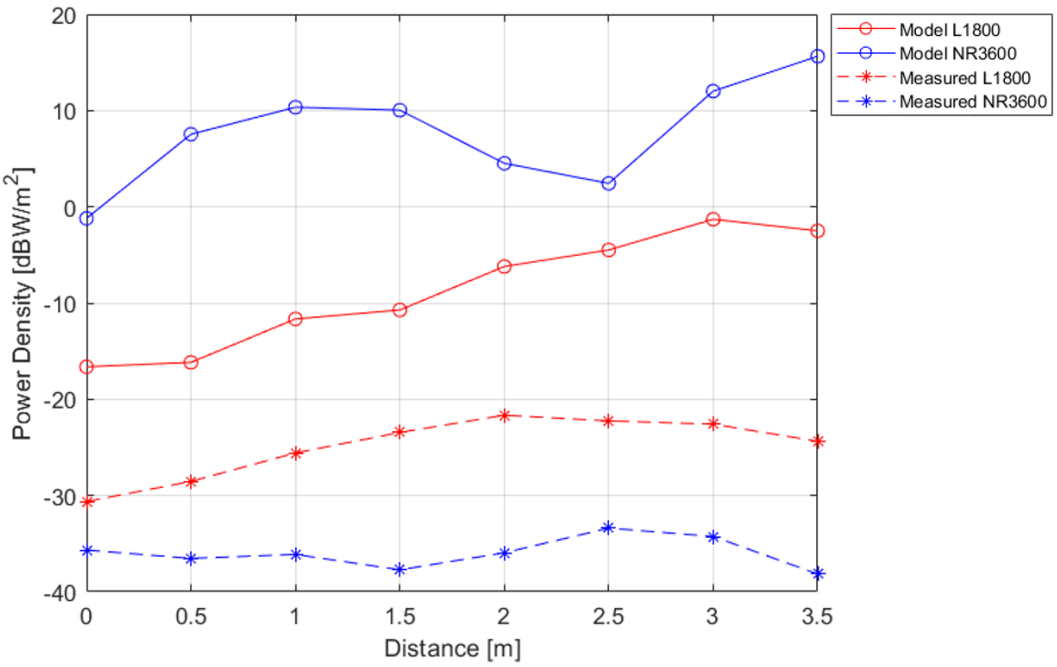

Figure D.2. Measured versus theoretical results of $S(d)$ for LTE1800 and NR3600, for set 1 of BS1's sector 1.

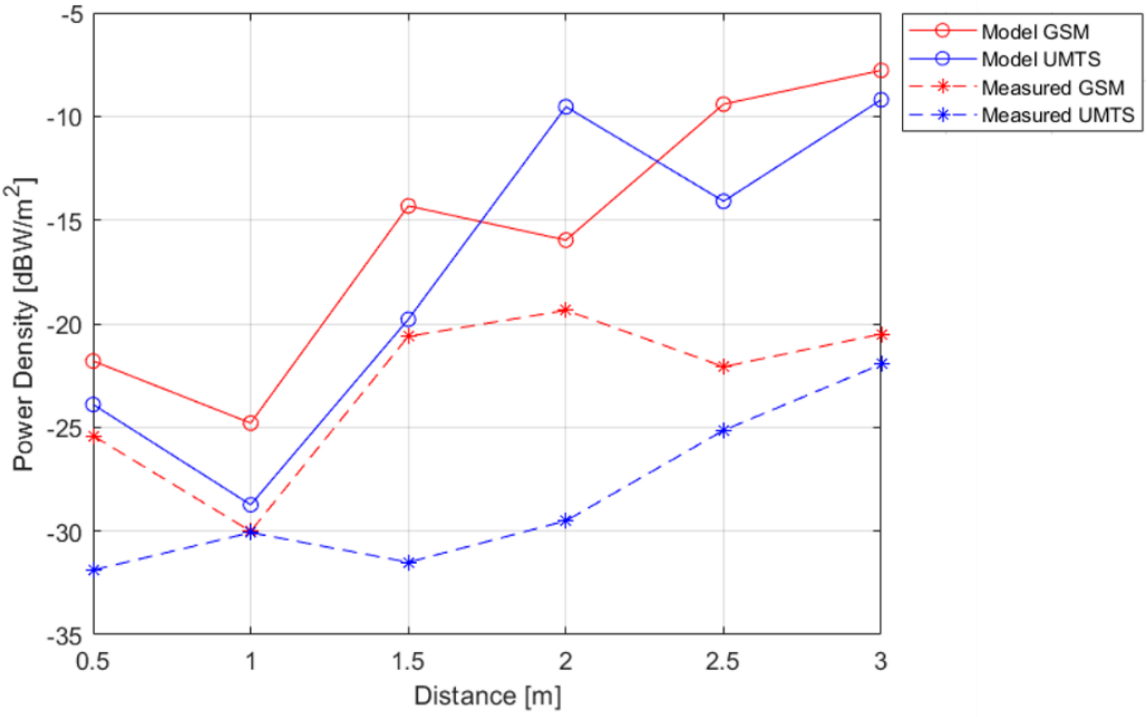

Figure D.3. Measured versus theoretical results of $S(d)$ for GSM900 and UMTS2100, for set 2 of BS1's sector 1.

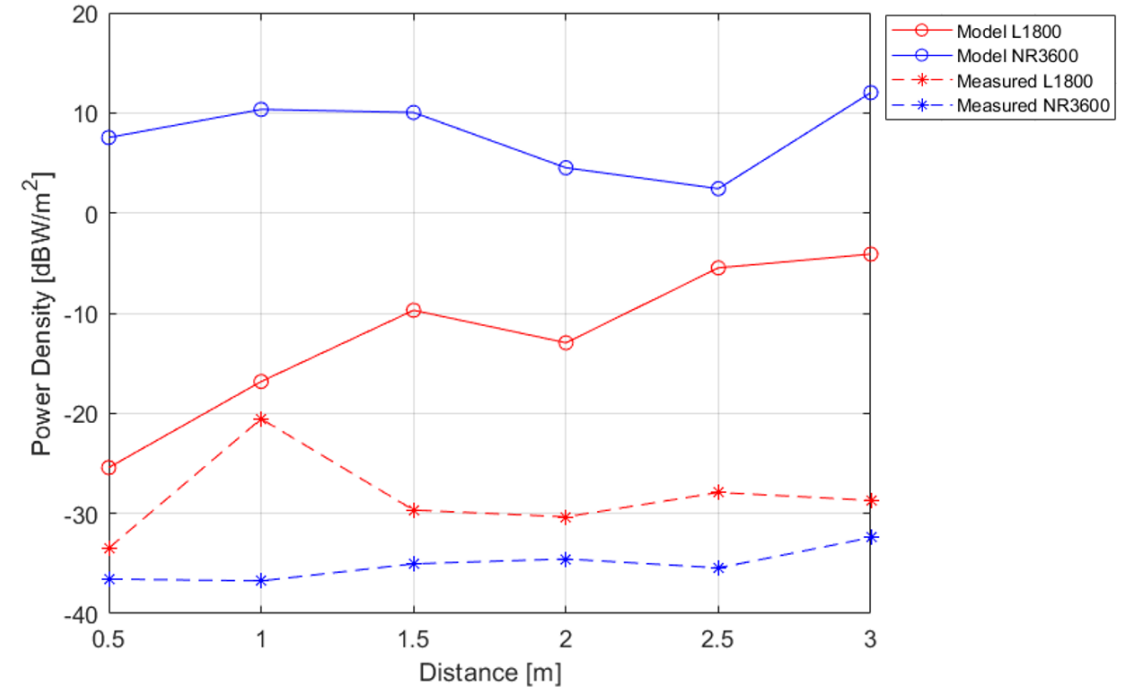

Figure D.4. Measured versus theoretical results of $S(d)$ for LTE1800 and NR3600, for set 2 of BS1's sector 1.

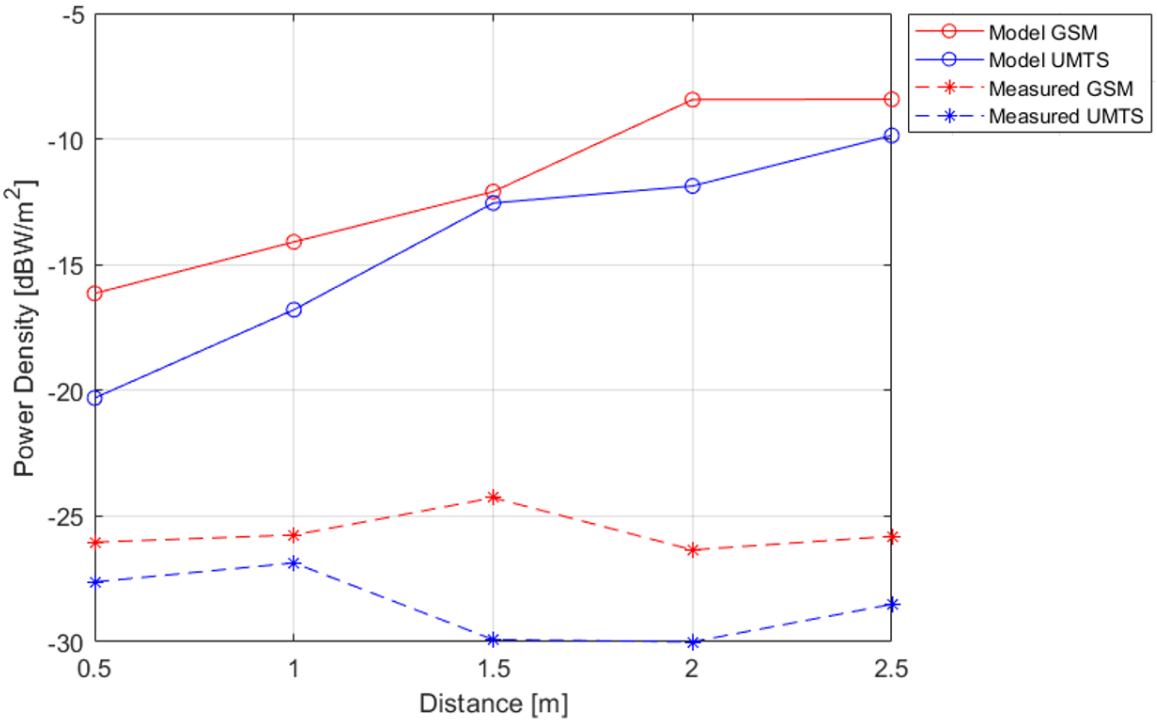

Figure D.5. Measured versus theoretical results of $S(d)$ for GSM900 and UMTS2100, for set 3 of BS1's sector 1.

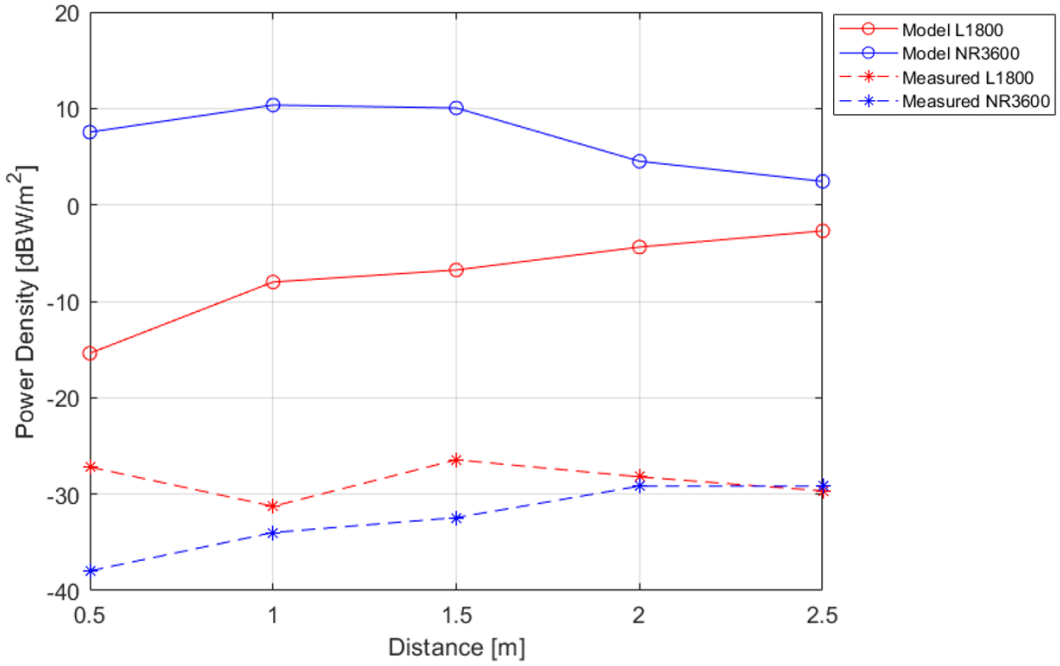

Figure D.6. Measured versus theoretical results of $S(d)$ for LTE1800 and NR3600, for set 3 of BS1's sector 1.

Table D.1. Measurement results for sector 1 of BS1.

Observation Point	Distance [m]	$S_{measure}[\mathrm{mW/m^2}]$			
		GSM900	UMTS2100	LTE1800	NR3600
1.1	0.0	2.180	0.643	0.865	0.271
1.2	0.5	2.575	0.312	1.396	0.222
1.3	1.0	16.825	1.334	2.769	0.244
1.4	1.5	9.290	1.571	4.517	0.169
1.5	2.0	5.635	2.460	6.827	0.254
1.6	2.5	12.510	2.755	5.958	0.458
1.7	3.0	15.435	2.600	5.507	0.375
1.8	3.5	7.700	2.840	3.660	0.153
2.1	0.5	2.880	0.648	0.450	0.221
2.2	1.0	0.997	0.983	0.880	0.212
2.3	1.5	8.690	0.707	1.075	0.314
2.4	2.0	11.570	1.118	0.924	0.351
2.5	2.5	6.195	3.058	1.615	0.286
2.6	3.0	8.920	6.373	1.348	0.574
3.1	0.5	2.490	1.732	1.912	0.160
3.2	1.0	2.660	2.060	0.748	0.400
3.3	1.5	3.735	1.019	2.275	0.571
3.4	2.0	2.320	0.999	1.512	1.212
3.5	2.5	2.630	1.405	1.079	1.212

D.1.2 Sector 2

The comparison between the measurements and theoretical results for the first, second, and third set are presented from figures D.7 to D.12, and the results obtained from the measurements are presented in Table D.2.

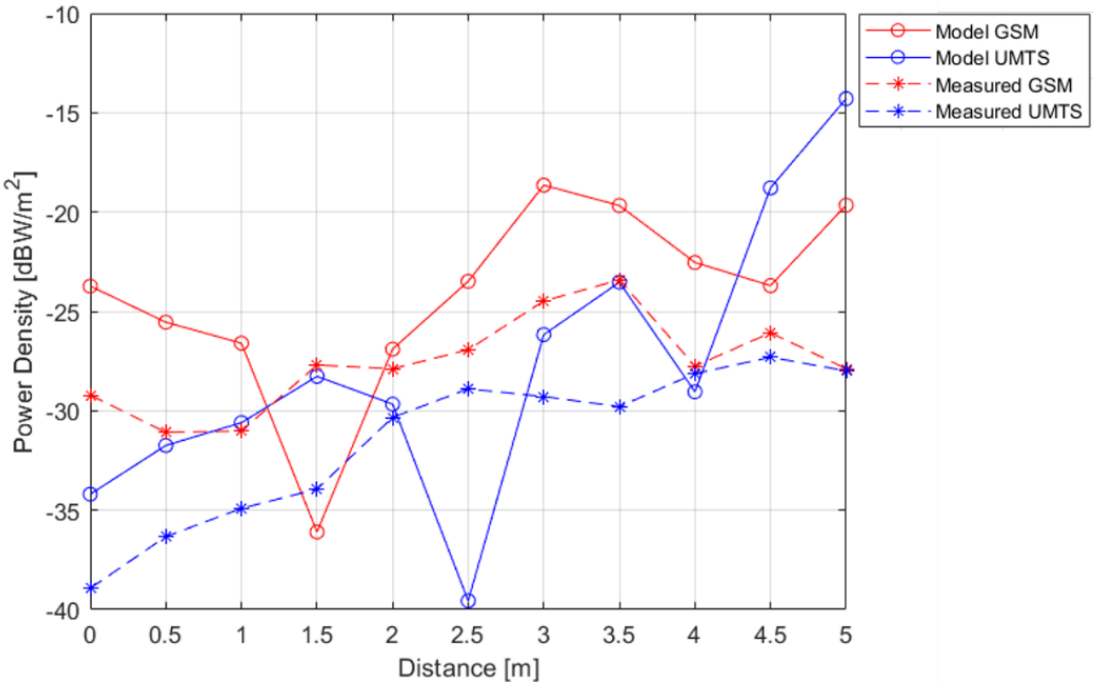

Figure D.7. Measured versus theoretical results of $S(d)$ for GSM900 and UMTS2100, for set 1 of BS1's sector 2.

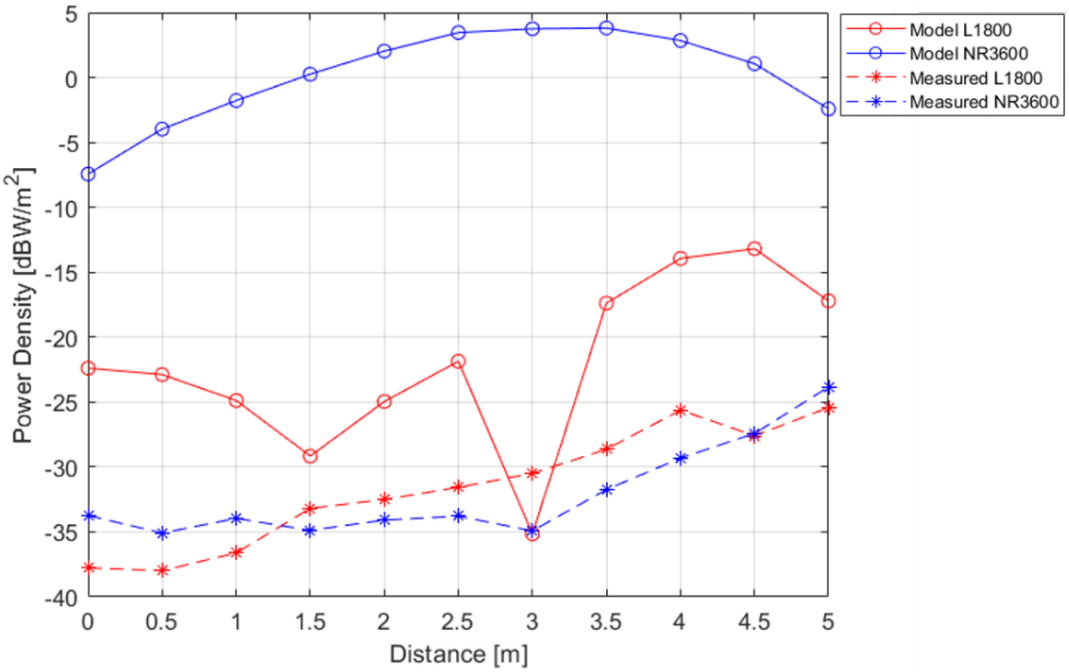

Figure D.8. Measured versus theoretical results of $S(d)$ for LTE1800 and NR3600, for set 1 of BS1's sector 2.

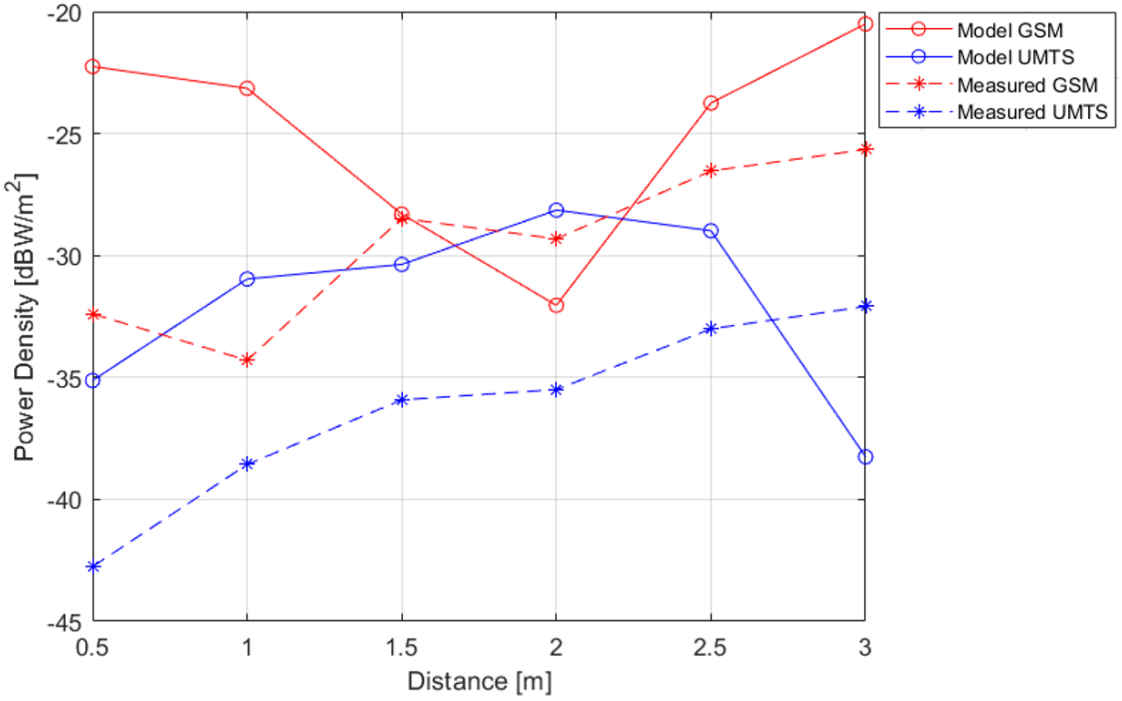

Figure D.9. Measured versus theoretical results of $S(d)$ for GSM900 and UMTS2100, for set 2 of BS1's sector 2.

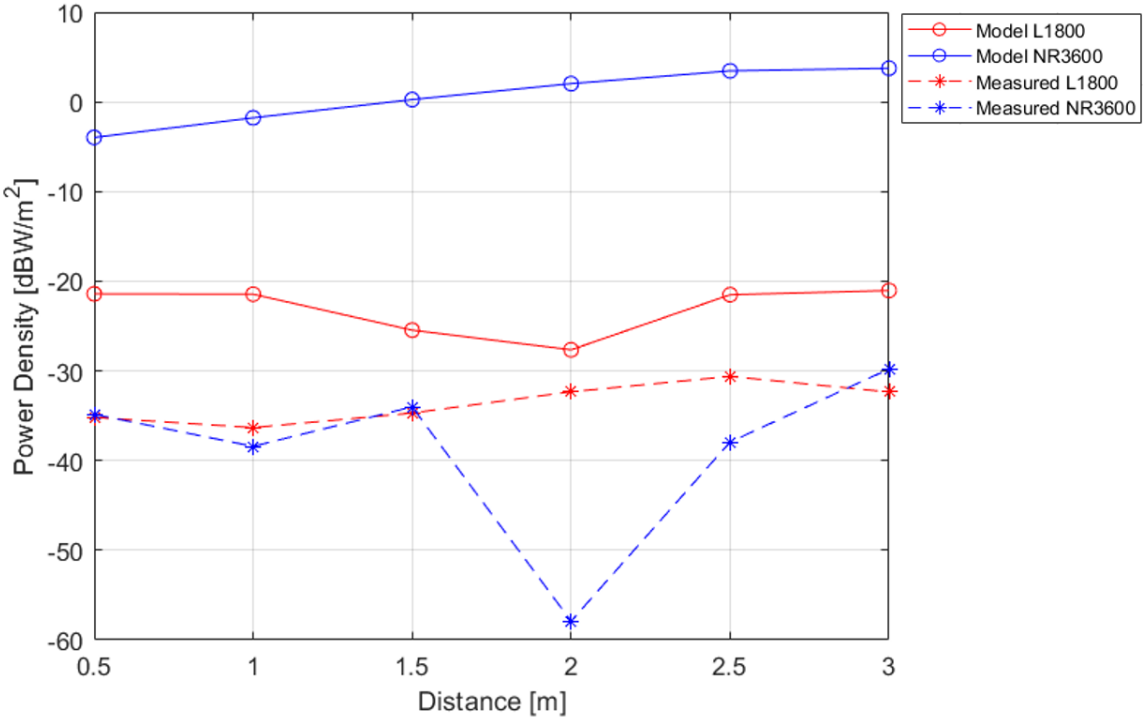

Figure D.10. Measured versus theoretical results of $S(d)$ for LTE1800 and NR3600, for set 2 of BS1's sector 2.

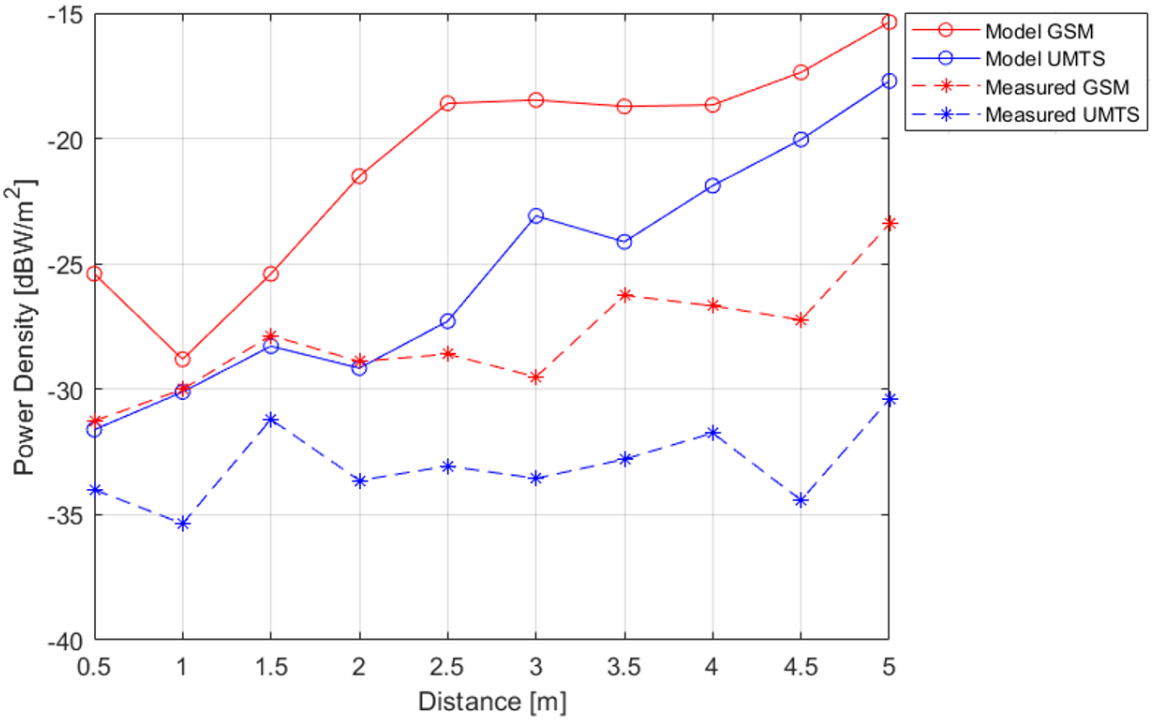

Figure D.11. Measured versus theoretical results of $S(d)$ for GSM900 and UMTS2100, for set 3 of BS1's sector 2.

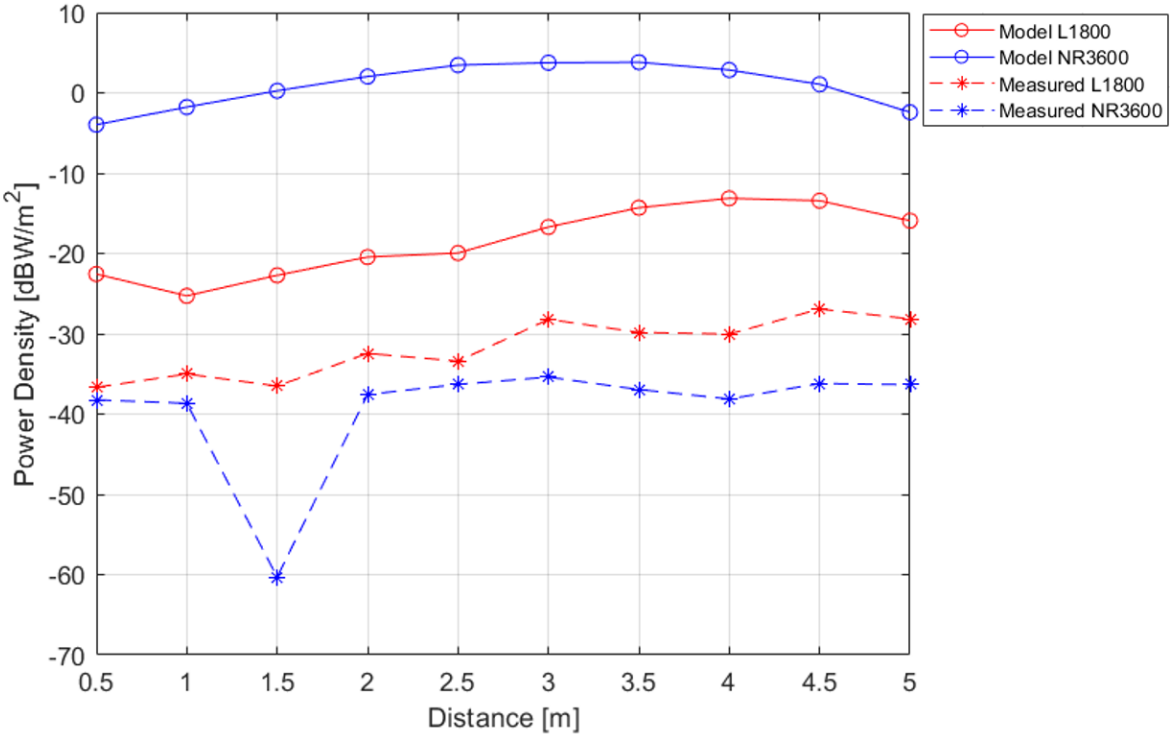

Figure D.12. Measured versus theoretical results of $S(d)$ for LTE1800 and NR3600, for set 3 of BS1's sector 2.

Table D.2. Measurement results for sector 2 of BS1.

Observation Point	Distance [m]	$S_{measure}[\mathrm{mW/m^2}]$			
		GSM900	UMTS2100	LTE1800	NR3600
1.1	0.0	1.200	0.128	0.167	0.423
1.2	0.5	0.780	0.233	0.159	0.310
1.3	1.0	0.792	0.323	0.218	0.402
1.4	1.5	1.700	0.404	0.480	0.325
1.5	2.0	1.630	0.927	0.526	0.390
1.6	2.5	2.030	1.295	0.697	0.418
1.7	3.0	3.565	1.185	0.893	0.322
1.8	3.5	4.555	1.048	1.368	0.670
1.9	4.0	1.675	1.542	2.742	1.167
1.10	4.5	2.465	1.857	1.742	1.812
1.11	5.0	1.630	1.592	2.868	4.132
2.1	0.5	0.576	0.053	0.303	0.327
2.2	1.0	0.372	0.139	0.233	0.144
2.3	1.5	1.420	0.256	0.339	0.397
2.4	2.0	1.170	0.282	0.585	0.002
2.5	2.5	2.220	0.500	0.868	0.161
2.6	3.0	2.720	0.618	0.581	1.046
3.1	0.5	0.747	0.398	0.215	0.150
3.2	1.0	1.002	0.291	0.315	0.136
3.3	1.5	1.640	0.758	0.223	0.001
3.4	2.0	1.285	0.433	0.569	0.175
3.5	2.5	1.375	0.494	0.455	0.234
3.6	3.0	1.123	0.441	1.512	0.288
3.7	3.5	2.370	0.526	1.042	0.202
3.8	4.0	2.145	0.669	0.990	0.154
3.9	4.5	1.885	0.361	2.025	0.240
3.10	5.0	4.555	0.914	1.530	0.232

D.2 Measurements Results of BS2

The comparison between the measurements and theoretical results for the first, second, and third set are presented from figures D.13 to D.18, and the results obtained from the measurements are presented in Table D.3.

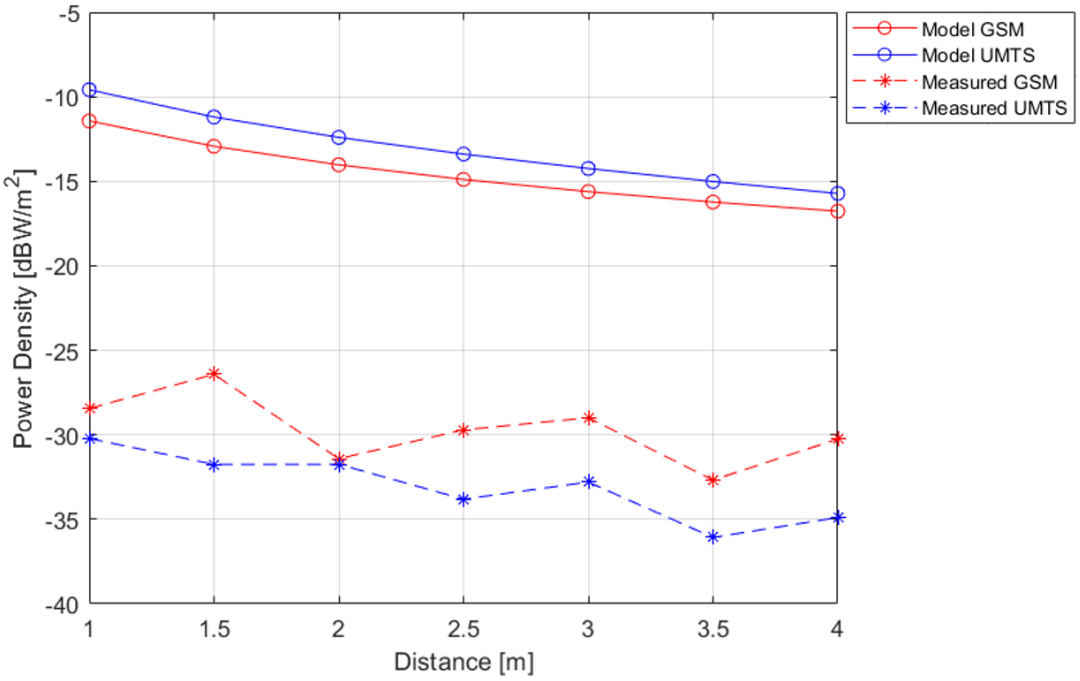

Figure D.13. Measured versus theoretical results of $S(d)$ for GSM900 and UMTS2100, for set 1 of BS2.

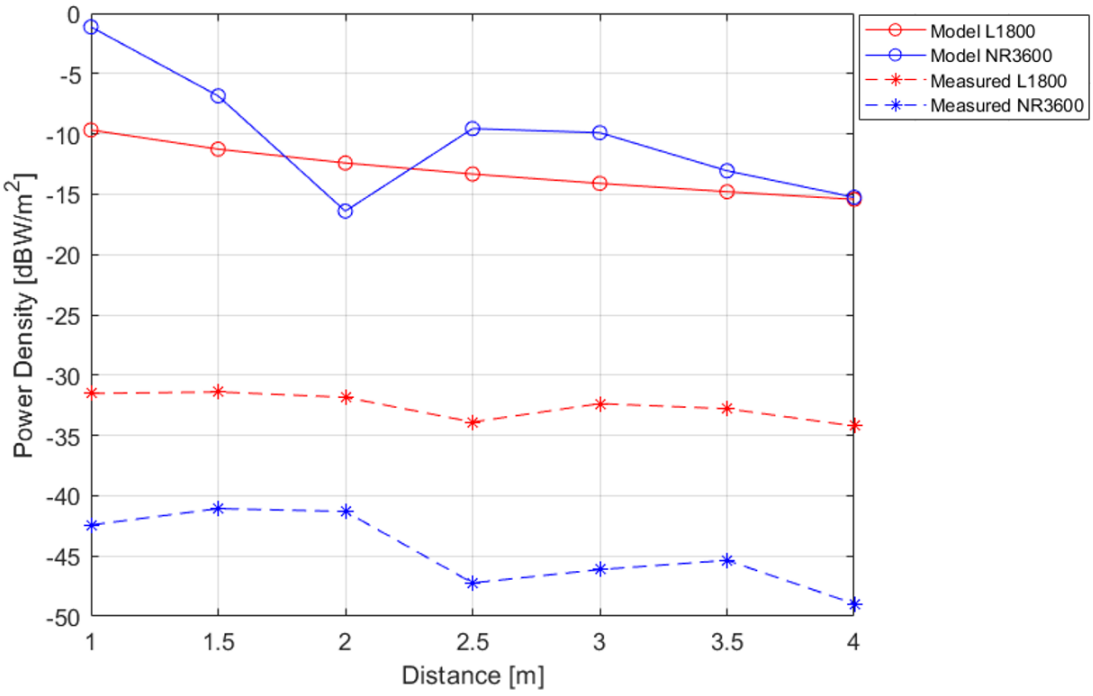

Figure D.14. Measured versus theoretical results of $S(d)$ for LTE1800 and NR3600, for set 1 of BS2.

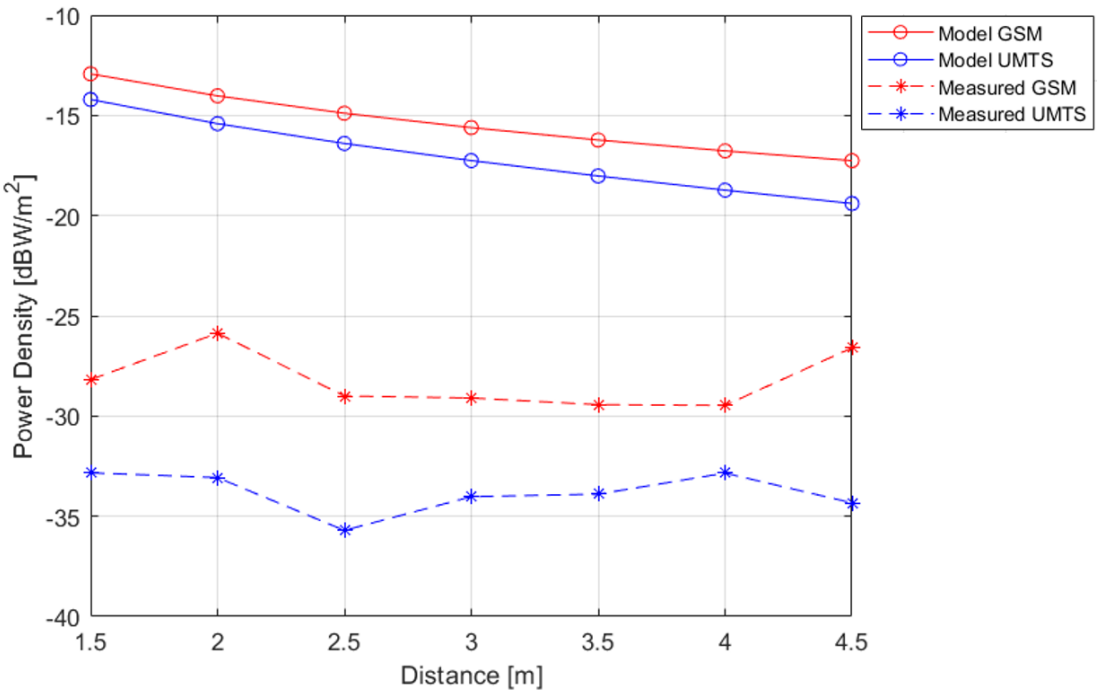

Figure D.15. Measured versus theoretical results of $S(d)$ for GSM900 and UMTS2100, for set 2 of BS2.

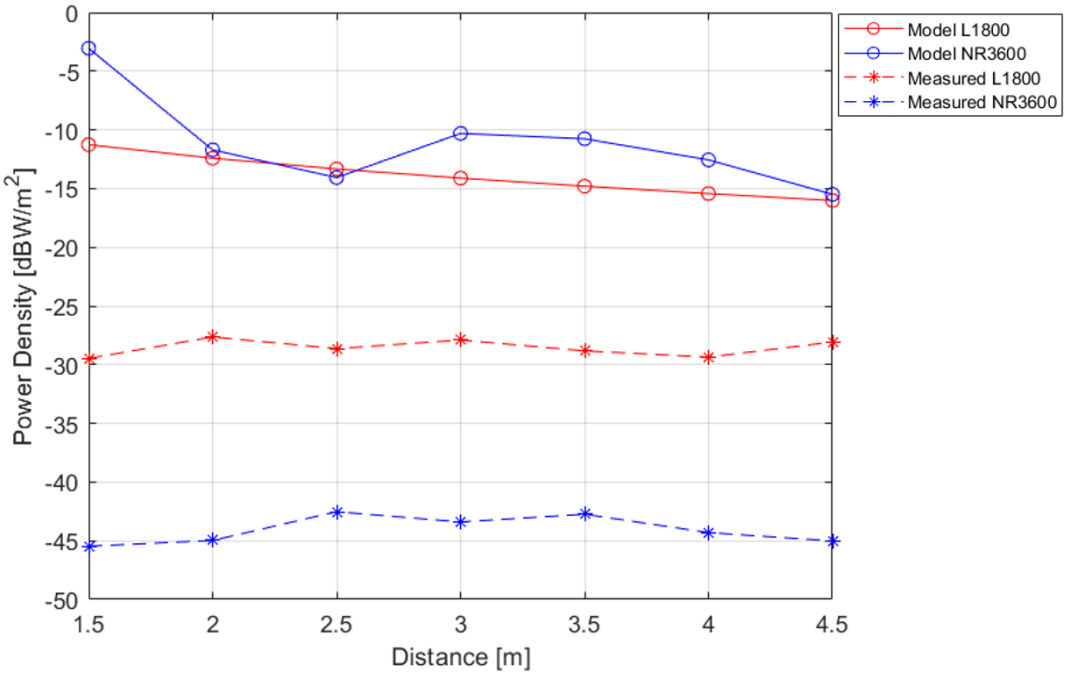

Figure D.16. Measured versus theoretical results of $S(d)$ for LTE1800 and NR3600, for set 2 of BS2.

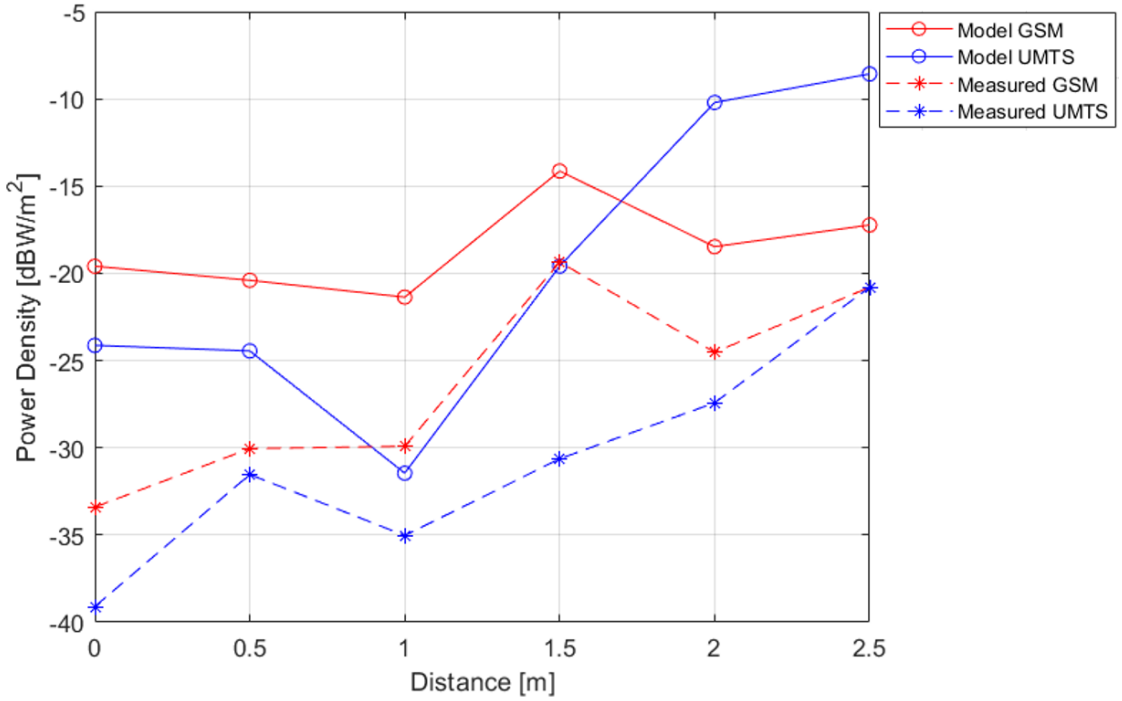

Figure D.17. Measured versus theoretical results of $S(d)$ for GSM900 and UMTS2100, for set 3 of BS2.

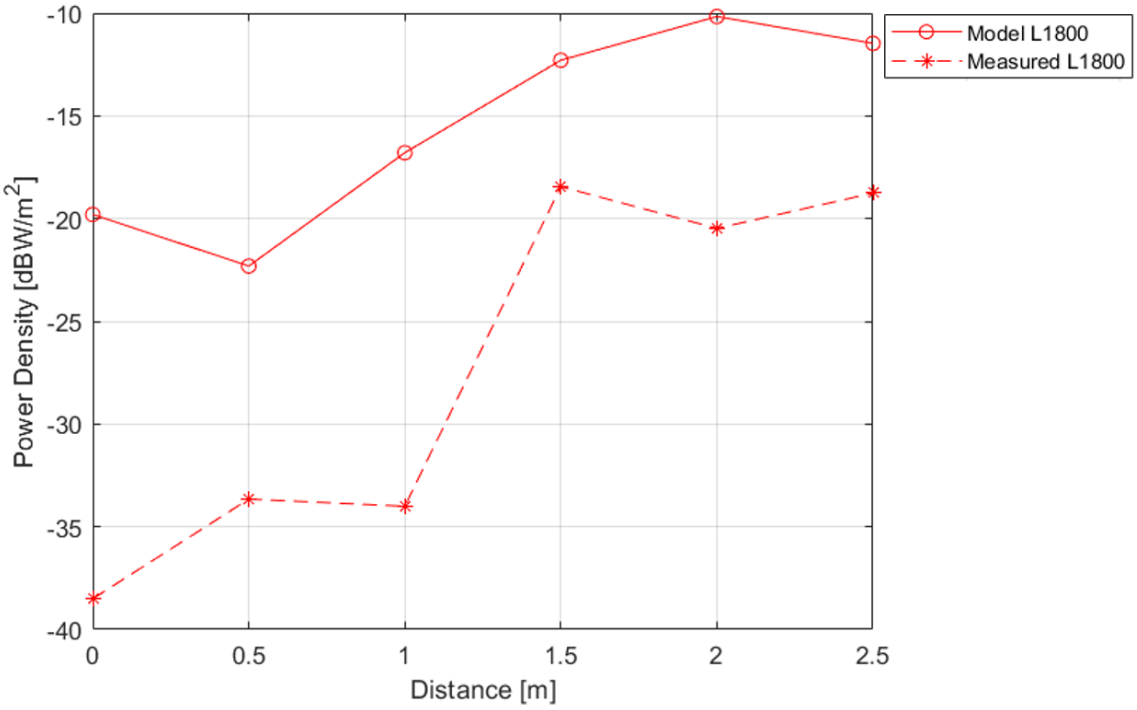

Figure D.18. Measured versus theoretical results of $S(d)$ for LTE1800, for set 3 of BS2.

Table D.3. Measurement results for BS2

Observation Point	Distance [m]	$S_{measure}[\mathrm{mW/m^2}]$			
		GSM900	UMTS2100	LTE1800	NR3600
1.1	1.0	1.425	0.951	0.704	0.057
1.2	1.5	2.280	0.668	0.725	0.078
1.3	2.0	0.722	0.669	0.654	0.074
1.4	2.5	1.069	0.416	0.408	0.019
1.5	3.0	1.260	0.525	0.580	0.024
1.6	3.5	0.540	0.247	0.526	0.029
1.7	4.0	0.944	0.324	0.378	0.013
2.1	1.5	1.515	0.521	1.134	0.028
2.2	2.0	2.590	0.493	1.718	0.032
2.3	2.5	1.255	0.269	1.365	0.056
2.4	3.0	1.225	0.396	1.618	0.046
2.5	3.5	1.144	0.408	1.314	0.053
2.6	4.0	1.113	0.519	1.164	0.037
2.7	4.5	2.185	0.369	1.555	0.032
3.1	0.0	0.457	0.123	0.141	-
3.2	0.5	0.990	0.703	0.431	-
3.3	1.0	1.020	0.314	0.398	-
3.4	1.5	11.620	0.865	14.347	-
3.5	2.0	3.530	1.811	8.957	-
3.6	2.5	8.320	8.325	13.253	-

Annex E

3D Radiation Pattern Interpolation Method

This annex presents the interpolation method used to compute the three-dimensional antenna radiation pattern.

The interpolation method proposed by [LCSF16] is based on the assumption that both vertical and horizontal antenna radiation patterns are available. The azimuth angle (φ) and elevation angle (θ) configurations used in the interpolation are presented in Figure E.1. In this method, the angular ranges considered for φ and θ are $[-\pi, \pi]$ and $[-\frac{\pi}{2}, \frac{\pi}{2}]$ respectively. This implementation sets then the maximum antenna gain for $\varphi = 0$ and $\theta = 0$.

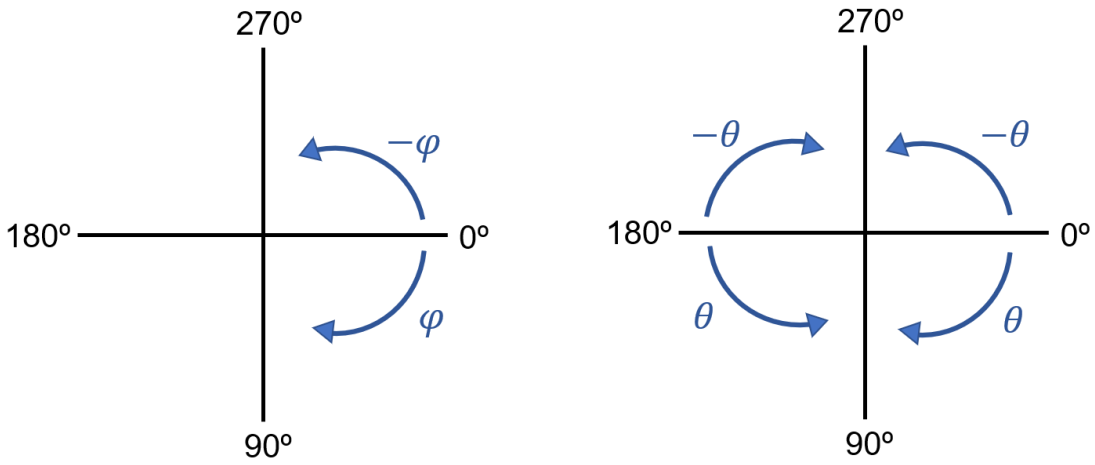

a) Horizontal Plane. b) Vertical Plane.

Figure E.1. Azimuth and elevation angle configuration.

According to [LCSF16], the reconstruction of the 3D radiation pattern is performed using two steps. Primarily, the weighted contribution from the horizontal ($\hat{G}_H(\theta, \varphi)$) and vertical planes ($\hat{G}_V(\theta, \varphi)$) are obtained by:

$$\hat{G}_H(\theta, \varphi)_{[\text{dBi}]} = G_{\theta_2}(\varphi)_{[\text{dBi}]}\ W_1(\theta) + G_{\theta_1}(\varphi)_{[\text{dBi}]}\ [1 - W_1(\theta)] \quad (E.1)$$

$$\hat{G}_V(\theta, \varphi)_{[\text{dBi}]} = G_{\varphi_1}(\theta)_{[\text{dBi}]}\ W_2(\varphi) + G_{\varphi_2}(\theta)_{[\text{dBi}]}\ [1 - W_2(\varphi)] \quad (E.2)$$

where:

- $G_{\theta_1}(\varphi)$: the top/bottom antenna gain;
- $G_{\theta_2}(\varphi)$: the antenna gain in the horizontal plane for φ;
- $G_{\varphi_1}(\theta)$: the antenna gain in the vertical plane for θ at the front of the antenna ($\varphi = 0$);
- $G_{\varphi_2}(\theta)$: the antenna gain in the vertical plane for θ at the back of the antenna ($\varphi = \pi$).

$$W_1(\theta) = 1 - \frac{2|\theta|}{\pi} \quad (E.3)$$

$$W_2(\varphi) = 1 - \frac{|\varphi|}{\pi} \quad (E.4)$$

Regarding $G_{\theta_1}(\varphi)$, the choice of whether to use the top or bottom antenna gain is dependent on the desired direction. If θ is inside the interval $[-\frac{\pi}{2}, 0]$ then the top antenna gain is chosen, on the other hand, if θ belongs to $[0, \frac{\pi}{2}]$ then the bottom antenna gain is chosen instead. Note that, for $\theta = 0$, the value taken for $G_{\theta_1}(\varphi)$ is irrelevant since, as can be observed from (E.1) and (E.3), $W_1(\theta)$ is equal to 1 in this

circumstance and thus no weight is attributed to $G_{\theta_1}(\varphi)$.

Finally, the interpolated antenna gain for any given direction ($\hat{G}(\theta, \varphi)$) is given by:

$$\hat{G}(\theta, \varphi)_{[\mathrm{dBi}]} = \hat{G}_H(\theta, \varphi)_{[\mathrm{dBi}]}\ W_3(\theta, \varphi) + \hat{G}_V(\theta, \varphi)_{[\mathrm{dBi}]}\ [1 - W_3(\theta, \varphi)] \qquad (E.5)$$

where:

$$W_3(\theta, \varphi) = \frac{2}{\pi}\left|\left(\frac{\pi}{4} - |\theta| + \frac{\pi}{2} - \left|\left(\frac{\pi}{2} - |\varphi|\right)\right|\right)\right| \qquad (E.6)$$

Annex F

Antennas Description

This annex presents the main technical characteristics of the antennas used in this work.

The ASI4517R3v06 is the passive antenna used in this thesis for the transmission of GSM, UMTS, LTE, and NR700. Its main technical characteristics of interest are presented in Table F.1.

Table F.1. Technical characteristics of the passive antenna (extracted from [HUAW19d]).

Technical Characteristics	Frequency Bands [MHz]					
	690-803	790-862	880-960	1695-1990	1920-2200	2490-2690
Polarisation	+45º, -45º (cross-polarisation)					
Electrical Downtilt [º]	0-10			2-12		
Gain [dBi]	14.9	15.5	16.0	15.5	15.9	16.7
Horizontal HPBW [º]	68 ± 4	63 ± 3	60 ± 3	63 ± 5	62 ± 5	60 ± 6
Vertical HPBW [º]	10.5 ± 0.9	9.5 ± 0.8	8.5 ± 0.7	10.4 ± 0.6	9.4 ± 0.5	7.4 ± 0.3
FTBR (±30º) [dB]	> 22	> 25	> 24	> 25		
Impedance [Ω]	50					
Dimensions [mm] (height/widht/depth)	1999/429/196					

The AAU5613 and the AAU5339w are the active antennas used in this thesis for the simulation of NR3600. Their main technical characteristics are presented in Table F.2.

Table F.2. Technical characteristics of the active antennas used in NR3600 (extracted from [HUAW20a] and [HUAW20b]).

Technical Characteristics	Antenna	
	AAU5613	AAU5339w
Frequency Range [Mhz]	3400 - 3800	
Polarisation	+45º, -45º (cross-polarisation)	
Gain [dBi]	25.0	23.8
Horizontal Beam Sweeping Range [º]	-60 to +60 (120º)	
Vertical Beam Sweeping Range [º]	-15 to +15 (30º)	
Number of MIMO Elements	64	32
Number of Antenna Elements	192	
Dimensions [mm] (height/widht/depth)	795/395/220	699/395/160

Annex G

General Zone Model Simulation

This annex presents the general zone model results for the different frequency bands and antennas used in this thesis, as well as the parameters used in the simulations.

G.1 Simulation Parameters

In this section, the communications systems' and the exclusion zone evaluation model's parameters for the simulation of the power density exposure are presented. The parameters of the utilized mobile systems are presented in Table G.1.

Table G.1. Simulation parameters for the utilized systems.

System	Central Frequency [MHz]	λ [m]	3λ [m]	$S_{ref}[\mathrm{W/m^2}]$
NR700	763	0.39	1.18	3.82
LTE800	816	0.37	1.10	4.08
GSM/UMTS900	943	0.32	0.95	4.72
LTE1800	1835	0.16	0.49	9.18
UMTS/LTE2100	2137	0.14	0.42	10.00
LTE2600	2660	0.11	0.34	10.00
NR3600	3650	0.08	0.25	10.00

The remaining values for the simulation's parameters are:

- $N_{samp} = 100000$;
- $d_{min} = \max\{3\lambda_i : i = 1, \dots, N_{sys}\}$;
- $d_{max} = \max\left\{\frac{2D_i^2}{\lambda_i} : i = 1, \dots, N_{sys}\right\} + 20$;
- $\psi_i = 0$;
- $\Delta_{es} = 1$;
- $L_{dip} = \frac{\lambda}{2}$;
- $N_{el} = 8$ (ASI4517R3v06);
- $N_{V,el} = 3$ (AAU5613);
- $N_{V,el} = 6$ (AAU5339w);
- The maximum number of iterations performed by the interpolation method: 1000.

G.2 Simulation Results

The general zone model results for the power density function coefficients and far-field distances for the mobile communications systems utilized in the simulations are presented in Table G.2. These were

obtained for the parameters presented in the previous section.

Table G.2. S_{nf}^{norm} coefficients and far-field distance for the utilized systems.

System		S_{nf}^{norm} Coefficients				$d_{ff}[\mathrm{m}]$
		$a_0[\mathrm{m}^2]$	$a_1[\mathrm{m}]$	$a_2[1]$	$a_3[\mathrm{m}^{-1}]$	
NR700		1.2753	16.9713	-0.6188	0.0418	20.35
LTE800		0.8111	16.0.732	-0.6551	0.0460	21.76
GSM/UMTS900		2.0898	12.2407	-0.3458	0.0384	25.15
LTE1800		0.4650	6.4919	-0.4062	0.0780	12.23
UMTS/LTE2100		0.5797	4.8327	-0.1404	0.0666	14.25
LTE2600		0.3720	3.7171	-0.1297	0.0850	17.73
NR3600	AAU5613	0.4486	-0.2272	1.0286	-	3.80
	AAU5339w	0.9188	-0.4736	1.0609	-	

Annex H

Variation of the Exclusion Zone Results

This annex presents the additional results obtained for the exclusion zone variation, such as the D_{front} variation, the compliance distance for the back, side, top, and bottom of the antennas, and the influence of downtilt on the implementation of physical barriers at street level.

H.1 Variation of D_{front}

The results of the variation of the D_{front} for the scenarios analysed in this thesis are presented in Table H.1.

Table H.1. D_{front} variation for the analysed scenarios.

Scenario	Δ_{front} [%]			
	$N_{c\,GSM900}/N_{c\,UMTS}$			
	1/1	2/1	4/2	4/4
Urban.1	248.7	213.4	146.7	123.8
Urban.2	152.6	141.8	115.3	104.1
Urban.3	127.5	119.9	101.2	92.3
Suburban.1	113.9	102.5	73.5	57.1
Suburban.2	41.5	34.2	21.7	17.3
Suburban.3	131.6	118.7	93.8	83.1
Rural.1	52.1	41.3	24.2	18.5
Rural.2	56.4	46.7	24.8	16.4
Rural.3	32.0	27.8	17.1	14.3

H.2 Exclusion Distance Results for Other Directions

In this subsection, the results for the front, back, side, and top exclusion borders regarding the suburban and rural scenarios are presented from Table H.2 to H.7.

Table H.2. Exclusion borders for the front, back, side, top and bottom for the Suburban.1 scenario.

	$N_{c\,GSM900}/N_{c\,UMTS}$		D_{front} [m]	D_{back} [m]	D_{side} [m]	D_{top} [m]	D_{bottom} [m]
Suburban.1	1/1	W/O NR	9.54	1.10	1.10	1.10	1.10
		W NR	20.41	1.10	3.64	1.10	1.10
	2/1	W/O NR	10.23	1.10	1.10	1.10	1.10
		W NR	20.72	1.10	3.66	1.10	1.10
	4/2	W/O NR	12.63	1.10	1.10	1.10	1.10
		W NR	21.91	1.10	3.74	1.10	1.10
	4/4	W/O NR	14.56	1.10	1.10	1.10	1.10
		W NR	22.87	1.10	3.81	1.10	1.10

Table H.3. Exclusion borders for the front, back, side, top and bottom for the Suburban.2 scenario.

	$N_{c\ GSM900}/N_{c\ UMTS}$		D_{front} [m]	D_{back} [m]	D_{side} [m]	D_{top} [m]	D_{bottom} [m]
Suburban.2	1/1	W/O NR	7.08	1.10	1.10	1.10	1.10
		W NR	10.02	1.18	1.18	1.18	1.18
	2/1	W/O NR	8.06	1.10	1.10	1.10	1.10
		W NR	10.82	1.18	1.18	1.18	1.18
	4/2	W/O NR	10.59	1.10	1.10	1.10	1.10
		W NR	12.89	1.18	1.18	1.18	1.18
	4/4	W/O NR	11.99	1.10	1.10	1.10	1.10
		W NR	14.06	1.18	1.18	1.18	1.18

Table H.4. Exclusion borders for the front, back, side, top and bottom for the Suburban.3 scenario.

	$N_{c\ GSM900}/N_{c\ UMTS}$		D_{front} [m]	D_{back} [m]	D_{side} [m]	D_{top} [m]	D_{bottom} [m]
Suburban.3	1/1	W/O NR	9.27	1.10	1.10	1.10	1.10
		W NR	21.47	1.18	3.72	1.18	1.18
	2/1	W/O NR	9.95	1.10	1.10	1.10	1.10
		W NR	21.76	1.18	3.74	1.18	1.18
	4/2	W/O NR	11.68	1.10	1.10	1.10	1.10
		W NR	22.63	1.18	3.80	1.18	1.18
	4/4	W/O NR	12.58	1.10	1.10	1.10	1.10
		W NR	23.03	1.18	3.83	1.18	1.18

Table H.5. Exclusion borders for the front, back, side, top and bottom for the Rural.1 scenario.

	$N_{c\ GSM900}/N_{c\ UMTS}$		D_{front} [m]	D_{back} [m]	D_{side} [m]	D_{top} [m]	D_{bottom} [m]
Rural.1	1/1	W/O NR	6.24	1.10	1.10	1.10	1.10
		W NR	9.49	1.18	1.18	1.18	1.18
	2/1	W/O NR	7.34	1.10	1.10	1.10	1.10
		W NR	10.37	1.18	1.18	1.18	1.18
	4/2	W/O NR	10.14	1.10	1.10	1.10	1.10
		W NR	12.59	1.18	1.18	1.18	1.18
	4/4	W/O NR	11.65	1.10	1.10	1.10	1.10
		W NR	13.81	1.18	1.18	1.18	1.18

Table H.6. Exclusion borders for the front, back, side, top and bottom for the Rural.2 scenario.

	$N_{c\,GSM900}/N_{c\,UMTS}$		D_{front} [m]	D_{back} [m]	D_{side} [m]	D_{top} [m]	D_{bottom} [m]
Rural.2	1/1	W/O NR	4.90	0.95	0.95	0.95	0.95
		W NR	7.68	1.18	1.18	1.18	1.18
	2/1	W/O NR	5.82	0.95	0.95	0.95	0.95
		W NR	8.54	1.18	1.18	1.18	1.18
	4/2	W/O NR	9.14	0.95	0.95	0.95	0.95
		W NR	11.40	1.18	1.18	1.18	1.18
	4/4	W/O NR	11.52	0.95	0.95	0.95	0.95
		W NR	13.40	1.18	1.18	1.18	1.18

Table H.7. Exclusion borders for the front, back, side, top and bottom for the Rural.3 scenario.

	$N_{c\,GSM900}/N_{c\,UMTS}$		D_{front} [m]	D_{back} [m]	D_{side} [m]	D_{top} [m]	D_{bottom} [m]
Rural.3	1/1	W/O NR	8.09	1.10	1.10	1.10	1.10
		W NR	10.68	1.18	1.18	1.18	1.18
	2/1	W/O NR	8.93	1.10	1.10	1.10	1.10
		W NR	11.40	1.18	1.18	1.18	1.18
	4/2	W/O NR	11.68	1.10	1.10	1.10	1.10
		W NR	13.68	1.18	1.18	1.18	1.18
	4/4	W/O NR	13.61	1.10	1.10	1.10	1.10
		W NR	15.56	1.18	1.18	1.18	1.18

H.3 Downtilt Influence on Physical Barriers

The results regarding the downtilt influence on the definition of physical barriers at street level for the different urban scenarios analysed in this thesis are presented from Table H.8 to H.10. The minimum antenna height ($h_{min,ant}$) and D'_{front} were obtained for a downtilt of 12º, a vertical SER of 30º (with active antenna), and person height (h_{person}) of 1.80 m.

Table H.8. Downtilt influence on the definition of physical barriers for the Urban.1 scenario.

	$N_{c\,GSM900}/N_{c\,UMTS}$		D_{front} [m]	D'_{front} [m]	$h_{min,ant}$ [m]
Urban.1	4/2	W/O NR	9.03	8.83	3.68
		W NR	22.28	19.85	11.91
	4/4	W/O NR	10.14	9.92	3.91
		W NR	22.69	20.22	12.10

Table H.9. Downtilt influence on the definition of physical barriers for the Urban.2 scenario.

	$N_{c\,GSM900}/N_{c\,UMTS}$		D_{front} [m]	D'_{front} [m]	$h_{min,ant}$ [m]
Urban.2	4/2	W/O NR	10.70	10.47	4.02
		W NR	23.04	20.53	12.26
	4/4	W/O NR	11.48	11.23	4.19
		W NR	23.43	20.88	12.44

Table H.10. Downtilt influence on the definition of physical barriers for the Urban.3 scenario.

	$N_{c\,GSM900}/N_{c\,UMTS}$		D_{front} [m]	D'_{front} [m]	$h_{min,ant}$ [m]
Urban.3	4/2	W/O NR	11.71	11.45	4.23
		W NR	23.56	20.99	12.50
	4/4	W/O NR	12.45	12.18	4.39
		W NR	23.94	21.33	12.67

Annex I

Influence on Coverage and Throughput Results

This annex presents the results obtained for the coverage radius as well as the throughput per RB at the cell-edge.

I.1 Coverage Radius Results

The results obtained for the coverage radius are presented from figures I.1 to I.8, and for the coverage radius variation are presented in Table I.1 and I.2.

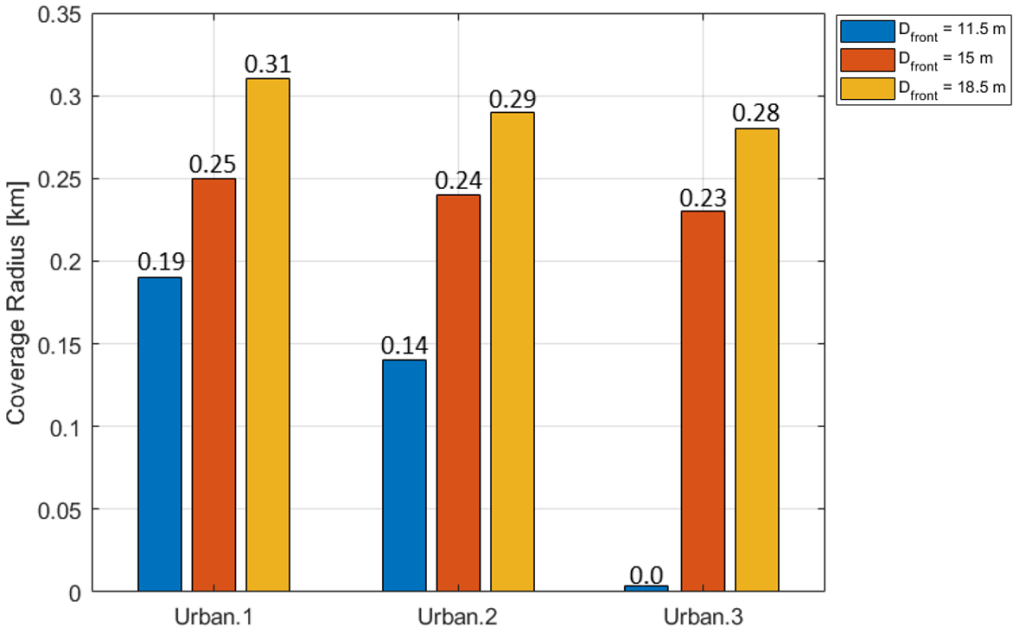

Figure I.1. Coverage radius for the urban scenarios for the 4/2 configuration with all communications systems.

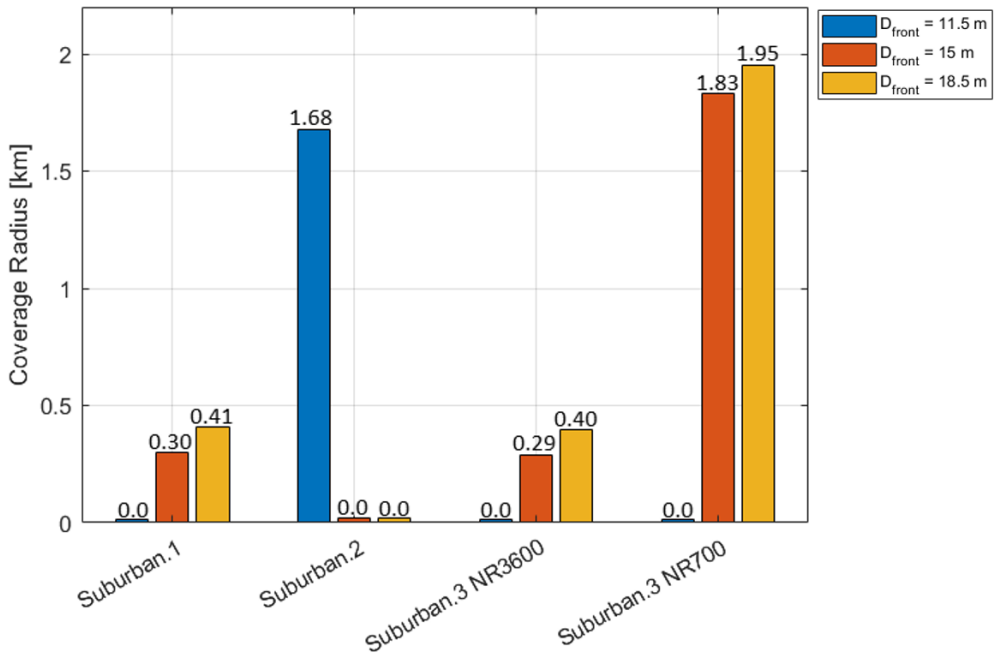

Figure I.2. Coverage radius for the suburban scenarios for the 4/2 configuration with all communications systems.

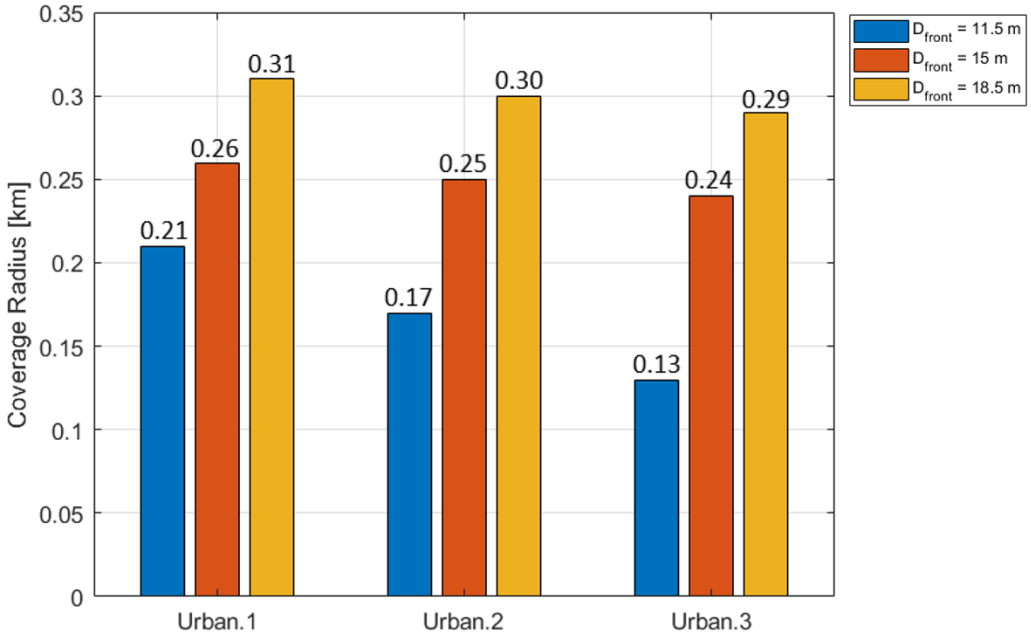

Figure I.3. Coverage radius for the urban scenarios for the 4/2 configuration without UMTS.

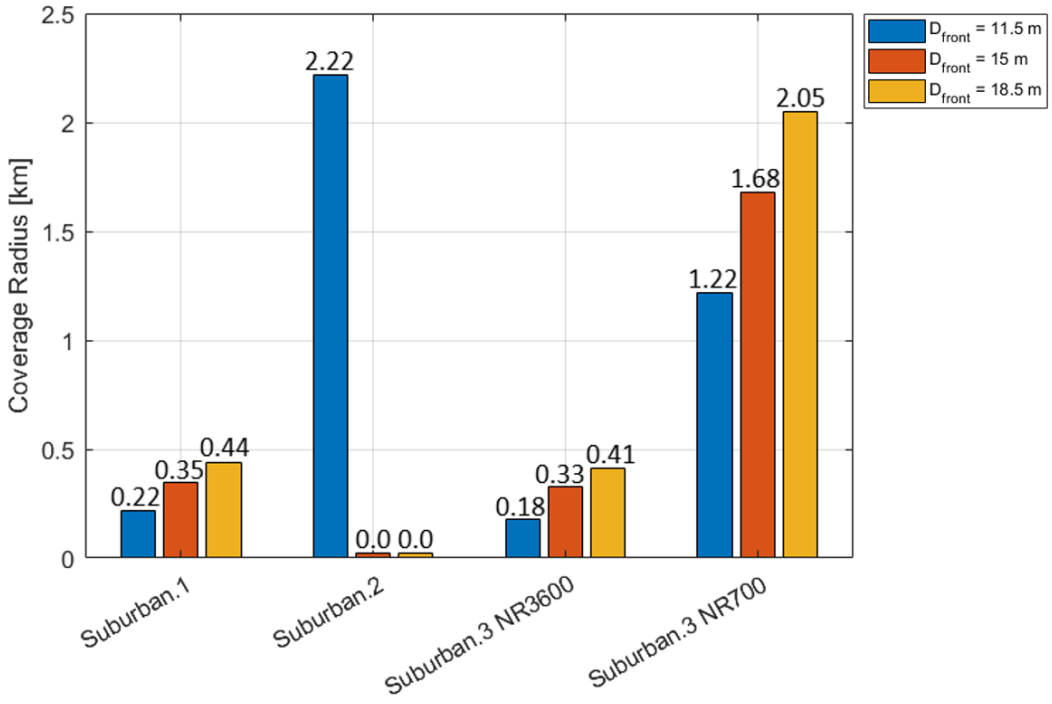

Figure I.4. Coverage radius for the suburban scenarios for the 4/2 configuration without UMTS.

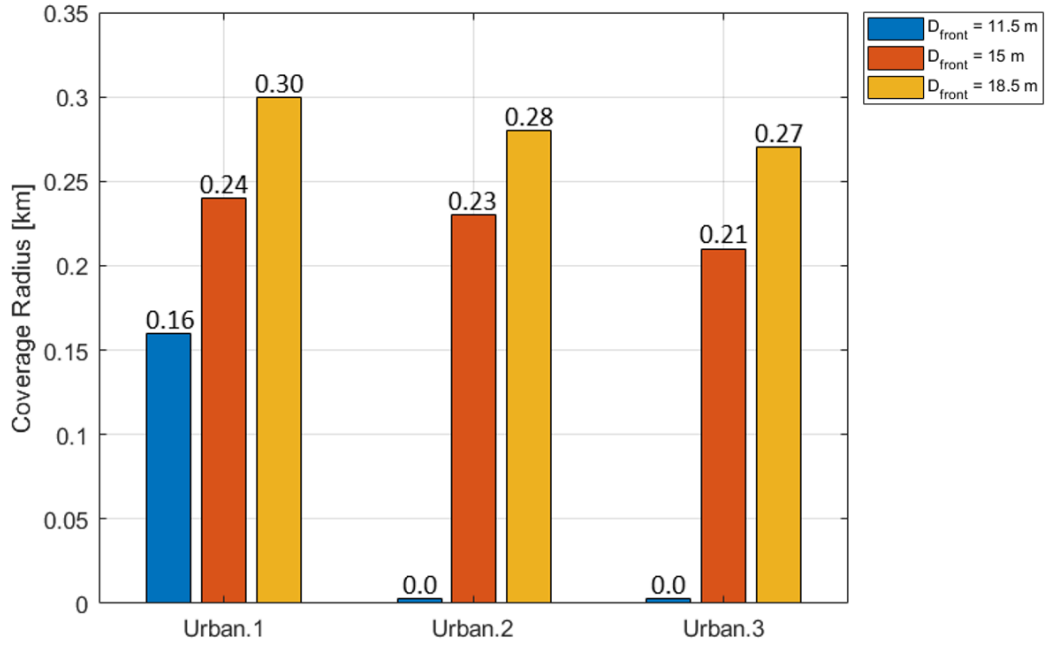

Figure I.5. Coverage radius for the urban scenarios for the 4/4 configuration with all communications systems.

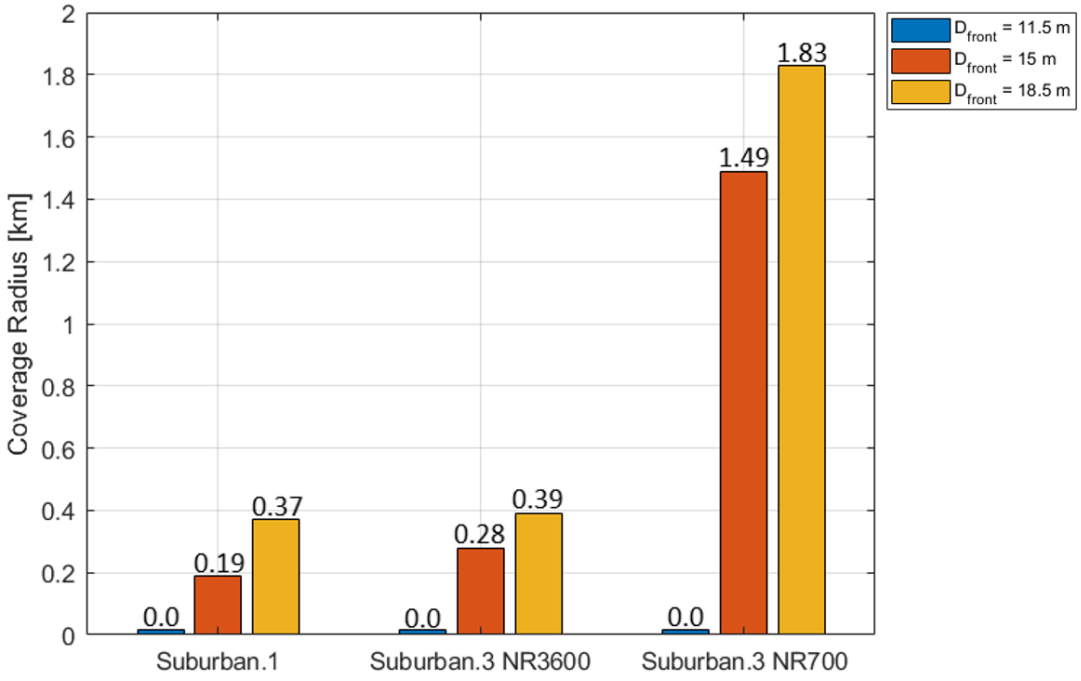

Figure I.6. Coverage radius for the suburban scenarios for the 4/4 configuration with all communications systems.

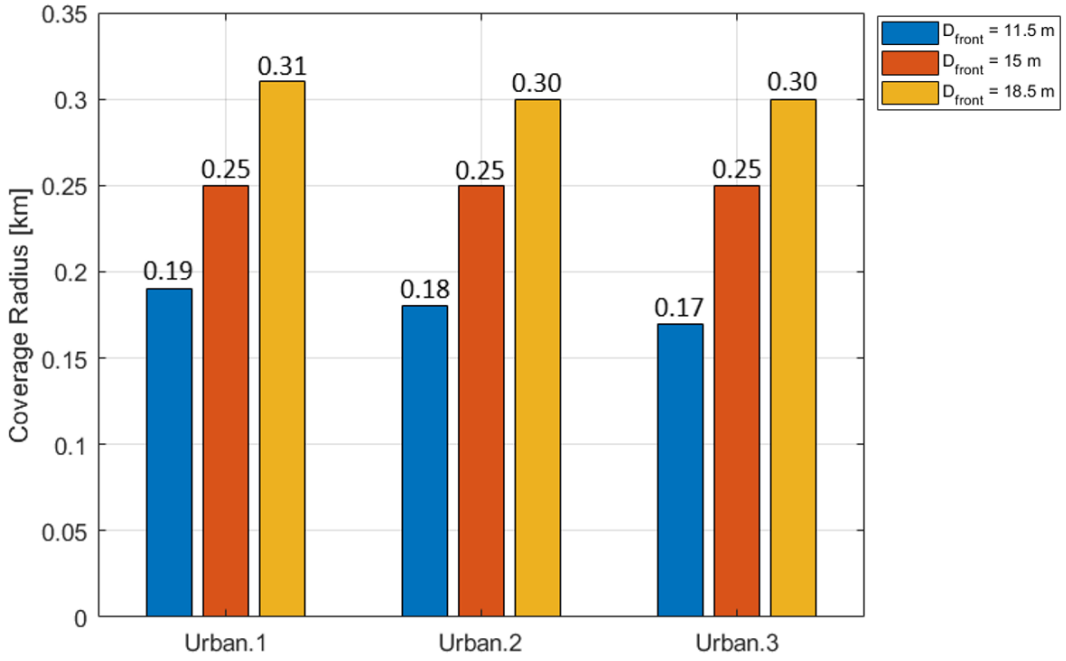

Figure I.7. Coverage radius for the urban scenarios for the 4/4 configuration with 20% of LTE's maximum transmission power.

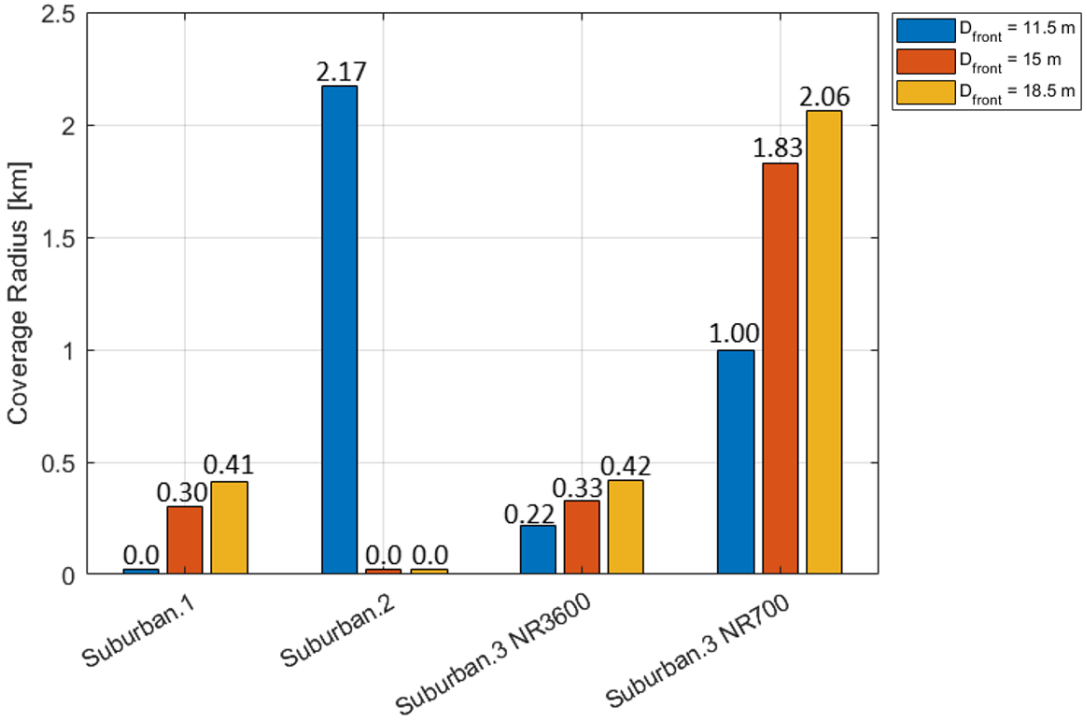

Figure I.8. Coverage radius for the suburban scenarios for the 4/4 configuration without LTE800.

Table I.1. Coverage radius variation for carrier configuration 4/2.

Characteristics	D_{front} [m]	$\Delta_{R_{cell}}$ [%]						
		Scenario						
		Urban.1	Urban.2	Urban.3	Suburban.1	Suburban.2	Suburban.3	
							NR3600	NR700
All Communications Systems	11.5	-45.7	-60.0	-	-	-25.0	-	-
	15.0	-28.6	-31.4	-34.3	-38.8	0.0	-40.8	-18.3
	18.5	-11.4	-17.1	-20.0	-16.3	0.0	-18.4	-12.9
Without UMTS	11.5	-40.0	-51.4	-62.9	-55.1	-0.9	-63.3	-45.5
	15.0	-25.7	-28.6	-31.4	-28.6	0.0	-32.7	-25.0
	18.5	-11.4	-14.3	-17.1	-10.2	0.0	-16.3	-8.5

Table I.2. Coverage radius variation for carrier configuration 4/4.

Characteristics	D_{front} [m]	$\Delta_{R_{cell}}$ [%]						
		Scenario						
		Urban.1	Urban.2	Urban.3	Suburban.1	Suburban.2	Suburban.3	
							NR3600	NR700
All Communications Systems	11.5	-54.3	-	-	-	-	-	-
	15.0	-31.4	-34.3	-40.0	-61.2	0.0	-42.9	-33.5
	18.5	-14.3	-20.0	-22.9	-24.5	0.0	-20.4	-18.3
Without LTE800 for Suburban and 20% of LTE for Urban	11.5	-45.7	-48.6	-51.4	-	-3.1	-55.1	-55.4
	15.0	-28.6	-28.6	-28.6	-38.8	0.0	-32.7	-18.3
	18.5	-11.4	-14.3	-14.3	-16.3	0.0	-14.3	-8.0

I.2 Cell-Edge Throughput per RB Results

The results obtained for the throughput per RB are presented from figures I.9 to I.16, and for the throughput per RB variation are presented in Table I.3 and I.4.

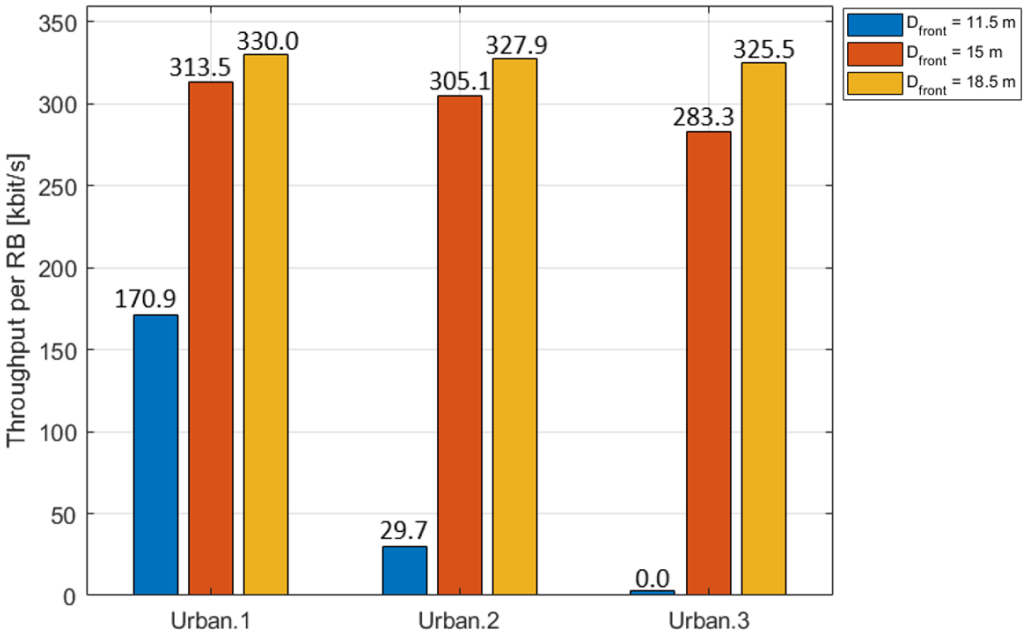

Figure I.9. Throughput per RB for the urban scenarios for the 4/2 configuration with all communications systems.

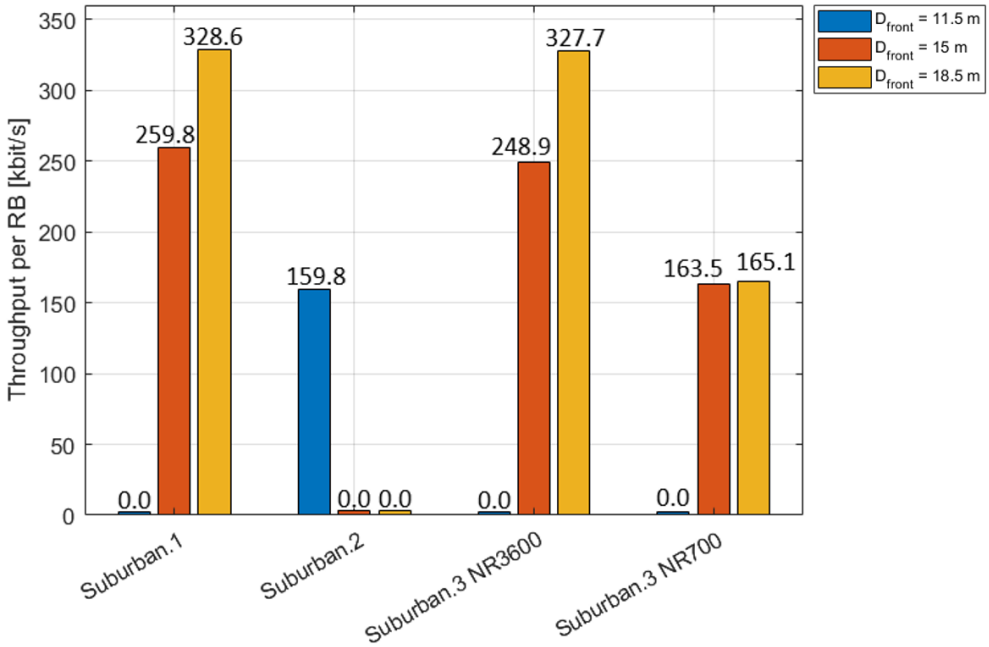

Figure I.10. Throughput per RB for the suburban scenarios for the 4/2 configuration with all communications systems.

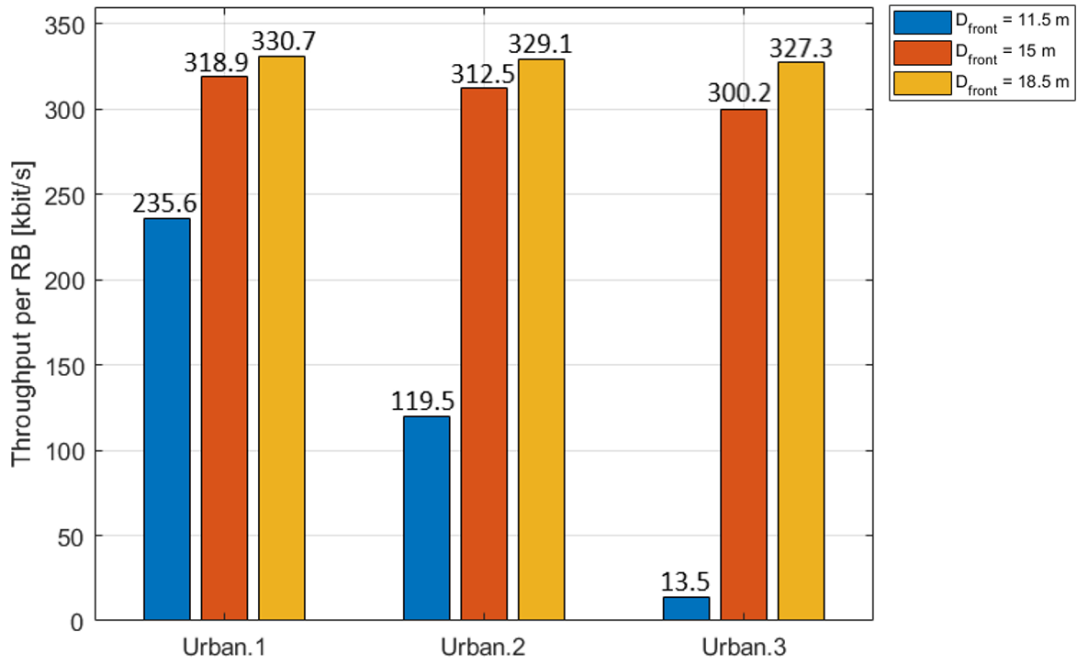

Figure I.11. Throughput per RB for the urban scenarios for the 4/2 configuration without UMTS.

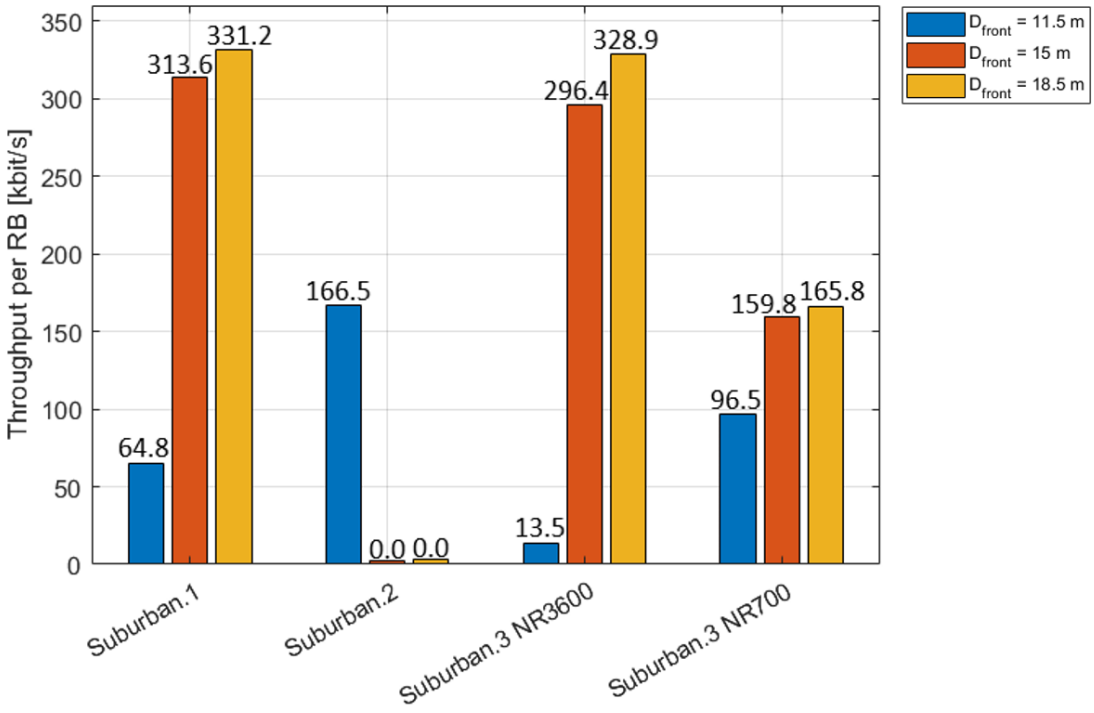

Figure I.12. Throughput per RB for the suburban scenarios for the 4/2 configuration without UMTS.

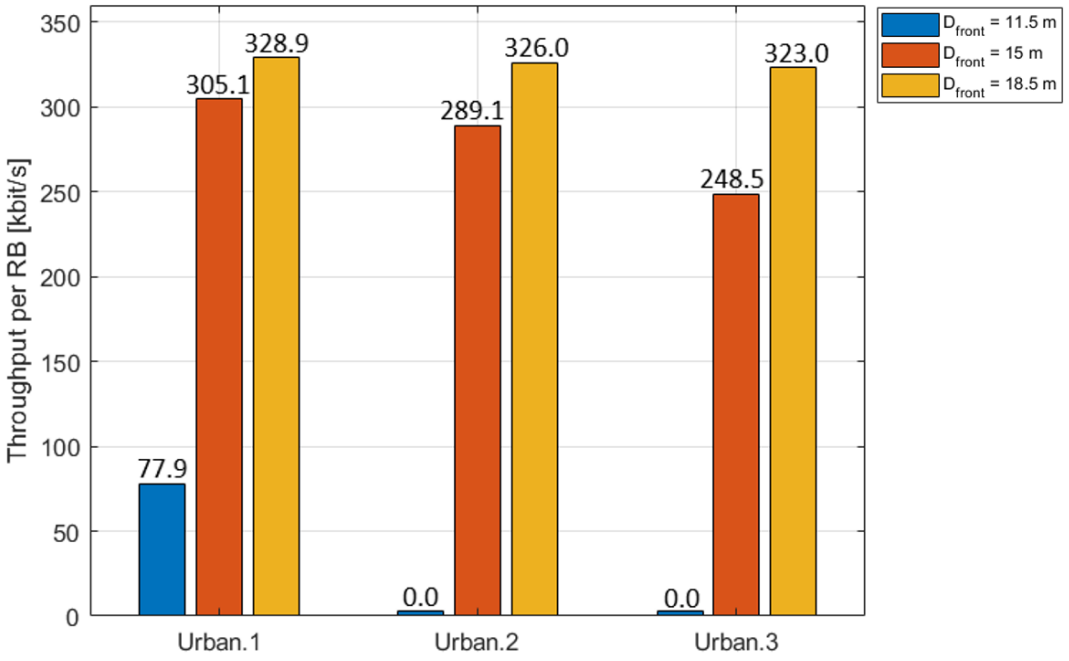

Figure I.13. Throughput per RB for the urban scenarios for the 4/4 configuration with all communications systems.

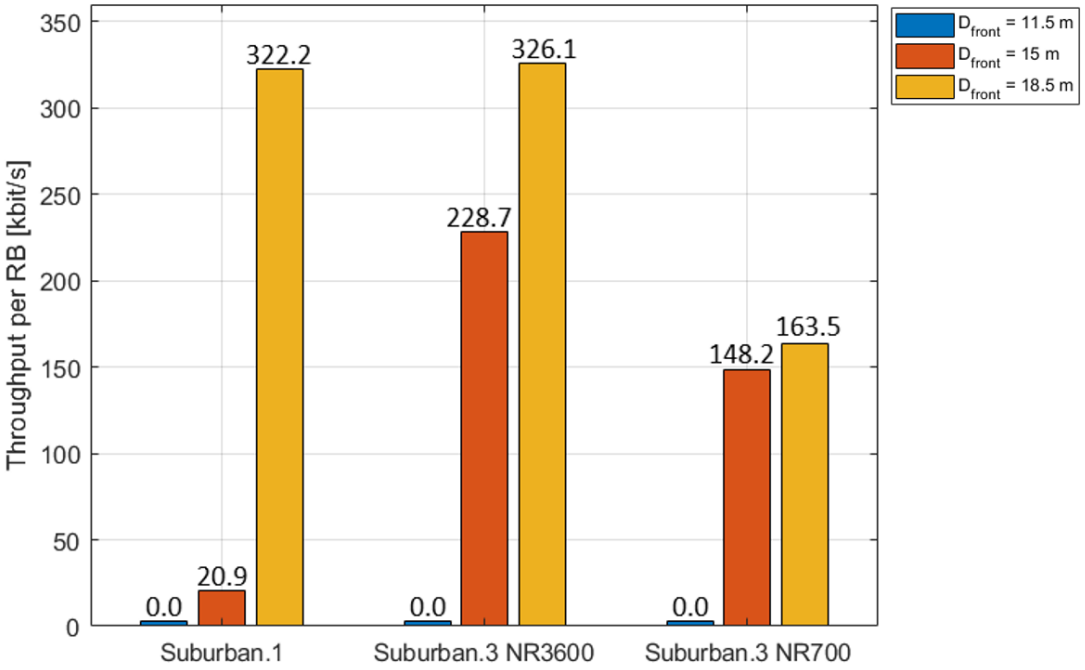

Figure I.14. Throughput per RB for the suburban scenarios for the 4/4 configuration with all communications systems.

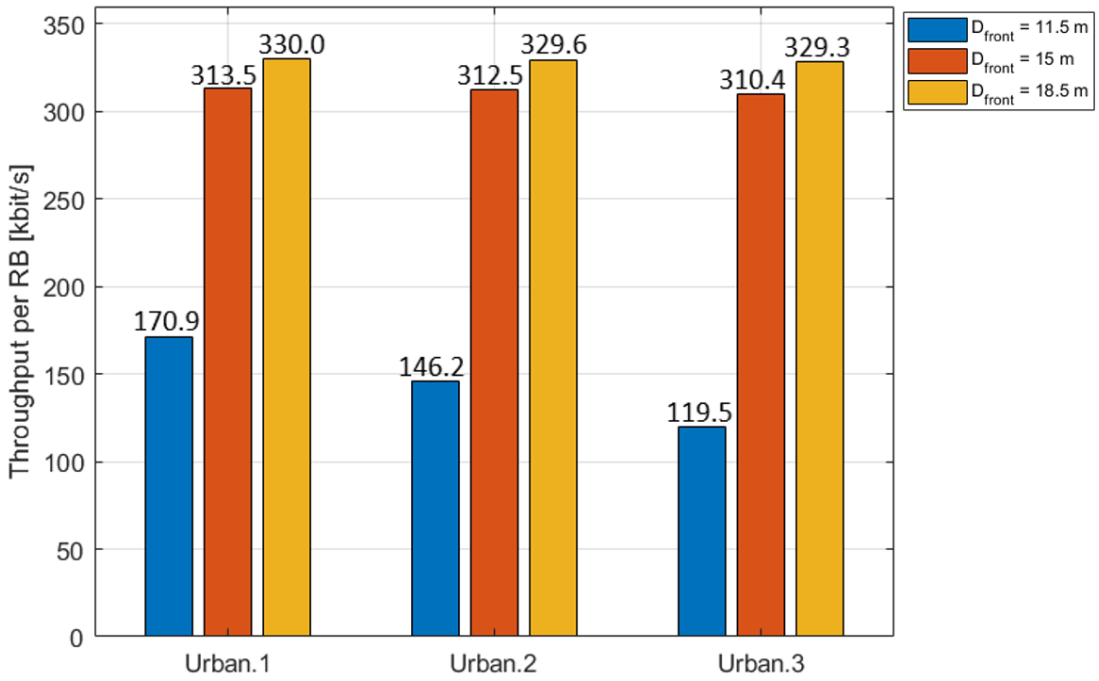

Figure I.15. Throughput per RB for the urban scenarios for the 4/4 configuration with 20% of LTE's maximum transmission power.

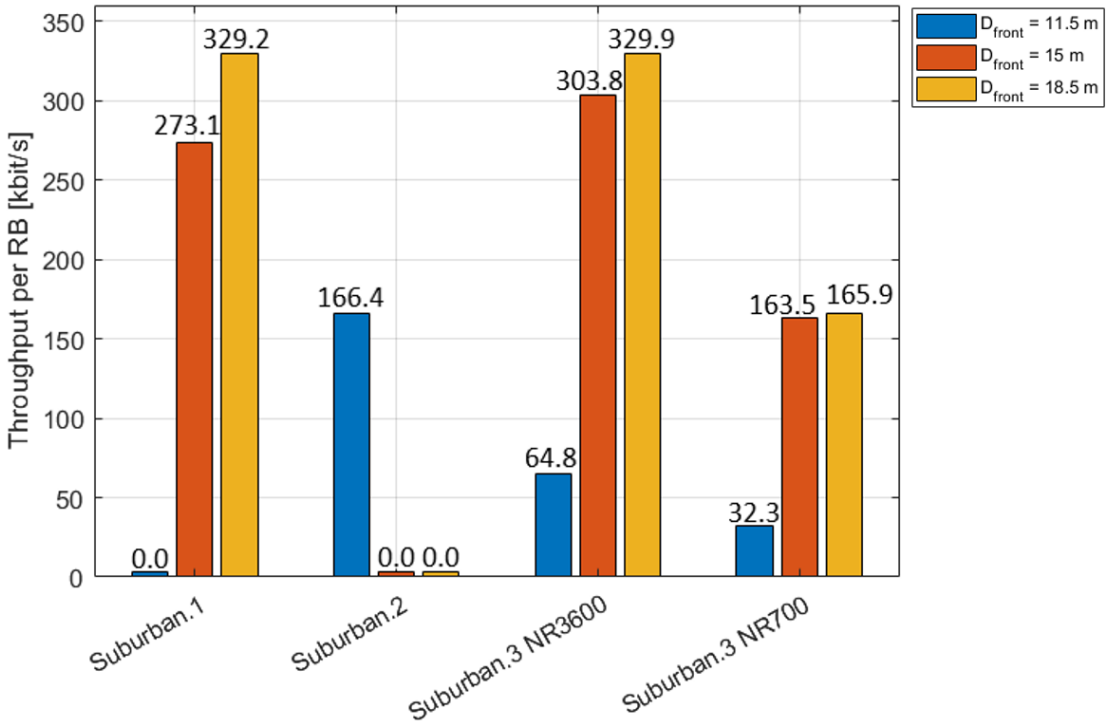

Figure I.16. Throughput per RB for the suburban scenarios for the 4/4 configuration without LTE800.

Table I.3. Throughput per RB variation for carrier configuration 4/2.

Characteristics	D_{front} [m]	$\Delta_{R_b^{RB}}$ [%]						
		Scenario						
		Urban.1	Urban.2	Urban.3	Suburban.1	Suburban.2	Suburban.3	
							NR3600	NR700
All Communications Systems	11.5	-48.7	-91.1	-	-	-4.1	-	-
	15.0	-5.9	-8.4	-15.0	-22.0	0.0	-25.3	-1.9
	18.5	-0.9	-1.6	-2.3	-1.4	0.0	-1.6	-0.9
Without UMTS	11.5	-29.3	-64.1	-95.9	-80.5	-0.1	-95.9	-42.1
	15.0	-4.3	-6.2	-9.9	-5.9	0.0	-11.0	-4.1
	18.5	-0.7	-1.2	-1.7	-0.6	0.0	-1.3	-0.5

Table I.4. Throughput per RB variation for carrier configuration 4/4.

Characteristics	D_{front} [m]	$\Delta_{R_b^{RB}}$ [%]						
		Scenario						
		Urban.1	Urban.2	Urban.3	Suburban.1	Suburban.2	Suburban.3	
							NR3600	NR700
All Communications Systems	11.5	-76.6	-	-	-	-	-	-
	15.0	-8.4	-13.2	-25.4	-93.7	0.0	-31.3	-11.0
	18.5	-1.3	-2.1	-3.0	-3.3	0.0	-2.1	-1.9
Without LTE800 for Suburban and 20% of LTE for Urban	11.5	-48.7	-56.1	-64.1	-	-0.1	-80.5	-80.6
	15.0	-5.9	-6.2	-6.8	-18.0	0.0	-8.8	-1.9
	18.5	-0.9	-1.1	-1.1	-1.2	0.0	-1.0	-0.4

References

[3GPP16] 3GPP, *Discussions on the frame structure design for NR*, TSG RAN WG1 Meeting #84bis, R1-163132, Busan, Korea, Apr. 2016.

[3GPP17] 3GPP, *Technical Specification Group Radio Access Network; Study on New Radio Acess Technology; Radio Interface Protocol Aspects (Release 14)*, TR 38.801, V14.0.0, Mar. 2017.

[3GPP19] 3GPP, *Technical Specification Group Services and System Aspects; Release 15 Description; Summary of Rel-15 Work Items (Release 15)*, TR 21.915 V15.0.0, Sep. 2019.

[Alca13] Alcatel-Lucent, *The LTE Network Architecture*, White Paper, Boulogne-Billancourt, France, 2013 (http://www.cse.unt.edu/~rdantu/FALL_2013_WIRELESS_NETWORKS/LTE_Alcatel_Whit e_Paper.pdf).

[Alme13] D.X.A. Almeida, *Inter-Cell Interference Impact on LTE Performance in Urban Scenarios*, M.Sc. Thesis, Instituto Superior Técnico, University of Lisbon, Oct. 2013.

[ANAC07] ANACOM, "86/2007 Regulation: Procedures for monitoring and measurement of electromagnetic field strength levels originated by radiocommunication stations" (in Portuguese), *Diário da República*, 2nd series, No. 98, May 2007, pp. 13650-13659.

[ANAC19a] ANACOM - Mobile Communications Systems Utilized Frequencies, https://www.anacom.pt/render.jsp?categoryId=382989, Dec. 2019.

[ANAC19b] ANACOM, *Decision about the designation of the 700 MHz band for electronic terrestrial communications services* (in Portuguese), Dec. 2019, (https://www.anacom.pt/streaming/dec23122019Atribuiao700_outrasfaixas.pdf?contentId=1498324&field=ATTACHED_FILE).

[Antu12] M.G.C. Antunes, *Estimation of exclusion regions in LTE base stations colocated with GSM/UMTS*, M.Sc. Thesis, Instituto Superior Técnico, University of Lisbon, Oct. 2012.

[Bala05] C. A. Balanis, *Antenna Theory: Analysis and Design (3rd edition)*, John Wiley & Sons, Inc., New Jersey, USA, 2005.

[Belc18] I. A. R. Belchior, *Evaluation of 5G Cellular Network Implementation over an Existing LTE One*, M.Sc. Thesis, Instituto Superior Técnico, University of Lisbon, Nov. 2018.

[BWWG18] P. Baracca, A. Weber, T. Wild, C. Grangeat, "A Statistical Approach for RF Exposure Compliance Boundary Assessment in Massive MIMO Systems", in *Proc. of WSA 2018 - 22nd International ITG Workshop on Smart Antennas*, Bochum, Germany, Mar. 2018.

[CCMF18] L. Chiaraviglio, A.S. Cacciapuoti, G. Martino, M. Fiore, M. Montesano, D. Trucchi, N.B. Melazzi, "Planning 5G Networks Under EMF Constraints: State of the Art and Vision", *IEEE Access*, Vol. 6, Sep. 2018, pp. 51021 - 51037.

[CFCO04] L.M. Correia, C. Fernandes, G. Carpinteiro, C. Oliveira, *A Procedure for Measurement of Electromagnetic Radiation in the Presence of Multiple BSs*, monIT Project, Report Ext_Tec_0147_03_COST281Paris, Ver. 3, Instituto de Telecomunicações, Lisbon, Portugal, Aug. 2004.

[Corr20] L.M. Correia, *Mobile Communications Systems*, Lecture Notes, Instituto Superior Técnico, University of Lisbon, Portugal, 2020.

[ECCC07] Electronic Communications Committee (ECC) European Conference of Postal and Telecommunications Administrations (CEPT), *Measuring Non-Ionizing Electromagnetic Radiation (9 kHz – 300 GHz)*, ECC Recommendation (02)04, Edition 060207, Helsinki, Finland, 2007.

[ELIF16] eLIFE, *A Century of Trends in Adult Human Height*, Research Article, McGill University, Canada, Jul. 2016 (https://elifesciences.org/articles/13410#metrics).

[ETSI08] ETSI, *Digital cellular telecommunications system (Phase 2+); Radio transmission and reception*, TS 145 005, V7.14.0, Jul. 2008.

[ETSI19a] ETSI - Technologies: 2nd Generation (GERAN), https://www.etsi.org/technologies/mobile/2g, Nov. 2019.

[ETSI19b] ETSI - Technologies: 3rd Generation (UMTS), https://www.etsi.org/technologies/mobile/3g, Nov. 2019.

[FIRR04] G. Franceschetti, A. Iodice, D. Riccio, and G. Ruello, ‘‘A tool for planning electromagnetic field levels in urban areas,’’ in *Proc. IEEE Antennas Propagation Society Symposium*, Monterey, CA, USA, Jun. 2004.

[GSMA20] GSMA - Brief History of GSM & the GSMA, https://www.gsma.com/aboutus/history, Dec. 2020.

[HoTo04] H. Holma and A. Toskala, *WCDMA for UMTS (3rd edition)*, John Wiley & Sons, West Sussex, United Kingdom, 2004, (http://citeseerx.ist.psu.edu/viewdoc/download?doi=10.1.1.87.7238&rep=rep1&type=pdf)

[HoTo11] H. Holma and A. Toskala, *LTE for UMTS: Evolution to LTE-Advanced (2nd edition)*, John Wiley & Sons, West Sussex, United Kingdom, 2011.

[HUAW19a] Huawei, *5G Advanced Wireless Knowledge*, Presentation, Aug. 2019.

[HUAW19b] Huawei, *5G Beamforming*, Presentation, Huawei Wireless Marketing, Aug. 2019.

[HUAW19c] Huawei, *5G Network Planning*, Presentation, 2019.

[HUAW19d] Huawei, *ASI4517R3v06*, Dec. 2019

[HUAW20a] Huawei, *AAU5613 Technical Specifications*, Apr. 2020

[HUAW20b] Huawei, *AAU5339w Description*, Mar. 2020

[ICNI09] ICNIRP, *Statement on the* "Guidelines for Limiting Exposure to Time-Varying Electric, Magnetic, and Electromagnetic Fields (up to 300 GHz)", *Health Physics Society*, Vol. 97, Supplement 3, pp. 257-258, 2009.

[ICNI20] ICNIRP, "ICNIRP Guidelines for Limiting Exposure to Electromagnetic Fields (100 kHz to 300 GHz)", *Health Physics Society*, Vol. 118, No. 5, 2020, pp. 483- 524.

[ICNI98] ICNIRP, "Guidelines for Limiting Exposure to Time-Varying Electric, Magnetic, and Electromagnetic Fields (up to 300 GHz)", *Health Physics Society*, Vol. 74, No. 4, 1998, pp. 494- 522.

[IMTT11] IMTT, *Road Network - Planning and Design Principles* (in Portuguese), Instituto da Mobilidade e dos Transportes Terrestres, Mar. 2011 (http://www.imt-ip.pt/sites/IMTT/Portugues/Planeamento/DocumentosdeReferencia/PacotedaMobilidade/Documents/Pacote%20da%20Mobilidade/Rede%20Vi%C3%A1ria_Princ%C3%ADpios%20de%20Planeamento%20e%20Desenho_Mar%C3%A7o%202011.pdf).

[ITUR15a] ITU-R, *Trends in Mobile Communications*, Presentation, Victoria, Republic of Seychelles, Oct. 2015, (https://www.itu.int/en/ITU-R/terrestrial/workshops/assistSeychelles/Documents/Presentations/Trends_in_mobile_communications_NV_for_presentation.pdf).

[ITUR15b] ITU-R, *IMT Vision – Framework and overall objectives of the future development of IMT for 2020 and beyond*, Recommendation ITU-R m.2083-0, Sep. 2015 (https://www.itu.int/dms_pubrec/itu-r/rec/m/R-REC-M.2083-0-201509-I!!PDF-E.pdf).

[KATH20] Kathrein, https://www.kathrein.com/en/products/antennas-accessories/outdoor-antennas, Jul. 2020

[LCSF16] N.R. Leonor, R.F.S. Caldeirinha, M.G. Sánchez, T.R. Fernandes, "A Three-Dimensional Directive Antenna Pattern Interpolation Method", *IEEE Antennas and Wireless Propagation Letters*, Vol.15, Sep. 2016, pp. 881- 884, https://www.researchgate.net/publication/281746121_A_Three-dimensional_Directive_Antenna_Pattern_Interpolation_Method

[Moli11] A.F. Molisch, *Wireless Communications (2nd edition)*, John Wiley & Sons Ltd, West Sussex, United Kingdom, 2011, (https://researchpapers4scolars.files.wordpress.com/2015/06/andreas-f-molisch-wireless-comm.pdf).

[OFRC05] C. Oliveira, C. C. Fernandes, C. Reis, G. Carpinteiro, L. Ferreira, L.M. Correia, D. Sebastião, *Definition of Exclusion Zones around typical Installations of Base Station Antennas*, monIT Project, Report Int_Tec_0102_15_BSExclZones, Ver. 15, Instituto de Telecomunicações, Lisbon, Portugal, Feb. 2005.

[OSLA08] C. Oliveira, D. Sebastião, D. Ladeira, M. Antunes, *Report of 5 Years of Measurements* (in Portuguese), monIT Project, Report monIT_Ext_Tec_0520_02_Rel5anos, Ver. 2, Instituto de Telecomunicações, Lisbon, Portugal, Jan. 2008.

[PKZu19] R. Pawlak, P. Krawiec, J. Zurek, "On Measuring Electromagnetic Fields in 5G", *IEEE Access*, Vol. 7, Mar. 2019, pp. 29826 - 29835.

[QUAL18] Qualcomm, *Designing 5G NR: The 3GPP Release 15 global standard for a unified, more capable 5G air interface*, Presentation, Sep. 2018, (https://www.qualcomm.com/media/documents/files/the-3gpp-release-15-5g-nr-design.pdf).

[ROSC08] Rohde & Schwarz, *RF chipset verification for UMTS LTE (FDD) with R&S®SMU200A and R&S®FSQ*, Application Note, Dec. 2008, (https://cdn.rohde-schwarz.com/pws/dl_downloads/dl_application/application_notes/1ma138/1MA138_0e_RF_chipset_verification_for_LTE.pdf).

[SDRh17] S. Sbit, M.B. Dadi, B.C. Rhaimi, *Interference Analysis: from 2G to 4G*, in *Proc. of IC_ASET - 2017 International Conference on Advanced Systems and Electric Technologies*, Hammamet, Tunisia, Jan. 2017 (https://ieeexplore.ieee.org/stamp/stamp.jsp?

tp=&arnumber=7983681).

[Shar17] K. Sharma, *Comparison of Energy Efficiency Between Macro and Micro Cells Using Energy Saving Schemes*, M.Sc. Thesis, Lund University, Lund, Sweden, 2017.

[SHTN20] ShareTechnote - 5G/NR Resource Grid, http://www.sharetechnote.com/html/5G/5G_ResourceGrid.html, Feb. 2020.

[Silv20] M.G. Silveirinha, *Antennas*, Lecture Notes, Instituto Superior Técnico, University of Lisbon, Portugal, 2020.

[SLAO10] D. Sebastião, D. Ladeira, M. Antunes, C. Oliveira, L.M. Correia, "Estimation of Base Stations Exclusion Zones", *in Proc. of VTC'10 - 72nd IEEE Vehicular Technology Conference*, Ottawa, Canada, Oct. 2010.

[STAT20] Statista - Number of mobile (cellular) subscriptions worldwide from 1993 to 2019, https://www.statista.com/statistics/262950/global-mobile-subscriptions-since-1993, Dec. 2020.

[TFCT17] B. Thors, A. Furuskar, D. Colombi, C. Tornevik, "Time-Averaged Realistic Maximum Power Levels for the Assessment of Radio Frequency Exposure for 5G Radio Base Stations Using Massive MIMO", *IEEE Access*, Vol. 5, Sept. 2017, pp. 19711 - 19719.

[Viei18] A.B. Vieira, *Analysis of 5G Cellular Radio Network Deployment over Several Scenarios*, M.Sc. Thesis, Instituto Superior Técnico, University of Lisbon, Nov. 2018.

[WINN07] WINNER II, *"WINNER II Channel Models - Part I Channel Models"*, V1.2, Feb. 2008, (https://cept.org/files/8339/winner2%20-%20final%20report.pdf).

[WSAI03] B. Walke, P. Seidenberg and M.P. Althoff, *UMTS The Fundamentals*, John Wiley & Sons, West Sussex, United Kingdom, 2003.